



High Strength Steel in Seismic Resistant Building Frames (HSS-SERF)

EUROPEAN COMMISSION

Directorate-General for Research and Innovation
Directorate D — Key Enabling Technologies
Unit D.4 — Coal and Steel

E-mail: rtd-steel-coal@ec.europa.eu
RTD-PUBLICATIONS@ec.europa.eu

Contact: RFCS Publications

European Commission
B-1049 Brussels

European Commission

Research Fund for Coal and Steel

High Strength Steel in Seismic Resistant Building Frames (HSS-SERF)

D. Dubina, C. Vulcu, A. Stratan, A. Ciutina, D. Grecea, A. Ioan
Universitatea Politehnica Timisoara, Piata Victoriei 2, RO-300006 Timisoara, Romania

A. Tremeeea, A. Braconi
RIVA Acciaio S.p.A., Viale Certosa 249, IT-20151 Milano, Italy

L. Fülöp
Valtion teknillinen tutkimuskeskus, Vuorimiehentie 3, FI-02044 Espoo, Finland

J.-P. Jaspart, J.-F. Demonceau, L. Hoang, L. Comeliau
University of Liège, Place du 20 Aout 7, BE- 4000 Liège, Belgium

U. Kuhlmann, A. Kleiner, C. Rasche
Universität Stuttgart, Keplerstraße 7, DE-70174 Stuttgart, Germany

R. Landolfo, M. D'Aniello, F. Portioli
University of Naples "Federico II", Corso Umberto 1, IT-80138 Napoli, Italy

D. Beg, B. Cermelj, P. Može
Univerza v Ljubljani, Kongresni Trg 12, SI-1000 Ljubljana, Slovenia

L.S. da Silva, C. Rebelo, A. Tenchini
Gabinete de Informática e Projecto Assistido por Computador Lda.
Trav. Padre Manuel da Nobrega 17, 4o Dto, PT-3000-323 Coimbra, Portugal

J. Kesti
Ruukki Construction Oy, Suolakivenkatu 1, FI-00810 Helsinki, Finland

W. Salvatore, S. Caprili, M. Ferrini
Università di Pisa, Lungarno Pacinotti 43, 56100 Pisa, Italy

Grant Agreement RFSR-CT-2009-00024
1 July 2009 to 30 June 2013

Final report

Directorate-General for Research and Innovation

LEGAL NOTICE

Neither the European Commission nor any person acting on behalf of the Commission is responsible for the use which might be made of the following information.

The views expressed in this publication are the sole responsibility of the authors and do not necessarily reflect the views of the European Commission.

***Europe Direct is a service to help you find answers
to your questions about the European Union***

**Freephone number (*):
00 800 6 7 8 9 10 11**

(*) Certain mobile telephone operators do not allow access to 00 800 numbers or these calls may be billed.

More information on the European Union is available on the Internet (<http://europa.eu>).

Cataloguing data can be found at the end of this publication.

Luxembourg: Publications Office of the European Union, 2015

ISBN 978-92-79-44081-6
doi:10.2777/725123

© European Union, 2015
Reproduction is authorised provided the source is acknowledged.

Printed in Luxembourg

PRINTED ON WHITE CHLORINE-FREE PAPER

Table of contents

TABLE OF CONTENTS	3
FINAL SUMMARY	7
1 INTRODUCTION.....	19
1.1 BACKGROUND	19
1.2 OBJECTIVES OF THE RESEARCH PROJECT	19
1.3 DESCRIPTION OF ACTIVITIES AND DISCUSSION / WORK-PLAN AND PROJECT STRUCTURE.....	19
2 DESIGN OF DUAL-STEEL MULTI-STOREY FRAMES.....	23
2.1 INTRODUCTION	23
2.2 STRUCTURAL TYPOLOGIES FOR DUAL-STEEL FRAMES.....	23
2.3 DESIGN OF DUAL-STEEL MULTI-STOREY FRAMES	23
2.3.1 <i>General assumption for the study cases</i>	24
2.3.2 <i>Study cases</i>	24
2.3.3 <i>Structural analysis</i>	25
2.3.4 <i>Design criteria for Moment Resisting Frames</i>	25
2.3.5 <i>Design criteria for (Dual) Concentrically Braced Frames</i>	26
2.3.6 <i>Design criteria for (Dual) Eccentrically Braced Frames</i>	26
2.3.7 <i>Design results</i>	27
2.4 DESIGN OF BEAM-TO-COLUMN JOINT ASSEMBLIES	27
2.4.1 <i>Definition of the experimental program on beam-to-column joint specimens.</i>	27
2.4.2 <i>Design and detailing of bolted and welded beam-to-column joint specimens.</i>	29
2.4.2.1 <i>Design of bolted joints with PE-WF & CFT columns</i>	29
2.4.2.2 <i>Design of welded joints with FE-WF columns</i>	30
2.4.2.3 <i>Design of welded joints with CFT columns</i>	31
2.5 CONCLUDING REMARKS	32
3 SEISMIC PERFORMANCE OF DUAL-STEEL FRAME TYPOLOGIES.....	33
3.1 INTRODUCTION	33
3.2 NUMERICAL PROGRAMME	33
3.3 NON-LINEAR ANALYSIS OF FRAMES.....	34
3.3.1 <i>Seismic hazard and performance levels</i>	34
3.3.2 <i>Selection of accelerograms</i>	35
3.3.3 <i>Overall overstrength factor</i>	40
3.3.4 <i>Behaviour factors</i>	40
3.3.5 <i>Failure criteria and relevant acceptance criteria</i>	40
3.3.6 <i>Numerical models</i>	41
3.4 PERFORMANCE BASED EVALUATION OF DUCTILITY AND OVER-STRENGTH DEMANDS	43
3.4.1 <i>Moment Resisting Frames</i>	43
3.4.2 <i>Concentric Braced Frames</i>	44
3.4.3 <i>Dual Concentric Braced Frames</i>	45
3.4.4 <i>Eccentric Braced Frames</i>	46
3.4.5 <i>Dual Eccentric Braced Frames</i>	48
3.5 PERFORMANCE DESIGN LEVELS AND RELATED Q-FACTORS.....	49
3.5.1 <i>Moment Resisting Frames</i>	49
3.5.1.1 <i>Peak interstorey drift ratios for MRF's</i>	49
3.5.1.2 <i>Overstrength factors for MRF's</i>	50
3.5.1.3 <i>Behaviour factors for MRF's</i>	51
3.5.2 <i>Concentric Braced Frames</i>	51
3.5.2.1 <i>Peak interstorey drift ratios for CBF's</i>	51
3.5.2.2 <i>Overstrength factors for CBF's</i>	52
3.5.2.3 <i>Behaviour factors for CBF's</i>	52
3.5.3 <i>Dual Concentric Braced Frames</i>	53
3.5.3.1 <i>Peak interstorey drift ratios for D-CBF's</i>	53
3.5.3.2 <i>Overstrength factors for D-CBF's</i>	54
3.5.3.3 <i>Behaviour factors for D-CBF's</i>	54

3.5.4	<i>Eccentric Braced Frames</i>	55
3.5.4.1	Peak interstorey drift ratios for EBF's	55
3.5.4.2	Overstrength factors for EBF's	55
3.5.4.3	Behaviour factors for EBF's	56
3.5.5	<i>Dual Eccentric Braced Frames</i>	56
3.5.5.1	Peak interstorey drift ratios for D-EBF's	56
3.5.5.2	Overstrength factors for D-EBF's	57
3.5.5.3	Behaviour factors for D-EBF's	57
3.6	CONCLUDING REMARKS	58
4	EXPERIMENTAL INVESTIGATION OF JOINT ASSEMBLIES AND COMPONENTS	59
4.1	INTRODUCTION	59
4.2	DUCTILITY AND STRENGTH DEMANDS OF WELD DETAILS AND T-STUBS	59
4.2.1	<i>Material tests</i>	60
4.2.1.1	General	60
4.2.1.2	Tests on bolts	60
4.2.1.3	Tests on base metal	61
4.2.1.4	Tests on filler metal	63
4.2.1.5	Hardness measurements	63
4.2.1.6	Macro investigations	64
4.2.2	<i>Welded Connections – Cruciform Joints</i>	64
4.2.2.1	General	64
4.2.2.2	Geometry	65
4.2.2.3	Loading protocol – Cruciform Joints	66
4.2.2.4	Experimental results from Cruciform Joints	67
4.2.2.5	Numerical investigations	69
4.2.2.6	Concluding remarks – Cruciform joints	70
4.2.3	<i>Bolted Connections – T-stubs</i>	71
4.2.3.1	General	71
4.2.3.2	Design	71
4.2.3.3	Loading protocol – T-stubs	72
4.2.3.4	Experimental results from T-stubs	73
4.2.3.5	Experimental results vs. analytical predictions	77
4.2.3.6	Concluding remarks – T-stubs	78
4.3	BOLTED BEAM-TO-COLUMN JOINTS IN MOMENT-RESISTING DUAL-STEEL FRAMES	79
4.3.1	<i>Experimental program</i>	79
4.3.2	<i>Tests on bolted beam-to-column joints</i>	81
4.3.2.1	Pre-test activities	81
4.3.2.2	Interpretation and evaluation of test results	84
4.3.3	<i>Load introduction tests</i>	88
4.3.3.1	Pre-test activities	88
4.3.3.2	Test results and discussions	89
4.4	WELDED BEAM-TO-COLUMN JOINTS IN MOMENT-RESISTING DUAL-STEEL FRAMES	92
4.4.1	<i>Experimental program</i>	92
4.4.2	<i>Tests on welded stiffened and welded cover plate beam-to-column joints with fully-encased wide-flange columns</i>	93
4.4.2.1	Experimental program and specimen configuration	93
4.4.2.2	Tests results	96
4.4.2.3	Interpretation and evaluation of results	102
4.4.3	<i>Load introduction tests on steel-concrete connection through the use of shot fired nails</i>	104
4.4.3.1	Experimental program and specimen configuration	105
4.4.3.2	Experimental test set-up, instrumentation and loading protocol	105
4.4.3.3	Material properties	105
4.4.3.4	Test results	106
4.4.3.5	Interpretation of results	106
4.4.4	<i>Tests on welded reduced beam section and welded cover plate beam-to-column joints with concrete filled rectangular hollow section (CF-RHS) columns ...</i>	107
4.4.4.1	Experimental program and specimen configuration	107
4.4.4.2	Experimental test set-up, instrumentation and loading procedure	108
4.4.4.3	Test results	109
4.4.4.4	Interpretation of results	114
4.4.4.5	Numerical investigation of beam-to-CF-RHS column joints	116
4.5	CONCLUDING REMARKS	122

5	RECOMMENDATIONS FOR SEISMIC DESIGN AND PERFORMANCE BASED EVALUATION OF DUAL-STEEL STRUCTURES.....	127
5.1	INTRODUCTION	127
5.2	DESIGN METHODOLOGY AND CRITERIA FOR DUAL-STEEL STRUCTURES	128
5.2.1	<i>Moment-resisting frames (MRF's)</i>	129
5.2.2	<i>Centrally braced frames (CBF's)</i>	130
5.2.3	<i>Dual centrally braced frames (D-CBF's)</i>	130
5.2.4	<i>Eccentrically braced frames (EBF's)</i>	130
5.2.5	<i>Dual eccentrically braced frames (D-EBF's)</i>	131
5.3	DESIGN AND DETAILING RULES FOR CONNECTIONS AND JOINTS	131
5.3.1	<i>Guidelines for welding</i>	131
5.3.2	<i>Design of load introduction in composite beam to column joints with concrete-filled tube (CFT) columns</i>	132
5.3.3	<i>Bolted hammer head end-plate to wide flange column joint</i>	133
5.3.4	<i>Bolted hammer head end-plate to RHS column joint with U channel</i>	134
5.3.5	<i>Bolted extended end-plate to RHS column joint with long bolts and reduced beam section</i>	136
5.3.6	<i>Welded rib stiffened beam to wide flange column joint, and welded cover plate beam to wide flange column joint</i>	137
5.3.7	<i>Welded external diaphragm reduced beam section to RHS column joint, and welded external diaphragm cover plated beam to RHS column joint</i>	141
5.3.8	<i>Design and detailing rules for bracing connections</i>	144
5.3.9	<i>Design and detailing rules for column bases</i>	144
5.4	RECOMMENDATION FOR PERFORMANCE BASED EVALUATION	145
5.4.1	<i>Framework for performance based evaluation</i>	145
5.4.2	<i>Modelling criteria for structural components</i>	147
5.4.3	<i>Model validation for non-linear dynamic analysis</i>	148
5.4.4	<i>Acceptance criteria for structural components</i>	148
5.5	CONCLUDING REMARKS	149
6	TECHNICAL AND ECONOMIC EFFICIENCY	151
6.1	INTRODUCTION	151
6.2	CASE STUDY REFERENCE FRAMES	151
6.2.1	<i>Design of reference frames</i>	151
6.2.2	<i>Design of beam-to-column joints</i>	152
6.3	EVALUATION OF THE TECHNICAL AND ECONOMIC EFFICIENCY	153
6.3.1	<i>Evaluation of frame weight</i>	153
6.3.2	<i>Evaluation of unitary price of frames</i>	153
6.3.2.1	General considerations	153
6.3.2.2	Average unitary frame price.....	153
6.3.2.3	Influence of the connection typology	153
6.3.2.4	Influence of the steel grade	155
6.3.3	<i>Frame price</i>	156
6.3.3.1	Economic benefit of using higher steel grades in non-dissipative members (columns particularly).....	156
6.3.4	<i>Beam-to-column joint price</i>	157
6.3.4.1	Economic indicators	157
6.3.4.2	Connection price.....	157
6.4	CONCLUDING REMARKS	158
7	CONCLUSIONS.....	161
	LIST OF FIGURES.....	167
	LIST OF TABLES	173
	LIST OF ACRONYMS AND ABBREVIATIONS	175
	LIST OF REFERENCES	177

Final Summary

Introduction

Multi-storey frame structures of high strength steel members for seismic resistant building frames represent an innovation in seismic design in Europe. This type of structures in which mild carbon steel (MCS) is used in dissipative members while high strength steel (HSS) is used in non-dissipative "elastic" members, can be reliable and cost efficient. Based on this conceptual framework, the purpose of "HSS-SERF" project was to investigate the seismic performance of dual-steel building frames, in order to evaluate the effectiveness of such solutions, compared with current homogeneous steel concept. Dual-steel structures enable to fulfil by design the three critical tasks of a robust structure: (i) to secure plastic deformation capacity in structural members, targeted as dissipative, which are key members in any seismic-resistant structure; (ii) to prepare multiple routes for transfer of forces and ensure their redistribution through yielding of other members; (iii) to provide sufficient over-strength to structural members that cannot be allowed to collapse at any cost. In dual-steel structures, the role of lower-yield steel is to work like a fuse, dissipating the seismic energy through plastic deformations, while the rest of the structure remains elastic or undamaged. To achieve these global performance targets, a proper detailing is compulsory, mainly for beam to column joints, in which by conception and sizing, a good balance between dissipative and non-dissipative components is needed.

Research objectives

The aim of the project was to investigate and evaluate the seismic performance of dual-steel building frames, realised from two different steel grades: mild carbon steel (MCS) and high strength steel (HSS). The main objectives of "HSS-SERF" research project can be summarized as follows:

- To find reliable structural typologies (e.g. moment-resisting frames, concentrically braced frames, eccentrically braced frames) and connection detailing for dual-steel building frames, and to validate them by tests and advanced numerical simulations;
- To develop design criteria and performance based design methodology for dual-steel structures using HSS;
- To recommend relevant design parameters (i.e. behaviour factor q , over-strength factor Ω) to be implemented in further versions of the seismic design code (EN 1998-1 [1]) in order to apply capacity design approach for dual-steel framing typologies;
- To evaluate technical and economic benefit of dual-steel approach involving HSS;

Research plan and work carried out

The main research activities of the project were divided into several working packages. The general flow-chart of research is illustrated in Figure I.

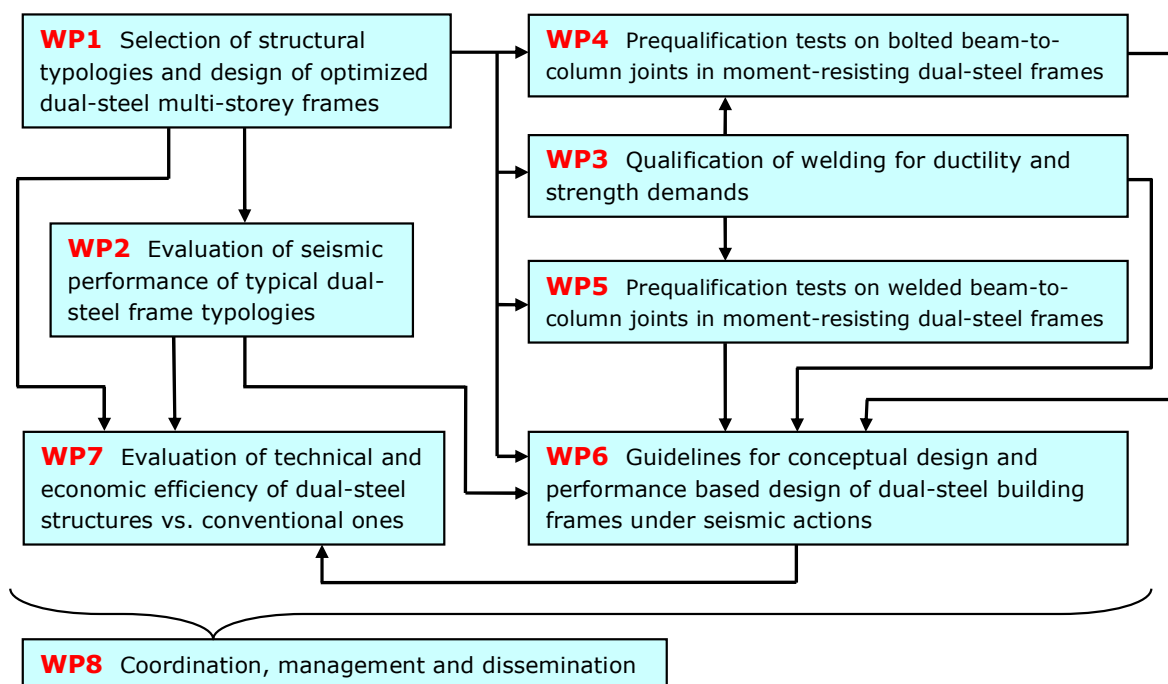


Figure I. General flow chart of research

Research team:

- UPT Politehnica University of Timisoara, Romania (project coordinator)
- RIVA Riva Acciaio S.p.A, Italy
- VTT Technical Research Centre of Finland
- ULG University of Liege, Belgium
- USTUTT University of Stuttgart, Germany
- UNINA University of Naples "Federico II", Italy
- UL University of Ljubljana, Slovenia
- GIPAC Gabinete de Informática e Projecto Assistido por Computador Lda., Portugal
- RUUKKI Ruukki Construction Oy, Finland
- UPI University of Pisa, Italy

In relation to the general flow chart of research, Table I summarises all working packages and nominates for each Working Package, the WP Leader and the Partners involved in the realisation of the specific tasks.

Table I – Working packages: WP leaders and partners involved in specific tasks

WP	WP Leader	Partners involved
WP1	GIPAC	UPT, VTT, ULG, UNINA, UL
WP2	UNINA	UPT, VTT, GIPAC
WP3	USTUTT	RIVA, ULG, UL, RUUKKI
WP4	ULG	RIVA, USTUTT, RUUKKI
WP5	UL	UPT, RIVA, USTUTT, RUUKKI
WP6	VTT	UPT, ULG, USTUTT, UNINA, UL, GIPAC, UPI
WP7	RIVA	UPT, VTT, UNINA, GIPAC, RUUKKI, UPI
WP8	UPT	RIVA, VTT, ULG, USTUTT, UNINA, UL, GIPAC, RUUKKI

Considering the general flow-chart of research and the containing working packages (WP's), the final report of the "HSS-SERF" project is structured considering the following outline:










1. Introduction
2. Design of dual-steel multi-storey frames
3. Seismic performance of dual-steel multi-storey frames
4. Experimental investigation of joint assemblies and components
5. Recommendations for seismic design and performance based evaluation of dual-steel structures
6. Technical and economic efficiency
7. Conclusions

In Introduction, a brief presentation is made in relation to the background, the main objectives of the research project, as well as the description of activities, work plan and outline of the final report. Chapter 2 is related to the design of the frames performed within WP1 and WP2, and Chapter 3 presents the seismic performance of dual-steel multi-storey frames investigated in WP2. Chapter 4 covers the experimental investigations conducted on joint assemblies within (WP4 and WP5) and on joint components (weld details and T-stubs) within WP3. Chapter 5 is related to the Guidelines elaborated within WP6, and Chapter 6 is related to the technical and economic efficiency of dual-steel structures vs. conventional ones (WP7). The main conclusions of the research activities from "HSS-SERF" project are presented in Chapter 7. In the following part, a brief presentation is made for each section covering the main activities and obtained results.

Design of dual-steel multi-storey frames

In WP1, a number of 18 dual-steel frame configurations were designed. The particular frame typologies covered moment resisting frames (MRF), dual concentrically braced frames (D-CBF) and dual eccentrically braced frames (D-EBF). Table II makes an overview of the frame configurations considered for the preliminary design. Beside the three frame typologies, two other parameters were taken into account, i.e. the column cross section (full encased wide flange FE-WF, partially encased wide flange PE-WF, concrete filled tube CFT) and steel grade for column (S355, S460, S690 → hot rolled sections and plates / S700 → rectangular hollow sections).

Table II – Frame configurations for preliminary design in WP1

Frame type		MRF – 8 storeys			D-CBF – 8 storeys			D-EBF – 8 storeys		
Column type										
Column steel grade	S355	1.1.1	1.2.1	-	-	-	-	-	-	-
	S460	1.1.2	1.2.2	-	2.1.2	2.2.2	2.3.2	3.1.2	3.2.2	3.3.2
	S690/S700	1.1.3	1.2.3	-	2.1.3	2.2.3	2.3.3	3.1.3	3.2.3	3.3.3

The design of the multi-story frames allowed the identification of realistic member sizes for both mild carbon steel beams and high strength steel composite columns (see Figure II).

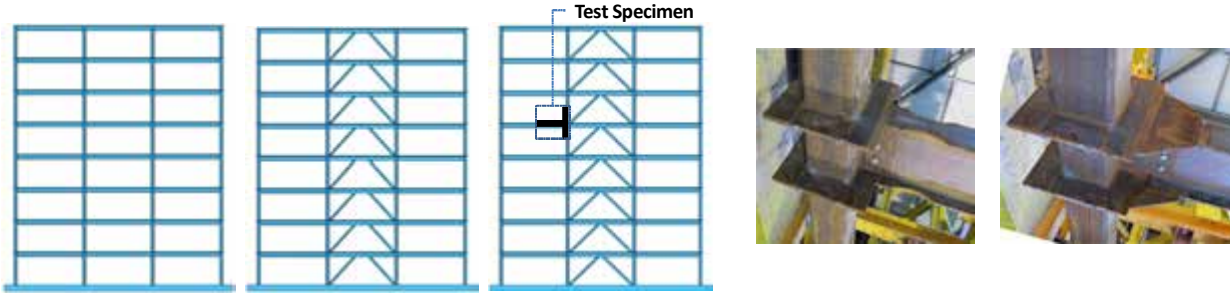


Figure II. Design of dual-steel multi-storey frames (MRF, D-EBF, D-CBF), choice of members (beams, columns) and design of beam-to-column joint specimens

Several practical solutions for bolted and welded beam-to-column joints were identified and designed. These are: bolted joints with hammer-heads and partially encased wide flange (PE-WF) columns (see Figure III-a) and respectively concrete filled rectangular hollow section (CF-RHS) columns (see Figure III-b), joints with long bolts for concrete filled tubes (see Figure III-c), welded joints with fully encased wide-flange (FE-WF) columns and rib or cover plate stiffened beam (see Figure IV-a), as well as welded joints with concrete filled rectangular hollow section (CF-RHS) columns and reduced beam section and cover plate stiffened beam (see Figure IV-b and Figure II). In addition, new T-stub configurations ("Box Section" T-stub & unstiffened T-stub with long bolts) whose design is not covered by Eurocode rules, were identified and considered further in the experimental program.

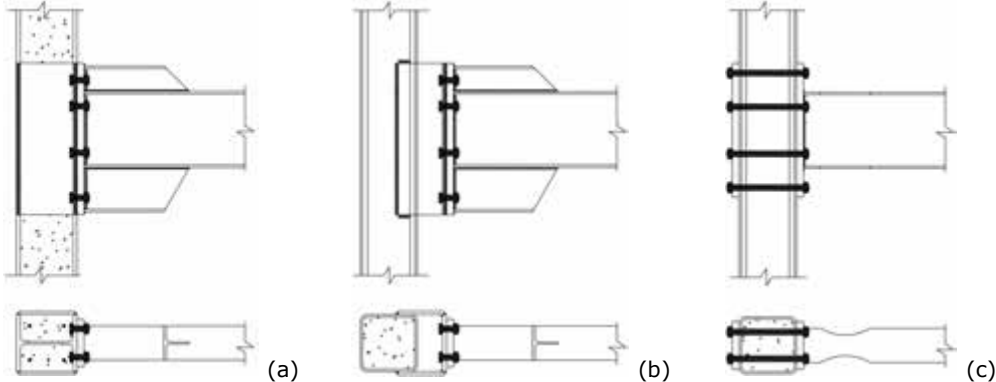


Figure III. Bolted beam-to-column joint configurations

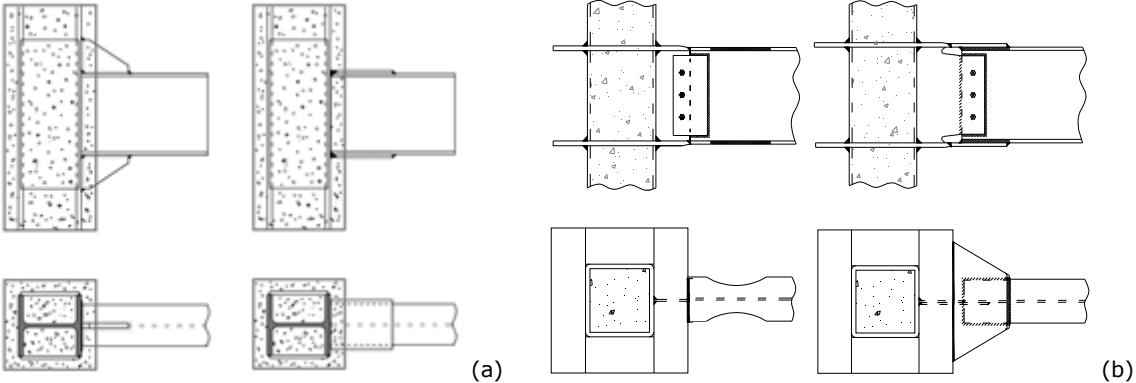


Figure IV. Welded beam-to-column joint configurations

Within WP2, the initial set of frames was extended to include standard concentrically and eccentrically braced frames, two additional height ranges (4 and 8 storeys for MRF's, respectively 8 and 16 storeys for braced frames), two span ranges (5 m and 7.5 m), and two different types of seismic action corresponding to stiff and soft soil (see Figure V-a-b). Consequently, a number of 120 frame configurations were designed.

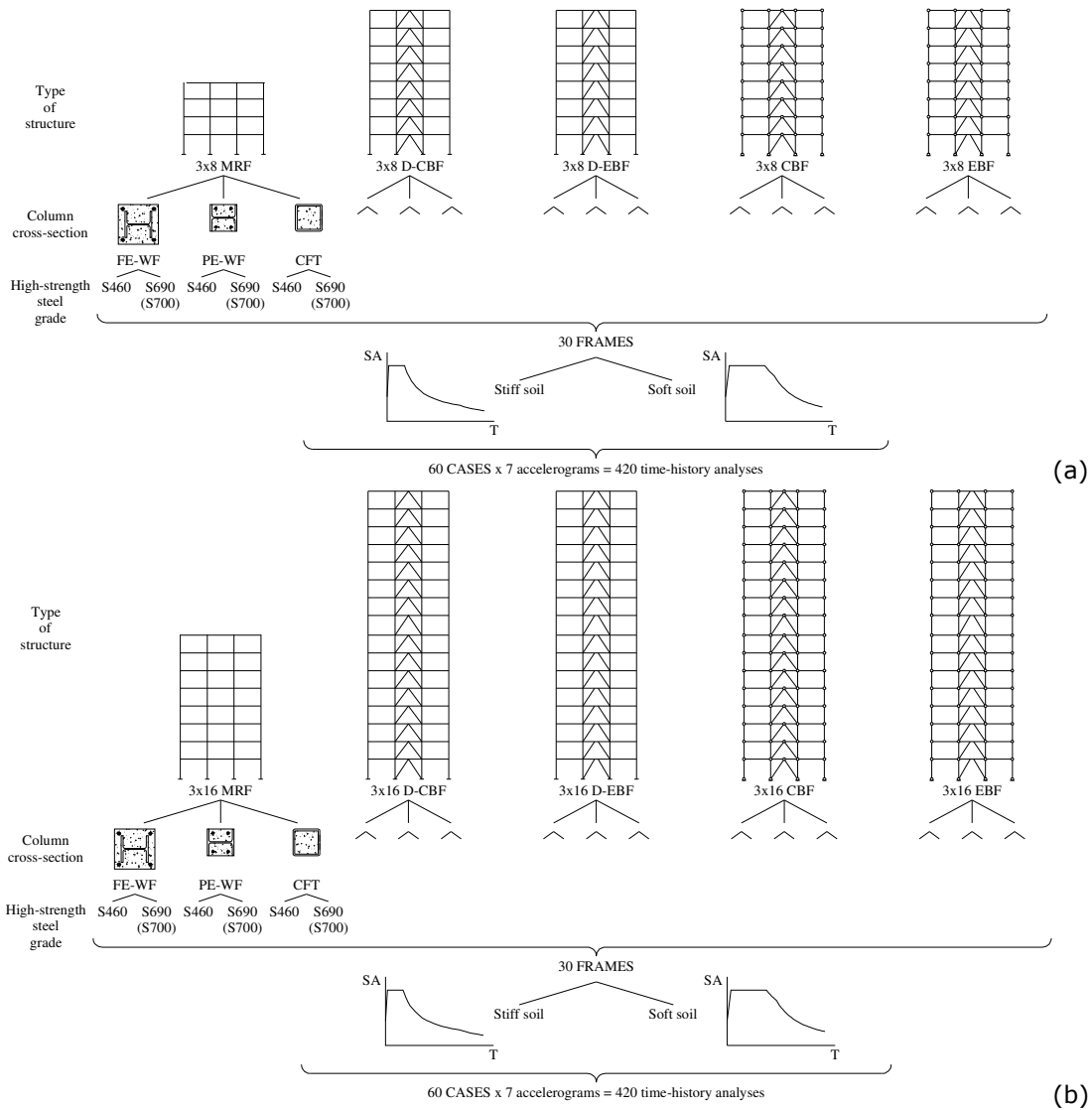


Figure V. Analysis cases for the seismic performance evaluation

Seismic performance of dual-steel multi-storey frames

Nonlinear analyses were carried out in order to assess the seismic performance of the 120 frame configurations summarized in Figure V-a-b. For the beginning, numerical modelling assumptions were validated on the basis of existing experimental results, both in static and dynamic conditions. The free computational framework Seismostruct [2] was used in the study. Further, static and dynamic non-linear analyses were carried out to identify the collapse modes and deformation demands. For this purpose, two sets of accelerograms compatible to EN 1998-1 [1] spectra for stiff and soft soil types were selected. The evaluation of ductility and over-strength demands, and evaluation of q-factors associated with different performance levels were also performed. The outcomes of the study can be summarised as follows:

- The use of HSS was proven to be an efficient solution especially in columns for CBF's (simple & dual), and in both columns and braces for EBF's (simple & dual); in contrast, the use of HSS was not an effective solution for MRF's, the seismic design procedure being governed by damage limitation;
- MRF's evidenced an adequate seismic performance with low ductility demands, and the exhibited overstrength was larger than the behaviour factor used in design;
- CBF's & D-CBF's: the dual-system structures presented higher over-strength and behaviour factors compared to the simple solutions; however, in all cases the behaviour factors were smaller compared to the values from EN 1998-1 [1], mainly due to the large brace ductility demand in compression; in addition, the frames with flexible beams in the braced bays showed the poorest performance – hence, the use of HSS for beams of braced bays is not advisable. Although, EN 1998-1 [1] makes no difference between the soil condition regarding the overstrength and behaviour factors, the frames designed on soft soil presented smaller overstrength and behaviour factors;
- EBF's & D-EBF's: the static and dynamic analyses showed that the performance of the structures designed according to EN 1998-1 [1] was affected by the brace buckling;

consequently, the behaviour factors were significantly lower compared to the values recommended by EN 1998-1 [1]; the same set of structures designed with modified capacity design criterion showed an effective performance avoiding the brace buckling, thus experiencing behaviour factors consistent to the codified values;

- In all examined structural typology, the behaviour factors obtained from incremental dynamic analyses, for significant damage (SD) limit state, were smaller than the code values. These results suggest the need to calibrate the behaviour factors given by EN 1998-1 [1].

Experimental investigation of joint assemblies and components

The experimental program within "HSS-SERF" project covered extensive experimental investigations of joint components (weld details and T-stubs – WP3), and respectively joint assemblies (WP4 & WP5).

Investigation of joint components (weld details and T-stubs)

The experimental investigations on weld details (see Figure VI) were aimed at studying the influence of the following parameters: steel grade (S460, S690), filler metal (G46, G69), type of weld (fillet weld, full penetration weld), loading procedure (monotonic, cyclic), and the loading rate (0.00025 s^{-1} , 0.06 s^{-1} , 0.12 s^{-1}). The outcomes of the study can be summarised as follows:

- The dynamic loading lead to an increase of the capacity and a reduction of the ductility compared to the quasi-static loading, and that the cyclic loading lead to a reduction of ductility compared to the monotonic loading.
- The experimental investigations validated the adopted welding procedure, as the failure occurred in the base metal in all cases. It is to be mentioned that the filler welds were designed based on the over-strength requirements from EN 1998-1 [1].
- For welds designed as full-strength, the loading type did not affect the failure of the connection, which occurred for all types of loading conditions in the base metal.
- As the design philosophy of a "full-strength" weld was successful, and only failure of the base metal occurred, the influence of the steel grade of the longitudinal plate (S460 / S690), the type of welding (fillet weld or full penetration weld) and the type of filler metal on the overall strength and ductility of the Cruciform Joint was negligible.

The experimental investigations on T-stubs were aimed at studying the components which are of relevance in bolted beam-to-column joints where mild carbon steel beams are connected to high strength steel columns. Several T-stub configurations were considered (see Figure VI), particularly: un-stiffened T-stub with normal bolts, stiffened T-stub, "box-section" T-stub, and un-stiffened T-stub with long bolts. The failure mode considered in the design process of the T-stubs was failure mode 2 according to EN 1993-1-8 [3], justified by a reasonable compromise between capacity and ductility. The outcomes of the study can be summarised as follows:

- The observed failure modes of bolted T-stubs involved combined bending and tension bolt fracture for specimens behaving ductile and nearly pure tension bolt fracture for specimens behaving brittle. Stripping of the nut threads was not observed at all. In one specimen (Series 400) complete cracking of the end-plate material in the HAZ occurred.
- The choice of thickness for the end-plate associated with steel grade is important in the conception of a proper connection, in order to obtain a good balance between stiffness, strength and ductility of components.
- The major contributions to the overall T-stub strength and deformation were the end-plate deformation capacity and the strength of the bolts, as far as its plastic failure mechanism was governed by mode 2.
- The choice of steel grade for the end-plate material does not significantly influence the load carrying capacity. In contrast, the geometry (bolt distance, end-plate thickness, etc.) and the stiffener have a more remarkable influence on the load carrying capacity. For stiffened situations (Series 200), a uniform load introduction of the bolt and therefore almost a pure tensile stress situation of the bolt provides a nearly independent high load carrying capacity without losing much ductility.



Figure VI. Welded details and T-stub typologies (Univ. of Stuttgart)

Investigation of beam-to-column joint assemblies (bolted and welded joints)

As part of WP4, three types of bolted beam-to-column joints were developed and investigated at the University of Liege. The joint typologies are illustrated in Figure III and correspond to the following cases: (a) partially encased wide flange column with reinforced end-plate connection; (b) concrete filled tube column with reinforced end-plate connection; (c) concrete filled tube column with end-plate connection and long bolts. The parameters of the experimental program, covering a number of 16 beam-to-column joint tests, were: steel grade for the columns (S460, S700), loading procedure (monotonic, cyclic), and failure mode (beam, connection zone). The outcomes of the study can be summarised as follows:

- The experimental investigations (see Figure VII) evidenced a stable hysteretic behaviour of the joints for which the plastic deformations developed in the dissipative zone of the beam.
- The test campaign allowed demonstrating the ability of the proposed bolted joint configurations to exhibit a full strength and fully rigid character.
- The analytical provisions of EN 1993-1-8 [3] have been extended in order to be able to characterise the proposed joint configurations. The analytical models developed for the innovative joint components have been validated against the experimental results.
- All joint configurations can be designed as full-strength and rigid/or semi-rigid solutions and can be used in moment-resisting dual-steel frames. Moreover, the cyclic tests show that the ductility requirement by EN 1998-1 [1] is satisfied.

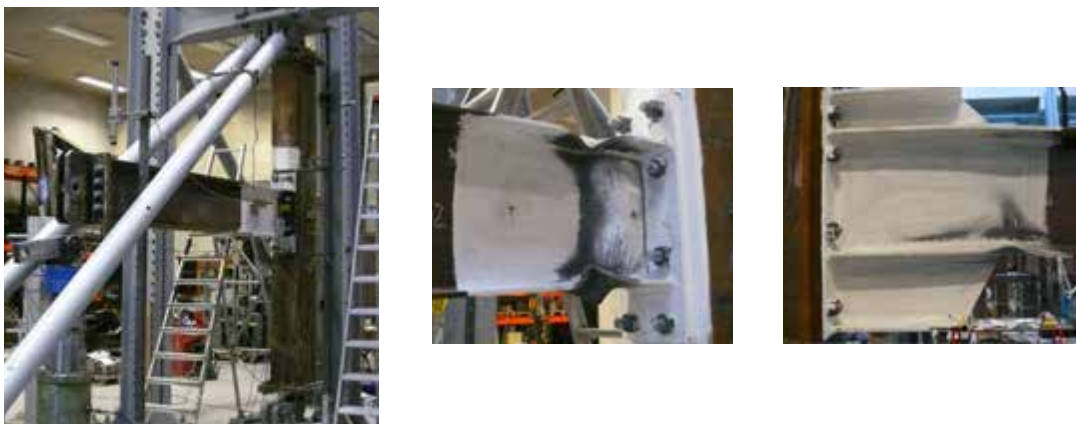


Figure VII. Experimental investigation of bolted beam-to-column joints (Univ. of Liege)

As part of WP5, experimental investigations were conducted on welded beam-to-column joints at University of Ljubljana and Politehnica University of Timisoara. The main tasks covered experimental investigations of joints with welded connections (rib stiffeners / cover plates) and fully encased wide flange columns (see Figure IV-a), and respectively joints with welded connection (reduced beam section / cover plates) and concrete filled rectangular hollow section columns (see Figure IV-b).

In case of joints with fully encased wide flange columns (Figure IV-a & Figure VIII), experimental and numerical investigations were performed with the aim to assess the influence of the following parameters: joint type (with rib stiffeners & with cover plates), steel grade for the column (S460 & S690), loading procedure (cyclic with variable amplitude & cyclic with constant amplitude), axial force level in the column. From the study, the following observations can be drawn:

- The proposed joints proved that the design and geometrical concept along with the considered weld details represent a good solution under variable and constant cyclic loading conditions.
- The design objective for the welded RS and CP connections, based on the capacity design concept, to relocate inelastic action away from the face of the beam-to-column connection, was fulfilled. In both cases connection zone and the column itself remained in elastic state.
- Both designed full strength connections proved to behave well under cyclic tests performed according to the ANSI/AISC 341-10 [7] loading protocol, with plastic rotation capacities greater than 0.044 and 0.051 rad, for bigger and smaller beam cross-sections, respectively, without degradation of strength and stiffness for more than 20% according to EN 1998-1 [1] criterion.
- In case of constant cyclic loading, the CP joint displayed better fatigue performance, attributed to the increased level of unfavourable strain concentrations, larger weld residual stress and HAZ at the end of the rib-stiffener in the RS joint.
- Axial force applied in the column did not have any noticeable effect on response of the specimens.



Figure VIII. Experimental investigation of welded beam-to-column joints (Univ. of Ljubljana)

In case of joints with concrete filled tubes (see Figure IV-b & Figure IX), two types of welded connections were considered, i.e. with reduced beam section (RBS) and with cover plates (CP). A number of 16 beam-to-column joint assemblies were investigated, varying parameters such as: loading procedure (monotonic, cyclic), joint type (reduced beam section, cover plate), steel grade for the column (S460, S700), and the failure mode (beam, connection zone). From the study, the following observations can be drawn:

- The monotonic and cyclic tests on beam-to-column joints evidenced a good conception and design of the joints (RBS and CP). This observation was justified by the elastic response of the connection zone, formation of the plastic hinge in the beam (see Figure IX), and a good response of joint detailing and welded connections. The joints were characterised by a significant over-strength.
- Corresponding to cyclic tests performed according to the ANSI/AISC 341-10 [7] loading protocol, the designed joints evidenced rotation capacities of 50 mrad (RBS joints) and respectively 40 mrad (CP joints) for which the degradation of strength and stiffness were not greater than the 20% limit defined in EN1998-1 [1].



Figure IX. Experimental investigation of welded beam-to-column joints (Univ. of Timisoara)

In the case of the partially encased and/or fully encased wide-flange columns, the load introduction is accomplished through shear studs. In contrast, for the case of rectangular hollow section columns, the connection solution between steel and concrete is more complex and can be realised in two methods, which were studied within HSS-SERF project:

- In case of joints with end-plate connection, long bolts and concrete filled tube columns, the long bolts have a double role, i.e. to assure the connection between beam and column, and respectively to assure the connection between the steel tube and the concrete core. For the study of the latter phenomenon, a set of load introduction tests were performed at the University of Liege as part of WP4 (see Figure X). Tests with and without bolt preloading have been performed to identify the effect of this preloading on the behaviour of the tested specimen. Also, different testing set-ups have been used in order to be able to characterise the slip resistance between the concrete and the tube, the resistance of the bolts subjected to pure shear and the resistance of the bolts subjected to combined bending and shear. The test results proved the effectiveness of the load transfer from the beams to the RHS composite columns through the use of long bolts.

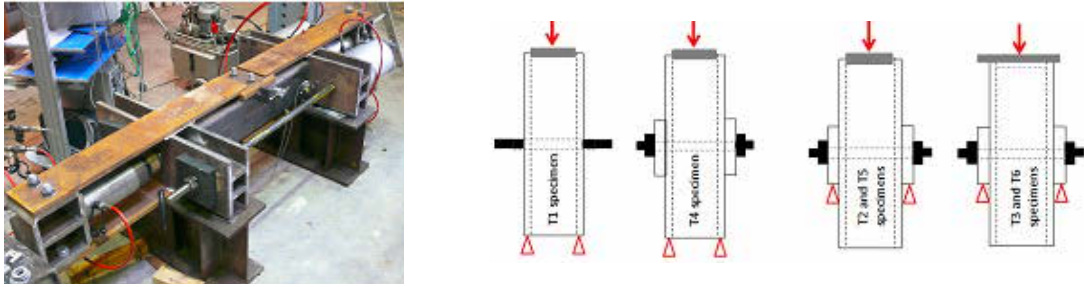


Figure X. Load introduction tests: steel-concrete connection through long bolts (Univ. of Liege)

- In case of joints with welded connection and concrete filled tube columns, the load introduction can be provided by shot-fired nails fixed from the exterior of the cross-section. In order to check the effectiveness of the shear connection between steel and concrete, a series of load introduction tests were performed on column stubs at the Politehnica University of Timisoara as part of WP5 (see Figure XI). The investigated parameters were: loading procedure (monotonic, cyclic), type of connection between steel tube and concrete core (friction only, friction combined with connectors), steel grade (S460, S700). The test results evidenced a significant contribution of the connectors to the load transfer from steel tube to the concrete core in both monotonic and cyclic loading. Additionally, the friction (0.4 N/mm^2) which developed between steel tube and concrete, was equal to the value recommended in EN 1994-1 [4] for rectangular hollow sections filled with concrete.

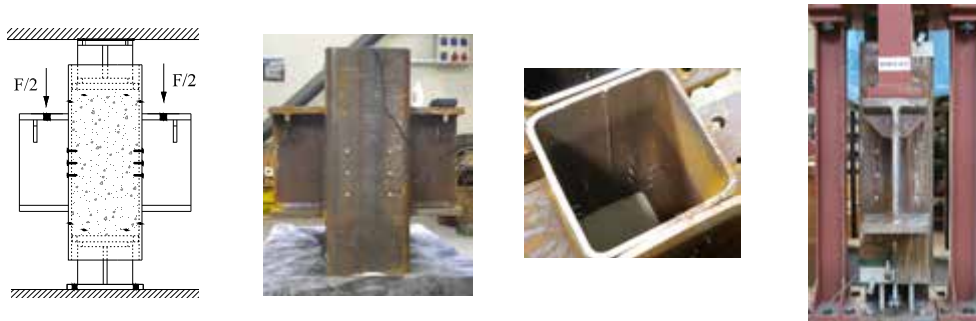


Figure XI. Load introduction tests: steel-concrete connection with shot fired nails (Univ. of Timisoara)

In addition to the experimental program, advanced numerical investigations were performed with regard to the beam-to-column joints assemblies. The first phase consisted in the calibration of the numerical models of the joint configurations based on the monotonic and cyclic test results (see Figure XII). From the calibration, a set of numerical models were obtained which were capable to reproduce with a good accuracy the response of the joints in both moment-rotation curve and failure mechanism, i.e. formation of the plastic hinge in the beam (designed joints) and yielding of components (joints with strengthened beam). This allowed for a better understanding of the joint behaviour and allowed the development and validation of simple design procedures for the studied joint configurations. The second phase consisted in the extension of the experimental program with the aim to evaluate the influence of the concrete core, axial force in the column, response of the joints with multiple beams and influence of the external diaphragm.

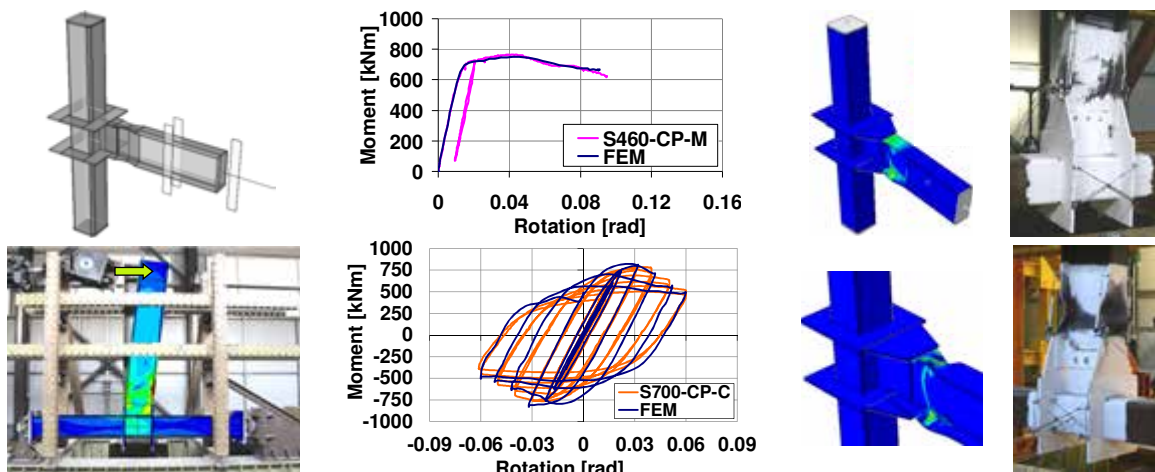


Figure XII. Advanced numerical investigations of beam-to-column joint assemblies subjected to monotonic and cyclic loading conditions (calibration of numerical models)

Recommendations for seismic design and performance based evaluation of dual-steel structures

The guidelines for conceptual design and performance based design of dual-steel building frames under seismic actions were developed within WP6, and cover the design and detailing rules for connections and joints, and design methodology and criteria for moment-resisting frames (MRF's), concentrically braced frames (CBF's), and eccentrically braced frames (EBF's). The outline of the guidelines can be summarised as:

- Introduction
- Seismic design of dual-steel structures
- Design and detailing rules for seismic resistant dual-steel structures
- Recommendation for performance based evaluation
- Concluding remarks
- Appendix A – Worked examples:
 - Design of bolted hammer head end plate to wide flange column joint
 - Design of bolted hammer head end plate to RHS column joint with U channel
 - Design of bolted extended end plate to RHS column joint with long bolts and reduced beam section
 - Design of welded rib stiffened beam to wide flange column joint
 - Design of welded cover plated beam to wide flange column joint
 - Design of welded external diaphragm reduced beam section to RHS column joint
 - Design of welded external diaphragm cover plated beam to RHS column joint

In relation to the acceptance criteria for structural components, a proposal was elaborated within the project concerning the definition of the acceptance criteria and evaluation of the seismic performance of the beam-to-column joints investigated in WP4 and WP5 (joints designed to develop the plastic hinge in the beam). In relation to the performance of the joints, the following observations were made:

- Corresponding to the Significant Damage performance level, all joint configurations evidenced rotation capacities larger than the 40 mrad, and therefore the seismic performance of the joints was considered acceptable;
- The state of the joints corresponding to the three performance levels was observed to reflect in a realistic manner the definition related to each performance level: Damage Limitation, Significant Damage, and Near Collapse.

Technical and economic efficiency

As part of WP7, the evaluation of the technical and economic efficiency of dual-steel structures compared to conventional ones was performed. Consequently, a number of 15 frame configurations (see Figure XIII) were selected and designed on a more detailed level. The frames were characterised by stiff soil conditions, eight stories, and 7.5 m span. The frame typologies were represented by dual frames (MRF+CBF, and MRF+EBF), and standard braced frames (CBF, EBF). The parameters from the case study frames are: frame type (D-CBF, CBF, D-EBF, EBF), steel grade for non-dissipative members (S355, S460, S690), and typology of the beam-to-column joints from the moment resisting bays (welded dog-bone, rib stiffened, hammer head, and long bolts joints – see Figure XIV). The evaluation of the technical and economic efficiency of dual-steel structures vs. conventional ones, showed that the use of high strength steel in non-dissipative members (columns of CBF & D-CBF, columns and braces of EBF & D-EBF) and connections, represented an effective solution from the technical and economical point of view, leading therefore to cost reduction.

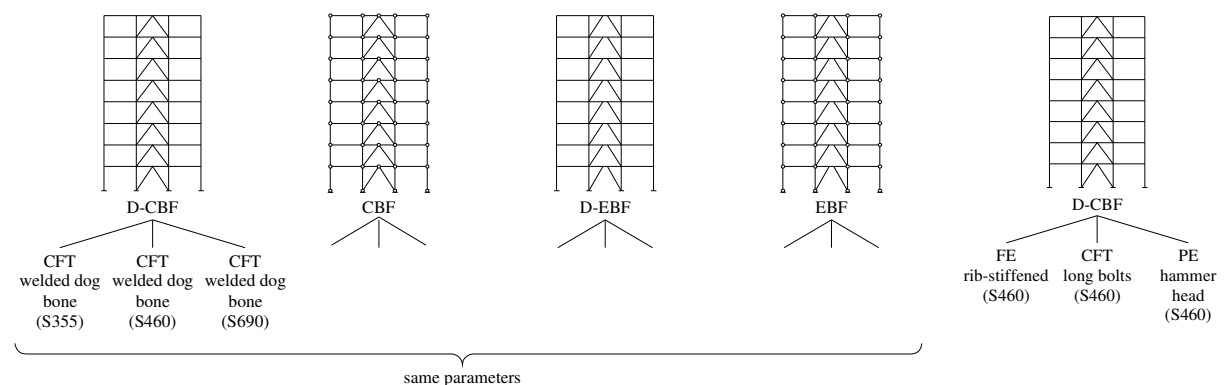


Figure XIII. Analysis cases for the evaluation of technical and economic efficiency

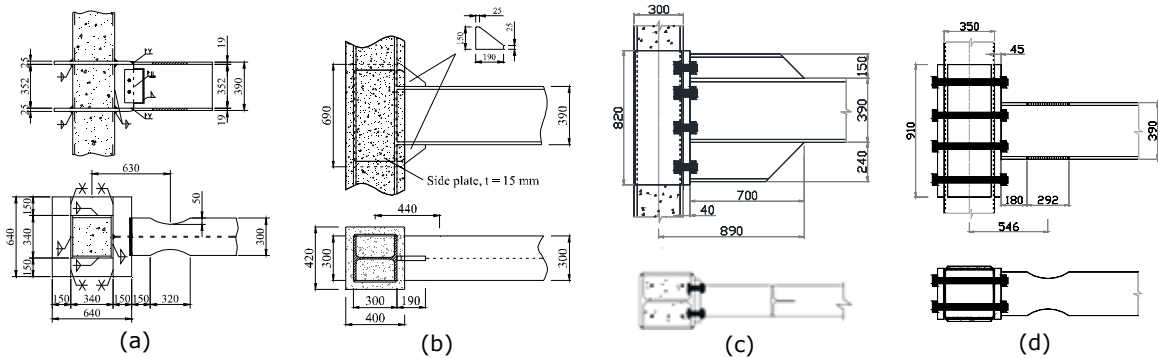


Figure XIV. Designed beam-to-column joints for the moment resisting bays: (a) ED-RBS – welded external diaphragm reduced beam section joint; (b) RS – welded rib stiffened joint; (c) HH – bolted hammer head joint; (d) LB-RBS – bolted reduced beam section joint with long bolts

Application of the dual-steel concept in the framework of SERIES / FP7 research project "DUAREM"

A particular application of the dual-steel concept was implemented within the research project "DUAREM" – Full-scale experimental validation of dual eccentrically braced frame with removable links (see Figure XV). The project involved a full scale pseudo-dynamic test of a dual structure (Eccentrically Braced Frame with removable links combined with Moment Resisting Frames) realized using the dual-steel concept (Mild Carbon Steel in dissipative members and High Strength Steel in non-dissipative members). "DUAREM" project, performed under SERIES TA User Agreement JRC N° 31817, started in September 2010 and is developed under the FP7 grant agreement "Seismic Engineering Research Infrastructures for European Synergies (SERIES)". The project was coordinated by the Politehnica University of Timisoara, while University of Liege, University of Naples "Federico II", University of Ljubljana, and University of Coimbra were partners in this research. The proposed research aimed at reducing the repair costs and downtime of a structure hit by an earthquake, and consequently more rational design approach in the context of sustainability. These objectives are to be attained through removable dissipative members and re-centering capability of the structure. The bolted links are intended to provide the energy dissipation capacity and to be easily replaceable, while the more flexible moment resisting frames would provide the necessary re-centering capability to the structure. The moment resisting frames and the columns of the eccentrically braced frames were fabricated from high strength steel, in order to keep these members in the elastic range even under strong seismic input.



Figure XV. Full-scale experimental validation of dual eccentrically braced frame with removable links

The full-scale pseudo-dynamic tests were performed at the ELSA facility of the Joint Research Centre in Ispra, Italy, and enabled a realistic evaluation and validation of the structural concept and dual-steel solutions developed within "HSS-SERF" Project. As a result, this complementary research in "DUAREM" provided an important added value to the "HSS-SERF" Project.

Conclusions and Future Perspectives

In recent years, significant developments in steel processing allowed obtaining high strength steels (HSS). Nowadays, in Japan and USA, HSS's are widely used for bridge and building construction. On the contrary, in Europe there are still a limited number of applications on buildings, and especially in seismic regions, although some examples exist for the use of HSS in bridge structures. The use of high strength steel within seismic resistant structures could be done considering two approaches: (i) dual-steel structures in which mild carbon steel (MCS) is used for dissipative members and HSS is used in non-dissipative members; (ii) structures realised of HSS, i.e. S460 which is characterised by a certain amount of ductility and therefore could be used in structures of medium ductility class (DCM). With these considerations, the aim of "HSS-SERF" project was to investigate and evaluate the seismic performance of dual-steel building frames, realised from two different steel grades: mild carbon steel and high strength steel. In addition, the main objectives can be summarized as follows:

- To find reliable structural typologies (e.g. moment-resisting frames, concentrically braced frames, eccentrically braced frames) and connection detailing for dual-steel building frames, and to validate them by tests and advanced numerical simulations;
- To develop design criteria and performance based design methodology for dual-steel structures using HSS;
- To recommend relevant design parameters (i.e. behaviour factor q , over-strength factor Ω) to be implemented in further versions of the seismic design code (EN 1998-1 [1]) in order to apply capacity design approach for dual-steel framing typologies;
- To evaluate technical and economic benefit of dual-steel approach involving HSS.

Considering the main objectives of "HSS-SERF" project, the following research activities have been accomplished:

- An initial set of 18 dual-steel frame configurations were selected and designed, considering MRF's, D-CBF's and D-EBF's, realised with composite columns (FE-WF, PE-WF, CF-RHS). The design of the frames allowed the identification of realistic member sizes for both mild carbon steel beams and high strength steel composite columns. Several practical solutions for bolted and welded beam-to-column joints were identified and designed. Based on the joint solutions, new T-stub configurations whose design is not covered by Eurocode rules, were identified and considered in the experimental program;
- A comprehensive parametric study was defined by selecting and designing a set of 120 frames representative for the design practice. An extensive numerical program was carried out for the seismic performance evaluation of the 120 frames. In addition, the ductility and over-strength demands, and evaluation of q -factors associated with different performance levels were performed;
- The experimental program covered the investigation of joint components (weld details and T-stubs), and respectively bolted and welded beam-to-column joint assemblies. In addition, advanced numerical investigations lead to the development and validation of simple design procedures for the studied joint configurations, and extension of the experimental program;
- Based on the outcomes from the design of frames and joints, numerical program on the 120 frames, and experimental investigation of joint assemblies and components – Guidelines were developed for the conceptual design and performance based design of dual-steel building frames under seismic actions. The main outline of the guidelines was related to the design and detailing rules for connections and joints, and design methodology and criteria for MRF's, CBF's and EBF's. In addition, several worked examples have been prepared covering the beam-to-column joint typologies investigated within the project;
- The technical and economic efficiency of dual-steel structures vs. conventional ones was finally evaluated.

The main contributions of the project can be summarised as follows:

- Principles and design recommendations for dual-steel frames (guidelines);
- The investigated frame typologies based on the dual-steel approach with composite columns, are solutions with a high innovative character in the European context; the dual-steel structures are not yet covered by the current code provisions (EN 1998-1 [1], EN 1993-1-8 [3], EN 1994-1 [4]); these configurations are to be taken into account within the further versions of the relevant Eurocodes;
- Characterisation in terms of global ductility and over-strength demands of dual-steel frames realised in simple and dual configuration;
- Modelling approach of members, such as braces, for non-linear analyses;
- Proposal of a series of innovative beam-to-column joint typologies with composite steel-concrete columns (i.e. PE, FE and CFT) for which the structural performance was confirmed by experimental and numerical investigations;
- Recommendations for weld details and appropriate component method design approaches.

Furthermore, the evaluation of the technical and economic efficiency of dual-steel structures vs. conventional ones showed that the use of high strength steel in non-dissipative members (columns of CBF & D-CBF, columns and braces of EBF & D-EBF) and connections represented an effective solution from the technical and economical point of view, leading therefore to cost reduction.

The outcomes of "HSS-SERF" project, have been disseminated through a large number of papers and presentations. In addition, the results obtained within "HSS-SERF" project have been presented and debated within the meetings of the technical committees TC10 (Structural Connections), TC11 (Composite Structures), and TC13 (Seismic Design), as well as within the framework of the following workshops:

- 7th International Workshop on Connections in Steel Structures 2012 – Connections VII, which took place between 30 May and 2 June, 2012, in Timisoara, Romania. The hosts were the Politehnica University and the Romanian Academy, under the supervision of ECCS and AISC.
- International Workshop on High Strength Steel in Seismic Resistant Structures, which took place between 28-29 June, 2013, in Naples, Italy, and was organised by the University of Naples "Federico II" and the Politehnica University of Timisoara (coordinator of the project), in cooperation with the Technical Committee TC13 (Seismic Design) of the European Convention of Constructional Steelwork.

1 Introduction

1.1 Background

Multi-storey frame structures of high strength steel members for seismic resistant building frames represent an innovation in seismic design in Europe. This type of structures in which mild carbon steel (MCS) is used in dissipative members while high strength steel (HSS) is used in non-dissipative "elastic" members, can be reliable and cost efficient.

A robust seismic resistant structure should be provided with balanced stiffness, strength and ductility among component members and connections. According to the dissipative design philosophy, such a structure will be able to dissipate a part of the energy induced by the ground motion, through plastic deformations in the dissipative zones of ductile members, e.g. beams in Moment Resisting Frames (MRF), links in Eccentrically Braced Frames (EBF), and braces in Concentrically Braced Frames (CBF). In order to avoid the premature collapse of the structure, development of plastic hinges in columns has to be prevented. To ensure such a scenario, in case of MRF's, for instance, the strong column-weak beam (SC-WB) concept applies, which in fact means to provide enough over-strength of the column with respect to adjoining beams.

In order to get an economic design of a structure, dissipative elements have to approach their plastic capacity under design forces, in order to reduce the demand on non-dissipative members (over-strength should be limited). The best way to accomplish this is not to reduce the cross-section of dissipative members and to increase the size of non-dissipative ones, but to use instead Mild Carbon Steel and High Strength Steel. To compensate for the loss of stiffness – important in MRF's of HSS columns, inherent due to reduction in steel cross-section, and to increase their axial compression strength – important in case of CBF and EBF typologies, and also to enhance fire resistance, the columns can be realized in composite solution.

Based on this conceptual framework, the purpose of "HSS-SERF" project was to investigate the seismic performance of dual-steel building frames, in order to evaluate the effectiveness of such solutions, compared with current homogeneous steel concept. Dual-steel structures enable to fulfil by design the three critical tasks of a robust structure: (i) to secure plastic deformation capacity in structural members, targeted as dissipative, which are key members in any seismic-resistant structure; (ii) to prepare multiple routes for transfer of forces and ensure their redistribution through yielding of other members; (iii) to provide sufficient over-strength to structural members that cannot be allowed to collapse at any cost. In dual-steel structures, the role of lower-yield steel is to work like a fuse, dissipating the seismic energy through plastic deformations, while the rest of the structure remains elastic or undamaged. To achieve these global performance targets, a proper detailing is compulsory, mainly for beam to column joints, in which by conception and sizing, a good balance between dissipative and non-dissipative components is needed.

1.2 Objectives of the research project

The aim of the project was to investigate and evaluate the seismic performance of dual-steel building frames, realised from two different steel grades: mild carbon steel (MCS) and high strength steel (HSS). The main objectives of "HSS-SERF" research project can be summarized as follows:

- To find reliable structural typologies (e.g. moment-resisting frames, concentrically braced frames, eccentrically braced frames) and connection detailing for dual-steel building frames, and to validate them by tests and advanced numerical simulations;
- To develop design criteria and performance based design methodology for dual-steel structures using HSS;
- To recommend relevant design parameters (i.e. behaviour factor q , over-strength factor Ω) to be implemented in further versions of the seismic design code (EN 1998-1 [1]) in order to apply capacity design approach for dual-steel framing typologies;
- To evaluate technical and economic benefit of dual-steel approach involving HSS;

1.3 Description of activities and discussion / Work-plan and Project Structure

The main research activities of the project were divided into several working packages. The general flow-chart of research is illustrated in Figure 1.1.

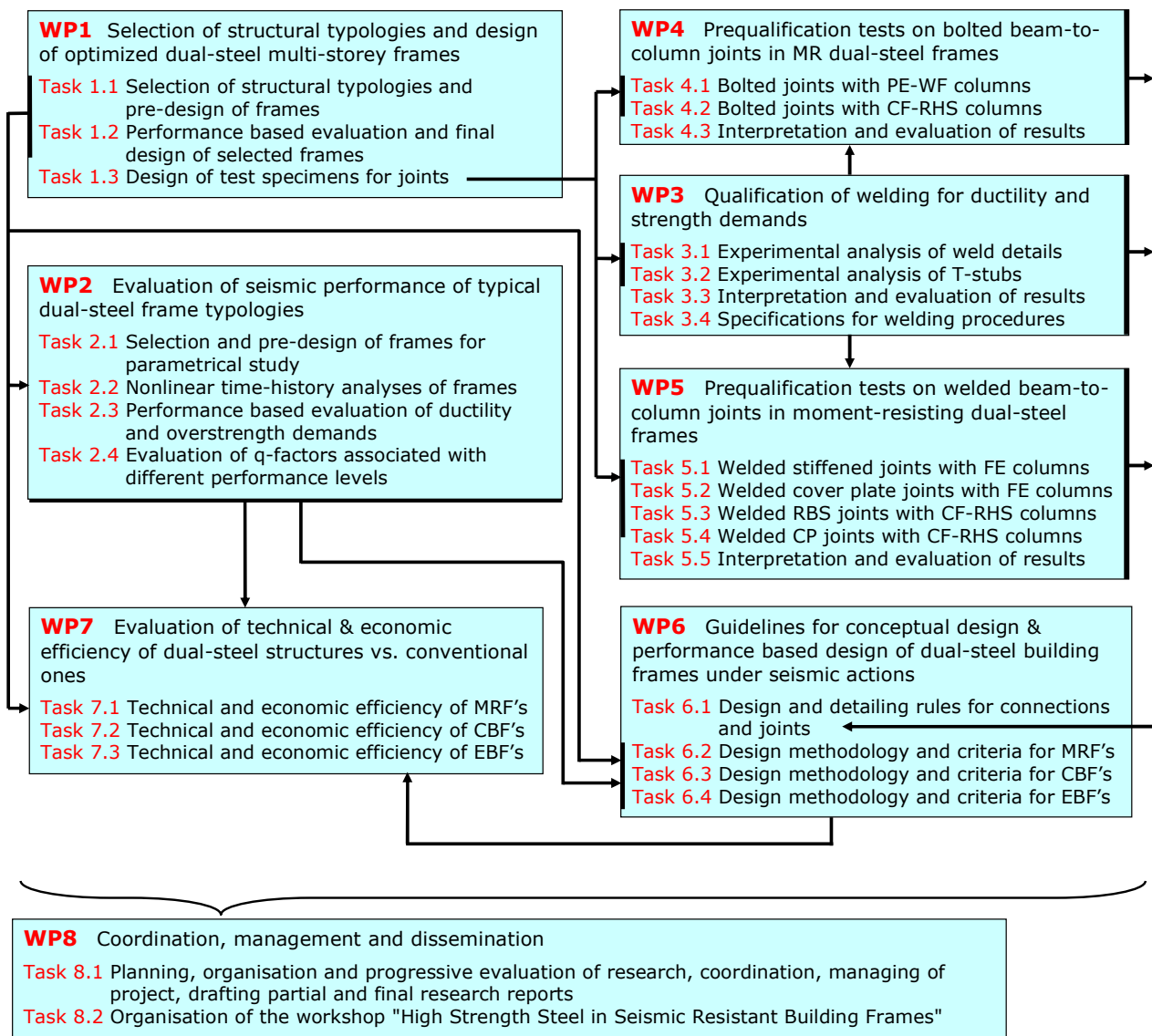


Figure 1.1. General flow chart of research

The selection of structural typologies and design of optimised dual-steel multi-storey frames were covered by Work Package 1. The main tasks were related to: selection of structural typologies and pre-design of frames, performance based evaluation and final design of selected frames based on pushover analysis, and design of test specimens for joints.

The evaluation of seismic performance of typical dual-steel frame typologies was performed in Work Package 2, with the following main tasks: selection and pre-design of frames for parametrical study, nonlinear time-history analyses of frames, performance based evaluation of ductility and over-strength demands, and evaluation of q-factors associated with different performance levels.

The qualification of welding for ductility and strength demands was accomplished as part of Work Package 3. The main tasks were related to: experimental analysis of welded details and T-stubs, interpretation and evaluation of results, and specifications for welding procedures to apply in fabrication of joint specimens.

Work Package 4 covered the tests on bolted beam-to-column joints in moment-resisting dual-steel frames. The main tasks were related to: tests on bolted beam-to-column joints with partially-encased wide-flange (PE-WF) columns, tests on bolted beam-to-column joints with concrete-filled rectangular hollow section (CF-RHS) columns, and interpretation and evaluation of results.

Work Package 5 covered the tests on welded beam-to-column joints in moment-resisting dual-steel frames. The main tasks were related to: tests on welded stiffened and welded cover plate beam-to-column joints with fully-encased wide-flange (FE-WF) columns, tests on welded reduced beam section and welded cover plate beam-to-column joints with concrete filled rectangular hollow section (CF-RHS) columns, and interpretation and evaluation of results.

The development of guidelines for conceptual design and performance based design (PBD) of dual-steel building frames under seismic actions was realised within Work Package 6. The main tasks were related to: design and detailing rules for connections and joints, and design methodology and

criteria for moment-resisting frames, concentrically braced frames, and eccentrically braced frames.

Work Package 7 was related to the evaluation of technical and economic efficiency of dual-steel structures vs. conventional ones.

The planning, coordination, progressive evaluation of the research and dissemination of results were realised within Work Package 8.

Considering the general flow-chart of research and the containing working packages (WP's), the final report of HSS-SERF project is structured considering the following outline:

1. Introduction
2. Design of dual-steel multi-storey frames
3. Seismic performance of dual-steel multi-storey frames
4. Experimental investigation of joint assemblies and components
5. Recommendations for seismic design and performance based evaluation of dual-steel structures
6. Technical and economic efficiency
7. Conclusions

Chapter 2 is related to the design of the frames within WP1 and WP2, and Chapter 3 presents the seismic performance of dual-steel multi-storey frames investigated in WP2. Chapter 4 covers the experimental investigations conducted on joint components (weld details and T-stubs) within WP3, and on joint assemblies (within WP4 and WP5). Chapter 5 is related to the Guidelines elaborated within WP6, and Chapter 6 is related to the technical and economic efficiency of dual-steel structures vs. conventional ones (WP7). The main conclusions of the research activities are presented in Chapter 7.

2 Design of dual-steel multi-storey frames

2.1 Introduction

The conceptual seismic design of the multi-storey frames and the design and detailing of the test specimens for joints make the subject of the current chapter. A total of 18 frames were designed within WP1, according to EN 1993-1-1 [6], EN 1994-1-1 [4] and EN 1998-1 [1], following the initial plan. The design of the frames allowed the identification of realistic member sizes for both mild carbon steel beams and high strength steel composite columns. Several practical solutions for bolted and welded beam-to-column joints were identified and designed.

The designed beam-to-column joint assemblies were investigated through experimental, numerical and analytical means as part of WP4 and WP5, and the results are presented in Chapter 4. As part of WP6, design procedures were developed for each joint typology, which are summarised in Chapter 5. Finally, Chapter 6 presents the outcomes of the technical and economic evaluation performed in WP7 for a number of 15 case study frames, as well as for a set of beam-to-column joint typologies, that were designed based on the configurations investigated in the project.

Furthermore, within WP2, a comprehensive parametric study was defined by selecting and designing a set of 120 frames representative for the design practice, extending the 18 frame configurations from WP1 to include standard braced frames (no dual action), two different building height ranges, and two span ranges. The design of the selected frames using current code provisions and a dual-steel composite solution was carried out.

2.2 Structural typologies for dual-steel frames

In order to evaluate the use of HSS in seismic resistant structures, five structural systems were selected (Figure 2.1):

- Moment-resisting Frames (MRF) – All beam-column joints were assumed as rigid and the column base were fixed on foundations (Figure 2.1-a).
- Concentrically Braced Frames (CBF) – Braces are inverted V-shape and are considered to be pinned in both joints. The beam-column joints in braced bay were assumed as rigid while the un-braced bays have pinned beam-to-column joints (Figure 2.1-b).
- Dual-Concentrically Braced Frames (D-CBF) – The dual-structures are characterized by contribution of two structural systems (CBF + MRF) to dissipate the seismic energy. In this case, one bay is composed by a concentrically braced system and adjacent bays are moment-resisting frames (MRF). All beam-to-column joints from the braced bays were assumed as rigid. Braces are inverted V-shape and are considered as pinned in both joints (Figure 2.1-b).
- Eccentrically Braced Frames (EBF) – The dissipative links are located in horizontal position. The beam-to-column joints are rigid for the braced bays, and respectively pinned for the adjacent non-braced bays. Braces are considered to be pinned at both ends (Figure 2.1-c).
- Dual-Eccentrically Braced Frames (D-EBF) – The dual-structures are characterized by contribution of two structural systems (EBF + MRF) to dissipate the seismic energy. One bay is composed by an eccentrically braced system and adjacent bays are moment-resisting frames (MRF). All beam ends from the braced bay are considered as rigid. The links are located in horizontal position. Braces are considered as pinned at both ends (Figure 2.1-d).

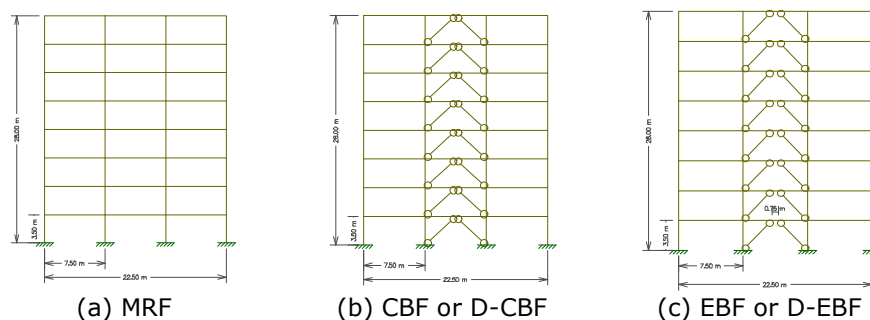


Figure 2.1. Structural configurations

2.3 Design of dual-steel multi-storey frames

The seismic design procedure described herein is strictly related to EN 1998-1 [1] adding one clause from ANSI/AISC 341-10 [7] code regarding to dual-structures. In detail, the frames with the combination of two structural systems (dual-structures) should be designed considering that the MRF system has minimum contribution of 25% with regard to the total lateral strength of the structures. The seismic design from European code is based on two requirements: no-collapse and damage limitation.

No-collapse requirement

The no-collapse requirement corresponds to seismic action with a return period of 475 years. The aim is to guarantee that the structures suffer severe damage in structural member. However, there is no local or global collapse ensuring the safety of people. The structure should be stable under the design seismic action. In addition, EN 1998-1 [1] requires that the structures should have on all joints a ratio for which the design capacity of the columns should be higher than the sum of the design capacity of the beams, see the following expression:

$$\Sigma M_{RC} \geq 1.3 \cdot \Sigma M_{RB} \quad (2.1)$$

being, M_{RC} the sum of design plastic moment capacity of columns in the joint; M_{RB} correspond to the sum of design plastic moment capacity of beam in the joint;

Damage limitation requirement

The damage limitation requirement is related to the criteria corresponding to the deformation capacity. In this case, it is used as a criterion for the inter-storey drift deformation. The following expression is applied in order to verify the inter-storey drifts limits:

$$d_r \cdot v \leq \beta \cdot h \quad (2.2)$$

where, d_r is the design inter-storey drift being obtained through seismic analyses multiplied by the employed behaviour factor; h is the storey height; v is a reduction factor which depends of the importance class of the building (EN 1998-1 [1] recommends a value of 0.4 for the importance classes III and IV, and respectively 0.5 for classes I and II); β is related to non-structural element (within the project, a value of 0.075 was utilized corresponding to buildings with ductile non-structural elements);

2.3.1 General assumption for the study cases

In order to define the study cases, some assumptions are considered as follows:

- The MRF's are assumed to be located in a region of moderate seismicity with peak ground acceleration (a_g) in amount of 0.24g and 0.16g, corresponding to Stiff and respectively Soft Soil. The braced frames are located in region with high seismicity with peak ground acceleration of 0.32g for both soil types;
- The behaviour factors were assumed as 2.5 and 4.8 for the CBF's and D-CBF's. The EBF's and D-EBF's were calculated considering the behaviour factors equal to 6.0 for both configurations. For MRF's a behaviour factor of 4.0 was assumed;
- The floor mass of each frame was calculated considering $G_k = 4.0 \text{ kN/m}^2$, and $Q_k = 3.0 \text{ kN/m}^2$;
- The frames were assumed to be retrieved from regular buildings with a side that is much wider than the other one and also is assumed that the analysed frame is effectively braced in the out-of-plane direction. Floors are composed by orthogonal steel beams (primary and secondary) and columns from composite steel-concrete cross-sections. Primary beams are taken as braced for out-of-plane buckling in order to obtain their full resistance in bending and greater resistance in axial compression;
- The floor mesh is regular and orthogonal with columns spacing $L \times L$. Values of L may be 5.0 m (not for 16 storey frames) or 7.5 m. Moreover, in all frames, the first storey is 4.0 m high and the rest are 3.5 m high.

2.3.2 Study cases

Hence, a parametrical study was carried out in order to evaluate the benefits of dual-steel concept on the performance based seismic design of five structural typologies compliant to both EN 1998-1 [1] and ANSI/AISC 341-10 [7]. Therefore, a total of 120 frames were selected and designed varying the following parameters:

- Span length – two span ranges were studied (5.0 m and 7.5 m);
- Storey number – for MRF's, a number of 4 and 8 storeys were considered. In contrast, 8 and 16 storeys were considered for braced frames;
- Type of composite column cross-section – three types of composite columns were used in the structures (see Figure 2.2), i.e.: Fully Encased Wide Flange (FE-WF) columns, Partially Encased Wide Flange (PE-WF) columns, and Concrete Filled Tube (CFT) columns;

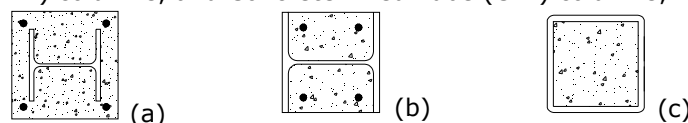


Figure 2.2. Types of composite columns: (a) FE-WF, (b) PE-WF, (c) CFT

- Soil conditions – two types of soil conditions have been examined (see Figure 2.3). The former representative of soil type C according to EN 1998-1 [1] (Stiff Soil), and the latter representative of very soft soil conditions with corner period of $T_c = 1.6 \text{ s}$, which are representative of specific soil condition in Bucharest (Soft Soil);

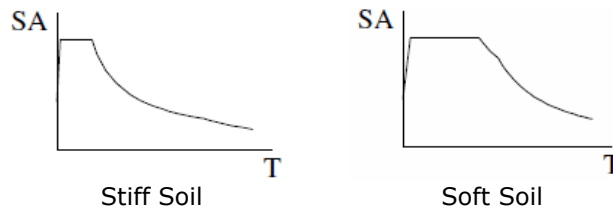


Figure 2.3. Types of soil conditions

- Steel grade for non-dissipative members – two steel grades were investigated in this project for the non-dissipative members, i.e. S460 and S690. All the dissipative members were designed considering an S355 steel grade.

Figure 2.4 shows the distribution of the 120 study cases. For each of the five structural configurations, a number of 24 frames were designed in accordance with current codes. In particular, MRF's were designed only for S460 and different storey number in comparison with braced frames, 4 and 8 storeys. In braced frames, a higher steel grade (S690) for non-dissipative members and higher number of stories (16) were also considered.

Storeys	Soil type	Span							
		5.00m			7.50m				
		Column		Column		Column			
		FE	PE	CFT	FE	PE	CFT		
		H	S	H	S	H	S		
4	S460								
8									

(a) Moment-Resisting Frames

Storeys	Soil type	Span							
		5.00m			7.50m				
		Column		Column		Column			
		FE	PE	CFT	FE	PE	CFT		
		H	S	H	S	H	S		
8	S460								
	S690								
16	S460								
	S690*								

(b) Braced Frames (CBF, D-CBF, EBF and D-EBF)

Figure 2.4. Definition of parametric study

Legend:

- H – Stiff soil
- S – Soft Soil
- FE – Fully Encased Column
- PE – Partially Encased Column
- CFT – Concrete Filled Tube

2.3.3 Structural analysis

The analysis was carried out with the finite element commercial software Autodesk Robot Structural Analysis Professional 2010 [8]. The analyses were carried out considering the linear type of analysis. In seismic design, modal response spectrum analyses were performed, according to EN 1998-1 [1] (clause 4.3.3.3). The responses of all modes of vibration with a significant contribution to the global response were taken into account.

All frames were modelled with 6 degree of freedom beam finite elements, in a 2D analysis. The finite elements mesh was refined until good convergence was obtained. Elements that are hot rolled steel profiles, such as beams and braces, were defined in the software using built-in databases. Cross-section characteristics of welded steel profiles and composite columns were calculated according EN 1994-1-1 [4] and EN 1998-1 [1] and directly input in the software.

2.3.4 Design criteria for Moment Resisting Frames

In order to obtain ductile plastic hinges in the beams, a set of rules for the dissipative and non-dissipative members were employed. The aim was to have beams where the full plastic moment resistance and rotation is not reduced due to axial and shear forces. Therefore, the applied moment (M_{Ed}) should not exceed the design plastic moment capacity of the beam ($M_{pl,Rd}$). On the other hand, the axial force (N_{Ed}) should not be higher than 15% of the plastic resistance ($N_{pl,Rd}$). For the shear force, the capacity design establishes that the section should not exceed 50% of the design plastic shear resistance ($V_{pl,Rd}$). In addition, the shear force (V_{Ed}) is obtained by the sum of the shear forces due to the gravity and moment components on the beam ($V_{Ed}=V_{Ed,G}+V_{Ed,M}$), respectively. The following expressions summarize these requirements:

$$\frac{M_{Ed}}{M_{pl,Rd}} \leq 1.0 \qquad \frac{V_{Ed}}{V_{pl,Rd}} \leq 1.0 \qquad \frac{N_{Ed}}{N_{pl,Rd}} \leq 0.15 \qquad (2.3)$$

Concerning the non-dissipative members (columns), the resistance capacity is given by unfavourable combination of bending moments, axial or shear forces:

$$X_{Rd} \geq X_{Ed,G} + 1.1 \cdot \gamma_{ov} \cdot \Omega \cdot X_{Ed,E} \quad (2.4)$$

where, X represents any member force – axial (N), shear (V) or bending moment (M); the indexes, “ $_{Ed,G}$ ” and “ $_{Ed,E}$ ”, correspond to seismic design situation for the gravity loads and lateral earthquake forces, respectively; in addition, the design axial forces on the columns should not exceed 30% of resistance capacity; Ω is the minimum overstrength in the connected beams defined as:

$$\Omega_i = \frac{M_{pl,Rd}}{M_{Ed,i}} \quad (2.5)$$

2.3.5 Design criteria for (Dual) Concentrically Braced Frames

In Concentrically V-inverted Braced Frames, the braces in tension and compression are considered to be the main ductile members. The yielding/buckling of braces should occur before yielding or buckling of beams or columns. Therefore, the braces are designed considering the seismic action for the design earthquake applying the requirements of EN 1993-1-1 [6] or EN 1994-1-1 [4], i.e., the yield or compression resistance of diagonals should be higher than the design axial force ($N_{pl,Rd}$ or $N_{b,Rd} > N_{Ed}$). Furthermore, the non-dimensional slenderness plays an important role in the behaviour of concentrically braced frames. Hence, EN 1998-1 [1] imposes a limit in which the concentrically braced frames in V should have braces with maximum non-slenderness of 2.0. The non-dissipative elements (beams and columns) are designed to resist the following condition:

$$N_{pl,Rd}(M_{Ed}) \geq N_{Ed,G} + 1.1 \cdot \gamma_{ov} \cdot \Omega \cdot N_{Ed,E} \quad (2.6)$$

where $N_{pl,Rd}(M_{Ed})$ is the design resistance of the beam or column taking account the influence of bending moment, $N_{Ed,G}$ and $N_{Ed,E}$ are the axial force in non-dissipative element to seismic design situation for the gravity loads and lateral earthquake forces, respectively. The Ω factor is the minimum overstrength corresponding to following ratio from diagonal members:

$$\Omega_i = \frac{N_{pl,Rd,i}}{N_{Ed,i}} \quad (2.7)$$

In order to obtain a homogenous distribution of ductility, EN 1998-1 [1] determines that the difference between the maximum and minimum value for Ω factor should not be more than 25%.

The beam from braced bays need to be designed for gravity loading without considering the intermediate support due to presence of braces, as well as account for a unbalanced vertical action due to brace buckling. According to EN 1998-1 [1], the post-buckling resistance should be considered as 30% of the yield resistance.

The Dual Concentrically Braced Frames combine the MRF and CBF systems. There is no information about the design of this structural system in EN 1998-1 [1]. Therefore, the ANSI/AISC 341-10 [7] was used for the design of the dual-system. According to this code, it is necessary to guarantee that the MRF system has a minimum lateral strength equal to 25%. The following expression was used to determine the lateral strength of MRF part:

$$V_{Rd,i}^{MRF} \geq 0.25 \cdot V_{Rd,i}^{DUAL} \rightarrow V_{Rd,i}^{DUAL} = \frac{1}{0.75} \cdot V_{Rd,i}^{CBF} = \frac{1}{0.75} \cdot (N_{pl}^+ + 0.3 \cdot N_{pl}^-)_i \cdot \cos \alpha_i \quad (2.8)$$

where, $V_{Rd,i}$ is the base shear resistance at the i-th storey, N_{pl} is the plastic axial resistance of the brace in tension⁽⁺⁾ or in compression⁽⁻⁾ and α is the angle that the braces make with the horizontal direction;

The members belonging to MRF part are designed in accordance with MRF requirements while the structural members from CBF part are designed considering the CBF rules. It is important to note that two values for the Ω factor can be calculated: (i) for MRF beams, (ii) for CBF braces.

2.3.6 Design criteria for (Dual) Eccentrically Braced Frames

The Eccentrically Braced Frames are designed in order that the links are able to dissipate the seismic energy through of plastic bending or shear mechanism. The links are classified into 3 categories: short links, long links or intermediate links. In this project, only short links were used due to their superior behaviour, in comparison with another links, related to their yield primarily in shear. Therefore, the links have to be checked for the following conditions:

$$\text{Short link if: } e \leq e_s = 1.6 \cdot \frac{M_{p,link}}{V_{p,link}} \quad \text{For } R < 0.30 \quad (2.9)$$

$$e \leq e_s = (1.15 - 0.5 \cdot R) \cdot 1.6 \cdot \frac{M_{p,link}}{V_{p,link}} \quad \text{For } R \geq 0.30 \quad (2.10)$$

$$\text{where: } R = N_{Ed} \cdot t_w \cdot (h - 2 \cdot t_f) / (V_{Ed} \cdot A) \quad (2.11)$$

$$V_{p,link} = f_y \cdot t_w \cdot (h - t_f) / \sqrt{3} \quad (2.12)$$

$$M_{p,link} = f_y \cdot b \cdot t_f \cdot (h - t_f) \quad (2.13)$$

being, $M_{p,link}$ and $V_{p,link}$ the plastic moment and plastic shear capacities of links, respectively; the letters: h , t_w , t_f , b and A are geometrical properties, and f_y is the nominal yield strength of the link;

The above expressions are applied to the cases where the axial force does not exceed 15% of the plastic capacity of the cross-section. Unless this happens, it is necessary to use reduced expressions for the moment and shear plastic capacities. Furthermore, the EN 1998-1 [1] determines limits of rotation for the links. For the short links, it is expected a maximum rotation capacity equal to 0.08 radians. On the other hand, the elements that do not contain links should be provided with sufficient overstrength. Therefore, these structural elements should be designed for un-favourable combination of the axial force and bending moments:

$$N_{pl,Rd}(M_{Ed}, V_{Ed}) \geq N_{Ed,G} + 1.1 \cdot \gamma_{ov} \cdot \Omega \cdot N_{Ed,E} \quad (2.14)$$

where $N_{pl,Rd}(M_{Ed}, V_{Ed})$ is the axial design resistance of the column or diagonal member taking account the influence of bending moment and shear, $N_{Ed,G}$ and $N_{Ed,E}$ are the axial force in non-dissipative element to seismic design situation for the gravity loads and lateral earthquakes forces, respectively. The Ω factor is the minimum overstrength in the connected beams defined as:

$$\Omega_i = 1.5 \cdot \frac{V_{p,link,i}}{V_{Ed,i}} \quad (2.15)$$

In order to obtain a homogenous distribution of ductility, EN 1998-1 [1] determines that the difference between the maximum and minimum value for Ω factor should not be more than 25%.

The Dual Eccentrically Braced Frames combine the MRF and EBF systems. There is no information about the design of this structural system in EN 1998-1 [1]. Therefore, the ANSI/AISC 341-10 [7] was used for the design of the dual-system. According to this code, it is necessary to guarantee that the MRF system has a minimum lateral strength equal to 25%. The following expression was used to determine the lateral strength of MRF part:

$$V_{Rd,i}^{MRF} \geq 0.25 \cdot V_{Rd,i}^{DUAL} \rightarrow V_{Rd,i}^{DUAL} = \frac{1}{0.75} \cdot V_{Rd,i}^{EBF} = \frac{1}{0.75} \cdot V_{p,link,i} \quad (2.16)$$

where $V_{Rd,i}$ is the base shear resistance at the i -th storey, $V_{p,link,i}$ is the plastic shear resistance of the link;

The members belonging to MRF part are designed in accordance with MRF requirements while the structural members from EBF part are designed considering the EBF rules. Again, two values for the Ω factor can be calculated, one related to MRF and another related to EBF.

2.3.7 Design results

The results related to the design of the 120 case study frames are presented in detail within the content of Deliverable D2 – "Report on seismic performance of dual-steel structures and evaluation of q-factors associated with different performance levels" [9].

2.4 Design of beam-to-column joint assemblies

2.4.1 Definition of the experimental program on beam-to-column joint specimens

The design of 18 dual-steel frame configurations was performed as part of WP1. The particular frame typologies covered moment resisting frames (MRF), dual concentrically braced frames (D-CBF) and dual eccentrically braced frames (D-EBF). Table 2.1 makes an overview of the frame configurations considering the number of storeys, column cross-section and column steel grade.

The design of the dual structural typologies (D-CBF & D-EBF) was governed by the strength of the members, while in the case of the MRF's the governing design criteria was related to the inter-storey drift limitation. With these considerations, but taking into account also aspects related to the steel quantity and testing capacity constraints, the members for the beam-to-column joint specimens were chosen from the dual concentrically braced frames D-CBF (see Figure 2.5). As a result, the design of the frames allowed the identification of realistic member sizes for both mild carbon steel beams and high strength steel composite columns. In addition, several practical solutions for bolted and welded beam-to-column joints were identified and designed, as further presented.

Table 2.1 – Frame configurations for preliminary design in WP1

Frame type		MRF – 8 storeys			D-CBF – 8 storeys			D-EBF – 8 storeys		
Column type										
Column steel grade	S355	1.1.1	1.2.1	-	-	-	-	-	-	-
	S460	1.1.2	1.2.2	-	2.1.2	2.2.2	2.3.2	3.1.2	3.2.2	3.3.2
	S690/S700	1.1.3	1.2.3	-	2.1.3	2.2.3	2.3.3	3.1.3	3.2.3	3.3.3

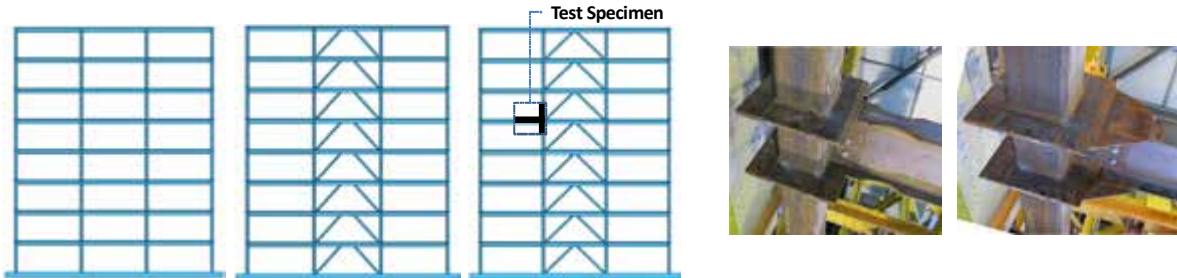


Figure 2.5. Design of dual-steel multi-storey frames (MRF, D-EBF, D-CBF), choice of members (beams, columns) and design of beam-to-column joint specimens

In case of the full-strength / full-rigid bolted beam-to-column joints, the columns were considered as PE-WF and CF-RHS. Different joint configurations were studied by the University of Liege, before suitable ones were found for the two column types. Finally, three kinds of joint specimens (see Figure 2.6) were considered: (a) partially encased wide flange column with reinforced end-plate connection; (b) concrete filled tube column with reinforced end-plate connection; (c) concrete filled tube column with end-plate connection and long bolts. Two particular joints were designed for each configuration, using two different steel grades for the column (S460 & S690).

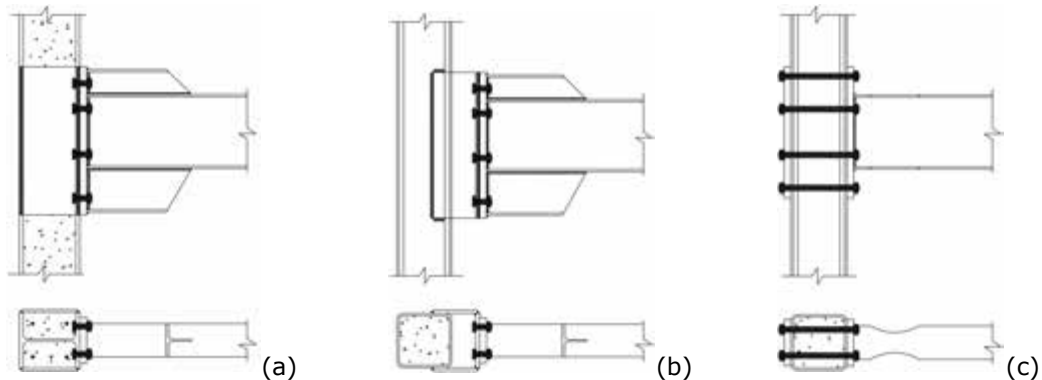


Figure 2.6. Bolted beam-to-column joint configurations (Univ. of Liege)

The welded beam-to-column joint typologies were analysed and tested at both University of Ljubljana and Politehnica University of Timisoara. The particular configuration of the joints studied at University of Ljubljana was characterised by full encased wide flange columns and welded connection with rib stiffeners and respectively cover plates (Figure 2.7-a-b). The beam-to-column joints investigated at the Politehnica University of Timisoara (Figure 2.7-c-d), were characterised by concrete filled tube columns and welded connections with reduced beam section and respectively cover plates.

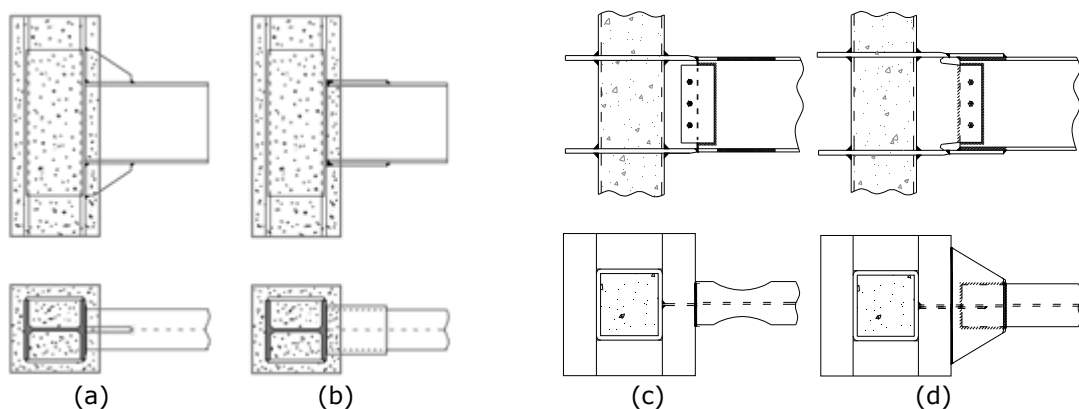


Figure 2.7. Welded beam-to-column joint configurations: (a) rib stiffener and (b) cover plate joints with FE-WF columns, (c) reduced beam section and (d) cover plate joints with CF-RHS columns

The outcome of this investigation was represented by design specifications and production drawings for experimental specimens: welded details and T-stubs for WP3, and beam-to-column joints for WP4 and WP5. Deliverable D1 – “Design specifications and drawings of joint specimens” [10] was prepared and contains the complete information (geometrical characteristics, material properties, preparation and welding details) in relation to the designed beam-to-column joint configurations, column stubs for load introduction tests, as well as cruciform joints and T-stubs. A brief description of the design and detailing of the beam-to-column joint specimens is further presented in Section 2.4.2.

2.4.2 Design and detailing of bolted and welded beam-to-column joint specimens

2.4.2.1 Design of bolted joints with PE-WF & CFT columns

The considered columns are partially-encased wide-flange H-columns and concrete-filled rectangular hollow-section RHS-columns. Three kinds of joint specimens were designed: one configuration for H columns and two configurations for RHS columns. Two particular joints were designed for each of these configurations using two different steel grades for the column (S460 and S690).

The “joint configuration 1” is related to an H column and is represented in Figure 2.8-a. Lateral plates are welded from one flange to the other on both sides of the column at the joint level and act as reinforcement for the following components: the column panel in shear, the column flange in bending, the column web in tension and the column web in compression. Hammer-heads are used to increase the lever arm between the compression and tension forces within the joint and to reinforce the end-plate in bending. The hammer-heads are extracted from the beam profile. Joints were designed with this configuration for the two cases summarised in Table 2.2. Additional information related to the detailing rules and the design procedure of the joint configuration are presented in Section 5.3.3, while the designed joint specimens are presented in Deliverable D4 [11].

Table 2.2 – Cross-section of members for “joint configuration 1”

Case 1	Beam:	IPE 400, S355
	Column:	HEB 320 (rolled profile), S460, concrete C30/37
Case 2	Beam:	IPE 400, S355
	Column:	“HEB 260” – welded plates ($t_{fc}=20$ mm, $t_{wc}=10$ mm, fillet welds: $a=8$ mm), S690, concrete C30/37

The “joint configuration 2” is related to a CFT column and is represented in Figure 2.8-b. The beam is fixed to the column using a U-shaped piece welded to the RHS column side walls. The bolted connection between the beam end-plate and the U front face is similar to the one proposed in “joint configuration 1” and hammer-heads are extracted from the beam profile. Joints were designed with this configuration for the two cases summarised in Table 2.3. Although the test specimens are single-sided, the design of both joint configuration 1 and 2 was first made considering double-sided joint configurations loaded with unbalanced moments ($\beta = 2$), which corresponds to the actual situation under seismic actions in moment-resisting frames. The design of the test specimens was also checked under the experimental conditions. Additional information related to the detailing rules and the design procedure of the joint configuration are presented in Section 5.3.4, while the designed joint specimens are presented in Deliverable D4 [11].

Table 2.3 – Cross-section of members for “joint configuration 2”

Case 1	Beam:	IPE 400, S355
	Column:	RHS 300x300x12,5, S460, concrete C30/37
Case 2	Beam:	IPE 400, S355
	Column:	RHS 250x250x10, S700, concrete C30/37

The “joint configuration 3” is also related to a CFT column and is represented in Figure 2.8-c. The connection is realised with long bolts passing through the tubular column. For this configuration it appeared that the tubular column, the walls of which are rather thin, cannot resist the double transverse compression force developed in case of $\beta = 2$ (due to “double compression effect”), even with a dog-bone in the beam. Consequently, it was decided to design these joints considering single-sided configurations ($\beta = 1$), which would correspond to a column at an extremity of a frame. Besides, for a double-sided joint involving a column which is adjacent to the brace in a dual concentrically or eccentrically braced frame, a plastic hinge will form at only one side under seismic circumstances while the moment at the other side will remain quite small. Joints were designed with this configuration for the two cases summarised in Table 2.4. Additional information related to the detailing rules and the design procedure of the joint configuration are presented in Section 5.3.5, while the designed joint specimens are presented in Deliverable D4 [11].

Table 2.4 – Cross-section of members for “joint configuration 3”

Case 1	Beam:	IPE 400, S355
	Column:	RHS 300x300x12,5, S460, concrete C30/37
Case 2	Beam:	IPE 400, S355
	Column:	RHS 250x250x10, S700, concrete C30/37

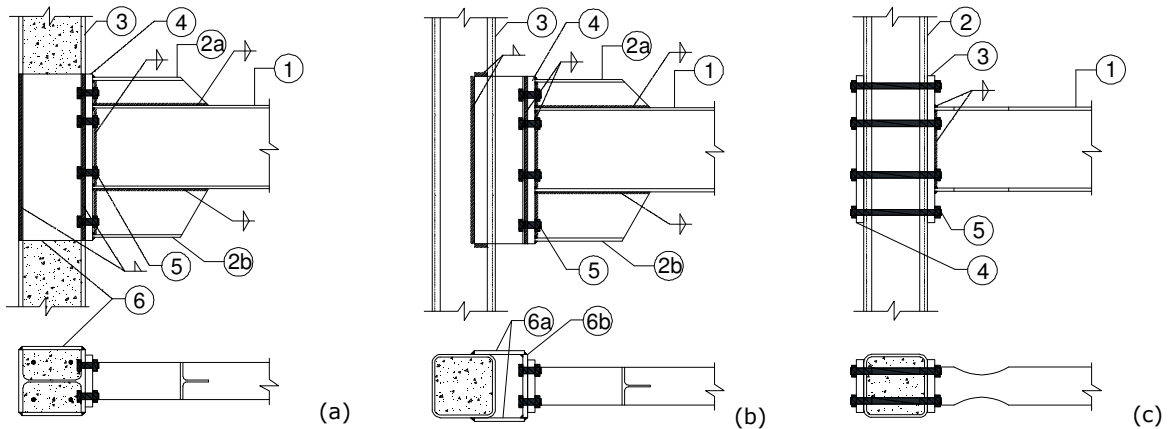


Figure 2.8. Bolted beam-to-column joints: (a) “joint configuration 1”, (b) “joint configuration 2”, (c) “joint configuration 3”

2.4.2.2 Design of welded joints with FE-WF columns

Two types of joints were considered: welded rib-stiffened joints (see Figure 2.7-a) and cover-plated joints (see Figure 2.7-b). The test specimens are one-sided beam-to-column joints simulating an exterior beam-to-column joint in moment resisting frame (MRF) or inner joint in dual braced frame. Especially in the latter case, the axial force level in column can be of significant value. Consequently, besides transverse force applied at the free end of the beam, compression axial force is provided at the top of the column as additional parameter of the study (see Section 4.4.2). The final composite column cross-section characteristics of the test specimens were designed in a way that a high level of ratio axial load – to – design plastic resistance (in compression) can be achieved during the test. Each of the two joint typologies was designed for the two cases summarised in Table 2.5.

Table 2.5 – Cross-section of members for welded joints with FE-WF columns

Case 1	Beam:	IPE 270, S355
	Column:	HEB 200, S460, concrete C30/37
Case 2	Beam:	IPE 240, S355
	Column:	HEB 160, S690, concrete C30/37

Rib stiffened joint: Two types of rib-stiffened moment connection typologies were observed: with single and dual tapered rib plates welded to the top and bottom beam flanges, see Figure 2.9-a-b. As no substantial advantage was gained with dual rib configuration in comparison with the single rib type, bearing in mind also the practical aspect that the first one is labour intensive and costly, the single rib type configuration was chosen, hereinafter referred to as rib-stiffened (RS) joint.

The geometry of the rib stiffener was determined taking into account the approach of seismic design of rib-reinforced moment connections according to Lee [12]. The following assumptions for preliminary rib sizing were used: rib height $b \approx h_b/3$; rib diagonal angle $\theta \approx 35^\circ$; rib length $a = b/\tan(\theta)$, and trimmed length $c = 25 \text{ mm}$, Figure 2.10-a. Rib thickness was determined by applying the design criterion that stiffened connection at the column face remains nominally elastic under maximum moment developed by the connected beam. Rib thickness ($t = 15 \text{ mm}$) met the applied design requirement for both designed RS joint specimens presented hereinafter. Fillet welds were used to join all the components together, including complete beam-column connection. In the latter case full-strength peripheral fillet weld was made all around the beam cross-section before attaching both rib plates. Throat thickness of fillet welds joining rib to the beam and column flange were designed to develop at least the yield strength of the rib. Additional information related to the detailing rules and the design procedure of the joint configuration are presented in Section 5.3.6, while the designed joint specimens are presented in Deliverable D5 [13].

Cover-plate joint: Two reinforcing plate geometries, rectangular and trapezoidal, and two fillet weld arrangements, two-sided and three-sided, adopted from [14], [15] and [16], were studied, see Figure 2.9-c-d. There was almost no difference in the global response of the joint using different reinforcing plates and weld geometries. However, comparison of local responses showed that the rectangular plate and the use of three-sided fillet weld arrangement are superior to both the trapezoidal plate and the use of only two longitudinal fillet welds. Therefore, configuration with

rectangular plate and three-sided fillet weld arrangement was chosen, hereinafter referred to as cover plate (CP) joint.

The length of the cover plate was chosen to permit the placement of sufficiently long fillet welds to develop at least the yield strength of the cover plate. The final length of reinforcing plates was chosen to be three quarters of the beam height. Complete joint penetration single-bevel butt weld was used to join the combined thickness of a cover plate and beam flange to the column flange, see Figure 2.10-b. No permanent backing bar was used, since its presence may be undesirable under fatigue conditions [17]. Butt weld was completed by depositing a sealing run on the back of the joint using fillet weld, which continued over the root radius of a beam section to the web connection. The complete solution, taking into account the robustness of elastic design, does not require the use of weld access holes. Additional information related to the detailing rules and the design procedure of the joint configuration are presented in Section 5.3.6, while the designed joint specimens are presented in Deliverable D5 [13].

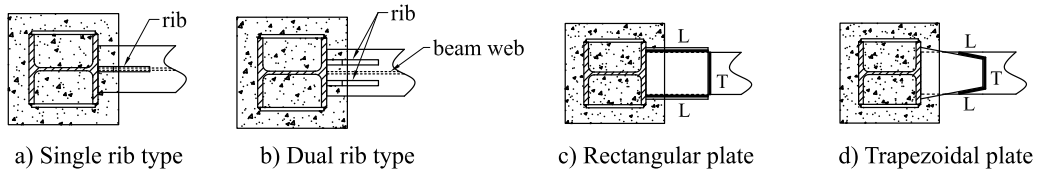


Figure 2.9. Rib- and cover plate- stiffened connection configurations studied

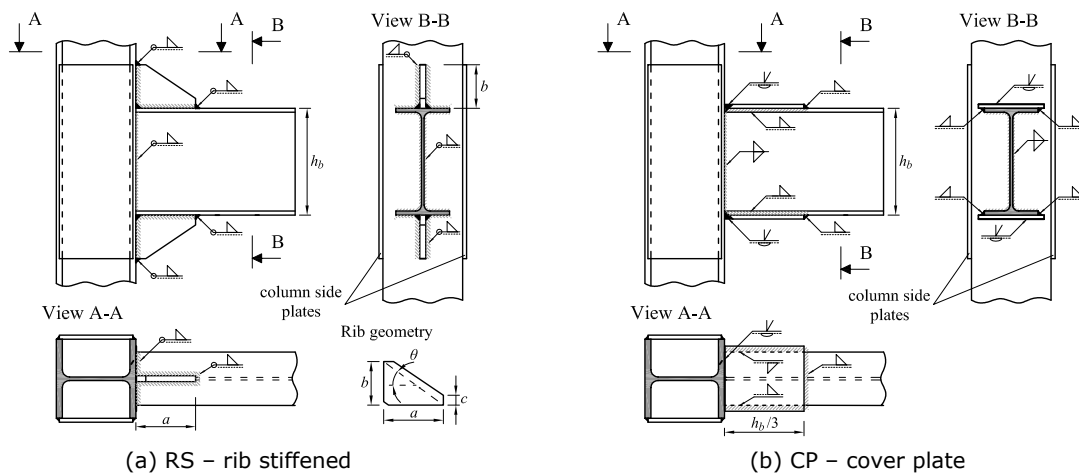


Figure 2.10. Welded RS and CP beam-to-column joint details (concrete encasement is not illustrated)

2.4.2.3 Design of welded joints with CFT columns

Two types of joints were considered: welded reduced beam section (RBS) joints (see Figure 2.7-c) and welded cover plate (CP) joints (see Figure 2.7-d). The test specimens are one-sided beam-to-column joints simulating an exterior beam-to-column joint in moment resisting frame (MRF) or inner joint in dual braced frame. Each joint configuration was designed for the two cases summarised in Table 2.6.

Case 1:	Beam:	IPE 400, S355
	Column:	RHS 300x12.5, S460, concrete C30/37
Case 2:	Beam:	IPE 400, S355
	Column:	RHS 250x10, S700, concrete C30/37

Reduced beam section joint configuration: The joint connects a wide-flange hot rolled beam with a concrete filled tube (CFT) column using field welding (see Figure 2.11). A reduced beam section is used in order to alleviate stresses in the beam-column connection and control the location of the plastic hinge. An external diaphragm is shop-welded to the column in order to transfer the forces from beam to the side walls of the column. Beam flanges are welded to the external diaphragm using full-penetration butt welds, for which the preparation details are shown in Figure 2.11. A shear tab bolted connection between the beam web and vertical column stiffener was considered for erection only. The final connection of the beam web is realized as full-penetration weld, using the shear tab as backing plate. The design of the reduced beam section was done based on provisions from AISC 358-05 [18]. Additional information related to the detailing rules and the design procedure of the joint configuration are presented in Section 5.3.7, while the designed joint specimens are presented in Deliverable D5 [13].

Cover plate joint configuration: The joint connects a wide-flange hot rolled beam with a concrete filled tube (CFT) column using field welding (see Figure 2.12). An external diaphragm is shop-welded to the column in order to reduce the out-of plane bending of the column walls. Cover plates are used in order to reinforce the beam-column connection, forcing the plastic hinge to form in the beam. The cover plates are welded to the external diaphragm using full-penetration butt welds. The preparation details shown in Figure 2.12 are based on the weld access hole details recommended in FEMA-350 [19]. A bolted connection between the beam web and vertical column stiffener was considered for erection only. The final connection of the beam web is realized using fillet welds. Additional information related to the detailing rules and the design procedure of the joint configuration are presented in Section 5.3.7, while the designed joint specimens are presented in Deliverable D5 [13].

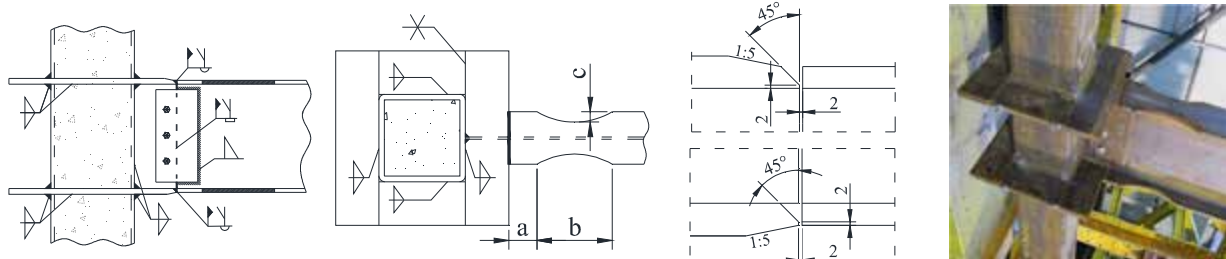


Figure 2.11. Welded RBS joint: configuration & preparation details for full penetration welds

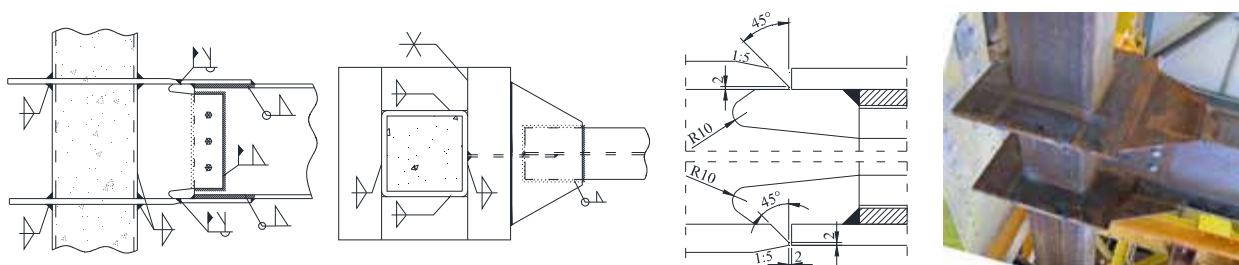


Figure 2.12. Welded beam-to-column joint with cover plates: joint configuration and preparation details for full penetration welds between external diaphragm and cover plates (top & bottom)

2.5 Concluding remarks

A total of 18 frames were designed within WP1, according to EN 1993-1-1 [6], EN 1994-1-1 [4] and EN 1998-1 [1], following the initial plan, i.e.:

- Three different frame typologies: moment resisting frames (MRFs), dual concentrically braced frames (D-CBFs) and dual eccentrically braced frames (D-EBFs);
- Three different column cross sections: fully encased wide flange sections, partially encase wide flange sections, and concrete filled rectangular hollow sections.
- Two different combinations of MCS/HSS, considering the dissipative members realized of S355 mild carbon steel, and non-dissipative members realised of high strength steel (S460 & S690).

The design of the dual structural typologies (D-CBF & D-EBF) was governed by the strength of the members, while in the case of the MRF's the governing design criteria was related to the inter-storey drift limitation. With these considerations, but taking into account also aspects related to the steel quantity and testing capacity constraints, the members for the beam-to-column joint specimens were chosen from the dual concentrically braced frames (D-CBF). It is to be mentioned that the size of the joint specimens has been established in close cooperation with RIVA and RUUKKI, the suppliers, in order to account for material availability that would be affected by the different steel grades, different dimensions and in the same time by the small quantities. As a result, the design of the frames allowed the identification of realistic member sizes for both mild carbon steel beams and high strength steel composite columns. In addition, several practical solutions for bolted and welded beam-to-column joints were identified and designed.

The studies performed in the first stage of the project contributed to the detailing of the experimental program and to its adjustment according to the requirements of the connection typologies resulted from the design of the considered structural typologies.

Furthermore, a comprehensive parametric study was defined by selecting and designing a set of 120 frames representative for the design practice, extending the initial set of frames (WP1) to include standard braced frames (no dual action), two different building height ranges, and two span ranges. The design of the selected frames using current code provisions and a dual-steel composite solution was carried out. An extensive numerical program was carried out for the seismic performance evaluation of the 120 frame configurations. The outcomes are therefore presented in the following Chapter 3.

3 Seismic performance of dual-steel frame typologies

3.1 Introduction

Chapter 3 is related to the evaluation of the seismic performance of typical dual-steel frame typologies. The study was carried out within WP2, and was correlated with the activities of WP1, in which several of the examined frame configurations have been designed, and respectively activities of WP6, where guidelines for conceptual design and performance based design of dual-steel building frames have been developed. The activities included a comprehensive set of nonlinear static and time-history analyses of different frame typologies. The main goals can be summarised as follows: (i) to establish ductility demands for members and connections for the structural systems investigated in the project; (ii) to determine overstrength factors to be used in the further versions of EN 1998-1-1 [1] for capacity design of non-dissipative members; (iii) to provide behaviour factors associated to different performance levels that could be used in code-based design procedures for design of dual-steel structures.

In the following sections, a brief description is made in relation to the numerical programme, non-linear analyses of frames (seismic hazard and performance levels, selection of accelerograms, overstrength and behaviour factors, failure criteria and relevant acceptance criteria, numerical models), and the main results (performance based evaluation of ductility and over-strength demands, and performance design levels and related q-factors).

3.2 Numerical programme

The numerical programme consisted in the following seismic analyses:

1. Pushover analyses. According to EN 1998-1 [1] (4.3.3.4.2.4) two lateral load distributions should be used: (i) 1st mode force distribution, (ii) uniform pattern (proportional to masses).
2. Nonlinear time history analyses. The performance was examined in terms of the inter-storey drift distributions recorded for two levels of seismic intensity corresponding to the serviceability (SLS) earthquake event and the damage (DLS) earthquake event.
3. Incremental non-linear dynamic analyses (IDA's). Each IDA was performed scaling 12 times the set of accelerograms as follows: 0.2 PGA to 1.2 PGA with a scaling step equal to 0.1 (to get the overall first yielding and the demand at both serviceability, 0.5 PGA, and ultimate, 1.0 PGA, seismic event) and from 1.2 PGA to 6.0 PGA with a scaling step equal to 0.4.

The numerical programme was applied on a comprehensive set of steel frames designed in WP1 and WP2 according to EN 1998-1 [1]. The details about the design criteria and assumptions are given in the relevant part of Chapter 2. As a result a total of 120 frame configurations have been analysed in order to assess the seismic performance of dual-steel structures. Figure 2.4 (see Section 2.3.2) summarizes the examined frame configurations, considering the following structural systems (Figure 3.1): (1) moment resisting frames (MRF), (2) concentrically braced frames (CBF), (3) eccentrically braced frames (EBF), (4) dual concentrically braced frames (D-CBF), and (5) dual eccentrically braced frames (D-EBF). These frames are representative of the class of mid-to-high rise multi-storey buildings. The basic typological properties have been assumed to be consistent with the common design practice, that are as follows: the floors are composed by composite steel decks simply rested on steel beams, which are restrained to avoid flexural-torsional buckling; all joints are simply pinned. Fully encased (FE), partially encased (PE), and concrete filled tube (CFT) cross-sections have been used for columns, alternatively.

In detail, the investigated design parameters are summarized in Table 3.1. For mid-rise buildings, two different values of span length (e.g. 5.0 m and 7.5 m) were investigated. The aim was to analyze two different overall structural behaviours: shear-dominant (racking), and flexural-dominant (cantilever).

According to Owens et al. [20], the flexural behaviour becomes important for relatively slender frames with a height-to-width (aspect) ratio of about 1.5. Hence, the span range 5.00 m – 7.50 m allows analysing both structural behaviours. The former for flexural-dominant frames, the second for those shear dominant, as better clarified by the aspect ratios reported in Table 3.2. For a proper organisation of the work, the following label code was developed for the numbering of the frame configurations:

(Storeys).(Steel).(Spans).(Soil).(Column type)

where:

- Storeys: 1 for 8 storeys / 2 for 16 storeys / 3 for 4 storeys;
- Steel (non-dissipative members): 1 for S460 / 2 for S690;
- Spans: 1 for 5.0 m / 2 for 7.5 m;
- Soil: 1 for Stiff / 2 for Soft;
- Column type: 1 for FE / 2 for PE / 3 for CFT.

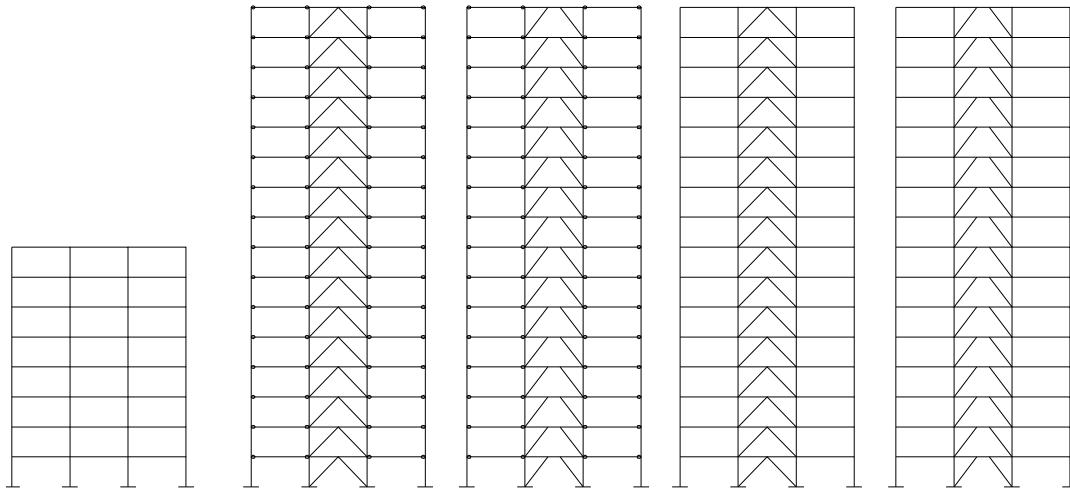


Figure 3.1. Investigated frame typologies

Table 3.1 – Parameter variations

No. of storeys	Span (m)	Interstorey height* (m)	Column types**	Accelerogram
8	5.0 – 7.5	3.5	3	2x7
16	7.5	3.5	3	2x7

* the first interstorey height is assumed equal to 4.0 m
 ** fully encased, partially encased, and concrete filled tubes

Table 3.2 – 8-storey frames: aspect ratios

Span (m)	H (m)	3L	Aspect ratio
5.0	28.5	15.0	1.90 > 1.5
7.5	28.5	22.5	1.27 < 1.5

3.3 Non-linear analysis of frames

3.3.1 Seismic hazard and performance levels

According to the seismic performance based design, structures designed against earthquakes must fulfil specific requirements for different level of seismic intensity, which correspond to criteria such as stiffness, strength and ductility. Hence, the current codes introduce different performance levels associated to specific seismic hazard. According to EN 1998-3 [21] the seismic hazard curve is defined with the following equation:

$$H(a_{gR}) = k_o (a_{gR})^{-k} \quad (3.1)$$

where a_{gR} is the reference peak ground acceleration, while the exponent k depends on seismicity, but being generally assumed equal to 3;

The seismic performance of the study cases has been evaluated considering three performance levels, which are associated to different annual rate of exceedance: damage limitation (DL), severe damage (SD), and near collapse (NC).

According to EN 1998-3 [21], at DL state, the building is subjected to the frequent earthquake with 95-year-return period, and the structure shall have no occurrence of damage and the associated limitations of use. EN 1998-3 [21] presented a reduction factor v to take into account the determination of the frequent earthquake from the design earthquake. In the examined cases, v is equal to 0.5 and the corresponding structural performance should provide interstorey drift ratios lesser than 0.75%.

The SD state corresponds to design condition where the structure shall have no local or global collapse under the design seismic action with 475-year-return period. At this performance level, the structure is strongly damaged but has some residual lateral strength and stiffness and vertical elements are capable of sustaining vertical loads, thus providing the strength to sustain moderate after-shocks.

At the NC state the structures are expected to be heavily damaged, with negligible residual lateral strength and stiffness, although vertical elements are still capable of sustaining vertical loads. Large permanent drifts are present. The structures are near collapse and are not able to resist to moderate earthquake after-shocks. In this study, it is assumed to verify this performance level against a seismic action with 2475-year-return period.

Table 3.3 summarizes the performance levels used for each of the three limit states where acceleration ratio A/A_d corresponds to peak ground acceleration used in design.

Table 3.3 – Performance levels vs. seismic intensity levels

Performance level	Return period (years)	A/A_d	Description of the performance level	Failure criteria
Damage limitation (DL)	95	0.50	Light damage, the component retaining the initial strength and stiffness	Interstorey drift/member buckling
Severe damage (SD)	475	1.00	Significant damage, with some margin against total collapse of the component	Interstorey drift/member capacity
Near collapse (NC)	2475	1.72	Heavy damage, with low residual strength and stiffness of the component	Interstorey drift/member residual capacity

3.3.2 Selection of accelerograms

The selection of acceleration records was mainly carried out by VTT with the aim to have two ensembles of records fitting the spectra of “stiff” and “soft” soil used in the design of the frames. The term “stiff soil” has been referred to the Ground C, Type 1 spectra of EN 1998-1 [1], while the “soft soil” was assumed to investigate the elastic spectra of Bucharest with an untypically large corner period $T_C=1.6$ s. This choice has been made in order to follow clearly distinguishable spectral typologies, so the conclusions of the parametric study can be focused for the two soil typologies.

The records have been used for the analysis of several typologies of moment resisting and braced frames, with a large range of fundamental periods. So the selection of the records was based on trying to match most properties of the spectrum, in order to achieve good fit over a large range of periods of vibration. Since the “earthquake scenario”, in term of magnitude and epicentre distance was not defined, the records were mixed, thus resulting in records with different frequency contents.

Both artificial and natural records have been selected. The former obtained using SIMQKE tool and the latter from the European Strong-Motion Data (ESMD) using the procedure reported by Kesti et al. [22]. The events at the basis of the selected records are presented in Table 3.4. The stiff soil records were mostly selected from an initial set provided by UNINA, being artificial records. For the soft soil typology all record are from events with $M_s > 5$, and the smallest PGA has been $PGA_{min}=0.33$ m/s². Selected properties of the 14 accelerograms are presented also in Table 3.5.

Table 3.4 – Basic data of the earthquakes behind the selected records

Soil C	Date	Measurement location	Focal depth (km)	Surface wave magnitude M_s	Foundation category	Epicentre distance (km)	Un-scaled records		Scaled $PGA=1$		Significant duration between 5-95% AI (s)
							PGA (m/s ²)	Arias Intensity (AI)	Arias Intensity (AI)	PGV (m/s)	
1S_2SR1	-	-	-	-	-	-	-	-	0.107	0.130	11.1
1S_2SR6	-	-	-	-	-	-	-	-	0.223	0.319	12.8
1S_2SR7	-	-	-	-	-	-	-	-	0.223	0.150	13.2
2S-R5-sc1	-	-	-	-	-	-	-	-	0.155	0.218	13.9
2S-R6-sc1	-	-	-	-	-	-	-	-	0.173	0.217	13.2
2S-R7-sc1	-	-	-	-	-	-	-	-	0.127	0.227	13.4
000296YA	23.11.80	Torre del Greco (Italy)	16	6.87	rock	80	0.4	0.046	0.284	0.121	35.2
000155XA	04.03.77	Bucharest (Romania)	86	7.05	alluvium	161	1.98	0.8	0.205	0.372	6.8
000184XA	16.09.78	Kashmar (Iran)	5	7.33	stiff soil	228	0.37	0.056	0.4	0.184	28.4
000297YA	23.11.80	Tricarico (Italy)	16	6.87	rock	72	0.343	0.050	0.424	0.154	37.9
000294XA	23.11.80	Bisaccia (Italy)	16	6.87	stiff soil	26	0.903	0.277	0.339	0.181	50.1
000479YA	20.06.90	Rudsar (Iran)	19	7.32	soft soil	65	0.84	0.302	0.426	0.182	26.5
000535XA	13.03.92	Erzincan (Turkey)	10	6.75	stiff soil	13	3.816	1.572	0.108	0.266	7.4
000303XA	23.11.80	Roccamonfina (Italy)	16	6.87	rock	127	0.230	0.019	0.353	0.193	19.9

The selected records present good correlation with the target design spectrum, but applying period dependent scaling can further reduce the scatter in the response data (Balling et al. [23]). Usually records are scaled to same PGA, based on the presumption that PGA is a good intensity measure

(IM). In this study a vibration period dependent scaling was implemented, and PGA was abandoned as IM of the records. Hence the PSA value corresponding to a certain period of vibration, or the range of periods in vicinity of the fundamental period, can be treated as IM. Particularly in this selection the average PSA value on a period interval T_l to T_u , was used. T_l represents the fundamental period of the studied structure (T_F), or a lower value $T_l < T_F$ if significant upper vibration modes are to be taken into account, and T_u is an upper value of period depending on the expected degree of softening resulting from the non-linear deformation. The upper limit should be about $\sqrt{\mu} \cdot T_l$, where T_l is the fundamental period and μ the expected level of ductility. As a principle, records should be scaled to the same level of average PSA on T_l to T_u as the elastic design spectra. The procedure was also used by Balling et al [23].

The selection of the period interval was based on the set of structures with different fundamental periods to be analyzed. Three typical structures to be analyzed were the basis for the periods of vibration: $T_{1-S1}=1.82$ s, $T_{1-S2}=0.78$ s, $T_{1-S3}=0.88$ s, these are values expected for 8th floor moment resisting frame, concentrically braced frame and eccentrically braced frame respectively.

Different design codes then simplify the definition of the period interval based on practical considerations. As an example, EN 1998-1 [1], §3.2.3.1.2(4), requires a comparison of the spectra on the interval $0.2 \cdot T_l$ to $2 \cdot T_l$, presuming a ductility of $\mu=4$. The UBC §1631.6.1 requires a comparison on the range $0.2 \cdot T_l$ to $1.5 \cdot T_l$. In case of the structures this would mean the period ranges from Table 3.5. As a result, the matching of the spectra is expected for approximately the first 3 modes of vibration of the structures. The values T_u indicate that both the EN 1998-1 [1] and the UBC expect significant softening of the structures. The intervals, shown in Table 3.6, do not bring much improvement, as they practically extend to the entire useful range of the spectrums, from 0.16 s to 3.64 s. The criteria of the two codes is also somewhat similar, with the difference that the UBS is focused on simultaneous 2 direction shaking, while the EN 1998-1 [1] defines acceptance criteria for single direction records. EN 1998-1 [1] requires that "between $0.2 \cdot T_l$ and $2 \cdot T_l$, no value of the mean 5% damping elastic spectrum, calculated from all time histories, should be less than 90% of the corresponding value of the 5% damping elastic response spectrum".

Table 3.5 – Period ranges for fitting the records

Structure	T_l (s)	T_l (s)	T_u (s)
S1	1.82	0.364	3.64 (2.73)
S2	0.78	0.156	1.56 (1.17)
S3	0.88	0.176	1.76 (1.32)

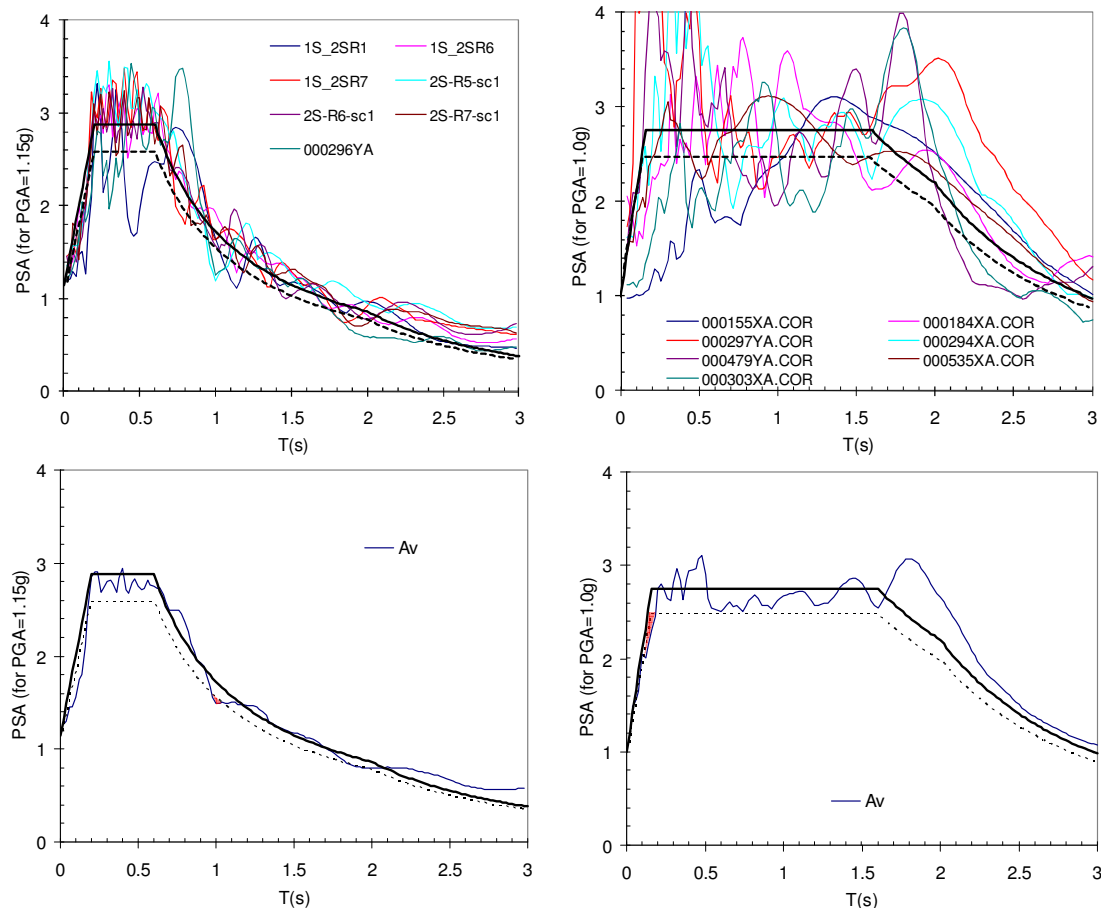


Figure 3.2. PSA spectra of the scaled records

EN 1998-1 [1] was decided to be used for acceptance criteria of the record sets. Records were scaled to the design spectrum using Balling et al. [23], for the range of fundamental periods $T = 0.78 \text{ s} - 1.82 \text{ s}$. The EN 1998-1 [1] acceptance criteria was then tested in the full range of $T = 0.16 \text{ s} - 3.00 \text{ s}$.

As it can be seen in Figure 3.2, some sections of the spectra still do not fulfil the EN 1998-1 [1] acceptance criteria. For the EN-1998-1 [1] Ground C type (stiff soil in this study) there is no significant difference, while for the Soft Soil type it affects the low range of periods. This can mean that the higher modes of vibration will not be correctly accounted.

In order to achieve the EN 1998-1 [1] criteria for the range of periods $0.16 - 3 \text{ s}$, all 7 records were scaled up uniformly with strict condition that average spectra > 0.9 target PSA. This leads to use of a uniform scaling up of the Ground C "Stiff Soil" records with 1.0385, and those of the "Soft Soil" by 1.0082. Final values of the scale factors for all records are presented in Table 3.6.

Table 3.6 – Scale factor based on equality of areas under spectra, corrected to fulfil the EN 1998-1 [1] requirement ($PSA_{\text{average}} > 0.9 \cdot PSA_{\text{target}}$)

Soil C	Scaling factor	Soil "Soft"	Scaling factor
1S_2SR1	1.027	000155XA	0.957
1S_2SR6	1.081	000184XA	1.249
1S_2SR7	1.129	000297YA	1.671
2S-R5-sc1	1.162	000294XA	1.567
2S-R6-sc1	1.070	000479YA	1.401
2S-R7-sc1	1.083	000535XA	1.372
000296YA	1.053	000303XA	1.100

In the non-linear time history analyses, a set of ground motion records were used (see Table 3.4) together with the scaling factors from Table 3.6. With the scaling, the average spectra of the records respect the conditions of EN 1998-1 [1] §3.2.3.1.2 imposed for using a set of records for time-history analyses (see Figure 3.3). Finally, Figure 3.4 and Figure 3.5 show the selected accelerogram records used for the nonlinear dynamic analyses.

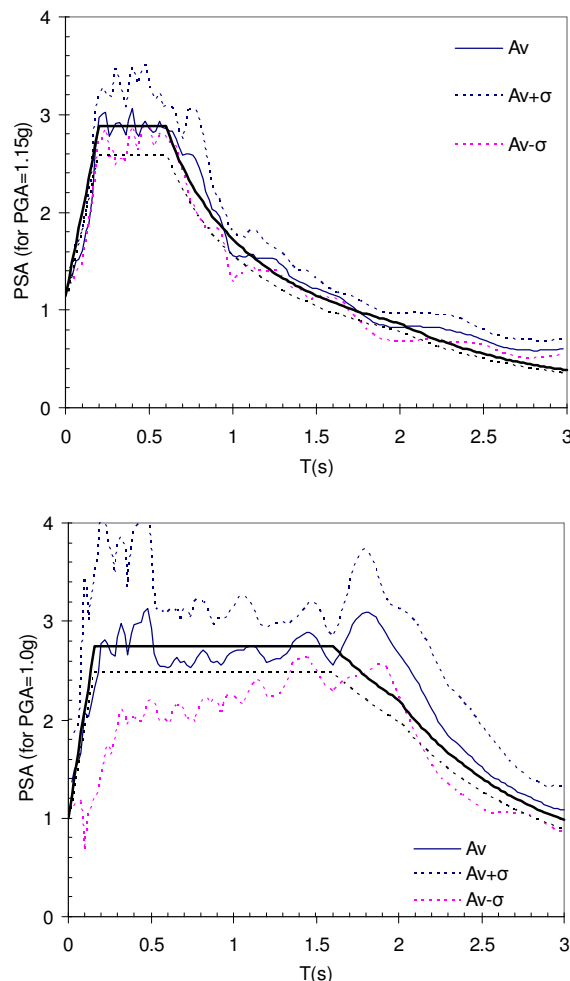


Figure 3.3. PSA spectra of the scaled records fulfilling EN 1998-1 [1] criteria, so that $PSA_{\text{average}} > 0.9 \cdot PSA_{\text{target}}$. (average & average $\pm 1\sigma$ are represented)

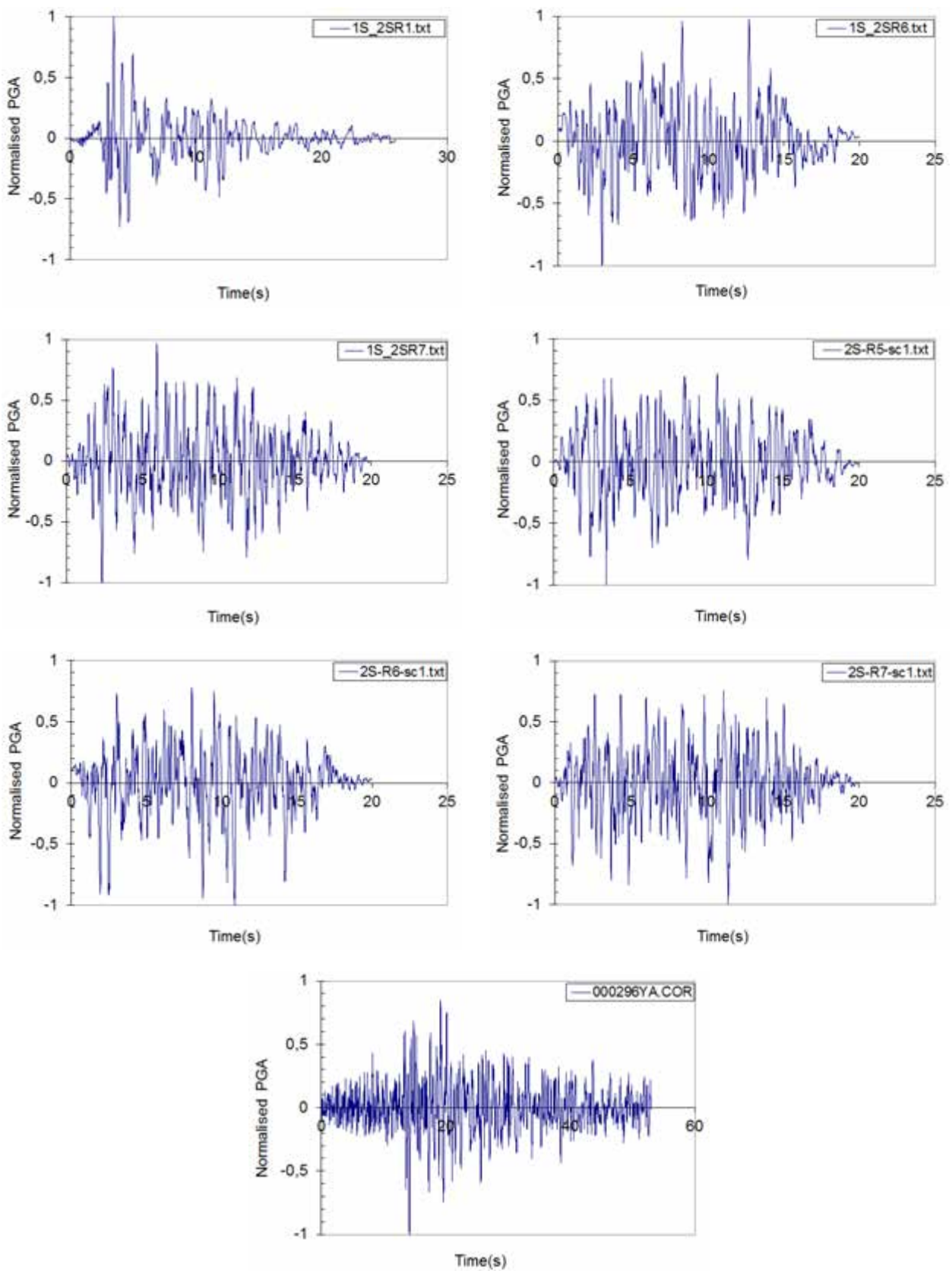


Figure 3.4. Earthquake records adopted in the analysis for stiff soil

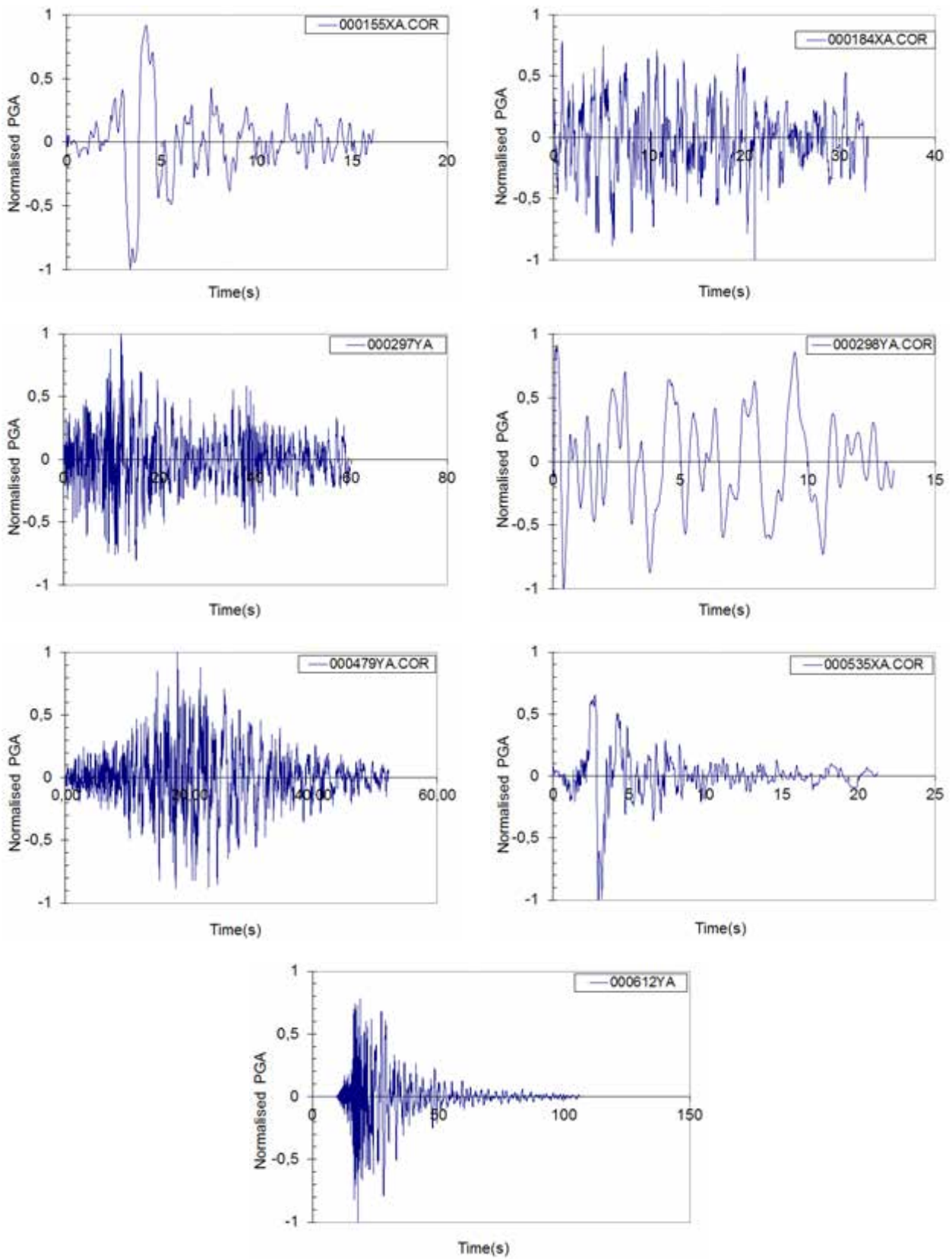


Figure 3.5. Earthquake records adopted in the analysis for soft soil

3.3.3 Overall overstrength factor

The overall overstrength factor Ω is defined as the ratio between the base shear corresponding to the overall yield strength of the frame and the design base shear. This ratio can be decomposed in two terms:

$$\Omega = \frac{V_y}{V_d} = \frac{V_y}{V_{1y}} \times \frac{V_{1y}}{V_d} \quad (3.2)$$

Where the first term, V_y/V_{1y} , corresponds to α_u/α_1 defined in the EN 1998-1 [1]. This value depends on the frame configuration, formation of the collapse mechanism, redistribution capacity and gravity loading (Elghazouli [24]). The second term (V_{1y}/V_d) is related to aspects of the design procedure such as differences between actual and nominal material strength, member oversizing due to choices of commercial cross-section and design governed by deformation and/or non-seismic loading. Therefore, this term may be associated to the degree of specialization of frame for seismic resistance.

According to EN 1998-1 [1] (4.3.3.4.2.4) the overstrength factor was determined by pushover analyses. In particular, two lateral load distributions were used: (i) 1st mode force distribution; (ii) uniform pattern (proportional to masses). The assumed value is the lower for the two lateral load distributions.

3.3.4 Behaviour factors

EN 1998-1 [1] states that the behaviour factor (q) can be obtained as the average ratio between the seismic intensity inducing an ultimate limit state in the structure, taking into account its non-linear behaviour, and the design seismic intensity used with a conventional linear model.

From a practical point of view, for a given earthquake, the behaviour factor (q) corresponds to the ratio between the seismic intensity A_u (in the sense of the peak value of the acceleration) which causes an ultimate limit state (failure) and the seismic intensity A_y associated to the elastic limit state of the structure (Mazzolani & Piluso [25], Elnashai & Broderick [26]). In the present study the values of A_y and A_u have been derived from IDA's.

In order to facilitate the comparison of the codified value of the behaviour factor with the ones determined from IDA, the total behaviour factor (q_t) should be used, which is obtained as the ratio between the seismic intensity A_u and the design seismic intensity A_d . The value of the total behaviour factor q_t is equal to the product between q and the design overstrength V_{1y}/V_d .

3.3.5 Failure criteria and relevant acceptance criteria

Separate failure criteria based on the limiting behaviour of each structural element have been assumed in order to assess the behaviour factors. In each examined frame, structural collapse has been assumed when one of the failure criteria is exceeded. This is plainly a conservative assumption, because local failure will need to occur in more than one area before overall collapse could experience.

Therefore, the performance criteria correspond to failure under seismic loading can be associated with:

- Buckling, local buckling, fracture and low cycle fatigue;
- Failure of a structural member;
- All phenomena causing deterioration of capacity or out-of service of the structure.

According to this approach the amplitude corresponding to the acceleration A_u is the minimum value corresponding to all possible theoretical states of collapse:

$$A_u = \min(A_\theta, A_c, A_R, A_{br}, A_{link}) \quad (3.3)$$

where:

- A_θ is the acceleration corresponding to the maximum permitted inter-story drift (3% for MRF and 2% for brace frames);
- A_c corresponds to the buckling of columns or the buckling of a bracing element in EBF's;
- A_R corresponds to the maximum permitted local rotation (defined according to EN 1998-3 [21]);
- A_{br} corresponds to the maximum permitted brace deformation in tension and compression (defined according to EN 1998-3 [21]);
- A_{link} corresponds to the maximum permitted link rotation (defined according to EN 1998-3 [21]).

The recommended acceptance criteria of member deformations, corresponding to the different performance levels are mainly consistent with those given by EN 1998-3 [21]. Since EN 1998-3 [21] does not provide indications for links of EBF's and D-EBF's, the performance limits given by Malley & Popov [27] have been used. Table 3.7 summarizes the acceptance criteria for assessing the seismic performance of dual-steel structures. For clarification, the meaning of the symbols from Table 3.7 are given as follows: Δ_t is the yield displacement of the bracing element in tension, Δ_c is the displacement corresponding to the buckling of the bracing element, γ is the shear rotation of the link, and γ_y is the yield shear rotation of the link.

Table 3.7 – Acceptance criteria at each limit state

Limit state	Interstorey drift ratio ^(*)	Bracing in tension ^(**)	Bracing in compression ^(**)	Beam ^(*)	Beam ^(**)	Column/bracing in EBF	Link ^(***)
DL	0.75% (transient)	0.25 Δ_t	0.25 Δ_c	1 θ_y	$\frac{M}{M_y} = 0$	buckling	$\gamma \leq 0.005rad$
SD	0.40% (residual)	7 Δ_t	4 Δ_c	6 θ_y	$\frac{M}{M_y} \leq 1$	buckling	$(\gamma - \gamma_y) \leq 0.08rad$
NC	3.0% (transient)	9 Δ_t	6 Δ_c	8 θ_y	$\frac{M}{M_y} \leq 1$	buckling	$(\gamma - \gamma_y) \leq 0.10rad$

(*) MRF / (**) CBF and D-CBF / (***) EBF and D-EBF

3.3.6 Numerical models

The models were developed using the force-based (FB) distributed inelasticity elements (Spacone et al. [28], Calabrese et al. [29]). The cross-section behaviour is reproduced by means of the fibre approach, assigning a uniaxial stress-strain relationship at each fibre. The stress-strain relationship for concrete fibres in the column elements was determined using the model proposed by Martinez-Rueda & Elnashai [30]. The effects of confinement provided by steel profile and/or reinforcement have been determined according to Mander et al. [31] and Susantha et al. [32], for fully encased sections, partially encased sections and respectively concrete filled tubes. In the case of steel members, the model proposed by Menegotto & Pinto [33] for the stress-strain curve was chosen. The average values of both concrete compression strength and steel yield stress have been used. The former has been assumed according to EN 1992-1-1 [34], while different values of material overstrength factor (γ_{ov}) were assumed for each steel grade. In particular, $\gamma_{ov}=1.25$ was assumed for S355, while 1.10 for S460 and S690 (OPUS [35]).

The numerical integration method used is based on the Gauss-Lobatto distribution (Abramowitz & Stegun [36], Szabo & Babuška [37]), which includes, at a minimum, monitoring points at each end of the element. Such feature allows each structural member to be modelled with a single FE element, thus requiring no meshing for each element. In the present study, 5 Gauss-Lobatto integration points have been used.

Second order effects have been accounted in all analyses presented in this paper, by assuming large displacements/rotations and large independent deformations relative to the chord of the frame element through the employment of the co-rotational formulation given by Correia & Virtuoso [38].

Concerning dynamic analyses a 2% Rayleigh tangent stiffness damping has been used at both first and second mode. Indeed, differently from initial damping formulation, it does not produce artificial over-damping at high ductility demand as shown by (Priestley & Grant [39], D'Aniello et al. [40]).

The effectiveness and the accuracy of the modelling assumptions have been verified against experimental results available from literature. In particular, concerning the steel beams and the MRF's, the validity of the modelling assumptions has been verified against the experimental results carried out by D'Aniello et al. [41] on steel beams, and by Wakawayashi et al. [42] on a single storey steel MRF. The comparison between experimental and numerical response curves are depicted in Figure 3.6, where the satisfactory accuracy of the implemented numerical models can be observed.

Differently from steel beams, the modelling of bracing elements needs additional assumptions and more refinement in order to simulate the complex hysteretic behaviour, given as follows:

1. The brace member should be subdivided into two inelastic beam-column elements.
2. It is suggested to use the value of the initial camber given by Dicleli & Calik [43], which is generally restrained in that range.
3. At least 200 fibres should be adopted to mesh the cross section for an accurate representation of inelastic strains for stable and less time consuming analysis.
4. Distributed plasticity elements have been used with more than 4 integrating sections.

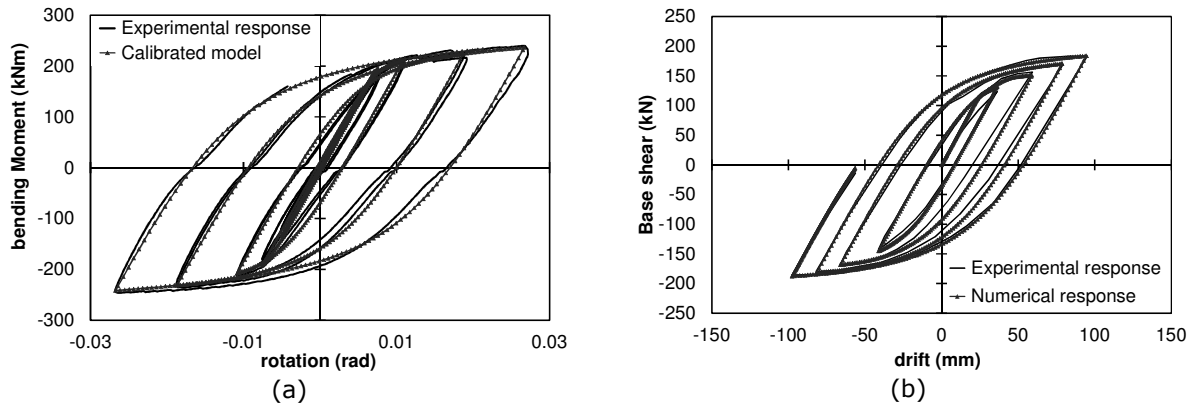


Figure 3.6. Comparison between numerical and experimental curves: (a) cyclic tests on beams by D'Aniello et al. [41]; (b) cyclic tests on single storey MRF by Wakawayashi et al. [42]

For brevity sake, a comparison is shown between experimental response curves (tests by Black et al. [44]) and those obtained by the so-defined numerical model. The examined brace is a simply pinned W8x20 (US measurements) steel wide flange brace, having a geometric slenderness $\lambda = kL/r$ equal to 118, and a nondimensional slenderness $\bar{\lambda}$ equal to 1.4. The axial force vs. axial displacement hysteretic loops and the axial force vs. lateral deflection are illustrated in Figure 3.7. More details about this issue can be found in D'Aniello et al. [40].

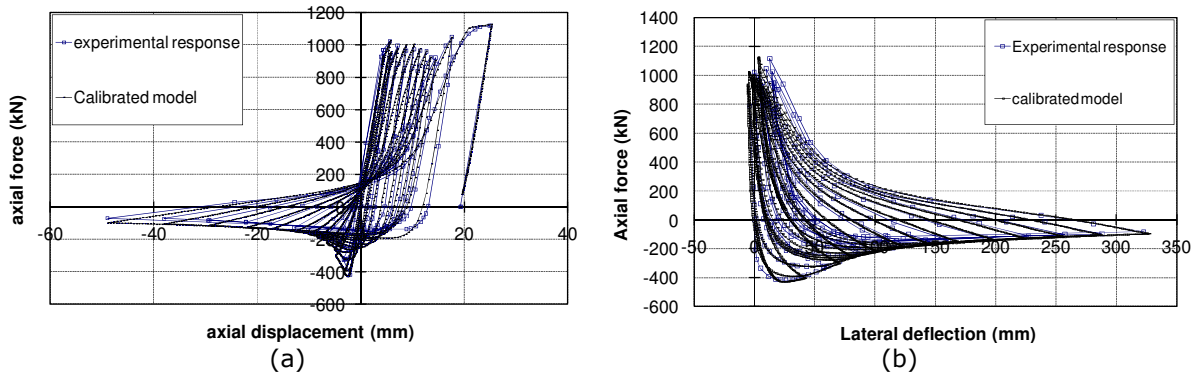


Figure 3.7. Brace model vs. experimental response: (a) axial behaviour, (b) out-of-plane behaviour

Finally, since shear fibre element are not currently implemented in the calculation software, the behaviour of shear links was also specifically simulated. For this purpose, the links were modelled by means of an inelastic fibre element and by a bi-linear kinematic spring at both ends. The central element has the same length and inertia as the link and simulates the flexural behaviour of links (the shear stiffness of this element is set to zero). The two ending springs are zero-length. They connect the beam segments outside the link to the flexural element of the link and reproduce the shear behaviour of the link. Only relative vertical displacements are permitted between the nodes of the shear element. The stiffness of the translational spring which causes this relative movement is defined to simulate the effect of the shear deformability of half a link.

Short links were considered. Hence, no interaction has been considered at yielding of links. The ultimate link shear force and bending moment are given by:

$$V_u = 1.5V_p \quad (3.4)$$

$$M_u = 0.5eV_u \quad (3.5)$$

being e the link length;

The post-yielding stiffness of the shear springs is defined as follows:

$$K_v = \frac{0.5V_p}{0.08} \quad (3.6)$$

being 0.08 the maximum plastic rotation in radians;

Accuracy of modelling assumptions was verified by comparison of theoretical outcomes with experimental results obtained by Okazaki & Engelhardt [45].

The examined link is made of an US wide flange hot-rolled profile W10x33, having $\frac{e \cdot V_p}{M_p} = 1.04$.

Figure 3.8 shows the comparison between experimental and numerical response of the examined link. As it can be observed the model matches very well the experimental response.

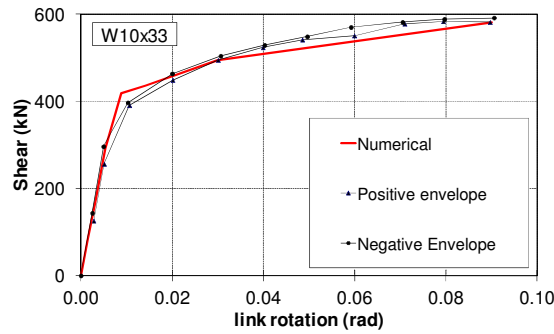


Figure 3.8. Link model vs. experimental response (W10x33 by Okazaki & Engelhardt [45]).

3.4 Performance based evaluation of ductility and over-strength demands

3.4.1 Moment Resisting Frames

The ductility demand for dissipative beams of MRF's is expressed in terms of total chord rotation. According to EN 1998-3 [21], the beam plastic rotation capacity should be no lesser than $10\theta_y$, $6\theta_y$ and respectively $8\theta_y$, for the DL, SD and NC performance levels, being θ_y the beam yield rotation.

Figure 3.9 illustrates the median ductility demand along the building height. As it can be observed the most of the beams are in the elastic range at SD limit state, while very limited plastic rotation demand can be recognized at NC limit state. Once more, these results can be explained by the design procedure that led to oversize the structural element to fulfil the requirement of damage limitation.

Another investigated important parameter was the beam flexural overstrength (s), which is the non-dimensional measure of the ultimate bending capacity of steel beams, due to the amount of strain hardening which can be exhibited prior beam failure (D'Aniello et al. [41]).

The maximum flexural overstrength (s) may be defined in terms of bending moments as follows:

$$s = \frac{M_u}{M_p} \quad (3.7)$$

where M_u is the peak bending moment experienced by the beam, and M_p is the beam plastic bending moment;

Figure 3.10 shows the median distribution of s^* along the building height. As it can be noted the most of beams behave elastically thus the median s^* is lesser than unity. Some cases slightly larger than 1 occur for 8-storey frames with soft soil at SD and NC limit states. Such results confirm that the design approach of EN 1998-1 [1] is consistent with the expected performance of the frames, namely limited ductility demand resulting in small hardening developed by plastic hinge.

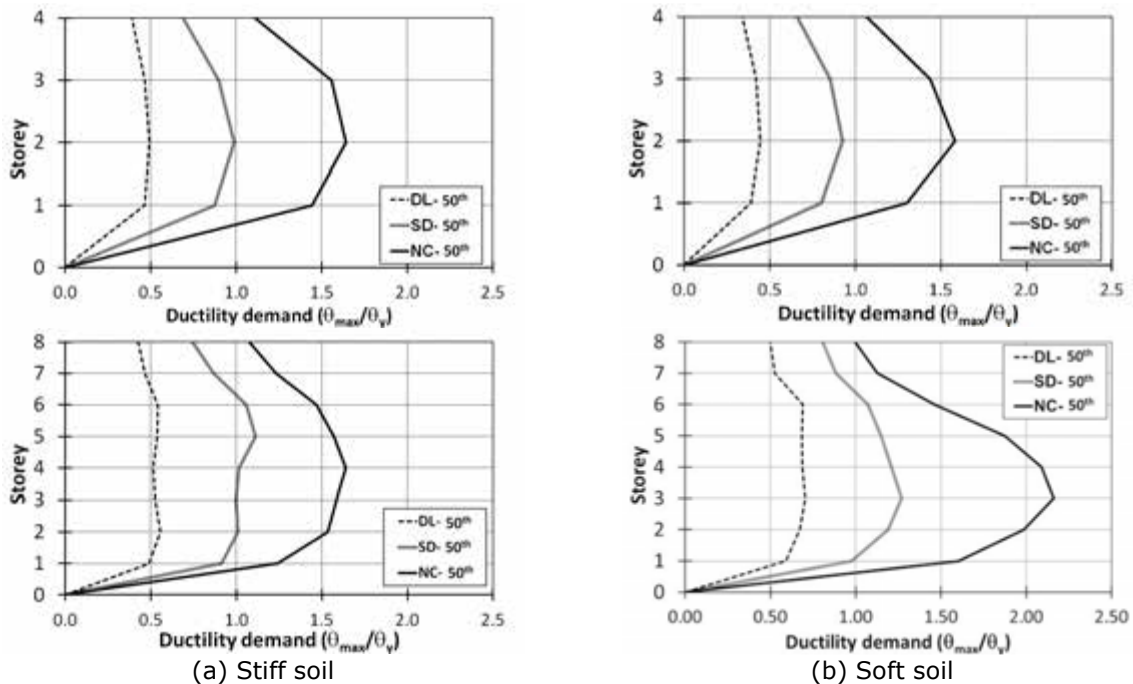


Figure 3.9. Ductility demand ratios

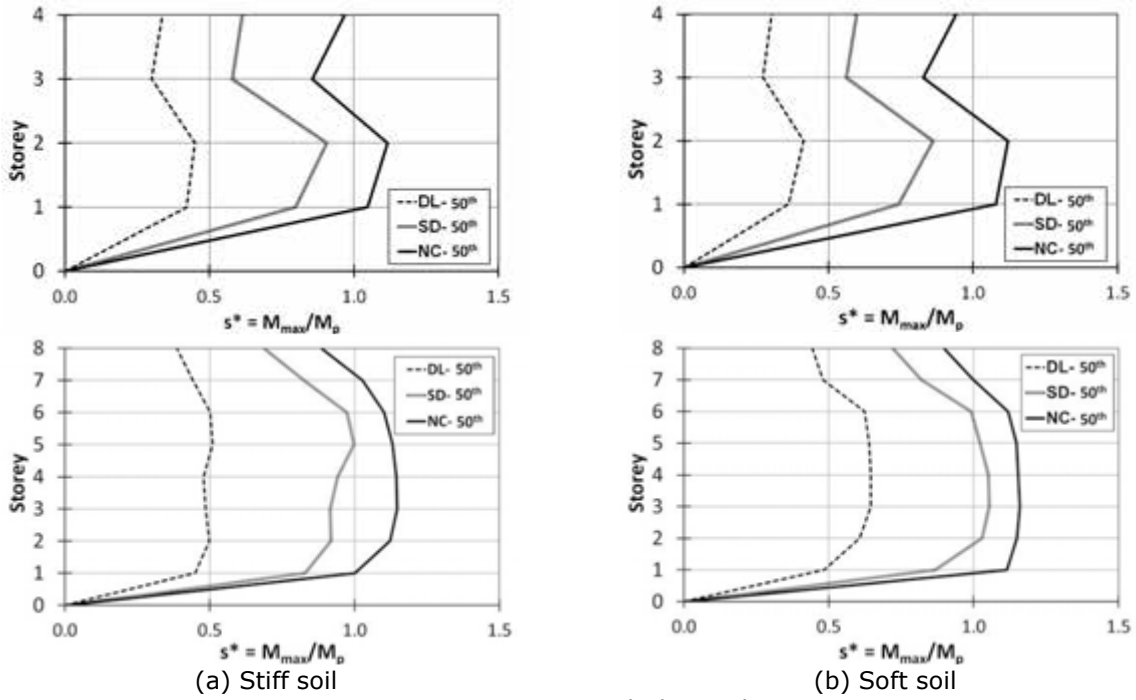
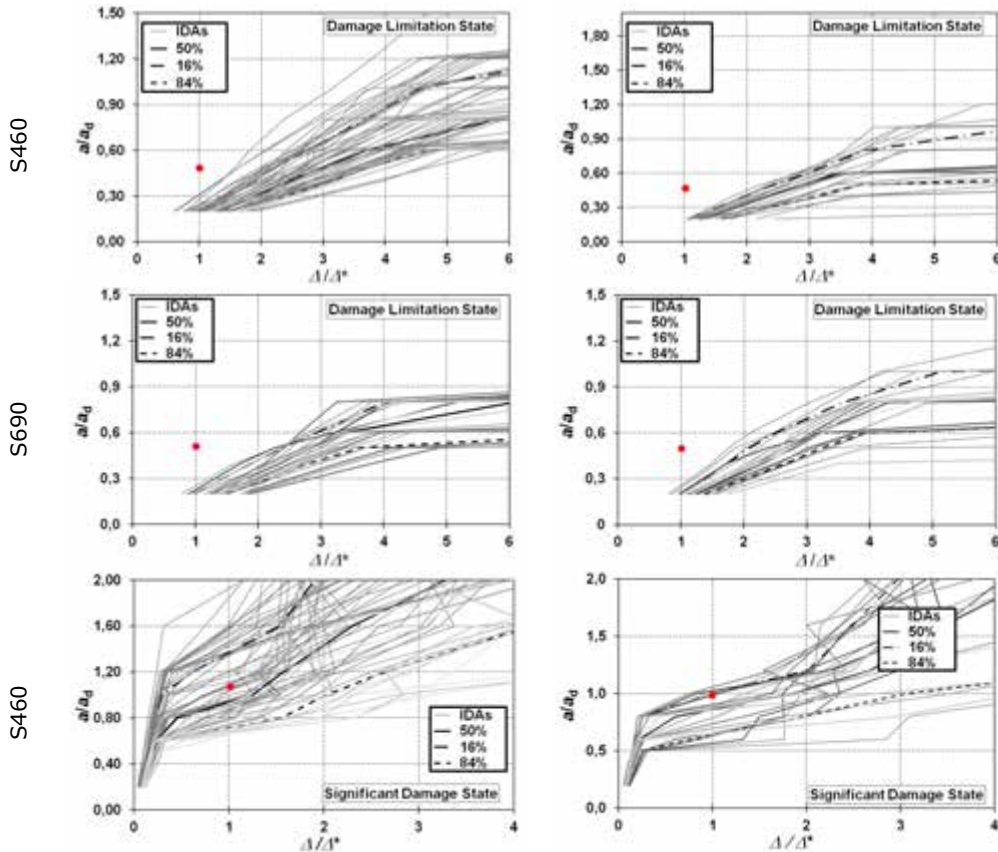


Figure 3.10. Overstrength demand ratios

3.4.2 Concentric Braced Frames

The ductility demand for CBF's is expressed in terms of brace axial deformation. According to EN 1998-3 [21], the limit values for braces cross section Class 1 are $0.25\Delta_c$, $4.0\Delta_c$ and $6.0\Delta_c$, for Class 2 are $0.25\Delta_c$, $1.0\Delta_c$ and $2.0\Delta_c$, corresponding to the DL, SD and NC limit states. In case of braces in tension the corresponding limits are $0.25\Delta_t$, $7.0\Delta_t$ and $9.0\Delta_t$, irrespectively of the cross section class.

The axial deformation of braces was investigated. Consequently, the analyses have shown that the shortening demand of braces exceeds the capacity for the most structures, while the braces in tension do not overcome their limits. The ratio between the maximum median value obtained for the seven records of each soil condition and the maximum value allowed in EN 1998-3 [21] is presented in Figure 3.11 for each limit state.



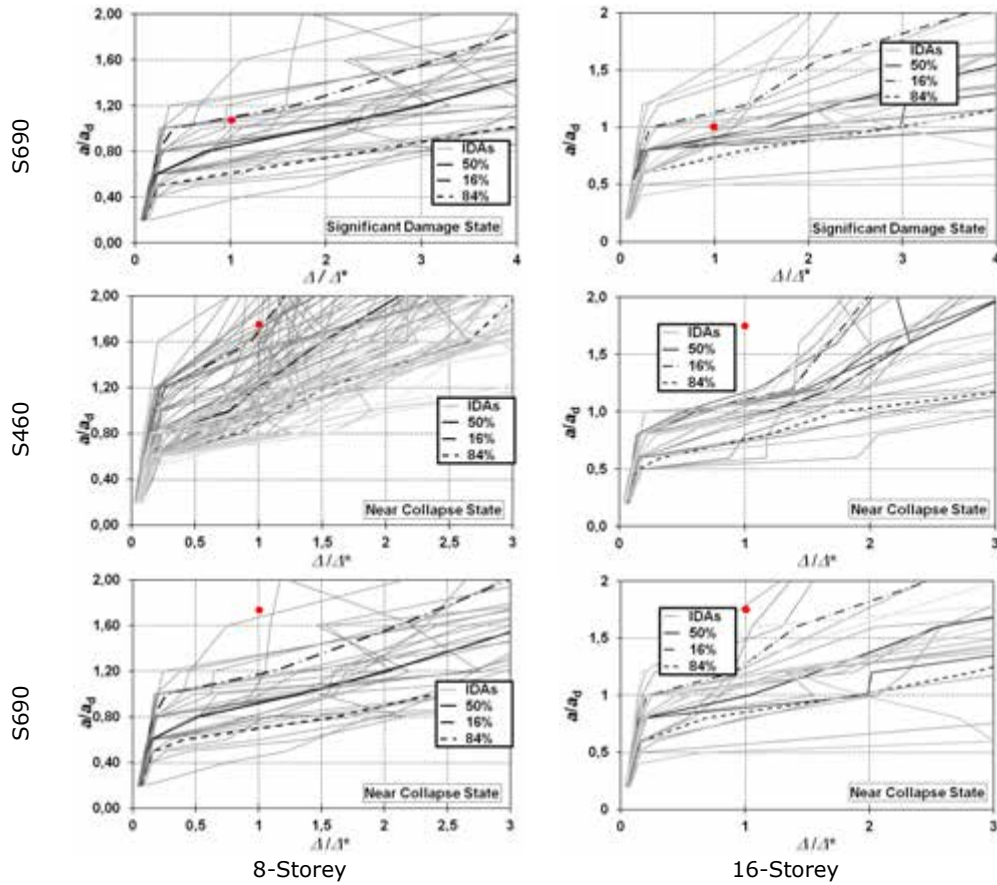


Figure 3.11. Brace ductility demand for the three limit states

The results show an inadequate performance of the frames, in special the values obtained for the DL that are heavily higher than the limit of $0.25\Delta_c$ showing a ratio around from 2.28 to 3.34 for the frames with S460, while this difference varies from 2.60 to 2.91 for the frames with higher steel grade. Concerning the steel grade used, its increase of strength provides a reduction of ductility demand mainly for the DL and NC limit states.

3.4.3 Dual Concentric Braced Frames

The ductility demand for D-CBF's is expressed in terms of both beam rotation, for the beams belonging to the MRF spans, and brace axial deformation (Δ) in the braced spans. The ductility capacity limits are given in Table 3.7.

As it can be easily recognized in Figure 3.12, the median value of beam rotation in the MRF span is lesser than the plastic rotation. Hence, the MRF's behave elastically in the most of cases.

The results in terms of axial deformation (Δ/Δ_c) are shown in Figure 3.13. The comparison between Figure 3.13 and Figure 3.11 highlight that D-CBF's may exhibit a smaller ductility demand than CBF's.

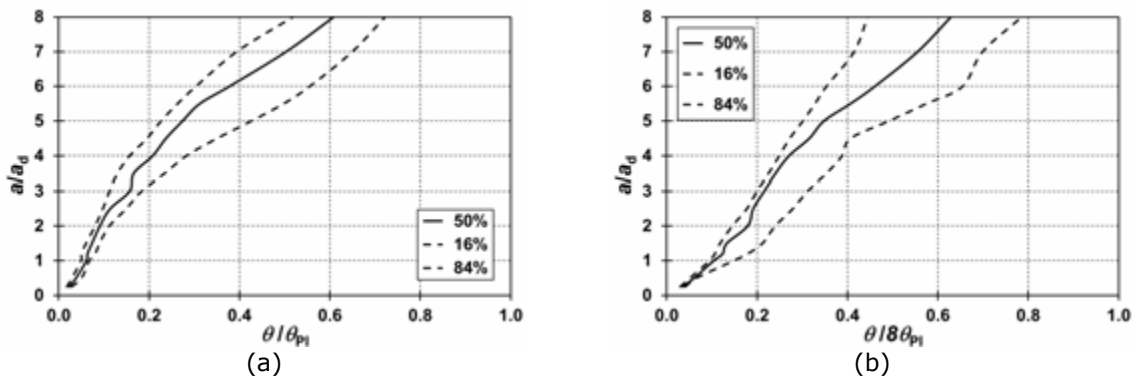
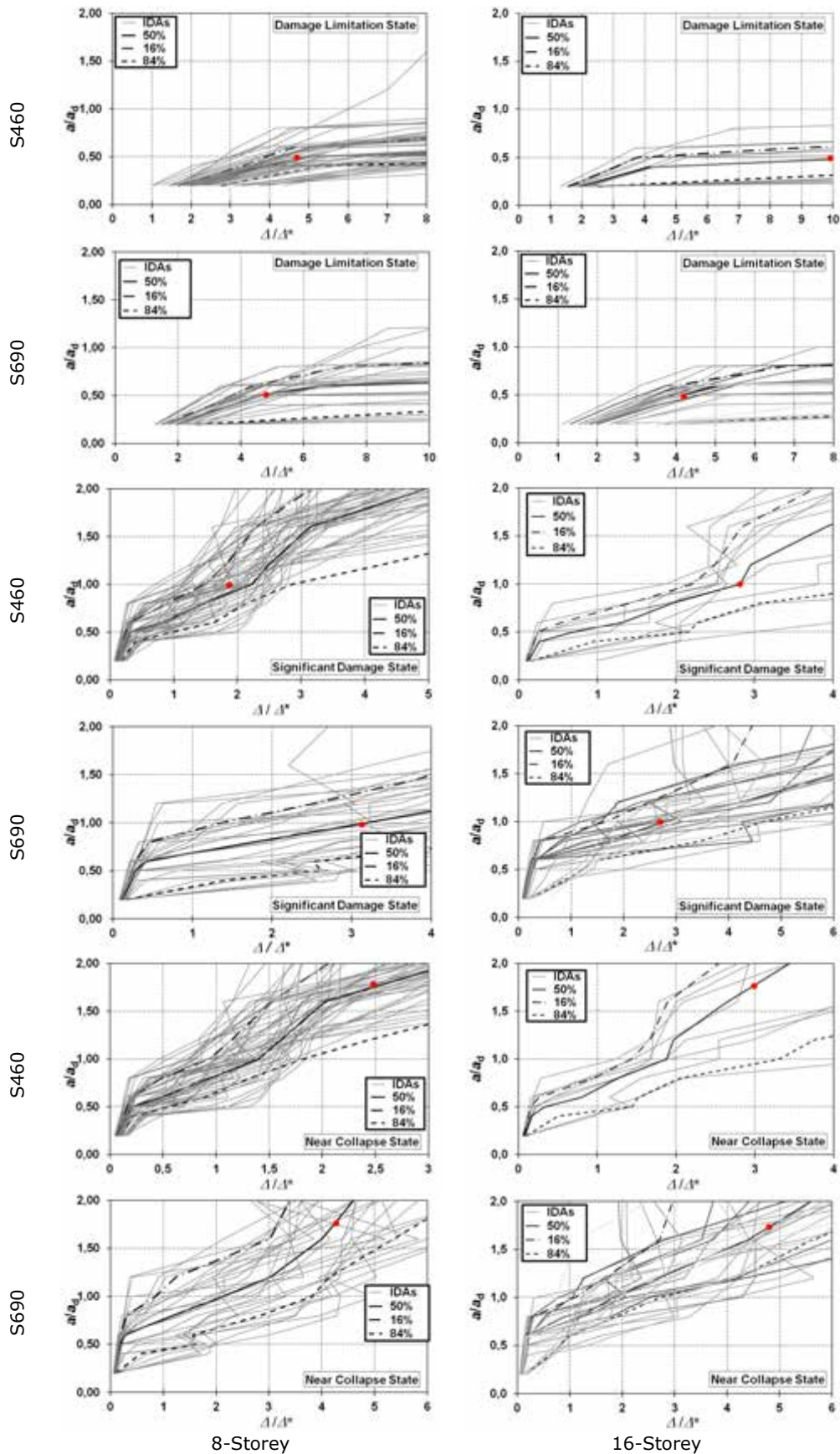


Figure 3.12. Rotation demand in beams of MRF spans: (a) 8-storeys, (b) 16-storeys



8-Storey 16-Storey
 Figure 3.13. Brace ductility demand for the three limit states

3.4.4 Eccentric Braced Frames

The ductility demand for EBF's is expressed in terms of link shear rotation (γ). According to Table 3.7, for DL $\gamma \leq 0.005$ rad, for SD $(\gamma - \gamma_v) \leq 0.08$ rad, while for NC $(\gamma - \gamma_v) \leq 0.10$ rad. The shear rotation (γ) was investigated and the ratio between the maximum values obtained for the seven records of each soil condition and the reference value allowed for each limit state is presented in Figure 3.14.

In addition, Figure 3.15 shows the median and the 16th and 84th percentiles of the maxima link shear overstrength (namely the ratio between the maximum shear and the plastic shear) against the corresponding peak shear rotation during the IDA's. It can be observed that the shear overstrength is consistent with the code values.

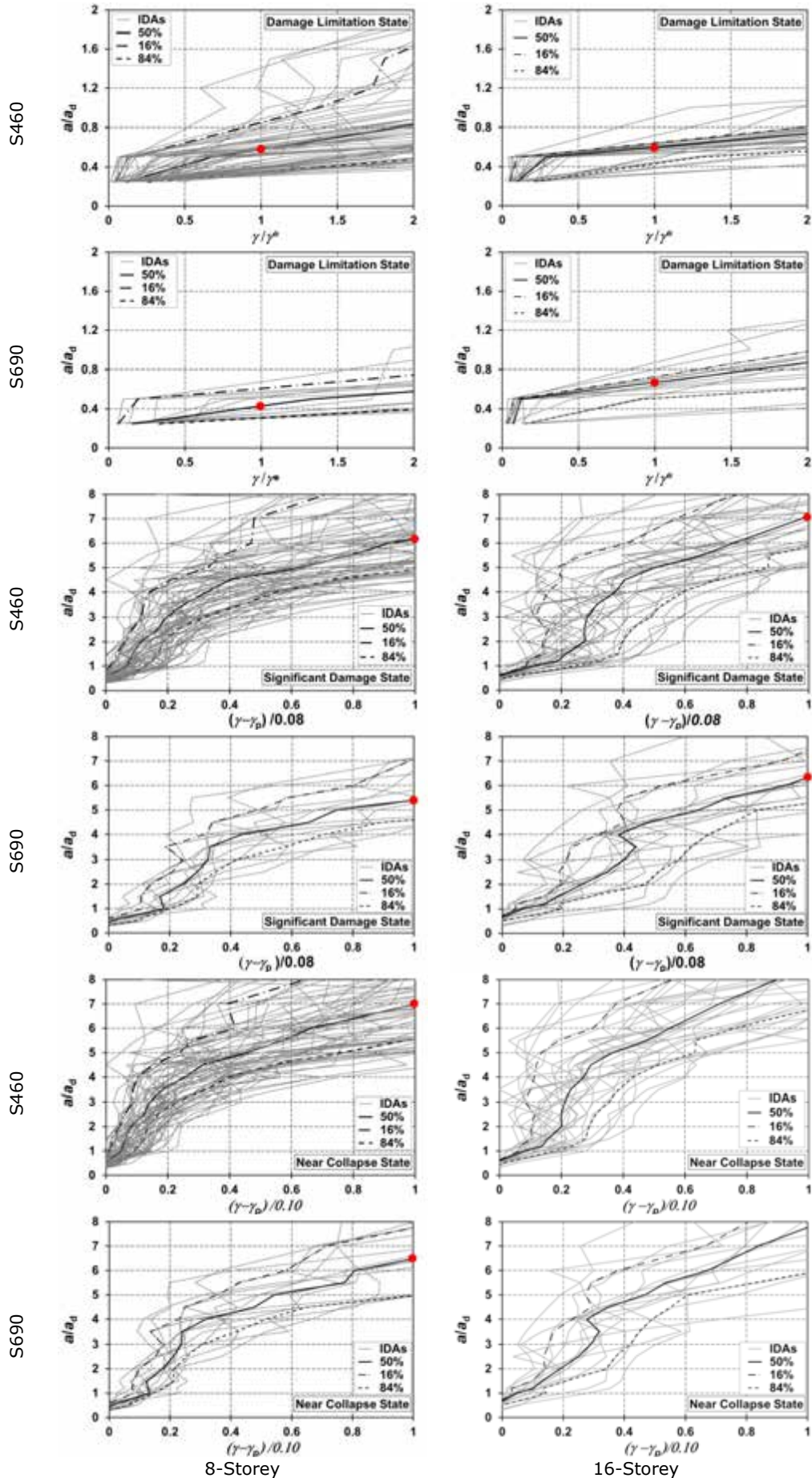


Figure 3.14. Link ductility demand for the three limit states

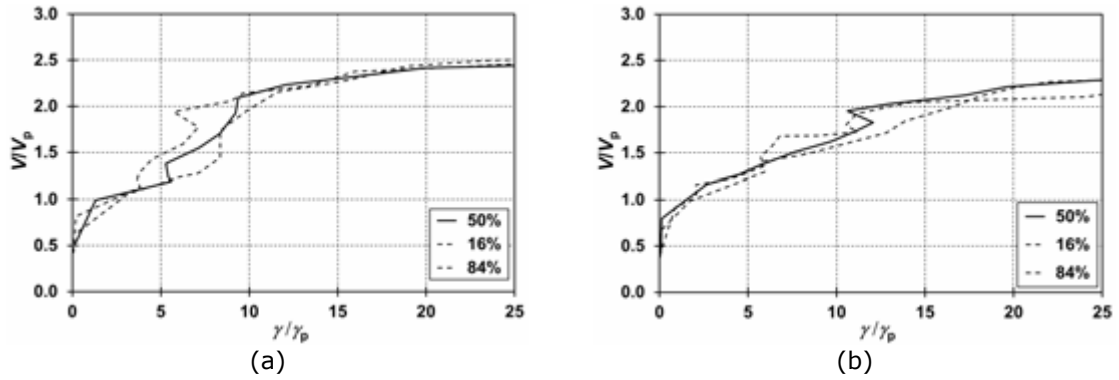


Figure 3.15. Link overstrength vs. link demand: (a) 8-storeys, (b) 16-storeys

3.4.5 Dual Eccentric Braced Frames

The ductility demand for D-EBF's is expressed in terms of both beam rotation, for the beams belonging to the MRF spans, and link shear rotation (γ), for the links in the braced spans. According to Table 3.7, the beam plastic rotation capacity should be no lesser than $10\theta_y$, $6\theta_y$ and respectively $8\theta_y$, for the DL, SD and NC performance levels, being θ_y the beam yield rotation. For what concerns the EBF's for DL $\gamma \leq 0.005$ rad, for SD $(\gamma - \gamma_y) \leq 0.08$ rad, while for NC $(\gamma - \gamma_y) \leq 0.10$ rad.

As it can be easily recognized in Figure 3.16, that the median value of beam rotation in the MRF span is lesser than the plastic rotation. Hence, the MRF's behave elastically in the most of cases.

The results in terms of shear rotation (γ) are shown in Figure 3.17. The comparison between Figure 3.14 and Figure 3.17 highlight that D-EBF's may exhibit a smaller rotation demand than EBF's.

Concerning the link shear overstrength, the results for D-EBF's are similar to those observed for EBF's as can be seen from the comparison between Figure 3.18 and Figure 3.15.

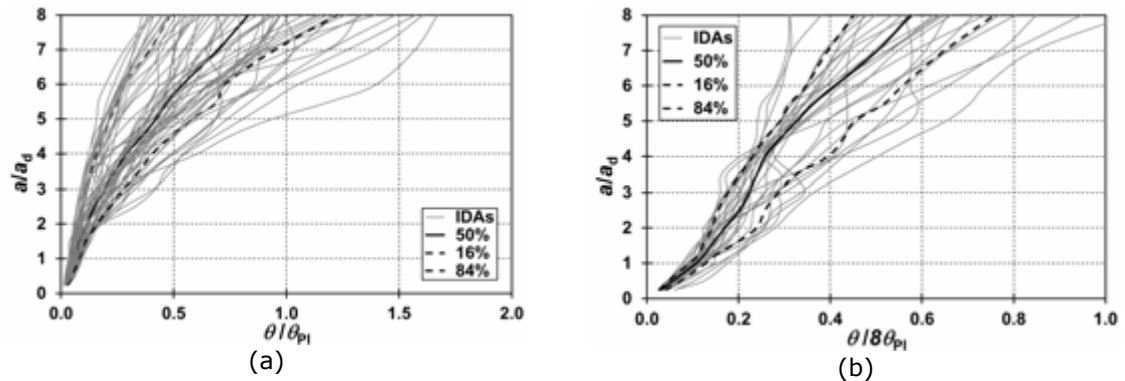
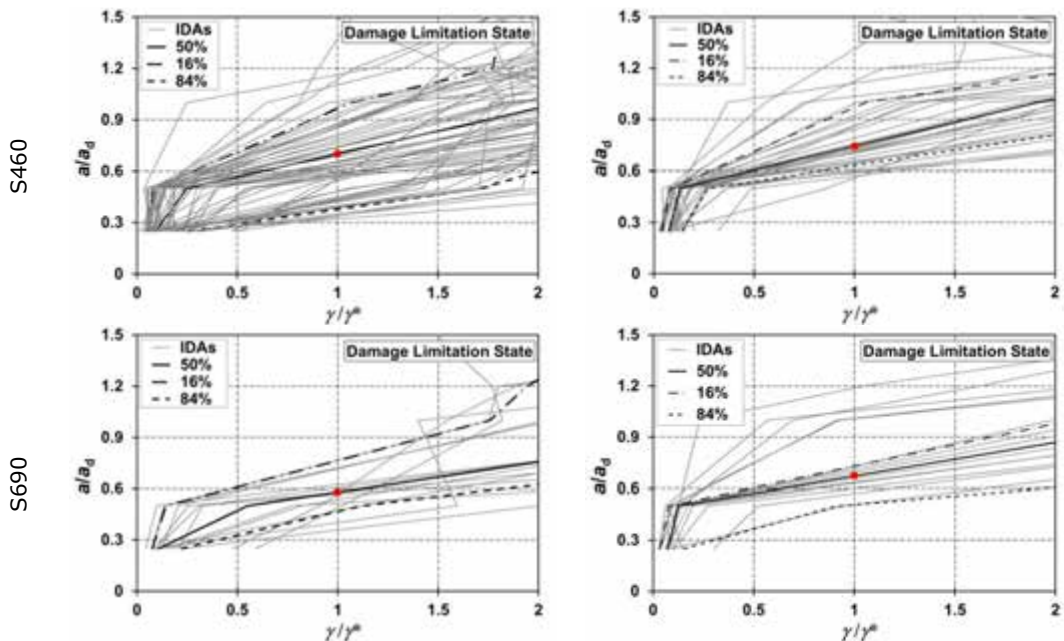


Figure 3.16. Rotation demand in beams of MRF spans: (a) 8-storeys, (b) 16-storeys



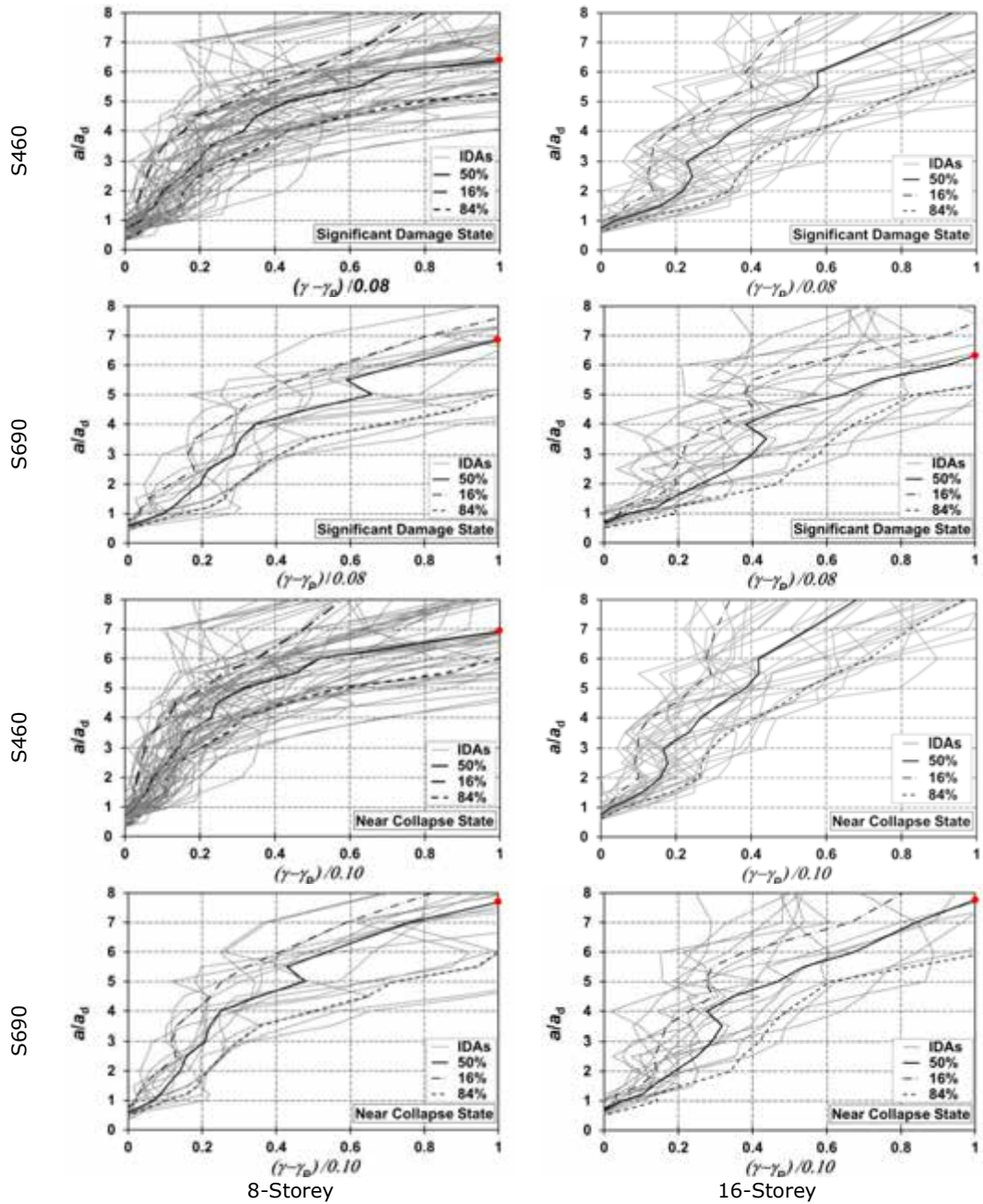


Figure 3.17. Link ductility demand for the three limit states

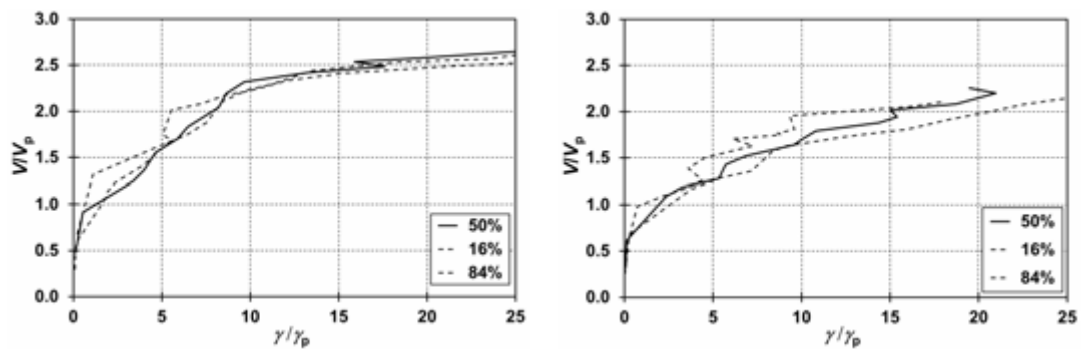


Figure 3.18. Link overstrength vs. link demand

3.5 Performance design levels and related q -factors

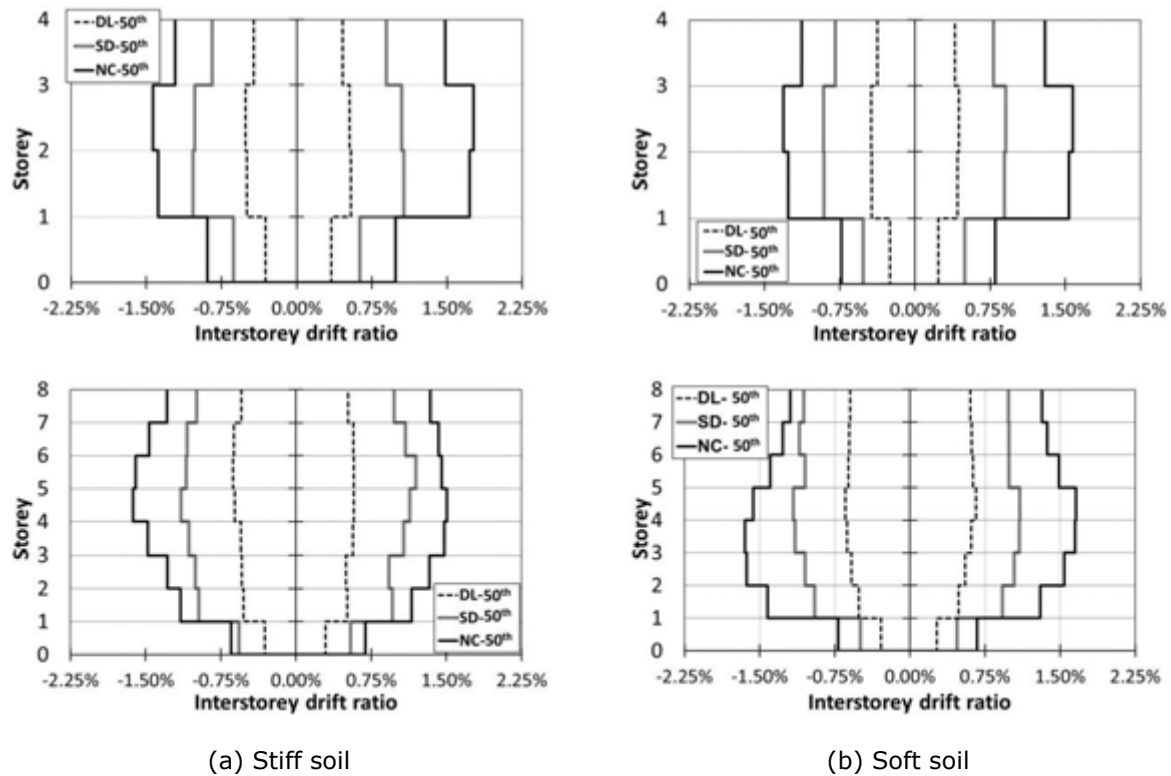
3.5.1 Moment Resisting Frames

3.5.1.1 Peak interstorey drift ratios for MRF's

Figure 3.19 depicts the median value of interstorey drift ratio (IDR) demand along the height for the three limit states. As a general remark, the examined design parameters do not highlight

appreciable influence on the IDR demand. However, it is interesting to note that the numerical results show an almost uniform distribution of IDR along the building height, expect for the first storey.

The IDR demand at each limit state was fairly lower than the performance limits. It is interesting to note that although the seismic design of the examined frames has been governed by drift limitation, the median values of IDR at DL state are significantly lower than the limit of 0.75%. At DL state, all frames behave in elastic field, being the yield IDR larger than 1% in most of the cases. Indeed, owing to this structural property a very limited inelastic demand can be observed at both SD and NC limit state. In particular, the median IDR for the SD also in the range 1% - 1.2% for 4- and 8-storey frames, thus significantly lower than the limit of 3.0%. Such results seem suggesting that dual-steel solution may lead to inefficient and uneconomical structures.



(a) Stiff soil (b) Soft soil
Figure 3.19. Interstorey drift demand for the three limit states: (a) 4 & 8 storey frames corresponding to stiff soil, (b) 4 & 8 storey frames corresponding to soft soil

3.5.1.2 Overstrength factors for MRF's

The overall overstrength factor (Ω) is defined in Eq. (3.2) as the product of two terms, namely the first terms is the ratio V_y/V_{1y} , (being V_y the ultimate base shear, and V_{1y} the base shear corresponding to the first yielding of the frame) and the second term V_{1y}/V_d (being V_d the design base shear force).

Table 3.8 reports the Ω factors obtained from the pushover analyses of the frames, summarizing also the two terms in which they are composed.

Analysing the ratio V_y/V_{1y} the pushover curves obtained with uniform load distribution show the lower values. As general outcome, the median value is equal to 1.36, thus very close to 1.30 recommended by EN 1998-1 [1]. Concerning the examined parameters, it is noticeable that frames having CFT columns show the higher overstrength factors, while the cases with FE and PE columns exhibit similar overstrength factors. The influence of the other design parameters is less significant on this factor.

Concerning the ratio V_{1y}/V_d , the pushover curves obtained with 1st mode load distribution show the lower values. Table 3.8 shows that significantly large values have been obtained. Indeed, the median of (V_{1y}/V_d) is equal to 3.85, thus very close to the design behaviour factor ($q = 4$). This result is ascribable to the need to satisfy the code drift requirements, which lead at oversizing the structural members to provide adequate lateral stiffness. This issue often arises in the design of ductile seismic resistant MRF's. However, in case of dual-steel frames this design procedure is even more necessary. Indeed, although the use of HSS allowed to guarantee the hierarchy criteria, the higher a steel grade of non-dissipative members is, the smaller is the corresponding size of cross sections, thus potentially resulting in very flexible frames.

Table 3.8 – Overstrength factors for MRF's

Frames	$\left(\frac{V_y}{V_{1y}}\right)_{\min}$	$\left(\frac{V_{1y}}{V_d}\right)_{\min}$	Ω	Frames (cont.)	$\left(\frac{V_y}{V_{1y}}\right)_{\min}$	$\left(\frac{V_{1y}}{V_d}\right)_{\min}$	Ω
MRF_1.1.1.1	1.17	3.78	4.60	MRF_3.1.1.1	1.35	4.00	5.59
MRF_1.1.1.2	1.19	3.84	4.80	MRF_3.1.1.2	1.45	4.16	6.10
MRF_1.1.1.3	1.20	3.86	4.66	MRF_3.1.1.3	1.49	4.19	6.28
MRF_1.1.2.1	1.21	2.94	3.60	MRF_3.1.2.1	1.43	3.71	5.34
MRF_1.1.2.2	1.21	3.09	3.79	MRF_3.1.2.2	1.46	3.92	6.27
MRF_1.1.2.3	1.54	3.11	4.91	MRF_3.1.2.3	1.49	3.96	6.23
MRF_1.2.1.1	1.43	3.44	5.02	MRF_3.2.1.1	1.26	4.22	5.55
MRF_1.2.1.2	1.44	3.52	5.26	MRF_3.2.1.2	1.29	4.38	5.94
MRF_1.2.1.3	1.54	3.71	7.46	MRF_3.2.1.3	1.36	4.53	6.30
MRF_1.2.2.1	1.28	3.18	4.32	MRF_3.2.2.1	1.24	4.52	5.91
MRF_1.2.2.2	1.31	3.24	4.44	MRF_3.2.2.2	1.29	4.67	6.37
MRF_1.2.2.3	1.44	3.25	4.46	MRF_3.2.2.3	1.38	4.76	6.96
				16 th	1.21	3.22	4.45
				50 th	1.36	3.85	5.45
				84 th	1.47	4.42	6.29

3.5.1.3 Behaviour factors for MRF's

The behaviour factor is given as the ratio between the peak ground acceleration leading to accepted failure for the selected performance level (A_U) and the peak ground acceleration corresponding to the yielding of the frame (A_Y). In the present study the values of A_Y and A_U have been derived from IDA's.

Table 3.9 shows the behaviour factors of MRF's and the 16th, 50th and 84th percentiles for both SD and NC limit state. The behaviour factors obtained for NC limit state are obviously larger than those for SD limit state, owing to the more demanding collapse criterion.

As a general remark, it should be noted that the median behaviour factors obtained from IDA's at SD are slightly lower than that used at the design stage (namely $q = 4$). However the median values of the total behaviour factor obtained from IDA's (q_t) are significantly larger than the codified ones, which means that the latter are conservative. Analysing the role of the examined design parameters it is not possible to define a general trend. Anyway, it is interesting to note that the frames located on soft soil present behaviour factors slightly lower than those designed for stiff soil.

Table 3.9 – Behaviour factors for MRF's

Frames	q-factors		Frames (cont.)	q-factors		
	SD	NC		SD	NC	
MRF_1.1.1.1	2.87	3.08	MRF_2.1.1.1	4.00	4.52	
MRF_1.1.1.2	2.86	3.50	MRF_2.1.1.2	3.93	4.05	
MRF_1.1.1.3	2.83	3.12	MRF_2.1.1.3	4.04	3.96	
MRF_1.1.2.1	2.62	3.10	MRF_2.1.2.1	3.38	3.47	
MRF_1.1.2.2	2.48	2.99	MRF_2.1.2.2	3.36	3.38	
MRF_1.1.2.3	3.40	3.86	MRF_2.1.2.3	3.30	3.69	
MRF_1.2.1.1	3.48	4.86	MRF_2.2.1.1	3.52	3.89	
MRF_1.2.1.2	3.39	4.10	MRF_2.2.1.2	3.29	3.42	
MRF_1.2.1.3	4.07	4.77	MRF_2.2.1.3	3.30	3.71	
MRF_1.2.2.1	3.36	7.16	MRF_2.2.2.1	2.63	2.62	
MRF_1.2.2.2	3.29	3.84	MRF_2.2.2.2	2.73	2.76	
MRF_1.2.2.3	3.79	4.23	MRF_2.2.2.3	3.09	2.84	
				16 th	2.80	3.05
				50 th	3.33	3.70
				84 th	3.83	4.32

3.5.2 Concentric Braced Frames

3.5.2.1 Peak interstorey drift ratios for CBF's

Figure 3.20 depicts the median value of interstorey drift ratio (IDR) demand along the height for the three limit states. The IDR demand at each limit state was lower than the performance limits. The median values of IDR at DL state are significantly lower than the limit of 0.5%. In particular, the median IDR for the SD is also in the range of 0.75% for 8- and 16-storey frames, while it is in the range of 1.5%-2% at NC. In all cases the larger demand has been recognized in soft soil conditions.

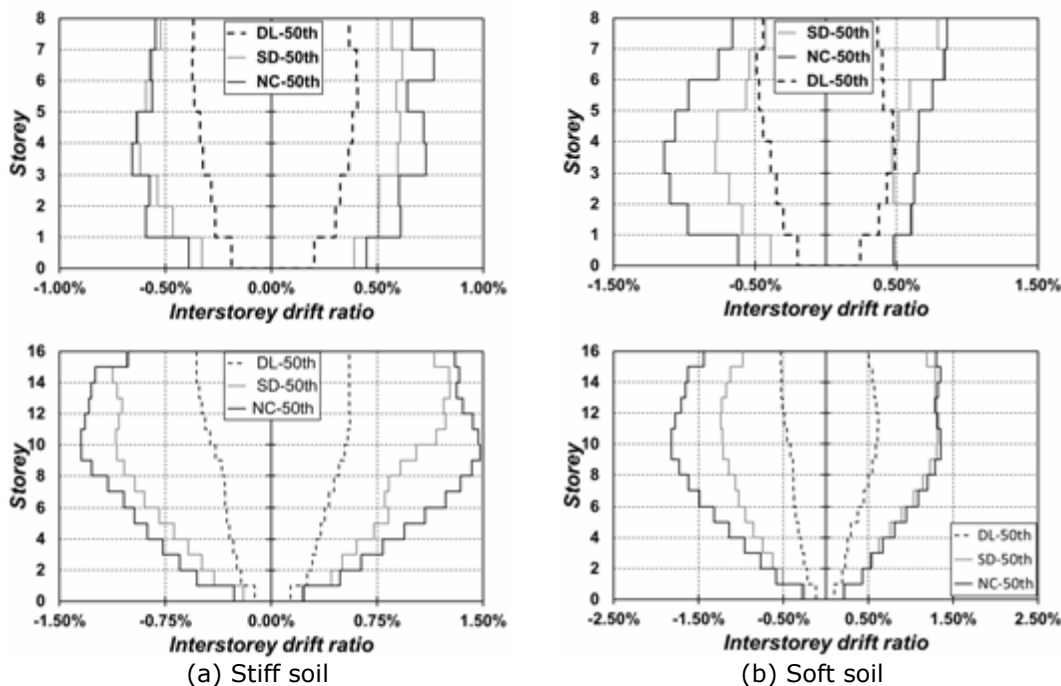


Figure 3.20. Interstorey drift demand for the three limit states

3.5.2.2 Overstrength factors for CBF's

The overstrength factors obtained from pushover analyses for CBF's are reported in Table 3.10. As it can be noted, the median value of the overstrength factor (Ω) is equal to 1.44.

Analysing the ratio V_y/V_{1y} , the median value is equal to 1.25, thus very close to the maximum value (namely 1.30) recommended by EN 1998-1 [1]. Concerning the examined parameters, the structures designed considering a soft soil condition show the smaller factor. Generally speaking, a reduction of overstrength when there is increasing of height. The influence of the other design parameters is less significant on this factor. Concerning the ratio V_{1y}/V_d , the pushover curves obtained with 1st mode load distribution show the lower values. Table 3.10 shows those values are close to 1 have been obtained. This result highlights that the design procedure allows selecting feasible sections for bracing members.

Table 3.10 – Overstrength factors for CBF's

Frames	$\left(\frac{V_y}{V_{1y}}\right)_{\min}$	$\left(\frac{V_{1y}}{V_d}\right)_{\min}$	Ω	Frames (cont.)	$\left(\frac{V_y}{V_{1y}}\right)_{\min}$	$\left(\frac{V_{1y}}{V_d}\right)_{\min}$	Ω
CBF_1.1.1.1.1	1.40	1.04	1.81	CBF_1.2.2.1.2	1.51	1.16	1.76
CBF_1.1.1.1.2	1.31	1.22	1.60	CBF_1.2.2.1.3	1.26	1.27	1.60
CBF_1.1.1.1.3	1.14	1.23	1.40	CBF_1.2.2.2.2	1.27	1.00	1.27
CBF_1.1.1.2.1	1.22	1.04	1.28	CBF_1.2.2.2.3	1.10	1.00	1.10
CBF_1.1.1.2.2	1.21	1.04	1.33	CBF_2.1.2.1.1	1.05	1.26	1.45
CBF_1.1.1.2.3	1.27	1.11	1.47	CBF_2.1.2.1.2	1.13	1.01	1.14
CBF_1.1.2.1.1	1.41	1.11	1.57	CBF_2.1.2.2.1	1.08	1.07	1.15
CBF_1.1.2.1.2	1.44	1.10	1.62	CBF_2.1.2.2.2	1.13	1.06	1.19
CBF_1.1.2.1.3	1.34	1.12	1.50	CBF_2.2.2.1.2	1.11	1.04	1.16
CBF_1.1.2.2.1	1.21	1.06	1.35	CBF_2.2.2.2.3	1.02	1.36	1.39
CBF_1.1.2.2.2	1.22	1.07	1.34	CBF_2.2.2.2.2	1.20	1.28	1.54
CBF_1.1.2.2.3	1.19	1.06	1.31	CBF_2.2.2.2.3	1.15	1.40	1.61
				16 th	1.21	1.04	1.33
				50 th	1.25	1.09	1.44
				84 th	1.40	1.14	1.60

3.5.2.3 Behaviour factors for CBF's

Table 3.11 shows the behaviour factors of CBF's and the 16th, 50th and 84th percentiles for both SD and NC limit state. The behaviour factors obtained for NC limit state are obviously larger than those for SD limit state, owing to the more demanding collapse criterion.

Table 3.11 – Behaviour factors for CBF's

Frames	q-factors		Frames (cont.)	q-factors	
	SD	NC		SD	NC
CBF_1.1.1.1	2.65	3.24	CBF_2.1.1.1	2.02	2.42
CBF_1.1.1.2	2.12	2.52	CBF_2.1.1.2	1.61	2.10
CBF_1.1.1.3	2.29	2.57	CBF_2.1.1.3	1.53	1.68
CBF_1.1.2.1	2.09	2.59	CBF_2.1.2.1	1.34	1.44
CBF_1.1.2.2	2.09	2.59	CBF_2.1.2.2	1.41	1.51
CBF_1.1.2.3	2.08	2.44	CBF_2.1.2.3	1.63	1.76
CBF_1.2.1.1	2.12	2.91	CBF_2.2.1.1	1.49	1.74
CBF_1.2.1.2	2.03	2.79	CBF_2.2.1.2	1.91	2.19
CBF_1.2.1.3	1.87	2.21	CBF_2.2.1.3	1.27	1.35
CBF_1.2.2.1	1.72	1.96	CBF_2.2.2.1	1.35	1.79
CBF_1.2.2.2	1.72	1.93	CBF_2.2.2.2	1.56	1.98
CBF_1.2.2.3	1.66	2.02	CBF_2.2.2.3	1.23	1.34
			16 th	1.39	1.63
			50 th	1.72	2.06
			84 th	2.10	2.59

As a general remark, it should be noted that the median behaviour factor (equal to 1.72) obtained from IDA's at SD is slightly lower than that used at the design stage (namely $q = 2.5$). Even the median values of the total behaviour factor obtained from IDA's (q_t) are lower than the codified ones. Analysing the role of the examined design parameters it is not possible to define a general trend. Anyway, it is interesting to note that the frames located on soft soil present behaviour factors slightly lower than those located on stiff soil.

Generally speaking, it should be noted that the small behaviour factors are due to the severe performance limits imposed by EN 1998-3 [21] for the brace ductility demand. In addition, the analyses showed that the beams from braced bays develop a plastic hinge in the mid-point, and that the braces suffer an increase of ductility demand associated to the large deformation of these beams.

3.5.3 Dual Concentric Braced Frames

3.5.3.1 Peak interstorey drift ratios for D-CBF's

Figure 3.21 depicts the median value of interstorey drift ratio (IDR) demand along the height of the D-CBF's for the three limit states. The IDR demand at each limit state was lower than the performance limits. The median values of IDR at DL state are significantly lower than the limit of 0.5%. In particular, the median IDR for the SD also smaller than 1% for 8- and 16-storey frames, while it is in the range 1.5%-2% at NC. In all cases the larger demand has been recognized in soft soil conditions.

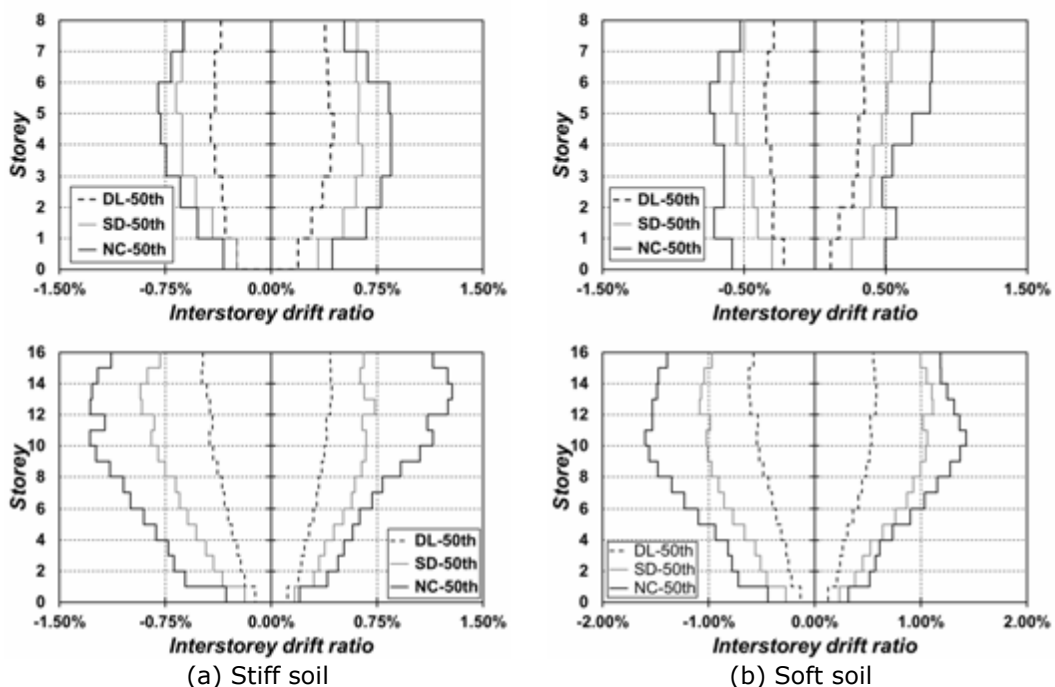


Figure 3.21. Interstorey drift demand for the three limit states

3.5.3.2 Overstrength factors for D-CBF's

The overstrength factors obtained from the pushover analyses of D-CBF's are reported in Table 3.12. As it can be noted, the median value of the overstrength factor (Ω) is equal to 2.21.

Analysing the ratio V_y/V_{1y} , the median value is equal to 1.51, thus larger than 1.30 (namely the value suggested by EN 1998-1 [1]), but smaller than the maximum value equal to 1.60. Concerning the examined parameters, the structures designed considering a soft soil condition show the smaller factor. Generally speaking, an overstrength reduction can be noticed when there is an increase of the height. The influence of the other design parameters is less significant on this factor. Concerning the ratio V_{1y}/V_d , the pushover curves obtained with 1st mode load distribution show the lower values. Table 3.12 shows those ratio have a median value equal to 1.44. This result highlights that the design procedure for D-CBF leads to larger oversizing of the bracing members.

Table 3.12 – Overstrength factors for D-CBF's

Frames	$\left(\frac{V_y}{V_{1y}}\right)_{\min}$	$\left(\frac{V_{1y}}{V_d}\right)_{\min}$	Ω	Frames (cont.)	$\left(\frac{V_y}{V_{1y}}\right)_{\min}$	$\left(\frac{V_{1y}}{V_d}\right)_{\min}$	Ω
D-CBF_1.1.1.1.1	1.36	1.60	2.18	D-CBF_1.2.2.1.2	1.75	1.78	3.12
D-CBF_1.1.1.1.2	1.36	1.57	2.14	D-CBF_1.2.2.1.3	1.81	1.77	3.20
D-CBF_1.1.1.1.3	1.39	1.62	2.25	D-CBF_1.2.2.2.2	1.42	1.53	2.17
D-CBF_1.1.1.2.1	1.47	1.44	2.12	D-CBF_1.2.2.2.3	1.40	1.44	2.02
D-CBF_1.1.1.2.2	1.45	1.00	1.45	D-CBF_2.1.2.1.1	1.92	1.18	2.27
D-CBF_1.1.1.2.3	1.55	1.48	2.29	D-CBF_2.1.2.1.2	1.86	1.23	2.29
D-CBF_1.1.2.1.1	1.66	1.64	2.72	D-CBF_2.1.2.2.1	1.39	1.10	1.53
D-CBF_1.1.2.1.2	1.70	1.68	2.86	D-CBF_2.1.2.2.2	1.87	1.30	2.43
D-CBF_1.1.2.1.3	1.65	1.62	2.67	D-CBF_2.2.2.1.2	1.98	1.10	2.18
D-CBF_1.1.2.2.1	1.40	1.25	1.75	D-CBF_2.2.2.2.3	1.46	1.00	1.46
D-CBF_1.1.2.2.2	1.39	1.33	1.85	D-CBF_2.2.2.2.2	1.87	1.26	2.36
D-CBF_1.1.2.2.3	1.33	1.45	1.93	D-CBF_2.2.2.2.3	2.14	1.37	2.93
				16 th	1.39	1.15	1.82
				50 th	1.51	1.44	2.21
				84 th	1.87	1.63	2.77

3.5.3.3 Behaviour factors for D-CBF's

Table 3.13 shows the behaviour factors of D-CBF's and the 16th, 50th and 84th percentiles for both SD and NC limit state. The behaviour factors obtained for NC limit state are obviously larger than those for SD limit state, owing to the more demanding collapse criterion.

As a general remark, it should be noted that the median behaviour factor (equal to 2.37) obtained from IDA's at SD are slightly lower than that used at the design stage (namely $q = 4.8$). Even the median values of the total behaviour factor obtained from IDA's (q_t) are lower than the codified ones. Analysing the role of the examined design parameters it is not possible to define a general trend. Anyway, it is interesting to note that the frames located on soft soil present behaviour factors slightly lower than those designed for stiff soil. Generally speaking, it should be noted that the small behaviour factors are due to the severe performance limits imposed by EN 1998-3 [21] for the brace ductility demand. In addition, as recognized for CBF's, also in D-CBF's the beams from braced bays presented plastic hinge in the mid-point, the braces suffer an increase of ductility demand associated to the large deformation of these beams. Indeed, this fact is more evident for the dual-system because they were designed for a higher behaviour factor resulting in a flexible structure, i.e. the beams from braced bays have smaller flexural stiffness.

Table 3.13 – Behaviour factors for D-CBF's

Frames	q-factors		Frames (cont.)	q-factors		
	SD	NC		SD	NC	
D-CBF_1.1.1.1	2.96	3.69	D-CBF_2.1.1.1	2.62	3.45	
D-CBF_1.1.1.2	3.23	3.72	D-CBF_2.1.1.2	2.6	3.05	
D-CBF_1.1.1.3	3.78	4.49	D-CBF_2.1.1.3	2.16	2.48	
D-CBF_1.1.2.1	2.64	3.67	D-CBF_2.1.2.1	2.00	2.29	
D-CBF_1.1.2.2	2.71	3.52	D-CBF_2.1.2.2	1.71	2.01	
D-CBF_1.1.2.3	2.39	2.89	D-CBF_2.1.2.3	2.49	2.76	
D-CBF_1.2.1.1	2.85	3.77	D-CBF_2.2.1.1	1.86	2.15	
D-CBF_1.2.1.2	3.25	4.18	D-CBF_2.2.1.2	2.25	2.44	
D-CBF_1.2.1.3	2.34	3.13	D-CBF_2.2.1.3	1.93	2.1	
D-CBF_1.2.2.1	1.89	2.31	D-CBF_2.2.2.1	1.78	1.92	
D-CBF_1.2.2.2	2.12	2.42	D-CBF_2.2.2.2	1.78	2.11	
D-CBF_1.2.2.3	2.23	2.52	D-CBF_2.2.2.3	2.76	2.74	
				16 th	1.88	2.14
				50 th	2.37	2.75
				84 th	2.89	3.70

3.5.4 Eccentric Braced Frames

3.5.4.1 Peak interstorey drift ratios for EBF's

Figure 3.22 depicts the median value of interstorey drift ratio (IDR) demand along the height of the EBF's for the three limit states. The IDR demand at each limit state was lower than the performance limits. The median values of IDR at DL state are significantly lower than the limit of 0.5%. In particular, the median IDR for the both SD and NC are smaller than 1% for 8-storey frames and 1.5% for 16-storey frames. In all cases the larger demand has been recognized in soft soil conditions.

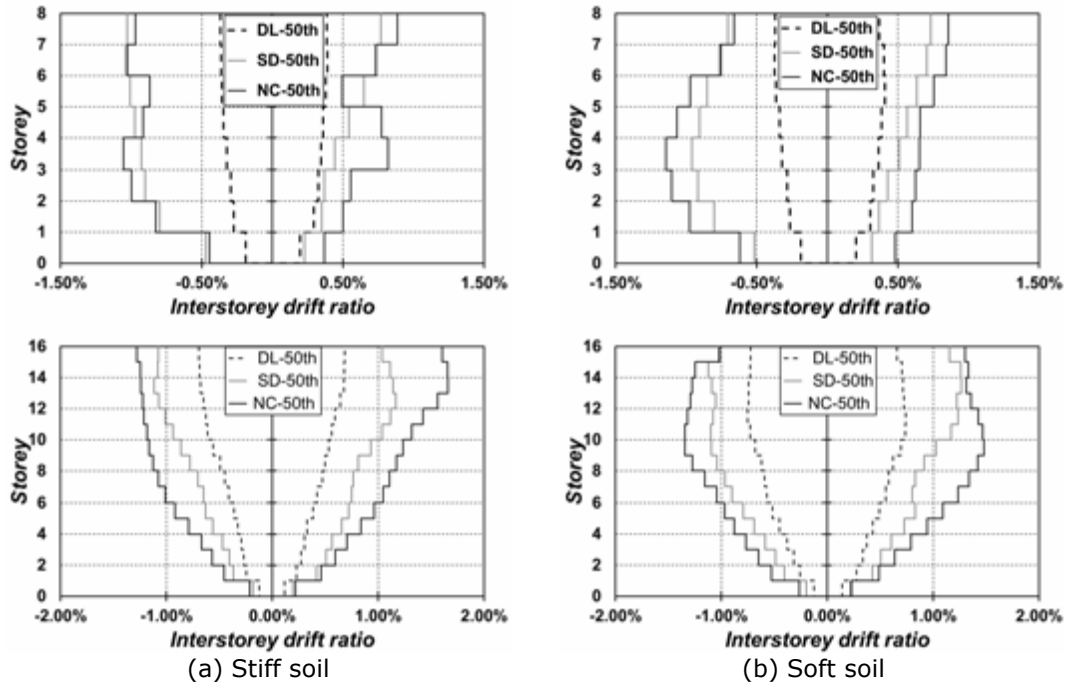


Figure 3.22. Interstorey drift demand for the three limit states

3.5.4.2 Overstrength factors for EBF's

The overstrength factors obtained from pushover analyses for EBF's are reported in Table 3.14. As it can be noted, the median of the overstrength factor (Ω) is equal to 3.18.

Table 3.14 – Overstrength factors for EBF's

Frames	$\left(\frac{V_y}{V_{1y}}\right)_{\min}$	$\left(\frac{V_{1y}}{V_d}\right)_{\min}$	Ω	Frames (cont.)	$\left(\frac{V_y}{V_{1y}}\right)_{\min}$	$\left(\frac{V_{1y}}{V_d}\right)_{\min}$	Ω
EBF_1.1.1.1.1	1.19	2.46	2.94	EBF_1.2.2.1.2	1.31	2.15	2.81
EBF_1.1.1.1.2	1.25	2.31	2.89	EBF_1.2.2.1.3	1.19	2.48	2.95
EBF_1.1.1.1.3	1.46	2.23	3.25	EBF_1.2.2.2.2	1.23	2.88	3.55
EBF_1.1.1.2.1	1.15	2.07	2.39	EBF_1.2.2.2.3	1.35	2.30	3.11
EBF_1.1.1.2.2	1.23	2.88	3.55	EBF_2.1.2.1.1	1.51	3.09	4.65
EBF_1.1.1.2.3	1.23	2.87	3.55	EBF_2.1.2.1.2	1.55	3.01	4.65
EBF_1.1.2.1.1	1.47	1.73	2.54	EBF_2.1.2.2.1	1.54	2.21	3.41
EBF_1.1.2.1.2	1.36	1.88	2.55	EBF_2.1.2.2.2	1.49	2.36	3.52
EBF_1.1.2.1.3	1.37	2.53	3.47	EBF_2.2.2.1.2	1.52	2.97	4.50
EBF_1.1.2.2.1	1.32	1.69	2.23	EBF_2.2.2.2.3	1.58	2.25	3.56
EBF_1.1.2.2.2	1.22	2.39	2.92	EBF_2.2.2.2.2	1.25	2.31	2.89
EBF_1.1.2.2.3	1.36	2.27	3.08	EBF_2.2.2.2.3	1.21	2.68	3.25
				16 th	1.22	2.12	2.73
				50 th	1.34	2.34	3.18
				84 th	1.51	2.88	3.55

Analysing the ratio V_y/V_{1y} the median value is equal to 1.34, thus close to 1.30 that is the value suggested by EN 1998-1 [1]. Concerning the examined parameters, the structures designed considering a soft soil condition show the smaller factor. Generally speaking, a reduction of overstrength when there is increasing of height. The influence of the other design parameters is less significant on this factor. Concerning the ratio V_{1y}/V_d , the pushover curves obtained with 1st mode load distribution show the lower values. Table 3.14 shows those ratio have a median value equal to 2.34. Consequently, the design procedure for EBF's leads to oversize the link section.

3.5.4.3 Behaviour factors for EBF's

Table 3.15 shows the behaviour factors of EBF's and the 16th, 50th and 84th percentiles for both SD and NC limit state. The behaviour factors obtained for NC limit state are obviously larger than those for SD limit state, owing to the more demanding collapse criterion.

As a general remark, it should be noted that the median behaviour factor (equal to 3.35) obtained from IDA's at SD are noticeably lower than that used at the design stage (namely $q = 6$). However the median values of the total behaviour factor obtained from IDA's (q_t) are significantly larger than the codified ones, which means that the latter are conservative. Analysing the role of the examined design parameters it is not possible to define a general trend. Anyway, it is interesting to note that the frames located on soft soil present behaviour factors slightly lower than those designed for stiff soil. Generally speaking, it should be noted that the small behaviour factors are due to the brace buckling, thus highlighting that the design criteria given by EN 1998-1 [1] are not effective to guarantee the expected performance.

Table 3.15 – Behaviour factors for EBF's

Frames	q-factors		Frames (cont.)	q-factors	
	SD	NC		SD	NC
EBF_1.1.1.1.1	3.10	3.10	EBF_1.2.2.1.2	3.85	4.60
EBF_1.1.1.1.2	2.94	2.94	EBF_1.2.2.1.3	3.28	3.45
EBF_1.1.1.1.3	3.02	3.02	EBF_1.2.2.2.2	2.37	2.37
EBF_1.1.1.2.1	4.43	5.40	EBF_1.2.2.2.3	3.14	3.29
EBF_1.1.1.2.2	3.10	3.10	EBF_2.1.2.1.1	4.44	4.44
EBF_1.1.1.2.3	3.52	3.84	EBF_2.1.2.1.2	4.57	4.57
EBF_1.1.2.1.1	3.26	3.26	EBF_2.1.2.2.1	4.26	4.26
EBF_1.1.2.1.2	3.31	3.31	EBF_2.1.2.2.2	3.86	3.86
EBF_1.1.2.1.3	3.36	3.47	EBF_2.2.2.1.2	4.80	4.80
EBF_1.1.2.2.1	2.81	2.81	EBF_2.2.2.2.3	3.50	3.88
EBF_1.1.2.2.2	2.83	2.83	EBF_2.2.2.2.2	4.08	4.18
EBF_1.1.2.2.3	3.33	3.50	EBF_2.2.2.2.3	3.58	4.16
			16 th	3.00	3.00
			50 th	3.35	3.49
			84 th	4.31	4.48

3.5.5 Dual Eccentric Braced Frames

3.5.5.1 Peak interstorey drift ratios for D-EBF's

Figure 3.23 depicts the median value of interstorey drift ratio (IDR) demand along the height of the D-EBF's for the three limit states. The IDR demand at each limit state was lower than the performance limits. The median values of IDR at DL state are significantly lower than the limit of 0.5%. In particular, the median IDR for the both SD and NC are smaller than 1% for both 8- and 16- storey frames. In all cases the larger demand has been recognized in soft soil conditions.

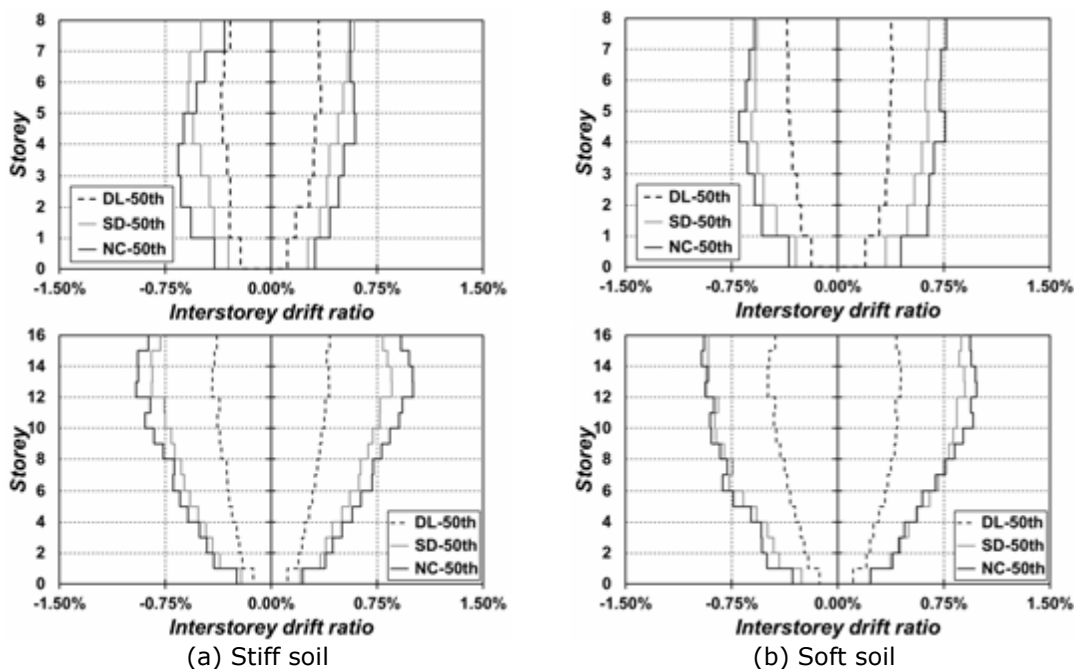


Figure 3.23. Interstorey drift demand for the three limit states

3.5.5.2 Overstrength factors for D-EBF's

The overstrength factors obtained from pushover analyses of D-EBF's are reported in Table 3.16. As it can be noted, the median value of the overstrength factor (Ω) is equal to 4.16.

Analysing the ratio V_y/V_{1y} , the median value is equal to 1.46, thus close to 1.30 that is the value suggested by EN 1998-1 [1]. Concerning the examined parameters, the structures designed considering a soft soil condition show the smaller factor. Generally speaking, a reduction of overstrength when there is increasing of height. The influence of the other design parameters is less significant on this factor.

Concerning the ratio V_{1y}/V_d , the pushover curves obtained with 1st mode load distribution show the lower values. Table 3.16 shows those ratio have a median value equal to 2.85. This result highlights that the design procedure for D-EBF's leads to oversize of the link section.

Table 3.16 – Overstrength factors for D-EBF's

Frames	$\left(\frac{V_y}{V_{1y}}\right)_{\min}$	$\left(\frac{V_{1y}}{V_d}\right)_{\min}$	Ω	Frames (cont.)	$\left(\frac{V_y}{V_{1y}}\right)_{\min}$	$\left(\frac{V_{1y}}{V_d}\right)_{\min}$	Ω
D-EBF_1.1.1.1.1	1.49	2.52	3.75	D-EBF_1.2.2.1.2	1.51	2.47	3.73
D-EBF_1.1.1.1.2	1.44	2.55	3.67	D-EBF_1.2.2.1.3	1.47	2.73	4.02
D-EBF_1.1.1.1.3	1.51	2.47	3.75	D-EBF_1.2.2.2.2	1.45	3.25	4.69
D-EBF_1.1.1.2.1	1.50	2.47	3.71	D-EBF_1.2.2.2.3	1.41	3.06	4.33
D-EBF_1.1.1.2.2	1.43	3.00	4.30	D-EBF_2.1.2.1.1	1.34	4.95	6.65
D-EBF_1.1.1.2.3	1.46	3.49	5.09	D-EBF_2.1.2.1.2	1.45	4.52	6.55
D-EBF_1.1.2.1.1	1.37	2.63	3.61	D-EBF_2.1.2.2.1	1.47	3.87	5.69
D-EBF_1.1.2.1.2	1.49	2.35	3.51	D-EBF_2.1.2.2.2	1.42	3.81	5.40
D-EBF_1.1.2.1.3	1.63	2.98	4.84	D-EBF_2.2.2.1.2	1.43	4.44	6.34
D-EBF_1.1.2.2.1	1.51	2.39	3.61	D-EBF_2.2.2.2.3	1.34	3.84	5.13
D-EBF_1.1.2.2.2	1.47	2.53	3.71	D-EBF_2.2.2.2.2	1.49	2.60	3.88
D-EBF_1.1.2.2.3	1.48	2.51	3.71	D-EBF_2.2.2.2.3	1.46	2.99	4.36
				16 th	1.42	2.47	3.70
				50 th	1.46	2.85	4.16
				84 th	1.51	3.85	5.50

3.5.5.3 Behaviour factors for D-EBF's

Table 3.17 shows the behaviour factors of D-EBF's and the 16th, 50th and 84th percentiles for both SD and NC limit state. The behaviour factors obtained for NC limit state are obviously larger than those for SD limit state, owing to the more demanding collapse criterion.

IDA's at SD are noticeably lower than that used at the design stage (namely $q = 6$). However the median values of the total behaviour factor obtained from IDA's (q_t) are significantly larger than the codified ones, which means that the latter are conservative. Analysing the role of the examined design parameters it is not possible to define a general trend. Anyway, it is interesting to note that the frames located on soft soil present behaviour factors slightly lower than those designed for stiff soil. Generally speaking, it should be noted that the small behaviour factors are due to the brace buckling, thus highlighting that the design criteria given by EN 1998-1 [1] are not effective to guarantee the expected performance.

Table 3.17 – Behaviour factors for D-EBF's

Frames	q-factors		Frames (cont.)	q-factors		
	SD	NC		SD	NC	
D-EBF_1.1.1.1.1	4.37	4.37	D-EBF_1.2.2.1.2	4.18	4.78	
D-EBF_1.1.1.1.2	4.59	4.59	D-EBF_1.2.2.1.3	4.69	4.89	
D-EBF_1.1.1.1.3	4.48	4.48	D-EBF_1.2.2.2.2	4.05	4.05	
D-EBF_1.1.1.2.1	5.67	5.67	D-EBF_1.2.2.2.3	4.57	4.75	
D-EBF_1.1.1.2.2	5.16	5.16	D-EBF_2.1.2.1.1	4.39	4.39	
D-EBF_1.1.1.2.3	5.10	5.10	D-EBF_2.1.2.1.2	4.80	4.80	
D-EBF_1.1.2.1.1	4.66	4.96	D-EBF_2.1.2.2.1	3.14	4.51	
D-EBF_1.1.2.1.2	6.03	6.41	D-EBF_2.1.2.2.2	2.99	2.99	
D-EBF_1.1.2.1.3	5.26	5.49	D-EBF_2.2.2.1.2	4.64	4.64	
D-EBF_1.1.2.2.1	3.75	3.75	D-EBF_2.2.2.2.3	4.53	4.69	
D-EBF_1.1.2.2.2	3.64	3.64	D-EBF_2.2.2.2.2	3.98	3.98	
D-EBF_1.1.2.2.3	4.91	5.02	D-EBF_2.2.2.2.3	4.51	4.67	
				16 th	3.91	4.02
				50 th	4.55	4.68
				84 th	5.12	5.12

3.6 Concluding remarks

Within Chapter 3, the outcomes of an extensive numerical programme have been presented. The aim was to investigate and evaluate the seismic performance of typical dual-steel frame typologies. The main objectives can be summarised as follows: (i) to establish ductility demands for members and connections for the structural systems investigated in the project; (ii) to determine overstrength factors to be used in the further versions of EN 1998-1-1 [1] for capacity design of non-dissipative members; (iii) to provide behaviour factors associated to different performance levels that could be used in code-based design procedures for design of dual-steel structures.

Following the introduction, a brief description was made in relation to the numerical programme, i.e. type of analyses, configuration of the case study frames. Further on, several topics were presented in relation to the non-linear analyses of frames, particularly: seismic hazard and performance levels, selection of accelerograms, overall overstrength factor, behaviour factors, failure criteria and relevant acceptance criteria, and numerical models. From the investigation of the case study frames, the main results are presented regarding: performance based evaluation of ductility and over-strength demands, and performance design levels and related q -factors.

The parametric study, based on nonlinear static and dynamic analyses, allowed to evaluate the seismic performance of dual-steel moment-resisting frames (MRF's), concentrically braced frames (CBF's), dual concentrically braced frames (D-CBF's), eccentrically braced frames (EBF's) and dual eccentrically braced frames (D-EBF's). The seismic performance-based evaluation has been carried out considering three limit states according to EN 1998-3 [21], namely damage limitation (DL), significant damage (SD) and near collapse (NC).

Based on the analysis of the results, the following conclusions can be drawn:

- For MRF's and for the moment resisting bays of dual structures, the use of HSS showed to be efficient to guarantee the weak-beam/strong-column behaviour.
- Regarding the MRF's, pushover analyses showed that the overall overstrength factors (Ω) could be larger than the design behaviour factor ($q = 4$). This result is ascribable to the codified design procedure, which leads to increase the member size to satisfy the drift limitations. Indeed, using HSS for columns small sections need to satisfy hierarchy criteria, thus having flexible structures.
- For CBF's and D-CBF's the pushover analyses showed that the design overstrength is slightly larger than 1.0, while the behaviour factors are smaller than the values employed in seismic design according to EN 1998-1 [1]. The analyses showed that the poor performance is mainly due to the large brace ductility demand in compression. In addition, the frames with flexible beams in the braced bays showed the poorest performance. Hence, the use of HSS for beams of braced bays is not advisable.
- For EBF's and D-EBF's pushover analyses showed that the average over-strength factor can be noticeably larger than the value indicated by EN 1998-1 [1]. This result is due to the design assumption, since the beams containing the links should be designed to resist vertical load that makes unfeasible the use of sections strictly sufficient for the seismic actions. It is also important to note that both static and dynamic analyses showed that the performance of the structures designed according to EN 1998-1 [1] are affected by the brace buckling. Due to the occurrence of this phenomenon, the behaviour factors of EN 1998-1 [1] compliant frames are significantly lower than the codified values.
- Nonlinear dynamic analyses showed that the frames have a seismic demand (namely, transient interstorey drift ratios, beam ductility) fairly below the proposed limit for DL, SD and NC states. In particular, only for MRF's at SD limit state the most of frames behave in elastic field. This result is mainly due to the design oversizing. Such results seem suggesting that dual-steel solution for MRF's may lead to inefficient and uneconomical structures.
- For MRF's, EBF's and D-EBF's, the total behaviour factors (q_t) obtained from incremental dynamic analyses, corresponding to SD limit state, are larger than the codified ones. However, in case of the analysed CBF and D-CBF structures, smaller behaviour factors were obtained from IDA in comparison with the considered values from the initial design. These results suggest that care should be taken for design of CBF's and D-CBF's.

4 Experimental investigation of joint assemblies and components

4.1 *Introduction*

Chapter 4 is related to the entire experimental program of "HSS-SERF" project carried out on joint assemblies and components, and which was focused on the following topics:

- Investigation of weld details and T-stubs;
- Investigation of bolted beam-to-column joints in moment-resisting dual-steel frames;
- Investigation of welded beam-to-column joints in moment-resisting dual-steel frames;
- Investigation of steel-concrete connection (load introduction tests) in case of concrete filled tubes, considering the use of long bolts and respectively shot fired nails;

The investigation of weld details and T-stubs were performed as part of WP3, which was focused on quantification of welded and bolted connections for the particular situation of joining High Strength Steel (HSS) and Mild Carbon Steel (MCS) elements used in dual-steel structural configurations. The experimental programme covering welded cruciform joints, bolted T-stubs and material tests was performed at the University of Stuttgart. The activities conducted in WP3 are linked to the activities conducted in other work packages. Particularly, the form, geometry and configuration of specimens were planned in cooperation with WP4 for the bolted connections and WP5 for the welded connections. The combination of HSS and MCS requires practical experiences in welding technology. Therefore welding procedures for the dual-steel cases (HSS and MCS) have been fixed in collaboration with the Italian Institute of Welding. Additionally, based on the outcomes of WP3, a set of guidelines for welding of dissimilar steel grades were developed within WP6.

The investigation of bolted beam-to-column joints were performed at University of Liege as part of WP4, which was focused on the pre-qualification of bolted beam-to-column joints in moment-resisting dual-steel frames. The activities conducted within WP4 are linked to the activities conducted within other work packages. Particularly, the design of the tested specimens was realised in WP1, the T-stubs extracted from the bolted joint configurations were investigated within WP3, the experimental results from WP4 have been used to validate the design guidelines of the joints within WP6, and the proposed joints were also used to evaluate the technical and economic efficiency of dual-steel structures in WP7.

The investigation of welded beam-to-column joints was performed at University of Ljubljana and Politehnica University of Timisoara as part of WP5, which was focused on the pre-qualification of welded beam-to-column joints in moment-resisting dual-steel frames. The activities conducted within WP5 are linked to the activities conducted within other work packages. Particularly, the design of the tested specimens was realised in WP1, the welding procedures for the dual-steel cases (HSS and MCS) have been established within WP3 which investigated the performance of weld details, the experimental results from WP5 have been used to validate the design guidelines of the joints developed in WP6, and the proposed joints were also used to evaluate the technical and economic efficiency of dual-steel structures in WP7.

The investigation of steel-concrete connection (load introduction tests) in case of concrete filled tube columns were performed as part of WP4 at University of Liege considering the use of long bolts, and respectively as part of WP5 at Politehnica University of Timisoara considering the use of shot fired nails.

The outcomes of the entire experimental program are presented in the containing sections of Chapter 4. Consequently, for each topic, a description is made with regard to the objectives, specimen configuration, experimental test set-up, instrumentation, loading procedure, material sample tests (bolts and nails, welds, concrete, steel plates and profiles), primary test results, interpretation and evaluation of results, and concluding remarks.

4.2 *Ductility and strength demands of weld details and T-stubs*

Within the framework of the project, University of Stuttgart was responsible for experimental investigations of welded details and bolted connections within WP3. The WP was focused on investigations quantifying the connection behaviour of welded and bolted connections for the particular situation of joining High Strength Steel (HSS) and Mild Carbon Steel (MCS) elements used in dual-steel structural configurations. An extensive experimental programme including 96 tests on welded Cruciform Joints (CJ), 86 tests on bolted T-stubs, and a high number of material tests were performed at the University of Stuttgart. The test configurations in WP3 should reproduce loading conditions to which critical welded and bolted connections are usually subjected under seismic action aiming at the evaluation of strength and ductility subjected to monotonic and cyclic loading.

The form, geometry and kind of specimens tested in WP3 at the University of Stuttgart were dependent and had been planned in cooperation with WP4 for the bolted connections, and WP5 for the welded connections. The design process for the beam-to-column connections led to very specific details in WP4 and WP5. Therefore the initially planned T-stub components according to the models in EN 1993-1-8 [46] were modified. For this reason the content of WP3 regarding the testing program was adapted for the specific cases in order to test T-stub specimens consistent with the beam-to-column connections applied in WP4 for the bolted connections and WP5 for the welded connections.

In the following part, experimental and numerical results are presented regarding the investigations carried out on material samples, as well as on welded and bolted connections. The extended information (experimental program, test results, interpretation and evaluation of results) are presented within Deliverable D3 – “Report on performance of welded details and T-stubs; Recommendations of welding procedures to be used in dual-steel structures for welded connections between HSS and MCS” [47].

4.2.1 Material tests

4.2.1.1 General

One of the purposes of material tests is to supply standard data on material properties in order to be able to compare them without any ambiguity. The tensile tests were realised according to EN ISO 6892-1 [48] and have been performed as static tensile tests in a hydraulic testing machine. The machine was controlled through the indications of the extensometer fixed on the test piece to ensure a constant deformation rate.

The material testing programme at the University of Stuttgart included material tensile tests on:

- Bolts;
- Base metal;
- Welds cut out of fillet welds (series KN);
- Filler metal (series SN).

In order to determine the throat thickness of the Cruciform Joint specimens and to verify the quality level for imperfections according to EN ISO 5817 [49] macro investigations and hardness measurements were accomplished according to EN ISO 9015-1 [50].

4.2.1.2 Tests on bolts

Tests on bolts are especially important to allow for a numerical recalculation of bolted connection T-stub tests, see Section 4.2.3.4 (numerical investigations). The entire experimental program for tensile tests on bolts was carried out at the internal laboratory of FUCHS Schraubenwerk in 57076 Siegen, due to the more appropriate testing equipment. Under displacement control, all bolts were subjected to a tensile axial force which was applied through the testing machine, in particular through a crosshead. The tensile tests were continued until fracture occurred.

Bolt assemblies in M24 HV property class 10.9 (hot-dip galvanised) according to EN 14399-4 [51] and a pair of washers according to EN 14399-6 [52] were used for all T-stub configurations to be tested in WP3. Bolt lengths from 60 mm up to 85 mm were required for the T-stubs to be tested. It was not possible to fix the testing equipment to these short bolt lengths, therefore it was decided to set up a testing programme on bolts consisting of 3 different test configurations (see Figure 4.1) in order to receive as much as possible information of the behaviour of the pure bolt material and the bolt behaviour itself subjected to tensile force.

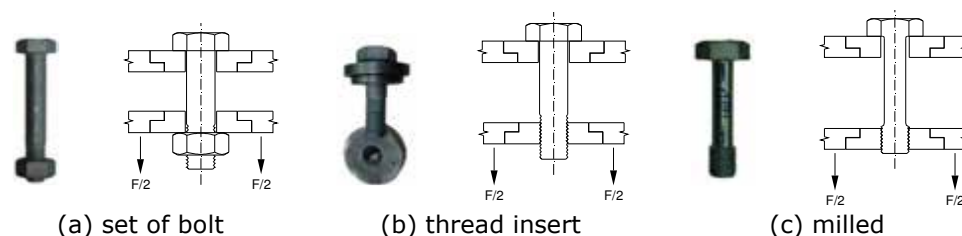


Figure 4.1. Experimental programme on bolts

A number of 6 tensile tests on "milled bolt shank" were accomplished in order to receive data for the behaviour of the pure bolt material. Consequently, the bolt shank was machined and milled to a defined diameter (D_0) and gauged length (L_0) in order to refer to while calculating strains and stresses. Additional 14 tests on the entire bolts were carried out in order to investigate the difference when the bolt is "thread inserted" or when the bolt is tested as "set of bolt" with nuts.

The curve "milled bolt shank" shown in Figure 4.2-a, is typical for a ductile material without a pronounced yield point. The initial part of the plot is linear since the material is behaving in an elastic manner (Hooke's law). If the load is released at any point the specimen will return to its original length. As it can be seen clearly in Figure 4.2-b for the tensile tests "thread insert" and "set of bolt" there is no clear difference in strength and ductility. The bolt failed in the free loaded threaded shank, contrarily to the well known failure mechanism, when the thread is being stripped. Equally to the failure mechanism of series "thread insert" the bolts in series "set of bolt" failed in the free loaded threaded shank.

In Table 4.1 the measured material characteristics for selected examples on the test configuration "milled", "thread insert" and "set of bolt" are given. The overstrength value γ_{ov} represents the ration between the measured yield strength $R_{p0.2}$ and the nominal yield strength for bolts M24 HV property class 10.9 (900 N/mm²).

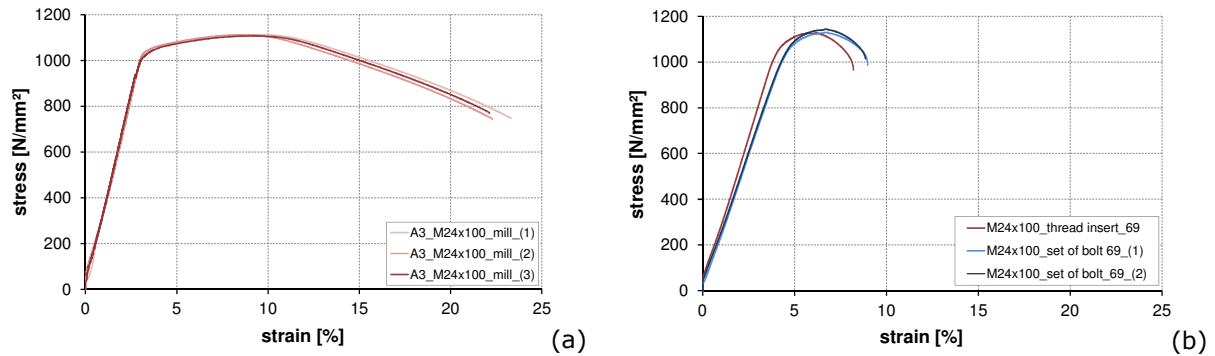


Figure 4.2. Results from tensile tests on bolts: (a) pure material, (b) thread insert & set of bolt

Table 4.1 – Extract from tensile tests on bolts shown in Figure 4.2

HV-bolt	Test configuration		$R_{p0.2}$ [N/mm ²]	R_m [N/mm ²]	A_g [%]	A_{gt} [%]	A [%]	A_t [%]	$R_m/R_{p0.2}$ [-]	γ_{ov} [-]
M24x100	milled	M24x100_mill_(1)	1031.2	1113.3	5.97	9.28	21.09	23.31	1.08	1.15
	milled	M24x100_mill_(2)	1043.7	1111.9	5.30	8.70	20.03	22.29	1.07	1.16
	milled	M24x100_mill_(3)	1015.2	1107.7	5.86	9.11	19.88	22.13	1.09	1.13
	thread insert	M24x100_thread insert_69	1080.0	1128.6	1.76	6.17	4.43	8.20	1.05	1.20
	set of bolt	M24x100_set of bolt_69_(1)	1048.9	1130.2	1.91	6.69	4.81	8.98	1.08	1.17
	set of bolt	M24x100_set of bolt_69_(2)	1076.4	1144.5	1.79	6.69	4.52	8.86	1.06	1.20

4.2.1.3 Tests on base metal

Considering that it is important to obtain the material characteristics through independent tests, for all plates and all thicknesses used both in Cruciform Joint (CJ) and T-stub (TS) specimens, a total number of 46 tensile tests were performed at the laboratory of Germanischer Lloyd (GL) in Esslingen near Stuttgart.

Figure 4.3 shows an excerpt of results from nominal engineering stress-strain relation tensile tests on steel grade S355. The experiments were driven under displacement control.

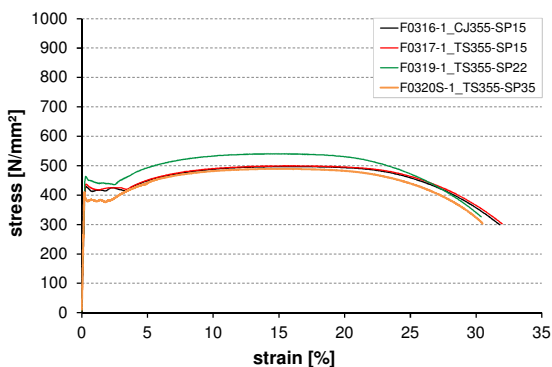


Figure 4.3. Stress-strain curve for tensile tests on steel grade S355

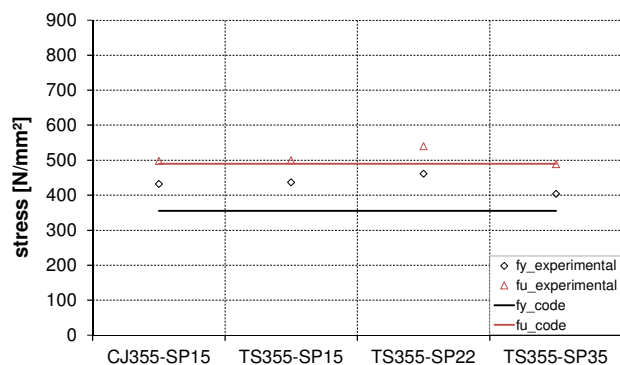


Figure 4.4. Yield strength and ultimate strength for steel grade S355

The four typical regions of the stress-strain curve of a low carbon structural steel are very clear: linear elastic region, yield plateau, strain hardening region and strain softening or necking portion, after the maximum load has been reached. As it can also be seen in Figure 4.3 non-consistent steel grades were delivered by RIVA. That means, no direct comparison among the different plate thicknesses is possible due to different technical delivery conditions (S355 J2+N / S355 J0+R / S355 J2+M). However, the overstrength factor γ_{ov} turned out to be relatively constant.

Besides, a pronounced material ductility could be observed. Figure 4.4 shows a comparison for yield strength and ultimate strength for steel grade S355 compared to the code provisions. Obviously, the measured data fulfil the code provisions. In general it has to be underlined that the independently made tensile test comply with the material certificates delivered by the steel supplier.

The stress-strain curves for steel grade S460 are shown in Figure 4.5. Additionally, Figure 4.6 shows a comparison for yield strength and ultimate strength for steel grade S460 compared to the code provisions. The test results also comply with the provisions.

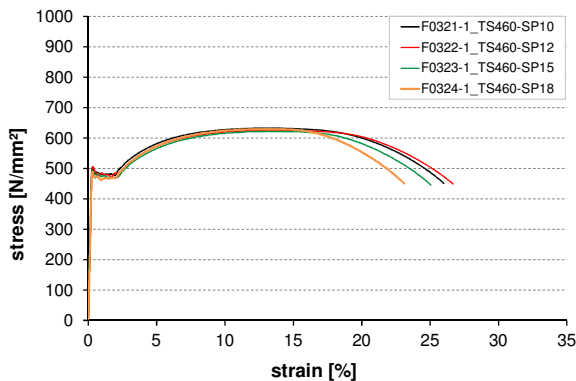


Figure 4.5. Tensile tests on steel grade S460

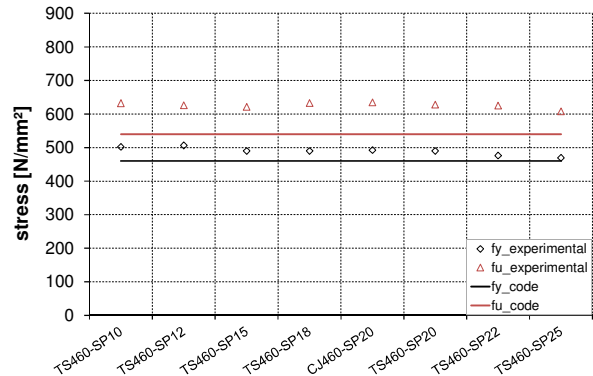


Figure 4.6. Yield strength and ultimate strength for steel grade S460

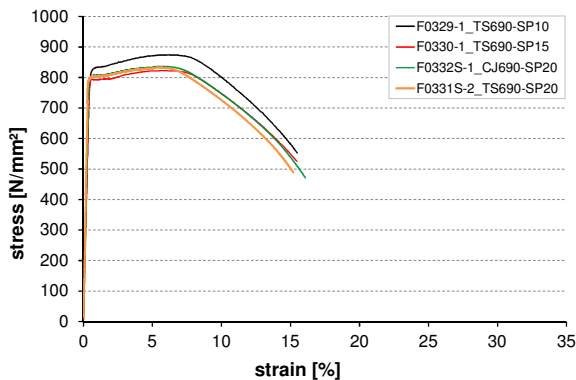


Figure 4.7. Tensile tests on steel grade S690

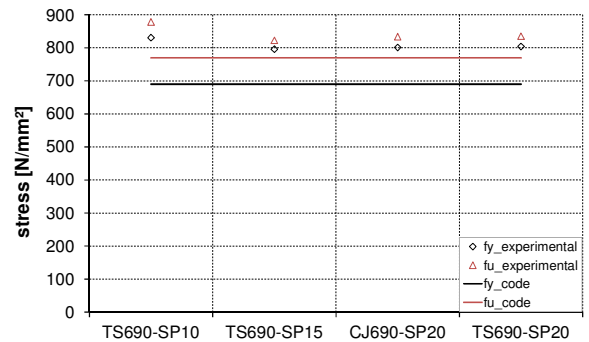


Figure 4.8. Yield strength and ultimate strength for steel grade S690

Whereas for steel grade S355 a very high ductility could be observed and furthermore for Mild Carbon Steel (MCS) a pronounced yield point was detected, for High Strength Steel (HSS) the yield strength was non-pronounced. Figure 4.8 points out that both the experimental measured yield strength and tensile strength for steel grade S690 exceeded the nominal code provisions. With regard to the tests performed on steel samples, the measurements satisfied the minimum requirements according to each steel grade as specified by the standards EN 10025-2 [53] and EN 10025-6 [54]. Therefore, the steel grade of each component for both Cruciform Joints and T-stubs was confirmed.

Figure 4.9 shows the distribution of modulus of elasticity for each steel plate thickness whereas in Figure 4.10 the percentage elongation after fracture (A) is demonstrated. A clear continuity among the steel grades and plate thicknesses could be observed.

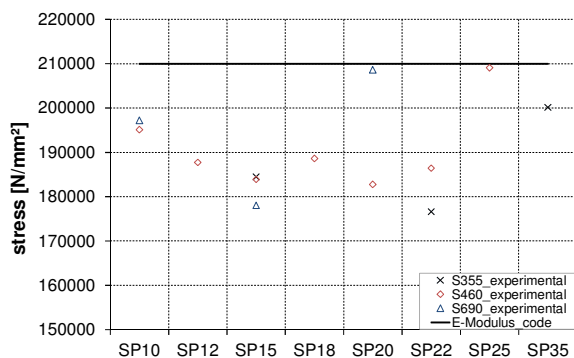


Figure 4.9. Modulus of elasticity

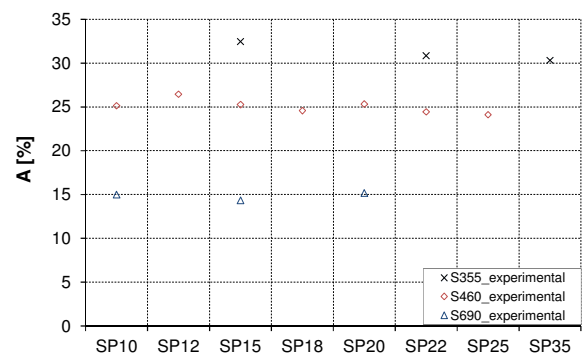


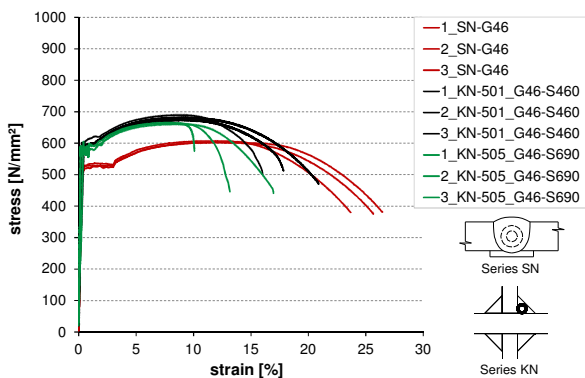
Figure 4.10. Elongation after fracture (A) [%]

4.2.1.4 Tests on filler metal

In order to observe yield strength, ultimate force and ductility and also to get material input data for FE simulations, a total number of 12 tensile tests on machined pieces of round cross-section cut out of filler metal from Cruciform Joint specimens were realised under quasi-static loading conditions (series KN).

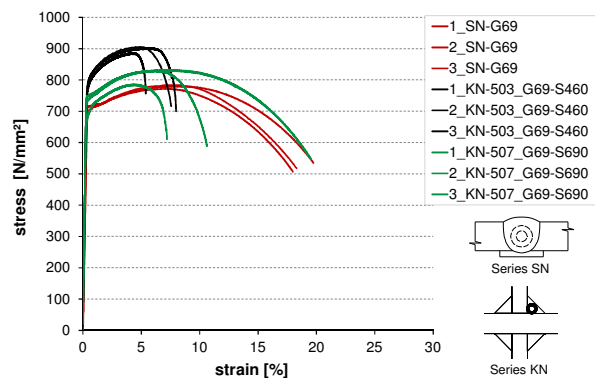
For Cruciform Joint specimens two different filler metals were used for both, fillet and full-penetration welds, G46 and G69. In order to obtain "pure" filler metal behaviour with regard to strength and ductility 6 tensile tests (3 for each filler metal) on machined test pieces of round cross-section from thick butt welds were realised under quasi-static loading conditions (series SN).

Figure 4.11 demonstrates the stress-strain curve for pure filler metal G46 compared to the results from the tensile test of series KN, where filler metal G46 is used. A clear tendency to increase in strength for tests out of fillet weld (KN) compared to tests out of pure filler metal (SN) can be observed. No significant influence on strength could be observed among fillet welds with matching base material and with overstrength base material, see KN-501 and KN-505 in Figure 4.11. Concerning the ductility, a certain decrease of the different series KN specimens could be observed. Figure 4.12 points out the difference between tests out of pure filler metal (SN) with filler metal G69 and series KN, where filler metal G69 was used. One reason for increased strength may be fusing of base and filler metal. The decrease in ductility for filler metal G69 is much more pronounced than for filler metal G46.



SN-G46 | KN-501_G46-S460 | KN-505_G46-S690

Figure 4.11. Stress-strain curves of filler metal G46



SN-G69 | KN-503_G69-S460 | KN-507_G69-S690

Figure 4.12. Stress-strain curves of filler metal G69

4.2.1.5 Hardness measurements

Additionally to the tensile tests on welded specimens, hardness measurements were accomplished on specimens for macro examination. As it is well known hardness measurements are widely used for the quality control of materials because they are quick and non-destructive tests if the marks or indentations produced by the measurements are in low stress areas. In general, hardness is the property of a material that corresponds to plastic deformation and therefore to the yield strength. To investigate the differences and influences between Cruciform Joints with different filler metals and different base metals Figure 4.15 and Figure 4.16 show hardness measurements on specimens for macro examination.

Hardness measurement were performed along two lines, see Figure 4.13 and Figure 4.14. Line 1 is placed near the surface of the weld starting from point 1 to point 15, and line 2 is placed through the weld root starting from point 16 to point 28. The regions of the base metal (Longitudinal Plate and Cross Plate), the heat affected zone (HAZ) and the filler metal (FM) are marked. It has to be underlined that the tensile strength placed on the right Y axis is based on a rough correlation between hardness and tensile strength, generally used for base plates, not for melted regions.

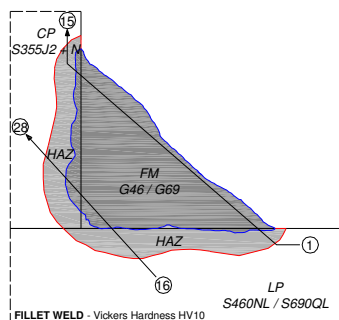


Figure 4.13. Testing scheme - indenter lines



Figure 4.14. Close up (indenter lines)

Comparing the values of hardness in the region of the weld (HAZ + FM + HAZ) no clear difference could be observed between connections G46/S460 and G46/S690, see Figure 4.15. This fact corresponds to the results of the tensile test of series SN (see Figure 4.11). In contrast, comparing the values of the hardness in the region of the weld (HAZ + FM + HAZ) for connections G69/S460 and G69/S690, Figure 4.16, it seems that the hardness of the weld made of filler metal G69 is 25 - 40 % higher than for the filler metal G46.

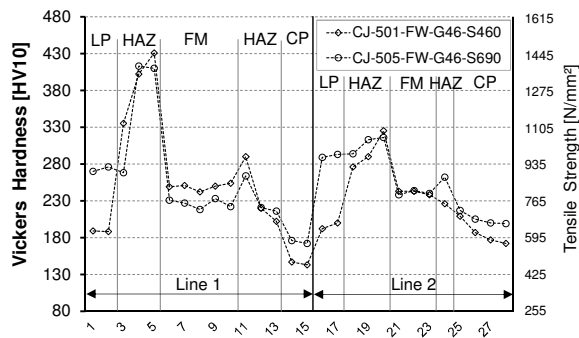


Figure 4.15. Comparison of hardness of filler metal G46 and different base metal (S460 / S690)

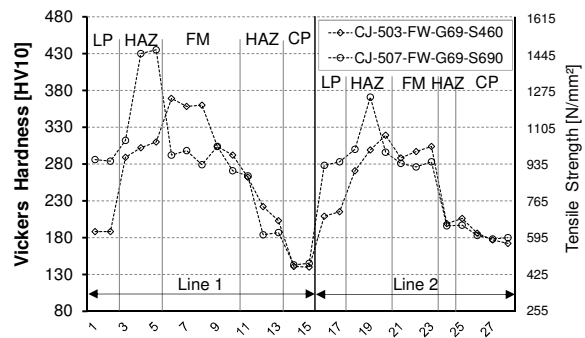


Figure 4.16. Comparison of hardness of filler metal G69 and different base metal (S460 / S690)

4.2.1.6 Macro investigations

Macro investigations presented in the current Section were performed in order to assess the quality and geometry of the weld. Figure 4.17 and Figure 4.18 demonstrate in an exemplary manner the macro investigation of a fillet weld, namely CJ-501-FW-G46-S460 and CJ-502-FPW-G46-S460.

As it can be clearly seen in Figure 4.17 (circled in red) the macro investigations indicated pores and lack of fusion at the weld root. Therefore the welds do not comply with the requirements according to EN ISO 15614-1 [55] and EN ISO 5817 [49], quality level B. The requirements for quality level B with regard to imperfections correspond to the level "high". Most of the tests observations showed offsets, lack of fusion at the root of the weld, incompletely filled groove and excessive asymmetry at some welds. This is especially remarkable because nevertheless the welds did not fail at the Cruciform Joints, see Section 4.2.2.4. Regarding the target value for the throat thickness of the fillet welds (12 mm) the actual measured throat thicknesses comply with the target value. More detailed information is given in the Deliverable D3 "Report on performance of welded details and T-stubs; Recommendations of welding procedures to be used in dual-steel structures for welded connections between HSS and MCS" [47].

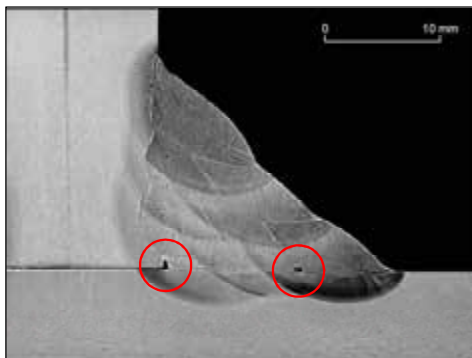


Figure 4.17. Close up CJ-501-FW-G46-S460

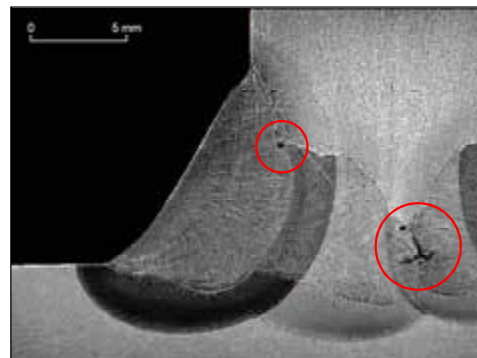


Figure 4.18. Close up CJ-502-FPW-G46-S460

4.2.2 Welded Connections – Cruciform Joints

4.2.2.1 General

The Cruciform Joints (Series 500) represent the welded plates of the beam flange with the column web in the welded joints of WP5 where columns were made of high strength steel (HSS) and beams of mild carbon steel (MCS). Therefore the Cruciform Joints can be considered as an extraction of the welded connection between HSS and MCS in the welded joints of WP5. Similar situations occur if a mild carbon steel flange is welded directly to a HSS end-plate.

These connections were experimentally analysed by "Cruciform Joints" combining rectangular welded plates of MCS (S355 J2+N) and HSS (S460 NL / S690 QL) in order to investigate the load-displacement or stress-strain behaviour and the ductility under loading conditions of seismic action.

The welds were designed as "full-strength" according to the rules for connections in dissipative zones in EN 1993-1-8 [46] and EN 1998-1 [1] with intended failure in the base plate and not in the

weld. For fillet welds the design was made in order to fulfil the rules according to EN 1998-1 [1], clause 6.5.5.(3), while full penetration welds were deemed to satisfy the overstrength criterion (EN 1998-1 [1], clause 6.5.5.(2)). As it is shown in Table 4.2 the parameters varied for the Cruciform Joint specimens are the choice of steel grade for the longitudinal plate (S460 NL or S690 QL), the filler metal (G46 or G69), the weld type (fillet weld (FW) or full penetration weld (FPW)) and the type of loading. It should be noted that the cross plate is always of MCS (S355 J2+N) plate material with a thickness of 15 mm and the longitudinal plate of HSS with a thickness of 20 mm, differing on S460 NL and S690 QL, see Table 4.2. In sum there are 8 cruciform joint variations, labelled with series number 501 to 508 and prefixed with the initials CJ, i.e. Cruciform Joints.

Table 4.2 – Cruciform Joint variations

#	Series number	Base metal 1 Cross Plate t = 15 mm	Base metal 2 Longitudinal Plate t = 20 mm	Filler metal	Fillet weld	Full penetration weld
501	CJ-501-FW-G46-S460	S355 J2+N	S460 NL	G46	✓	
502	CJ-502-FPW-G46-S460	S355 J2+N	S460 NL	G46		✓
503	CJ-503-FW-G69-S460	S355 J2+N	S460 NL	G69	✓	
504	CJ-504-FPW-G69-S460	S355 J2+N	S460 NL	G69		✓
505	CJ-505-FW-G46-S690	S355 J2+N	S690 QL	G46	✓	
506	CJ-506-FPW-G46-S690	S355 J2+N	S690 QL	G46		✓
507	CJ-507-FW-G69-S690	S355 J2+N	S690 QL	G69	✓	
508	CJ-508-FPW-G69-S690	S355 J2+N	S690 QL	G69		✓

For each series, the type of loadings realised were at least 1 monotonic quasi-static, 2 monotonic dynamic, 3 cyclic quasi-static and 6 cyclic dynamic loadings for each variations. Additionally pre-tests (in sum 7) were done in order to calibrate the machine control, the instrumentation as well as the testing procedure. A total number of 96 Cruciform Joint specimens were tested and evaluated. Concerning the dynamic loadings, two different strain rates were accomplished, typical for steel members yielding under seismic action:

- Strain rate (a): $\dot{\epsilon} = 0.06 \text{ s}^{-1}$
- Strain rate (b): $\dot{\epsilon} = 0.12 \text{ s}^{-1}$

Special focus was given to the influence of strain rate, the behaviour of fillet and full penetration welds and the influence of the type of loading regarding the strength of welds and the ductility of the welded connections.

Combining HSS and MCS requires practical experiences in welding technology. Therefore welding procedures for the dual steel cases (HSS and MCS) have been fixed in close collaboration with the Italian Institute of Welding on the basis of EN 1011-1 [57] and EN 1090-2 [58]. In the past, the Italian Institute of Welding gained experiences in several bridges for Italian construction companies applying these types of welding. These procedures cover all combinations proposed for Cruciform Joint specimens as well as T-stub specimens (steel grade, filler metal and weld type). Only two process parameters were changing: type of filler metal and preheating temperature. Other properties as gas composition, technique and electrical characteristics were kept the same. The intention was to focus on suitable combinations both in practice activities and not only in laboratory activities to guarantee the real feasibility of the process.

4.2.2.2 Geometry

The procedure for cutting the specimens out of welded plates after assembling is shown in Figure 4.19.

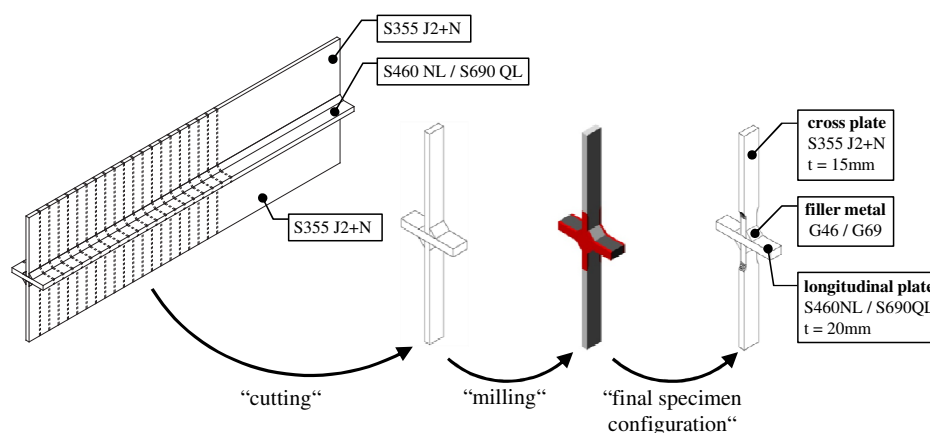


Figure 4.19. Fabrication for Cruciform Joint specimens

After cutting the welded plates for each variation additional test specimens for pre-tests were worked out. The remnant part was used for material testing, especially for specimens of macro examination and tensile tests on filler metal taken from realised fillet welds. In order to obtain the intended two different strain rates ($\dot{\epsilon} = 0.06 \text{ s}^{-1}$ and $\dot{\epsilon} = 0.12 \text{ s}^{-1}$) for dynamic loading the gauge length L_0 had to be reduced by milling the specimens after cutting. That means the specimens should be weakened in the vicinity of the welds. The longitudinal plate as well as the cross plate and the weld itself had been milled. The reduced area assured that all plasticization took place within L_0 considering also effects of strain hardening.

4.2.2.3 Loading protocol – Cruciform Joints

Monotonic quasi-static tests helped to establish the basic material joint properties, like the initial stiffness K_{ini} , the conventional limit of elastic range F_y^+ and the corresponding yield displacement D_y . In addition, this information was significant to establish the cyclic loading strategy. First all monotonic tests were performed and the yield displacement D_y was determined. The initial stiffness was obtained by fitting a linear polynomial to the force-displacement curve between 0% and 25% of the maximum force. The yield displacement D_y was determined at the intersection of the initial stiffness and tangent stiffness line, where the tangent stiffness was obtained by fitting a linear polynomial to force-displacement curve between 75% and 100% of the maximum force F_{max} . It has to be noted that the yield displacement D_y used for cyclic loading protocol for Cruciform Joint specimens scattered remarkably.

The ECCS document [5] enables the modification of the loading procedure for cyclic loading. Therefore, in case of tests on Cruciform Joints and T-stubs, a modified ECCS procedure was applied. The reason was to have larger increments in the inelastic cycles in order to have an assessable number of inelastic cycles up to attainment of the monotonic ultimate displacement. Consequently, the modified ECCS loading history for Cruciform Joints was stated as follows and it is shown in Figure 4.20:

$$0.25 D_y \pm 0.5 D_y \pm 0.75 D_y \pm D_y \pm 3x(6n) D_y \pm \dots \text{ with } n=1,2,3,\dots \quad (4.1)$$

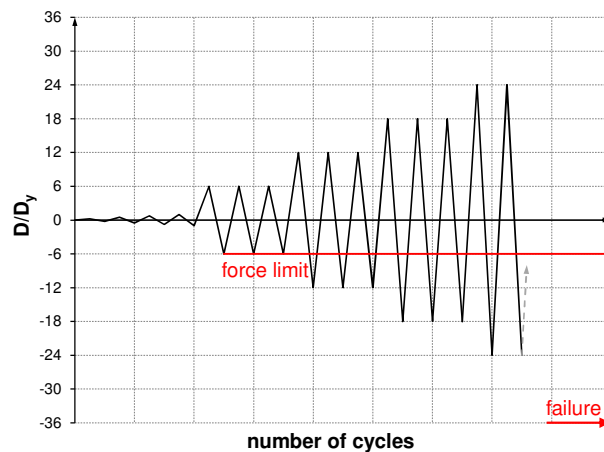
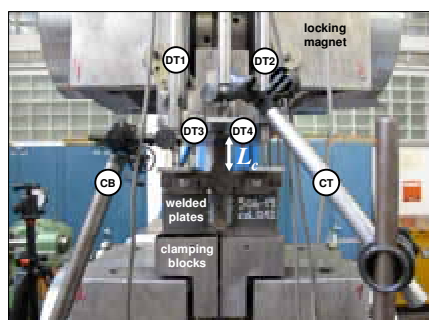


Figure 4.20. Modified loading protocol

It had to be taken into account that in case of compression, the specimen might fail due to global buckling. In order to prevent buckling during the cyclic tests the loading history was adapted as follows: displacement control in tension and force control in compression. That means a fixed force value (force limit) was used for cyclic loading. The experimental tests on Cruciform Joints were carried out at the laboratory of MPA University of Stuttgart. The tests were accomplished through a "closed-loop strain control" for machine controlling. The displacements (and strains) were measured with 4 Linear Variable Displacement Transducers DT1 - DT4, fixed over the length L_c and the mean value of these 4 DT's was used for machine controlling. The length L_c is defined as the distance from the end of the milled area to the surface of the longitudinal plate (see Figure 4.21).



DT	Displacement Transducer for machine controlling
E4D	Mean Value of DT1 - DT4
CB	Displacement Transducer BOTTOM (control)
CT	Displacement Transducer TOP (control)

Figure 4.21. Final instrumentation for Cruciform Joint specimens - Displacement Transducers

“Clamping blocks” were designed and fabricated in order to optimize the prevention of buckling. Reduction of the milled length L_m was accomplished to fix two problems: (i) reducing the loading velocity v_c to half, because the crosshead velocity was limited, (ii) reducing the buckling length and stabilizing the specimens through side plates (see Figure 4.21) which were welded subsequently.

4.2.2.4 Experimental results from Cruciform Joints

Figure 4.22 shows a comparison of the force-displacement curves for all configurations on Cruciform Joints under monotonic loading condition, see Schlecker [59]. From the graphs a larger tensile strength for series 505 and series 508 can clearly recognised in the force-displacement curves. Independently made tensile tests cut out of the cross plate indicated that different plate material from different lots were used for fabrication of Cruciform Joint specimens in particular for the cross plate. This fact had to be taken into account for the further evaluation.

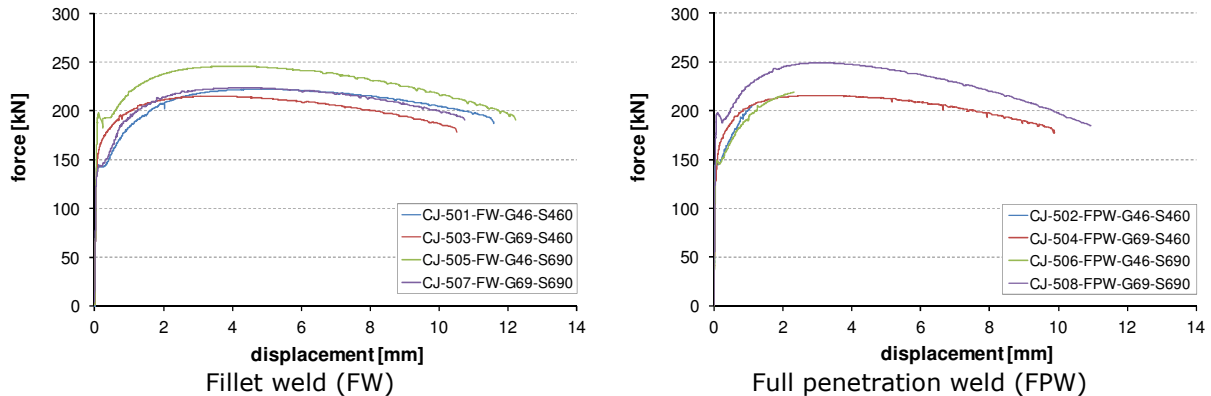


Figure 4.22. Test results for Cruciform Joints under monotonic quasi-static loading

Comparing the ultimate force F_{max} for all monotonic loading conditions a clear tendency to increased values for dynamic loading can be observed. High strain rates ($\dot{\epsilon} = 0.06 \text{ s}^{-1}$ and $\dot{\epsilon} = 0.12 \text{ s}^{-1}$) caused a slightly increase in ultimate strength (F_{max}) of about 4.8-5.6% considering that the values for series 505 and 508 are not representative for comparison due to the different material for the cross plate. Figure 4.23 summarizes the results for monotonic loaded specimens: Monotonic quasi-static (mq-s), monotonic dynamic with strain rate 0.06 s^{-1} (md_0.06) and monotonic dynamic with strain rate 0.12 s^{-1} (md_0.12).

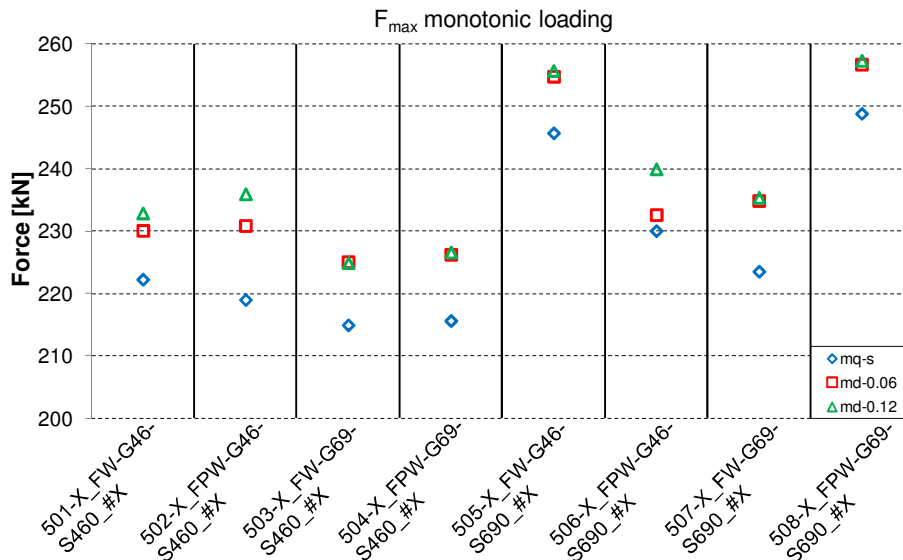


Figure 4.23. Comparison F_{max} for mq-s / md_0.06 / md_0.12

As shown in Figure 4.24 to Figure 4.26, no weld failure occurred for both monotonic and cyclic loading conditions, quasi-static as well as dynamic. That means, the “full strength” design, see Section 4.2.2.1, was successful and there is no influence of the strain rate on the behaviour of fillet and full penetration welds regarding failure. Concerning the ductility, a clear tendency of a decrease in ductility towards higher strain rates could be observed. Comparing the ultimate force F_{max} for cyclic loading protocol also a clear tendency for increase towards dynamic loading protocols is shown, see Figure 4.27.



Figure 4.24. 504-9_mq-s_#1



Figure 4.25. 504-16_cd_0.06_#1



Figure 4.26. 504-18_cd_0.12_#1

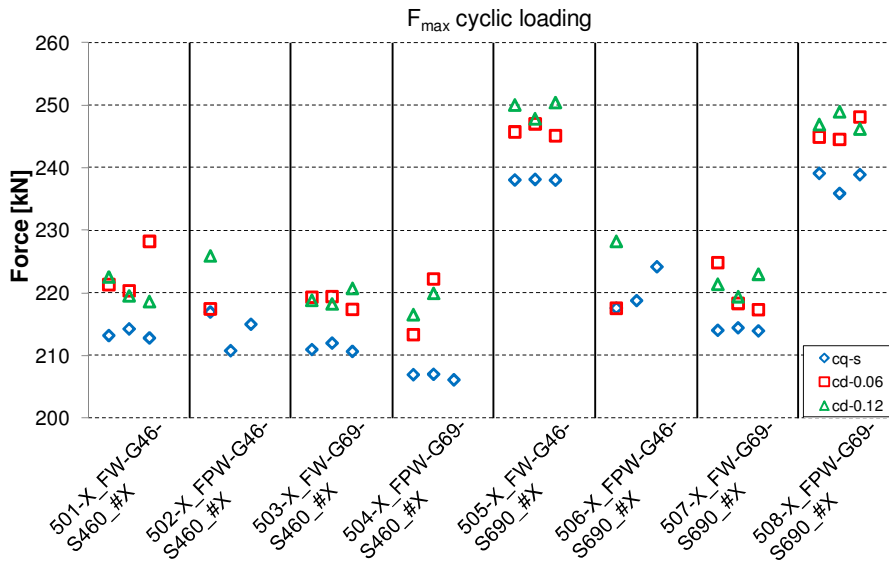


Figure 4.27. Comparison F_{max} for cq-s / cd_0.06 / cd_0.12

In the case of cyclic quasi-static (cq-s) and cyclic dynamic (cd) loaded specimens (cd_0.06 and cd_0.12), the ultimate strength F_{max} is less sensitive to the strain rate (difference of 3.5% to 4.5% F_{max} compared to cyclic quasi-static loading), see Figure 4.27. Strain rate affects the ultimate strength of welded specimens approximately in the same extent as observed in case of component materials, see Dubina & Stratan [60]. Comparing test results under monotonic quasi-static loading conditions with cyclic quasi-static loading conditions a loss of ductility for cyclic loading could be observed. Figure 4.28 and Figure 4.29 illustrate, that the decrease in ductility is more pronounced for dynamic loading conditions.

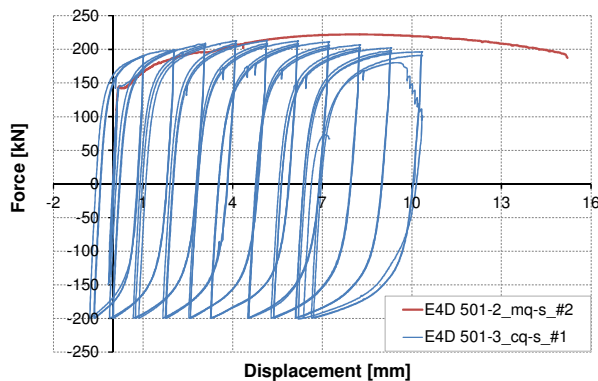


Figure 4.28. Comparison of mq-s & cq-s

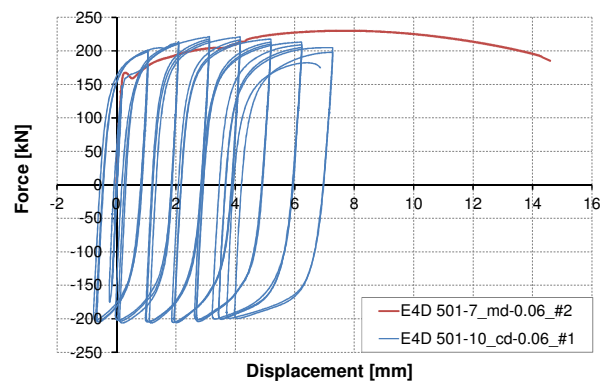


Figure 4.29. Comparison of md_0.06 & cd_0.06

In Figure 4.30 and Figure 4.31 the displacement is shown for each configuration at the time when F_{max} is reached for monotonic as well as cyclic loading conditions.

Comparing quasi-static and dynamic monotonic loaded specimens, dynamic loading caused a decrease of about -2.7% to -4.1% related to the displacement D_{max} , see Figure 4.30. Regarding dynamic loaded specimens the displacement D_{max} is more sensitive than monotonic loading (see Figure 4.31). Dynamic loading caused a decrease of about -15.3 % to -21.1 % compared to cyclic quasi-static loading. Generally, a clear loss of ductility can be observed for cyclic loading protocol.

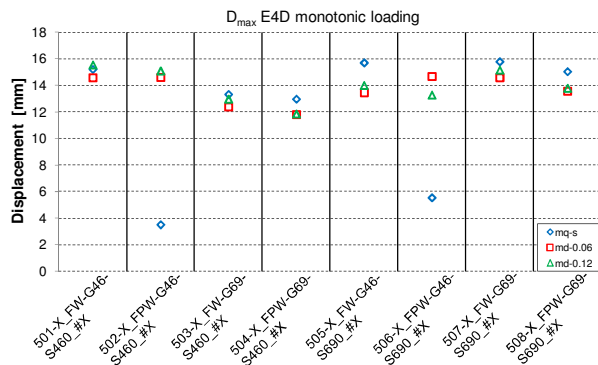


Figure 4.30. Comparison D_{max} for mq-s / md_0.06 / md_0.12

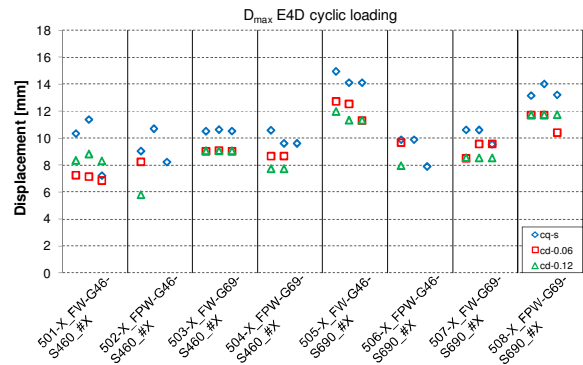
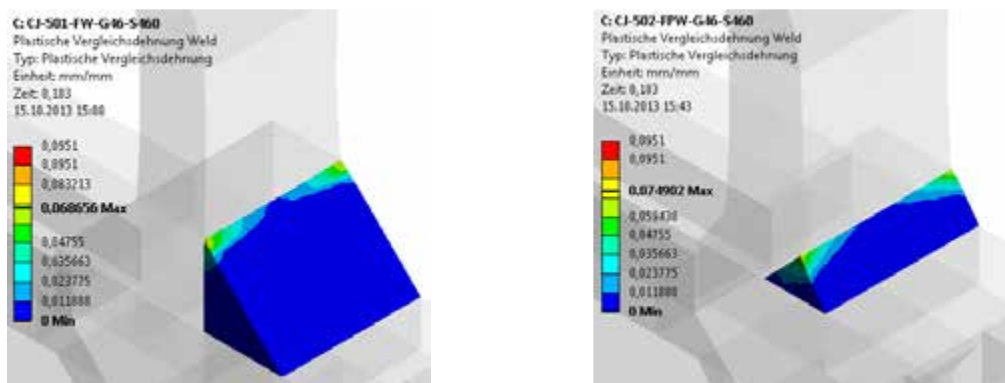


Figure 4.31. Comparison D_{max} for cq-s / cd_0.06 / cd_0.12

4.2.2.5 Numerical investigations

In order to find out more in detail about the behaviour of the weld, elastic as well as plastic, numerical simulations were performed on Cruciform Joint specimens in Schwab [61] with the finite element modelling software ANSYS Workbench (WB) V14.0 [62]. In a first step the material model was calibrated based on results from tensile tests on steel samples and weld material. Using the calibrated material model, the behaviour of each Cruciform Joint configuration was therefore obtained. Steel components were modelled based on true stress-true strain material data available from uniaxial tests with the same nominal mechanical properties as those used in the tests.

The extraction of the ANSYS material input data from the stress-strain relationship was done according to the procedure of Ling [63] and Bridgman [64]. In Figure 4.32 the plastic strains for e.g. series 501 and series 502 are shown under monotonic quasi-static loading conditions. In the figures the ultimate plastic strain for the filler metal is given, $\epsilon_{u,G46} = 0.0951$ and $\epsilon_{u,G69} = 0.0655$. The plots were taken at the point when the tensile strength of the cross plate ($\sigma_{u,cp}$) was reached.



CJ-501-FW-G46-S460

CJ-502-FPW-G46-S460

Figure 4.32. Plastic strains in the weld

It can clearly be observed that the ultimate plastic strains had not exceeded the yield strain for both specimens with fillet welds and with full penetration welds. To have a more detailed view on the development of the plastic strains inside and on the weld surface, evaluations were done along numerical paths, see Figure 4.33.

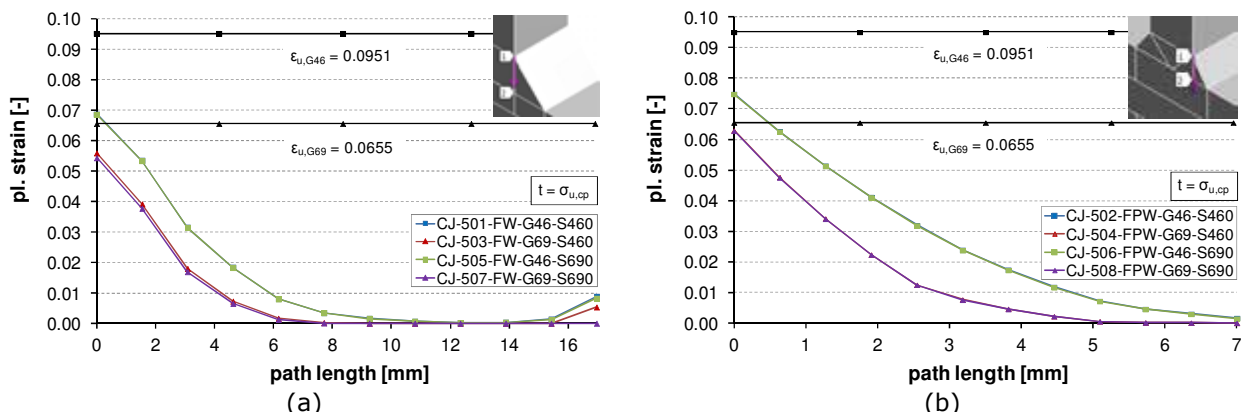


Figure 4.33. Plastic strains of specimens with (a) fillet welds, and (b) full penetration welds

Figure 4.33 illustrates the plastic strains of specimens with fillet welds depending on the length of the path. For instance, the difference for series 501 and 505 only depends on the steel grades of the longitudinal plate. The curves show the distribution of the plastic strains at the time when $t = \sigma_{u,cp}$. That means the ultimate strength for the cross plate material (S355) was reached. The values for ultimate plastic strain for filler metal G46 are given to $\epsilon_{u,G46} = 0.0951$ and for filler metal G69 to $\epsilon_{u,G69} = 0.0655$.

For all Cruciform Joint configurations with fillet and full penetration welds, the plastic strain of the weld did not reach or exceed the ultimate plastic strain of the corresponding pure weld material.

Figure 4.34 illustrates the plastic strains in the longitudinal plate at the time when the ultimate stress in the Cross Plate was reached. Series 501 represents the fillet weld configurations, and series 502 the full penetration weld configurations. It can be clearly seen that the longitudinal plate is not directly affected by plastic strains both FW specimens and FPW specimens.

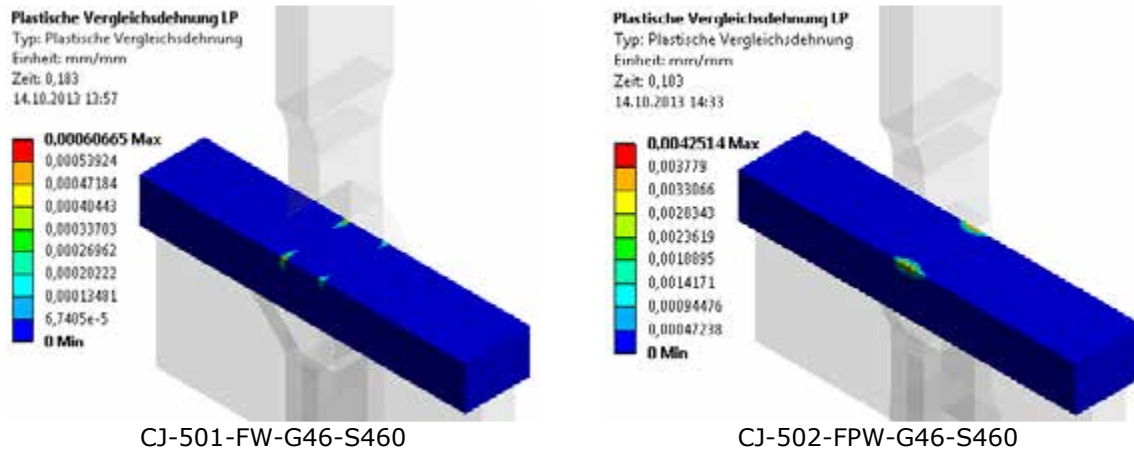


Figure 4.34. Plastic strains at longitudinal plate

4.2.2.6 Concluding remarks – Cruciform joints

To conclude, for welds designed as full-strength, the loading type did not affect the failure of the connection. This means in detail, cyclic quasi-static as well as cyclic dynamic loading had no influence on the behaviour of the weld itself. Only one failure type was observed: the failure occurred for all types of loading conditions in the cross plate (base metal) and no rupture in the weld occurred.

Ruptures in the cross plate (base metal) under both, monotonic and dynamic loading, were accompanied with substantial plastic elongation and necking, produced by sliding in planes at nearly 45° with respect to specimen faces which is typical for ductile ruptures of usual carbon steel used in constructions.

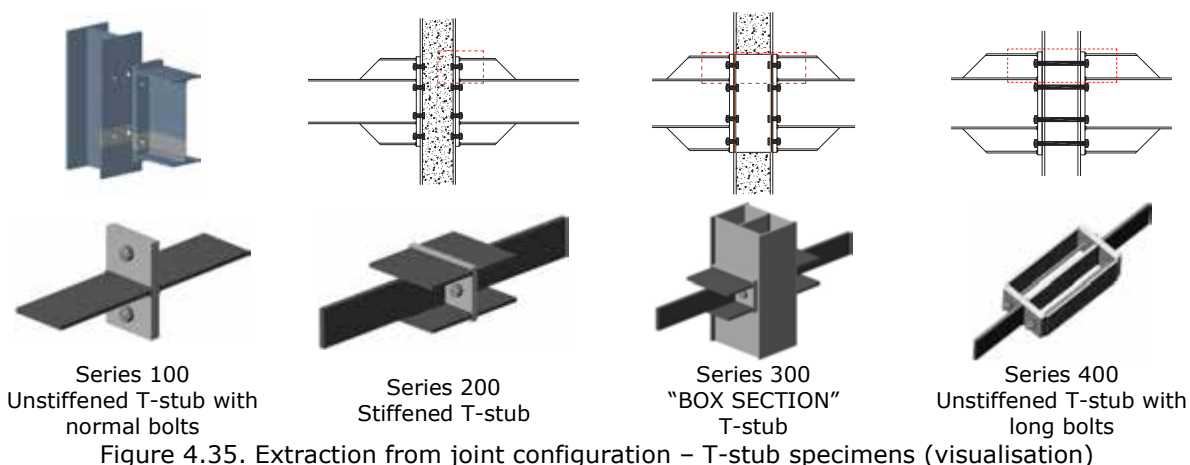
The most important consequences on the cyclic behaviour of the Cruciform Joints were the reduced ductility and the increased strength for the dynamic loading protocol. Indeed, for cyclic quasi-static loadings more stable hysteretic loops could be observed compared to cyclic dynamic loading. Investigations on the cross plate material of each Cruciform Joint configuration revealed differences in yield and tensile strength for the cross plate material, so it can be concluded that they were taken from different lots. Based on macro examination of cut out specimens defective welding could be observed which however had no influence on the overall behaviour of the weld under the different types of loading.

Based on the experimental results, a strain rate in the range of $0.06 \div 0.12 \text{ s}^{-1}$ (typical for steel members yielding under seismic action) showed an increase in the ultimate strength of welded connections. Additionally, a reduction of ductility was present in the case of high strain rates for monotonic loading as well as cyclic loading, which is an essential characteristic for an adequate seismic performance of beam-to-column joints. As the design philosophy of a “full-strength” weld was successful and only failure of the base metal occurred, the influence of the steel grade of the longitudinal plate (S460 / S690) related to the ultimate strength, the type of welding (fillet weld or full penetration weld) and the type of filler metal on the overall strength and ductility of the Cruciform Joint was negligible. Different base metal grades for the cross plate (S355) showed the sensibility against scatter of material characteristics which has to be considered in the over-strength design. Generally, failure was quite ductile due to the elongation and necking of the cross plate material.

4.2.3 Bolted Connections – T-stubs

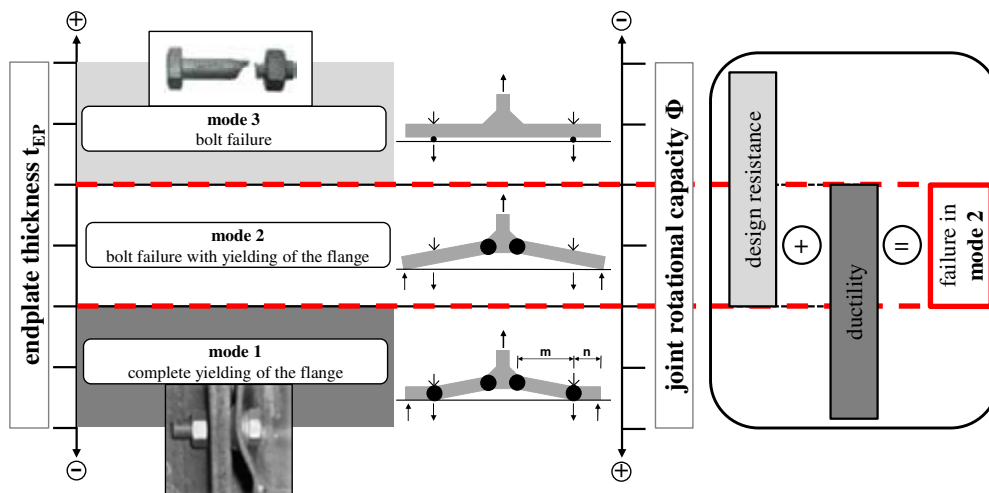
4.2.3.1 General

The experimental program on bolted connections had required the testing of 86 T-stub specimens reproducing loading conditions to which critical bolted connections are usually subjected under seismic action. Four T-stub configurations were “cut out” of bolted joints between HSS columns and MCS beams of WP4 (see Figure 4.35) and subjected to monotonic quasi-static and cyclic quasi-static loading. The individual extractions from joint configurations of WP4 are shown in Figure 4.35.



4.2.3.2 Design

In general there are two main strategies to improve the plastic rotation of welded moment connections during severe seismic events: (a) strengthening of the critical area close to the column flange, and (b) weakening of the beam section close to the beam-to-column connection (reduced beam section connections). Aside of these two options, bolted connections represent an alternative design approach for increasing the capacity to dissipate the seismic energy through the cyclic response of the connecting elements of bolted beam-to-column joints. On the basis of the component approach in EN 1993-1-8 [46] a prediction of the joint rotational stiffness, especially under cyclic loads, requires the preliminary characterization of both monotonic and cyclic behaviour of the components.



In general, a T-stub connection may fail according to one of the three known failure mechanism: yielding of the flange (mode 1), bolt failure with yielding of the flange (mode 2), and bolt failure (mode 3). The specimens for the four T-stub series were designed aiming at a mode 2 failure, one group being close to mode 1 (ductile) and one group respectively close to mode 3 (brittle) by varying the thickness and the steel grade (S460 / S690) of the end-plate, and the distance of the bolts. Failure of the T-stubs in mode 2 combines both adequate design resistance and sufficient rotational capacity of the joint, which tends to be an optimal solution in seismic design approach (see Figure 4.36).

All T-stub specimens were built up by welding of plates and not extracted from rolled profiles in order to reach defined ratios of thicknesses etc. All welds regarding T-stub assemblages were designed as “full-strength”, that means failure should not occur in the welds. Extensive analytical

calculations were realised in advance in order to identify the planned failure mode for all T-stub series and to obtain the design strength of T-stubs and failure modes according to the predictions in EN 1993-1-8 [46].

Therefore, one of the main objectives in the experimental program was to obtain the stiffness and strength corresponding to mode 2 failure, for comparison to the EN 1993-1-8 [46] predictions under monotonic as well as cyclic loading conditions. In Table 4.3 the four T-stub series are presented and the quantity of specimens tested under monotonic quasi-static and cyclic quasi-static loading conditions.

Table 4.3 – Experimental programme on T-stubs

T-stub label		Monotonic quasi-static loading	Cyclic quasi-static loading
Series 100: Unstiffened T-stub		12 specimens	24 specimens
Series 200: Stiffened T-stub		12 specimens	8 specimens
Series 300: "BOX SECTION" T-stub		4 specimens	6 specimens
Series 400: Unstiffened T-stub with long bolts		8 specimens	12 specimens

4.2.3.3 Loading protocol – T-stubs

T-stub specimens were tested under a cyclic loading sequence taken from the ECCS recommendations [5]. Thus, following the ECCS procedure, the yield displacement D_y and the corresponding yielding force F_y were obtained from the force-displacement curve of the monotonic quasi-static tests as explained for Cruciform Joint specimens in Section 4.2.2.3.

In order to apply a reasonable number of cycles up to failure the incremental step size (labelled with X) was adjusted.

$$0.25 D_y \pm 0.5 D_y \pm 0.75 D_y \pm D_y \pm 3x(Xn) D_y \pm \dots \text{ with } n=1,2,3,\dots \quad (4.2)$$

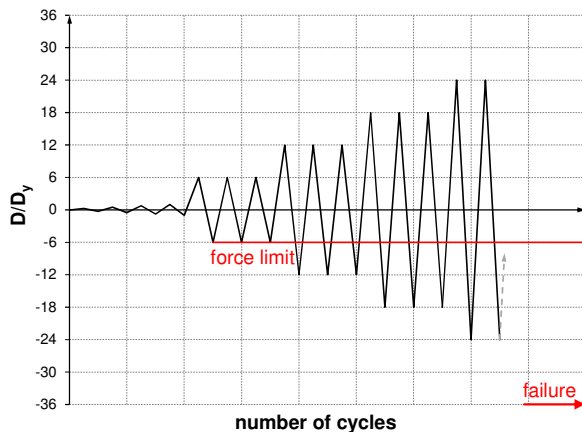


Figure 4.37. Modified loading protocol with X=6

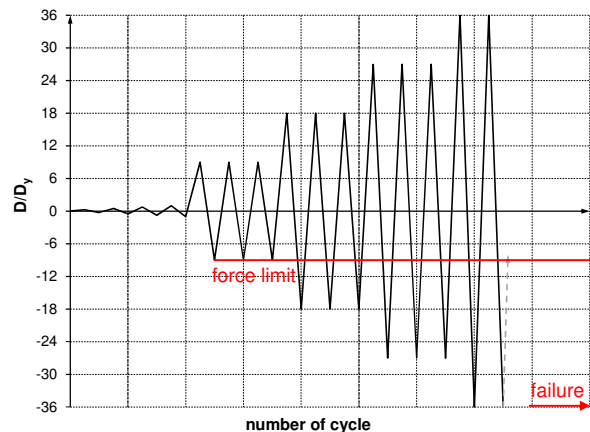


Figure 4.38. Modified loading protocol with X=9

Figure 4.37 and Figure 4.38 clearly indicate the development and increase related to the inelastic increments (XD_y) depending as above mentioned on the yield displacement D_y .

In order to avoid failure by premature buckling in compression range, the loading history was adapted as follows: displacement control in tension and force control in compression. That means a fixed force value (elastic force limit of ~ 400 kN in compression) was used for cyclic loading to prevent buckling of the specimens.

Due to the large scatter of D_y for T-stub series 100, 200 and 400 while monotonic loading the values for yield displacement D_y was split into two parts:

- D_y for ductile mode (thinner end-plates) \Rightarrow [Mode 2-1 / with prying forces]
- D_y for brittle mode (thicker end-plates) \Rightarrow [Mode 2-3 / no prying forces]

4.2.3.4 Experimental results from T-stubs

Test set-up

The experimental tests on T-stubs were carried out at the MPA University of Stuttgart. Under displacement control, all the specimens were subjected to an axial force which was applied to the webs tightened by jaws of the testing machine Schenck 1000 kN and increased up to collapse of the specimens. The type of loading was restricted to monotonic quasi-static (mq-s) and cyclic quasi-static (cq-s), and no dynamic loading was performed.

Four displacement transducers ($a_1 - b_2$) were fixed to the specimen, centred in bolt-line, see Figure 4.39. The deformation of the end-plates was measured in the centreline of the webs by means of Linear Variable Displacement Transducers (LVDT's). The measured mean value of these two LVDT's (D-c) was simultaneously used for machine controlling. Transducers were not removed before collapse in order to record as much as possible information about the deformation capacity.

Wood blocks were applied as safety measure to the testing machine in order to dissipate the energy of bolt failure. The end-plates were connected with bolts M24 HV class 10.9 (hot-dip galvanised) according to EN 14399-4 [51]. Tightening of the bolts was realised according to EN 1090-2 [58] using the combined method by means of a rotation-angle controlled electric nut runner.

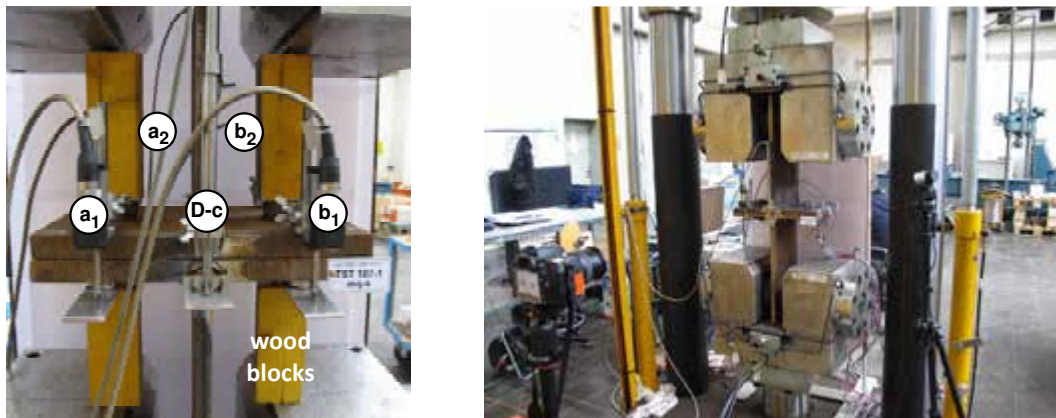


Figure 4.39. T-stub instrumentation (e.g. series 100)

Overview

In general, for all T-stub specimens, the following parameters were determined for each experimental test: initial stiffness K_{ini} , yield displacement D_y , yield force F_y , maximum force F_{max} and several characteristic elongation values. Additionally another aspect while evaluating the experimental results was to obtain the energy dissipation of both monotonic and cyclic loaded specimens. A common procedure for characterizing the energy dissipation capacity of steel members subjected to load reversals is the "envelope curve". Thereby stiffness, strength and ductility between monotonic and cyclic loading can be directly compared. Figure 4.40 shows an overview of the distribution of the experimental measured ultimate load carrying capacity F_{max} for all specimens of series 100 and series 200 under monotonic quasi-static as well as cyclic quasi-static loading conditions. The comparison is also focused on the difference between the load carrying capacity of the T-stub and the pure load carrying capacity of the bolts, respectively the threaded rods (see Figure 4.35). In the following, the red horizontal line represents the ultimate load carrying capacity of the bolts (rods) as an average of the different bolt (rod) lots used in the T-stub specimens. The maximum load carrying capacity of the bolts was ~ 776.6 kN and of the rods ~ 767.4 kN. Additionally a mean value is plotted in the figures covering monotonic and cyclic loaded specimens. The coefficient of variation CoV is a measure of the scattering of the results F_{max} for each configuration.

Generally a small scatter of results for monotonic as well as cyclic loaded specimens could be observed related to the load carrying capacity of series 100 and series 200. In other words, concerning the difference in monotonic and cyclic behaviour, no significant influence was observed. A clear tendency of an increased load carrying capacity within series 100 can be stated for T-stubs failing in mode 2-3 (brittle) whereas the end-plate made of steel grade S460 tends to be the most appropriate solution regarding ultimate behaviour and ductility capacity, see Figure 4.40-a. Failure mode 2-1 combining bending and tension of the bolts lead to a reduction in strength compared to failure mode 2-3. The results of series 200 of stiffened T-stubs show high loading capacity without any remarkable influence of the failure mode and the steel grade, see Figure 4.40-b.

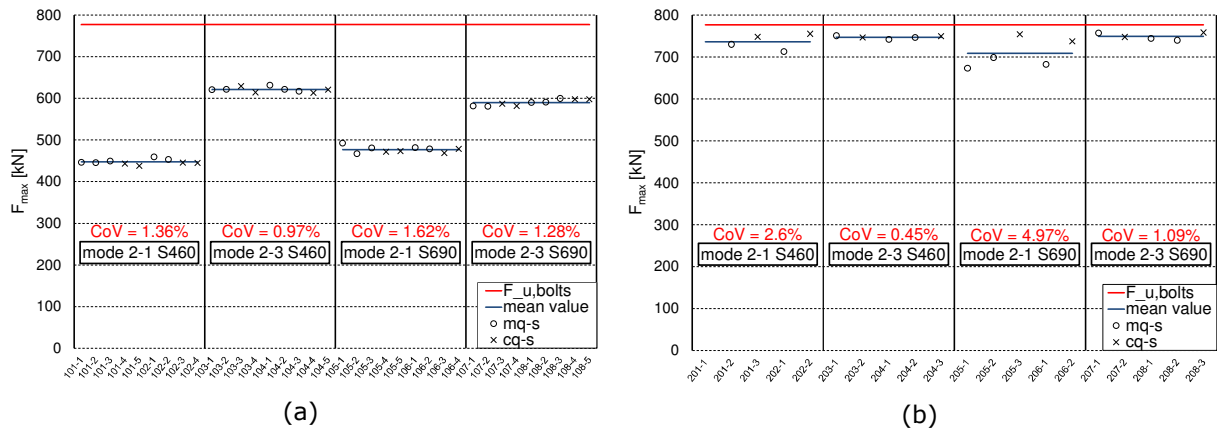


Figure 4.40. Load carrying capacity for T-stub (a) series 100, and (b) series 200

Numerical investigations

Figure 4.41 and Figure 4.42 show individual results of numerical investigations on unstiffened T-stub series 100. As it is well known, while experimental testing on T-stubs it is nearly impossible to measure prying forces Q and bolt forces B . Numerical investigations allow an appraisal of the development of the prying forces. The graphs in Figure 4.41 illustrate the numerical results for series 100 T-stubs (a) end-plate made of steel grade S460, and (b) end-plate made of steel grade S690 where the total applied load on the T-stub is shown against the bolt forces.

The results in Figure 4.41-a and Figure 4.41-b correspond to the results shown in Figure 4.40-a in terms of load carrying capacity. Prying forces $2Q$ reduce the strength of the T-stub failing in mode 2-1 (ductile), due to the bending of the end-plate and the related tensile stresses and bending of the bolt, see Figure 4.42-b. The reduction is more significant for end-plates made of steel grade S460 (prying force $2Q=326.5$ kN) compared to end-plates made of steel grade S690.

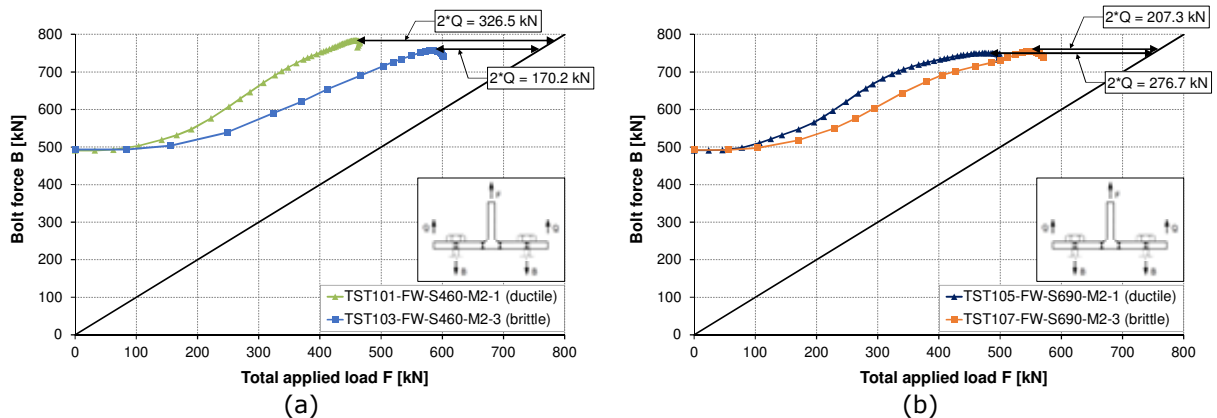


Figure 4.41. FE-results e.g. T-stub series 100 (a) end-plate S460, and (b) end-plate S690

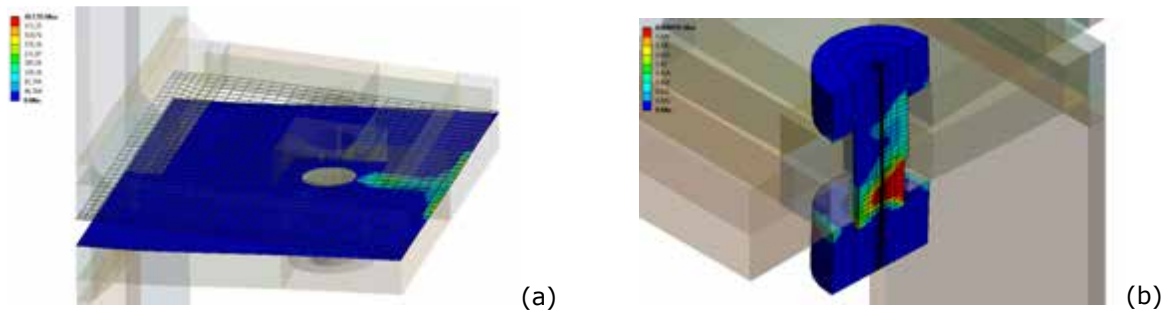


Figure 4.42. FE-results (a) development of prying forces, and (b) bolt failure

Experimental behaviour of different T-stub series

As it can be clearly recognised in Figure 4.43, ductile failure behaviour completely differed from brittle failure where the ultimate behaviour is remarkably varying: in general a clear influence can be observed for T-stubs subjected to ductile behaviour related to the combined bending and tension forces subjected to the bolts after bending deformation of the end-plate. The strength and the ductility of the T-stub specimens directly correlate to the stress distribution of the bolts.

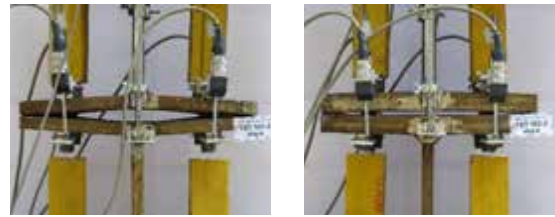
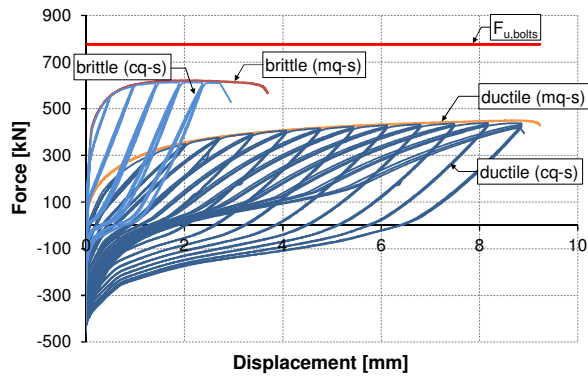


Figure 4.43. (a) F-D-curve: Unstiffened T-stub (series 100); (b) & (c) Immediately before failure

For series 200 the ultimate strength for stiffened T-stubs (see Figure 4.44) are nearly coincident with the ultimate strength of the bolts due to bolt governed collapse. Also cyclic loading affected the ultimate displacement respectively ductility for specimens, though the difference was not significant.

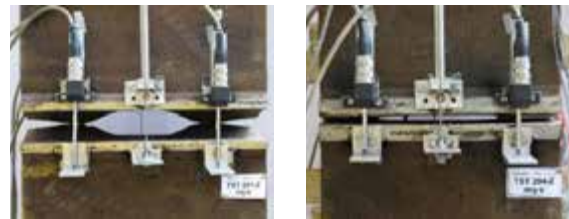
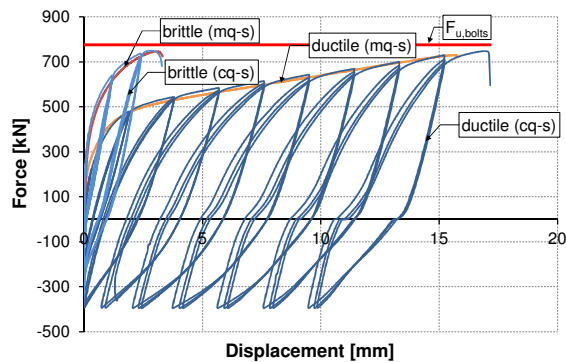


Figure 4.44. (a) F-D-curve: Unstiffened T-stub (series 200); (b) & (c) Immediately before failure

Regarding the development of strength it is evident to underline that for stiffened T-stubs the strength increases continuously up to failure due to membrane effects in the end-plate whereas unstiffened T-stubs show a nearly constant behaviour up to large plastic deformations ending in sensible strength degradation compared to the bolt strength in ultimate conditions. This yielding behaviour was more pronounced for specimens failing in mode 2-1 where large bending deformations developed in the end-plate, compared to tests failing in mode 2-3 (see Figure 4.44). In summary concerning the influence of the type of weld: fillet weld or full penetration weld, no significant effect was detected regarding both, series 100 and series 200.

Comparing the load carrying capacity of series 300 (BOX SECTION), see Figure 4.45 and Figure 4.46, and series 200 (stiffened T-stub) there is no significant difference. This is related to the uniform load introduction of the bolt subjected to nearly pure tension. It has to be noted that for T-stub specimens 301-3, 301-4 and 301-5 (subjected to cyclic loading) punching of the column flange occurred, evidenced by the lower strength. For the specimens, where the column flange is made up of S690 steel grade, nearly the ultimate bolt strength was reached.

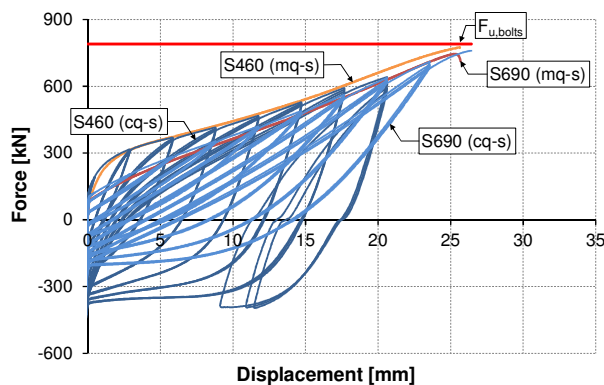


Figure 4.45. F-D-curve: T-stub series 300

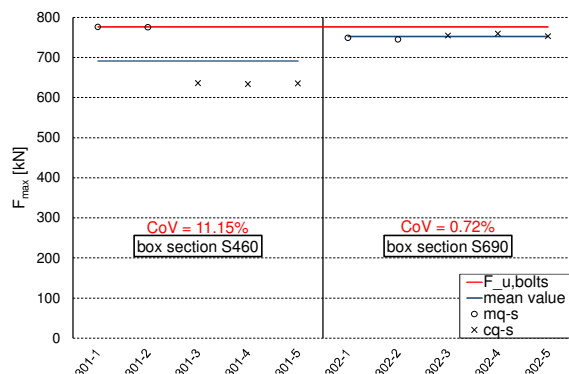


Figure 4.46. Load carrying capacity: T-stub series 300

Concerning ductility and energy dissipation no clear statement can be provided regarding the influence of steel grade for column flange and loading type due to the wide dispersion comparing

monotonic and cyclic loading. However, steel grade S690 for column flange seems to be the lightly more appropriate solution.

T-stub specimens of series 400 developing prying forces were governed by failure of the rods due to the significant bending of the rod caused by the local deformation of the end-plate (Figure 4.47).

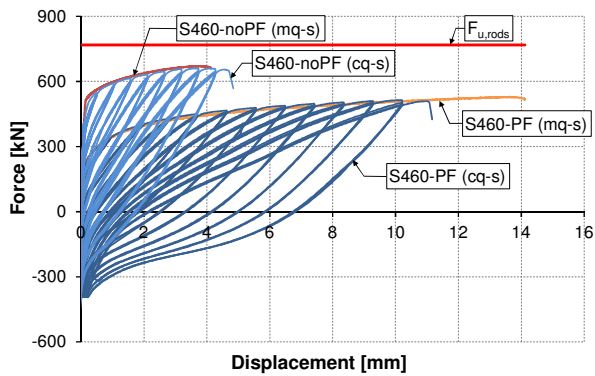


Figure 4.47. F-D-curve: T-stub series 400

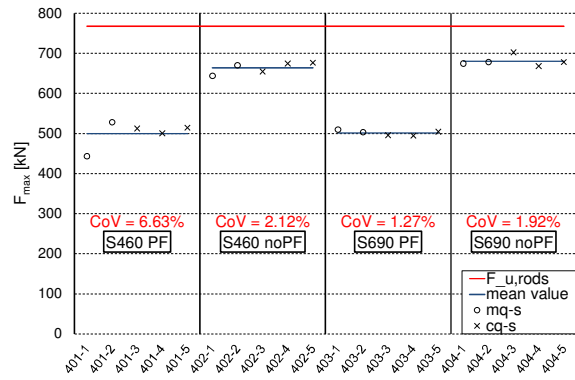


Figure 4.48. Load carrying capacity: T-stub series 400

A clear decrease in strength for T-stubs designed for developing of “prying forces” is stated in Figure 4.48. In general, a higher deformation capacity and respectively energy dissipation of the T-stub series 400 was observed if the end-plate material was made of steel grade S460 and the failure mechanism was governed by the developing of prying forces.

Special failure modes under cyclic loading

A special feature could be observed for series 300 “BOX SECTION” T-stub, especially for TST-301-3_cq-s. Within these configurations the box, representing the column flange was made of steel grade S460 and a thickness of 10 mm. The development of a “membrane effect” for T-stub series 301 may be clearly seen in Figure 4.50. The membrane effects resulted from a deformation of the column flange in the vicinity of the bolt.



TST-301-3_cq-s

Figure 4.49. Punching failure

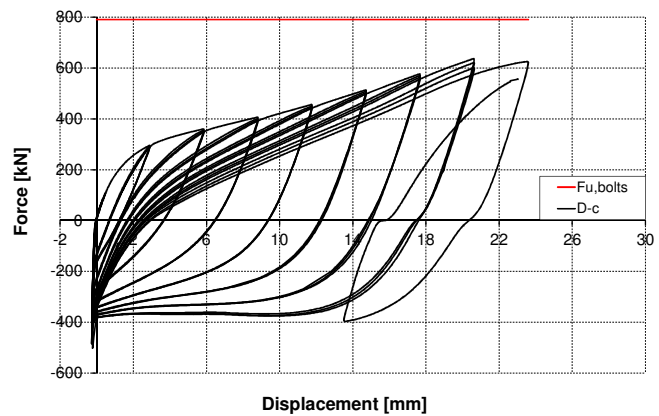


Figure 4.50. F-D-curve TST-301-3_cq-s

In fact, bolt failure was planned related to the analytical calculations, but while testing, the column flange around the bolt hole area tore open, leading to some bolts pulling out from the box face (see Figure 4.49). This punching failure occurred at a load of approximately 555 kN (TST-301-3_cq-s), see Figure 4.50. It has to be noted that punching only occurred for cyclic loaded specimens.

One time, the failure mode for series 400 (Unstiffened T-stub with long bolts), in particular specimen TST-401-4_cq-s, was characterized by premature cracking of the end-plate-to-web connection which prevented the development of the typical collapse mechanism (fracture of the rods), see Figure 4.51.

Regarding in particular the cyclic test, cracking of the end-plate initially developed in the central part of the end-plate at the end-plate-to-web connection zone. By increasing the number of cycles these cracks progressively propagated towards the end-plate edges up to the complete fracture of one end-plate which produces the complete loss of the load carrying capacity (Figure 4.52). This behaviour gave rise to a progressive deterioration, up to failure, of stiffness and energy dissipation capacity. It is important to underline that for these series of specimens the collapse mechanism under cyclic loading condition was different from that shown under monotonic tests, where the yielding of the end-plate was accompanied by the bolt fracture [65]. Finally, all other specimens of series 400 T-stubs failed as already described governed by rod failure.



Figure 4.51. Failure mode TST-401-4_cq-s

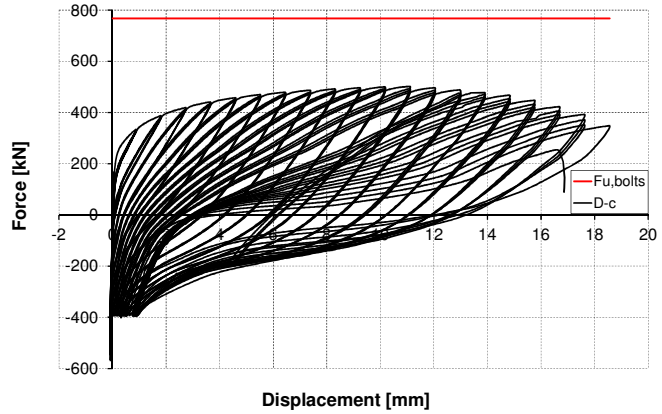


Figure 4.52. Cyclic F-D-curve TST-401-4_cq-s

4.2.3.5 Experimental results vs. analytical predictions

In order to get an overview of the T-stub response a comparison between test and theoretical results according to EN 1993-1-8 [46] and other models from literature [66] was made in Kittel [67]. Figure 4.53 and Figure 4.54 show the comparison of the experimental results (mq-s and cq-s) with the corresponding analytical predictions of plastic resistance derived from EN 1993-1-8 [46], taken into account the nominal values for the steel grades. Herein the theoretical characteristics were evaluated by component method from EN1993-1-8 [46]. Remarkable reserves are obvious.

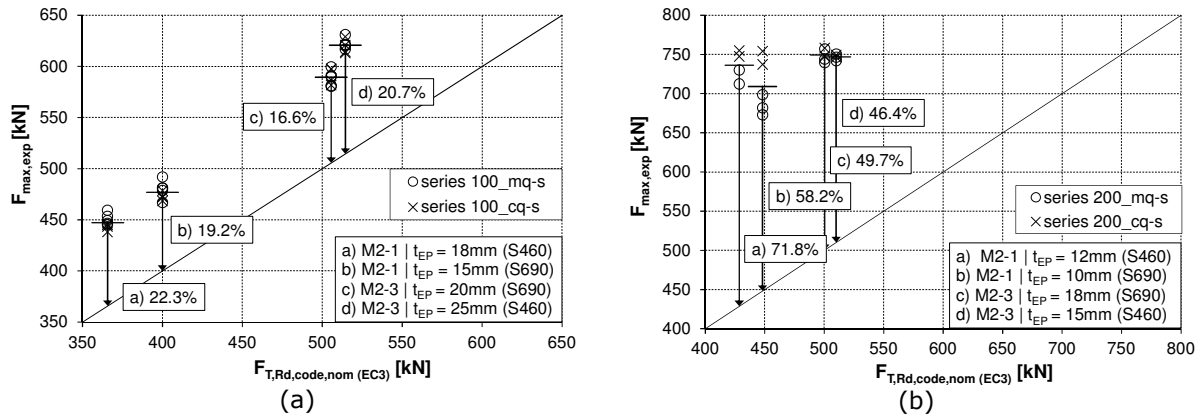


Figure 4.53. Experimental vs. analytical: (a) series 100; (b) series 200

Finally, an advantage related to the load carrying capacity for T-stubs designed for failure mode 2-1 could be observed (19.2% to 22.3%). A small increase with respect to the T-stubs with an end-plate made of S460 (20.7% and 22.3%) was exhibited, see Figure 4.53-a. Figure 4.53-b points out once more the effect of membrane forces developing for thinner end-plates of series 200 T-stubs. The safety margin accounts for 58.2% to 71.8% for T-stubs designed to fail in mode 2-1. As already mentioned the “T-stub” approach proposed by EN 1993-1-8 [46] neglects such important contributions, which can be considered as a reserve of strength and deformation capacity, contributing to fulfil the ductility requirements for joints in the case of seismic loading conditions. This however might lead to an underestimation of the T-stub components if combined with other components in a joint. In general the experimental measured ultimate strength values for T-stub series 200 do not differ significantly for all configurations, see also Figure 4.40-b in Section 4.2.3.4. The comparison of the experimental results with the corresponding analytical predictions of plastic resistance derived from EN 1993-1-8 [46] for series 100, exhibits significant reserves on the safe side. On the basis of the results it seems possible to conclude that the approach proposed by the EN 1993-1-8 [46] enables an accurate definition of the collapse mode and a regular safety margin for all configurations.

It has to be noted that for T-stub series 300 “BOX SECTION T-stub” the analytical load carrying capacity for T-stub series was not calculated according to the component method of EN 1993-1-8 [46] but in line with the CIDECT report [66]. Indeed the observed membrane effect led to a remarkable reserve on the safe side (70.5% and 76.2%). The evaluation of the experimental and analytical results points out a significant advantage in load carrying capacity for T-stubs failing without developing of prying forces (Figure 4.54-b), see also explanations in Section (experimental behaviour of different T-stubs). In summary it can be concluded, by comparing the results, that a clear increase (64.3% and 66.8%) was observed. For all tested specimens it has to be underlined that the Eurocode underestimates the plastic resistance and the elastic stiffness (not listed here).

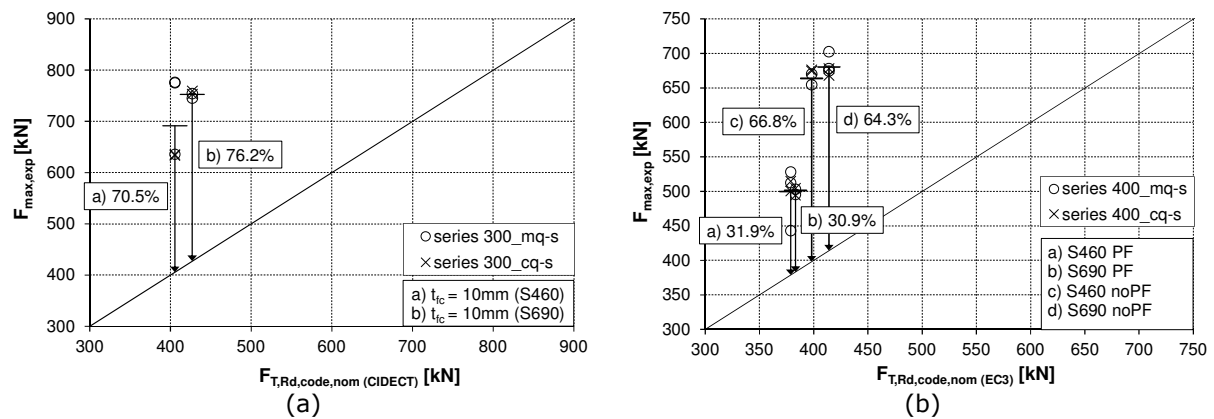


Figure 4.54. Experimental vs. analytical: a) series 300; b) series 400

4.2.3.6 Concluding remarks – T-stubs

The study on the response of bolted T-stubs under monotonic quasi-static and cyclic quasi-static loading conditions aiming at the characterisation of components which are of relevance in joints where Mild Carbon Steel beams are connected to High Strength Steel columns are presented. In particular, on the basis of 86 experimental tests on T-stub assemblages, the strength and ductility have been evaluated.

The observed failure modes involved combined bending and tension bolt fracture for specimens behaving ductile and nearly pure tension bolt fracture for specimens behaving brittle. Stripping of the nut threads was not observed at all. In one specimen (T-stub series 400) complete cracking of the end-plate material in the HAZ occurred.

The experimental results demonstrate that the end-plate can deliberately be designed, taken into account the thickness and the steel grade, in order to achieve sufficient ductility as requested by code provisions.

The degree in which cyclic loading affected the ductility of T-stubs is much dependent on the failure mode. Specimens failing by mode 2-3 (brittle) were characterized by an important decrease of ductility coupled with a significant load carrying capacity. On the other hand, ductility of specimens failing in mode 2-1 (ductile) was much more pronounced achieving however a smaller load carrying capacity.

It can be summarised that the choice of thickness of the end-plate associated with steel grade is important in the conception of a proper connection, in order to obtain a good balance between stiffness, strength and ductility of components.

As a key outcome it can be concluded in case of bolted T-stub connections and respectively bolted beam-to-column joints, the major contributions of the overall T-stub strength and deformation are the end-plate deformation capacity and the strength of the bolts, as far as its plastic failure mechanism was governed by mode 2.

The comparison between the experimental results and the corresponding analytical predictions of plastic resistance derived from EN 1993-1-8 [46], taking into account the nominal values for the steel grades, showed remarkable reserves which however might lead to an underestimation of the T-stub components if combined with other components in a joint. The results led to the assumption that the choice of steel grade for the end-plate material does not significantly influence the load carrying capacity. On the contrary, the geometry (bolt distance, end-plate thickness, etc.) and the stiffener have a more remarkable influence on the load carrying capacity. For stiffened situations, see e.g. series 200 a uniform load introduction of the bolt and therefore almost a pure tensile stress situation of the bolt provides a nearly independent high load carrying capacity without losing much ductility.

4.3 Bolted beam-to-column joints in moment-resisting dual-steel frames

4.3.1 Experimental program

Three innovative full-strength bolted end-plate joint configurations were proposed to be tested:

- Bolted hammer head end-plate to wide flange column joint (B-EP-H) (Figure 4.55): the end-plate welded to the hammer head beam is directly bolted to the flanges of partially-encased wide-flange columns reinforced by lateral plates (pieces 6 in Figure 4.55);
- Bolted hammer head end-plate to RHS column joint with U channel (B-EP-U) (Figure 4.56): the end-plate welded to the hammer head beam is connected to a concrete-filled tube column through a reverse U channel (pieces 6 in Figure 4.56) and;
- Bolted extended end-plate to RHS column joint with long bolts and reduced beam section (B-EPL-RBS) (Figure 4.57): extended end-plates are bolted to concrete-filled tube column using long bolts passing through the column.

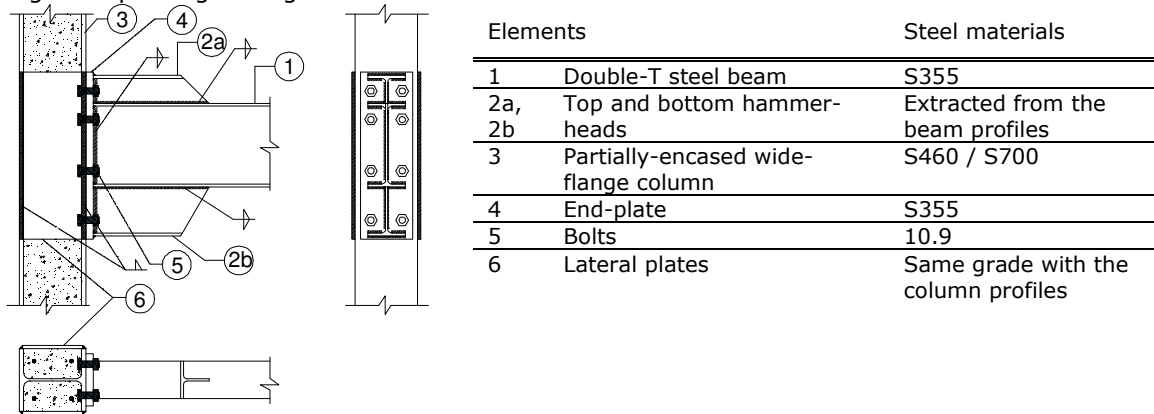


Figure 4.55. B-EP-H joint configuration

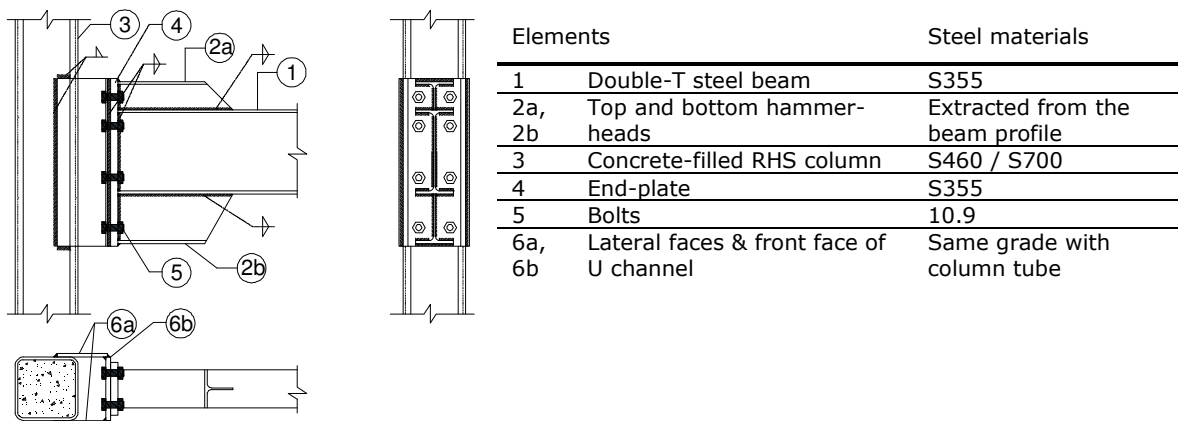


Figure 4.56. B-EP-U joint configuration

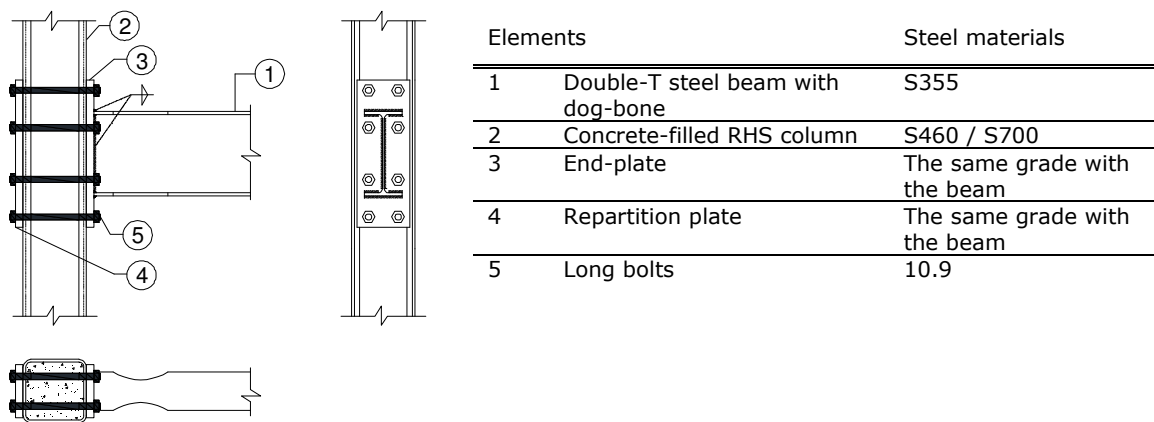


Figure 4.57. B-EPL-RBS joint configuration

A number of 16 large scale specimens were designed for the test campaign to be conducted at ULG (Table 4.4): 8 B-EP-H joints, 4 B-EP-U joints, and 4 B-EPL-RBS joints. The tested specimens were extracted from reference buildings designed within WP1. As the joints have been designed to be full strength, the beams in some specimens are reinforced by welding vertical plates between the

flanges (see Figure 4.61) to be able to reach the resistance of the joints during the tests and, so, to characterise the behaviour of new joint components that are not yet covered by Eurocodes.

Table 4.4 – Test program on the beam-to-column joints

N ^o	Test	Joint type ^(a)	Column	Reinforcement degree of the beam (Figure 4.61)	Loading ^(b)
1	A1	B-EP-H	HEB 320, S460	Partially reinforced	Monotonic M ⁺
2	A2			Totally reinforced	Monotonic M ⁻
3	A3			Not reinforced	Monotonic M ⁺
4	A4			Not reinforced	Cyclic
5	B1	"HEB260", S690		Totally reinforced	Monotonic M ⁺
6	B2			Totally reinforced	Monotonic M ⁻
7	B3			Not reinforced	Monotonic M ⁺
8	B4			Not reinforced	Cyclic
9	C1	B-EP-U	SHS 300x12.5, S460	Totally reinforced	Monotonic M ⁺
10	C2			Totally reinforced	Monotonic M ⁻
11	D1	B-EPL-RBS		Not reinforced	Monotonic
12	D2			Not reinforced	Cyclic
13	E1	B-EP-U	SHS 250x10 S700	Totally reinforced	Monotonic M ⁺
14	E2			Totally reinforced	Monotonic M ⁻
15	F1	B-EPL-RBS		Not reinforced	Monotonic
16	F2			Not reinforced	Cyclic

^(a): IPE400 with S355 steel grade, M30 10.9 bolts and C30/37 concrete are used for all specimens.
^(b): M⁺ and M⁻ are hogging and sagging moments, respectively.

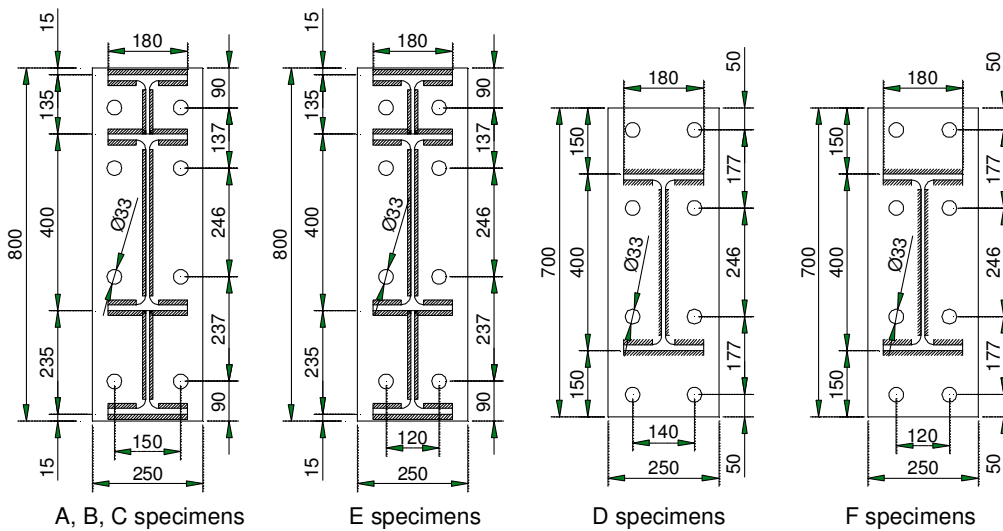


Figure 4.58. End-plate details

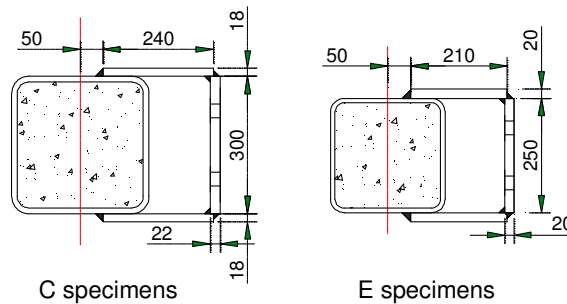


Figure 4.59. Reverse U channel details

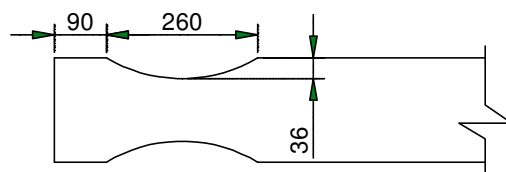


Figure 4.60. Dog-bone detail (D and F specimens)

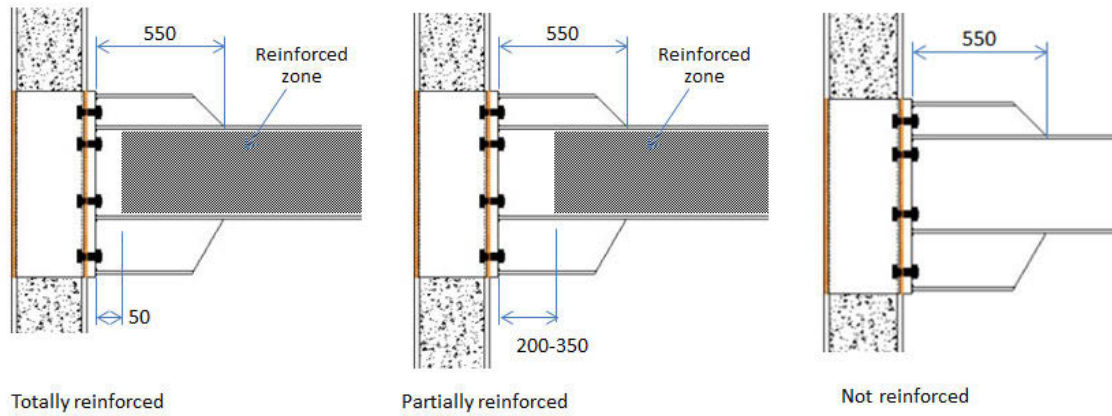


Figure 4.61. Different reinforcements of the beams

Beside the tests on the beam-to-column joints, tests on the column stubs were also conducted, in order to investigate the load introduction from the beam to the column inside the B-EPL-RBS joints. The geometrical properties of the specimens are described in Figure 4.62 and the test program is summarized in Table 4.5.

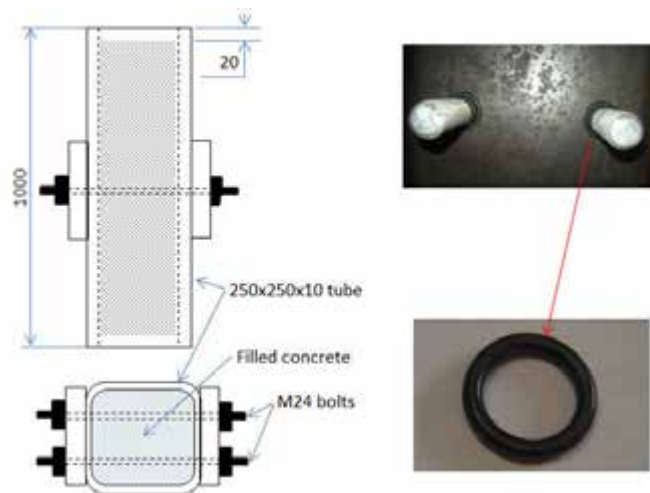


Figure 4.62. Description of column stub specimens

Table 4.5 – Test program on the column stubs ^(a)

Nº	Specimen	Configuration	Preloaded bolts?	Set-up ^(b)
1	T1	Tube 250X250x10 C30/37 concrete M24 10.9 long bolts, 10.9 (Figure 4.62)	No	Set-up 1
2	T2		No	Set-up 2
3	T3		No	Set-up 3
4	T4		Yes	Set-up 1
5	T5		Yes	Set-up 2
6	T6		Yes	Set-up 3

^(a) It is important to note that there are some changes in the test program for the column stubs if compared to the project proposal. Initially, three monotonic and three cyclic tests using the testing same set-up were planned. It was finally decided to perform only monotonic tests using three different testing set-ups in order to highlight some specific characteristics of the column stub behaviour (see Section 4.3.3.2);


^(b) see Figure 4.72 (in Section 4.3.3.1);

4.3.2 Tests on bolted beam-to-column joints

4.3.2.1 Pre-test activities

Tightening tests on bolts: as the bolts are preloaded for almost all the tested specimens, tightening tests on the bolts have been performed, using a specific equipment, in order to estimate the actual value of the friction coefficient k that allows calculating the ratio between the moment of tightening M and the preload in the bolt S , using the formula $M=k \cdot S \cdot d$, where d is the diameter of the bolt, EN 1090-2 [58]. The test results are presented in Table 4.6 for the different bolts used for the tested specimens, showing that the k factor given by the tests are quite in good agreement with the recommended value in EN-1090-2 [58]. For the definition of the tightening procedure in the laboratory, $k = 0.13$ is used.

Table 4.6 – Results of the tightening tests on bolts

	Bolt	k (test)	k recommended in EN 1090-2 [58]
	M30x100 (test 1)	0,140	0,13 (0.1-0.16)
	M30x100 (test 2)	0,138	
	M30x95 (test 1)	0,135	
	M30x95 (test 2)	0,145	

Tensile tests on bolts: two tensile tests were performed for each bolt type. The results are summarized in Table 4.7. The capacities and the failure modes obtained through the performed tests show that the quality of the bolt shanks, nut and washers are in good agreement with the bolt grades.

Table 4.7 – Results of the tensile tests on bolts

Bolt type	Nominal capacity	Test load	Actual ultimate strength
M30x500, 10.9 grade	565 kN	607 kN	1074 N/mm ²
M30x450, 10.9 grade	565 kN	618 kN	1093 N/mm ²
M30x100, 10.9 grade	565 kN	606 kN	1072 N/mm ²
M24x430, 10.9 grade (*)	362 kN	365 kN	1008 N/mm ²





(*) this bolt is used for the column stub specimens (Section 4.3.3)

Tests on steel material: the steel elements (plates, profiles, hollow tubes) identified in the tested specimens have been characterized through coupon tests. The main results are summarized in Table 4.8.

Table 4.8 – Coupon tests on plates, profiles and hollow sections

No	Specimen	Results (N and mm units)			Extracted from
		f _y	f _u	E	
1	HEB320 flange 1	-	-	-	Column of A specimens ^(a)
2	HEB320 flange 2	-	-	-	
3	HEB320 flange 1	-	-	-	
4	HEB320 flange 2	-	-	-	
5	HEB260 flange 1	789	827	200880	Column of B specimens
6	HEB260 flange 2	788	826	214186	
7	HEB260 web 1	827	872	194382	
8	HEB260 web 2	825	869	222024	
9	IPE400 flange 1	400	491	212162	Beams of all specimens
10	IPE400 flange 2	394	489	250536	
11	IPE400 web 1	438	518	211595	
12	IPE400 web 2	422	506	205548	
13	300x300x12.5 SHS 1	485	550	191694	Column of C and D specimens
14	300x300x12.5 SHS 2	501	557	166999	
15	250x250x10 SHS 1	734	833	187953	Column of E and F specimens
16	250x250x10 SHS 2	712	821	195596	
17	35mm, S355 plate 1	401	491	217740	Joint end-plate of A, B, C, and E specimens
18	35mm, S355 plate 2	398	491	201884	
19	35mm, S460 plate 1	438	586	215904	Joint end-plate of D and F specimens
20	35mm, S460 plate 2	433	578	211532	
21	15mm, S460 plate 1	461	616	201884	Lateral plate of HEB 320 (A specimens)
22	15mm, S460 plate 2	461	609	204662	
23	15mm, S690 plate 1	778	810	197819	Lateral plate of HEB 260 (B specimens)
24	15mm, S690 plate 2	774	808	227455	

25	18mm, S355 plate 1	419	526	206778	U lateral faces of C specimens
26	18mm, S355 plate 2	422	526	215306	
27	22mm, S355 plate 1	447	538	213660	U front faces of C specimens
28	22mm, S355 plate 2	450	539	225675	
29	20mm, S355 plate 1 ^(b)	440	-	-	U plates of E specimens
30	20mm, S355 plate 2 ^(b)	440	-	-	

Remarks:

^(a) as no extra length of HEB320 profile was delivered to extract the coupon to be tested, no coupon tests were performed for this profile. However, this has not been critical for the interpretation of the test results as no column components were activated at failure.

^(b) the properties of this plate have been estimated using a hardness test as it appeared that the S355 20 mm plate which was delivered to extract the coupons (for which f_y values of about 830 N/mm² were obtained) was not the one used for the realization of the reverse U channel.

Tests on concrete material: the strength of concrete material that was used in the column has been characterized through compression tests on 150x150x150mm cubes (see results in Table 4.9).

Table 4.9 – Compression tests on concrete cubes

Specimen	Resistance (N/mm ²)	Specimen	Resistance (N/mm ²)	Specimen	Resistance (N/mm ²)
1	53.3	9	54.3	17	57.2
2	54.2	10	57.5	18	54.3
3	52.8	11	59.3	19	56.9
4	55.4	12	58.7	20	57.6
5	55.3	13	57.1	21	56.7
6	54.0	14	56.1	22	57.3
7	55.0	15	57.5	23	54.3
8	54.9	16	55.5	24	55.3

Remark: as it can be observed, the results are similar for all the tests, which show that the concrete is "stabilized" during the test campaign. An average value of 55.8 N/mm² has been considered for the test interpretation. According to EN 1992-1-1 [34], it corresponds to a cylinder strength of $f_{cm} \approx 45$ N/mm².

Test set-up: the test set-up for the beam-to-column joints is presented in Figure 4.63. A fixed hinge at the bottom and a hinge allowing a vertical displacement at the top are used at the column extremities. Possible displacements of the hinges have been anyway recorded during the tests. A vertical load is applied at the free end of the beam introducing a bending moment and a shear force in the joints. Lateral supports on the beam length have been added to avoid the lateral torsional buckling of the beam.

Instrumentation: the instrumentations for the specimens is presented in Table 4.10.

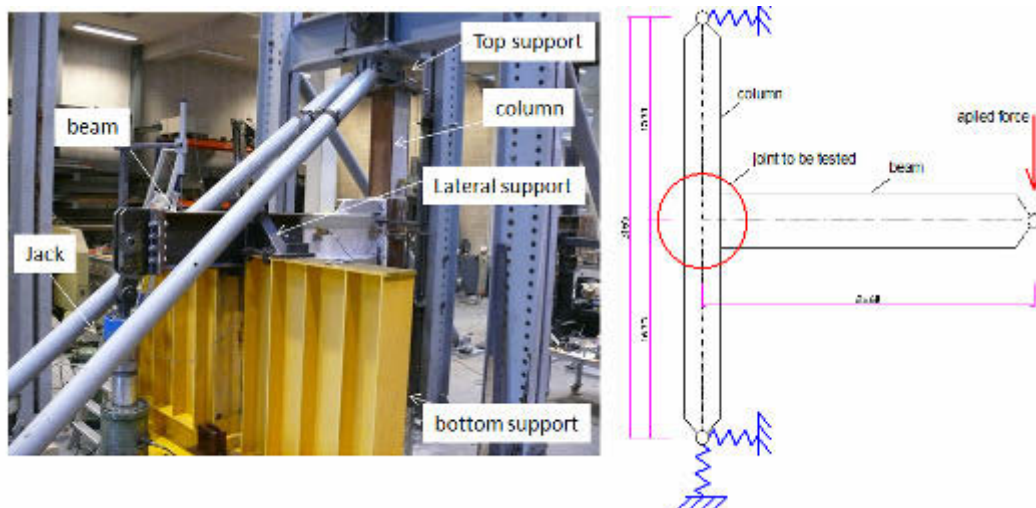


Figure 4.63. Test set-up for the beam-to-column joints

Table 4.10 – Instrumentation for the beam-to-column specimens

Quantities to be recorded	Instruments	Referent figures
Beam displacement	D1 and R1	Figure 4.64
Beam end rotation	R1 and R2	
Connection rotation	R2 and R4	
Panel rotation	R3, R4 and R5	
Support displacements	D1, D8, D9 and D10	
Supplementary info	D2, D3, D5-D7, and D11	

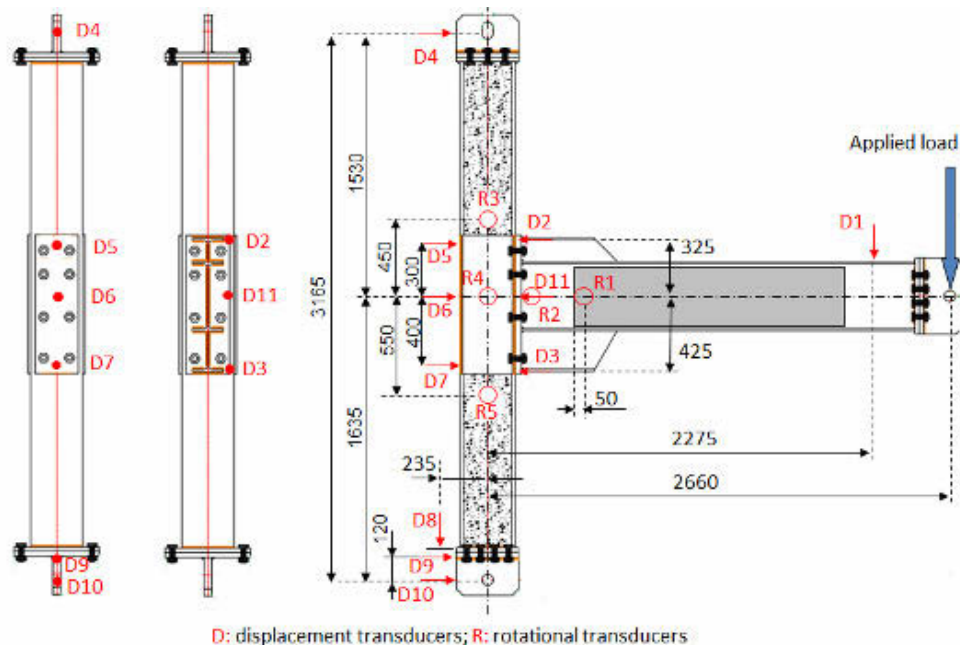


Figure 4.64. Instrumentation for A1, A2, B1 and B2 specimens (detail for C, D, E, F specimens can be found in Deliverable D4 [11] of the present project)

Loading protocols: for the monotonic tests, a quasi-static load is applied until the failure of the specimens; some unloading-reloading are made during the tests in order to estimate accurately the joint stiffness. For the cyclic tests, the ANSI/AISC 341-10 [7] loading procedure is adopted, in which the inter-storey drift is used as control parameter.

4.3.2.2 Interpretation and evaluation of test results

Test results

The resistance, initial stiffness and failure modes of the specimens are summarised in Table 4.11. The load-displacement curves of B-EP-H, B-EP-U and B-EPL-RBS joints are presented in Figure 4.68, Figure 4.69 and Figure 4.70 respectively. The average stiffness of each joint type is shown in Figure 4.71 through the k_b factor representing the relative stiffness between the joint ($S_{j,ini}$) and the associated beam (EI_b/L_b). The joint classification in terms of resistance and stiffness are summarized in Table 4.12.

Table 4.11 – Summary of the test results on the beam-to-column joints

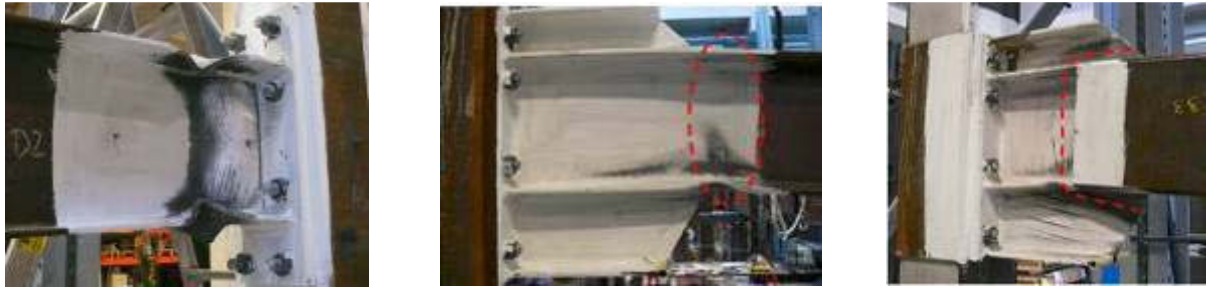
Test	$M_{max}^{(a)}$ [kNm]	Stiffness ^(b) [kNm/rad]	Failure modes
A1	820	193 000	Plastic hinge in the hammer head zone (Figure 4.65)
A2	1187	187 000	Joint failure (bolts + hammer head) (Figure 4.66)
A3 ^(d)	550	210 100	Plastic hinge in the beam (Figure 4.65)
A4 ^(d)	575	182 400	Plastic hinge in the beam (Figure 4.65)
B1	1160	154 500	Joint failure (bolts + hammer head) (Figure 4.66)
B2 ^(c)	944	177 700	
B3 ^(d)	550	214 000	Plastic hinge in the beam (Figure 4.65)
B4 ^(d)	566	144 000	Plastic hinge in the beam (Figure 4.65)
C1	980	82 027	Yield mechanic in reverse U channel (Figure 4.67)
C2	877	80 000	Yield mechanic in reverse U channel (Figure 4.67)
D1	435	154 900	Plastic hinge at the dog-bone (Figure 4.65)
D2	437	144 820	Plastic hinge at the dog-bone (Figure 4.65)
E1	972	70 100	Yield mechanic in reverse U channel (Figure 4.67)
E2	946	68 300	Yield mechanic in reverse U channel (Figure 4.67)
F1	435	113 850	Plastic hinge at the dog-bone (Figure 4.65)
F2	433	112 950	Plastic hinge at the dog-bone (Figure 4.65)

^(a): maximal bending moment at the critical section.

^(b): in the cyclic tests, the stiffness under hogging moment is reported.

^(c): the weld between the beam and the reinforcing plate failed and the test was stopped.

^(d): for these tests (A3, A4, B3 and B4), a lateral buckling occurs in the beam despite the use of systems to avoid this phenomenon. Therefore the reported values are not the ultimate capacities of the beam sections; however, the plastic hinges at the beam level are clearly identified (Figure 4.65). These tests can anyway be considered as successful as the estimation of the ultimate capacity of IPE400 cross-section was not the objective of these tests; indeed, the objective was to demonstrate that the proposed joints are fully rigid and full strength ones, what was demonstrated through these tests.



at dog-bone

in the beam close to the hammer heads

in the hammer head zone

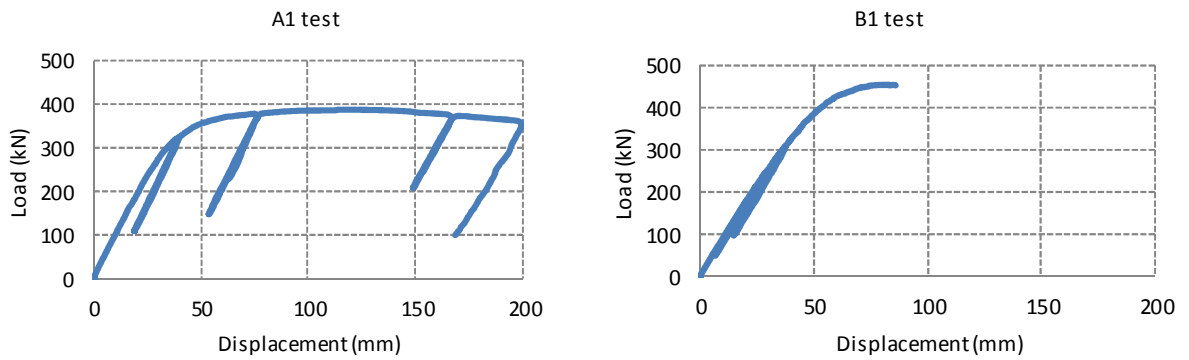
Figure 4.65. Plastic-hinge failure mode



Figure 4.66. B-EP-H joint – failure in the connection (4 bolts in the tension zone failed and the hammer head in compression yielded)



Figure 4.67. Failure mode of the B-EP-U joints (reverse U channels yielded)



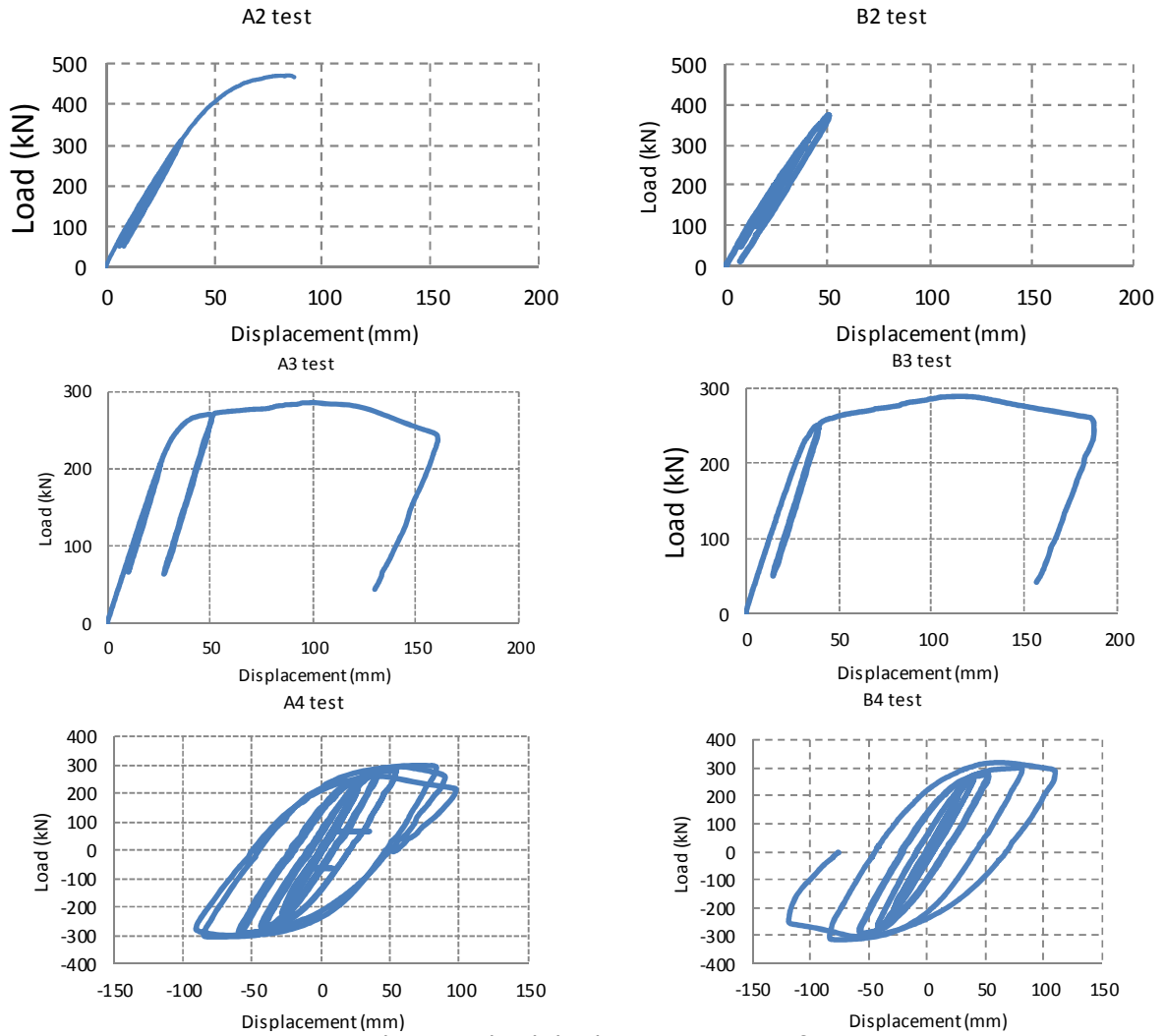


Figure 4.68. Load – point load displacement curves for B-EP-H joint

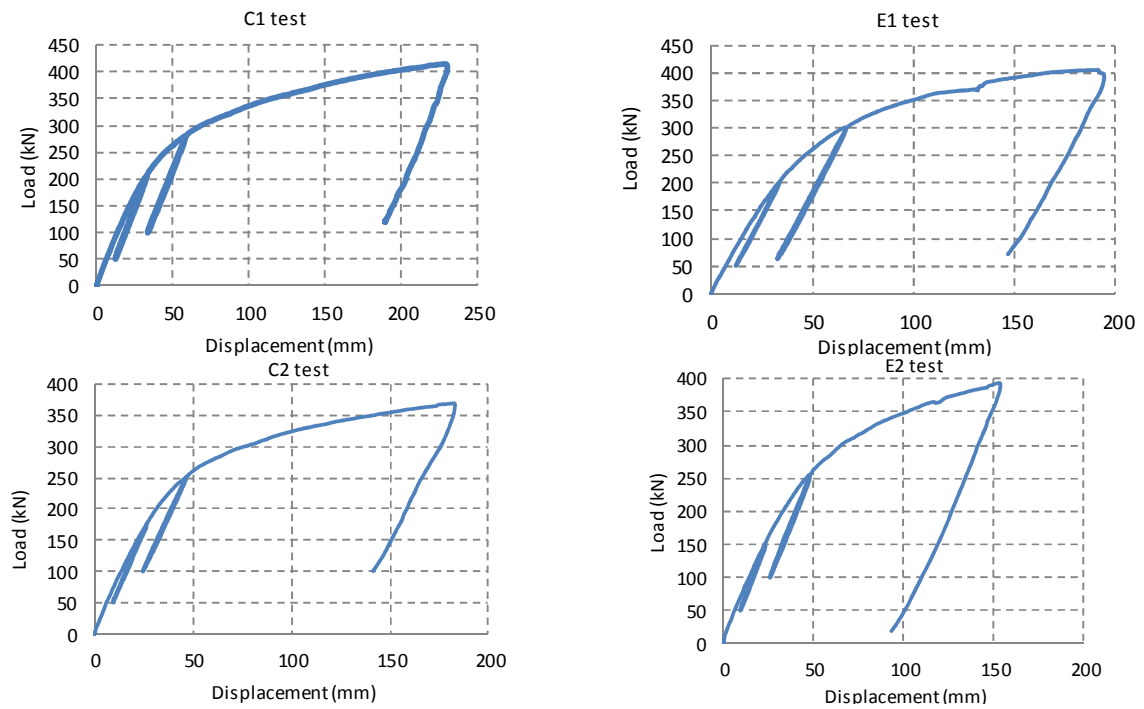


Figure 4.69. Load – point load displacement curves for B-EP-U joints

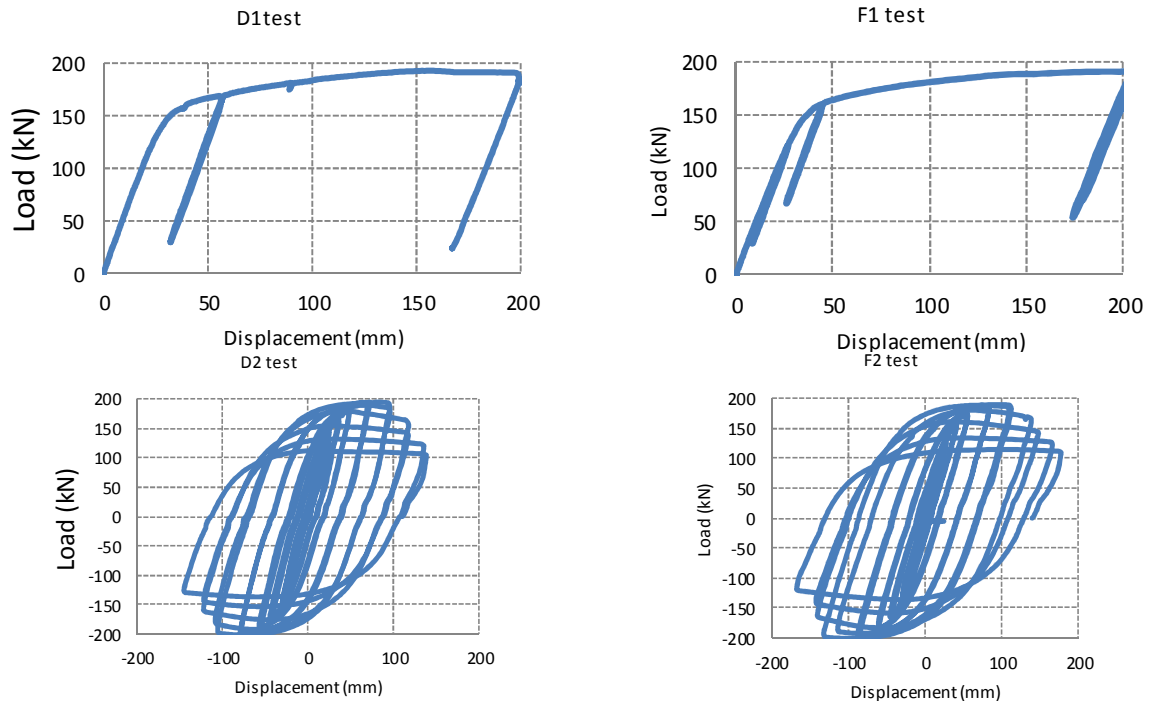


Figure 4.70. Load – point load displacement curves for B-EPL-RBS joints

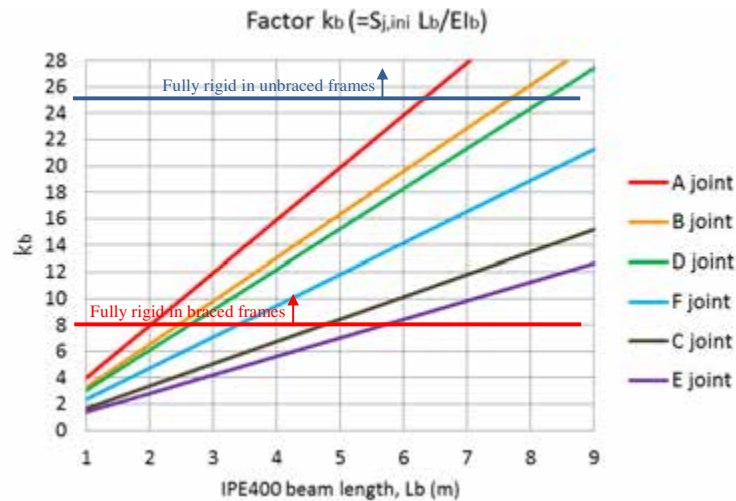


Figure 4.71. k_b factor for the joint types

Table 4.12 – Summary of joint characterization from the test results

Joint type	Resistance	Stiffness (IPE400 beam length requirement)			
		Braced frames		Unbraced frames	
		Semi-rigid	Rigid	Semi-rigid	Rigid
B-EP-H, NS (A)	Full	0 – 2.0 m	≥ 2.0 m	0 – 6.2 m	≥ 6.2 m
B-EP-H, HSS (B)	Full	0 – 2.6 m	≥ 2.6 m	0 – 8.0 m	≥ 8.0 m
B-EP-U, NS (C)	Partial	0 – 4.8 m	≥ 4.8 m	0 – 15.0 m	≥ 15.0 m
B-EP-U, HSS (E)	Full	0 – 5.6 m	≥ 5.6 m	0 – 17.5 m	≥ 17.5 m
B-EPL-RBS, NS (D)	Full	0 – 2.6 m	≥ 2.6 m	0 – 8.0 m	≥ 8.0 m
B-EPL-RBS, HSS (F)	Full	0 – 3.4 m	≥ 3.4 m	0 – 10.7 m	≥ 10.7 m

Note that the span of the referent building is 7.5m.

Summary of the observations from the test results

B-EP-H joint: this joint solution has a very high resistance and stiffness, as the main sources of the deformation are strengthened. Indeed, the extended part of the end-plate is reinforced by the hammer-head while the column flanges in bending and the column web panel in shear are reinforced by the lateral plates welded on the column flanges. Due to the hammed-head shape, stress concentrations at the beam level can be avoided. It has been demonstrated through these tests that a redistribution of loads between different compression zones, i.e. the hammer-head flange in compression and the beam flange in compression, occurs and should be taken into account in the estimation of the joint resistance. More details can be obtained within Deliverable D4 [11].

B-EP-U joint: the behaviour of the hammer-head zone and of the end-plate in this joint configuration is similar to the B-EP-H joint. However, the U reverse channel is the main source of the joint deformation and is generally the critical component mainly affecting the joint behaviour. The full strength and rigid requirements for B-EP-U joints are more difficult to be met in comparison to the B-EP-H joints.

B-EPL-RBS joint: the behaviour of the joints was not totally exposed during the tests, in particular in terms of resistance as the plastic hinges occurred at the dog-bone section of the beams. However, the test results show that the rigidity of the joints is quite high even the use of long bolts.

Obtained information for the analytical developments

The proposed joint configurations include some new components that are not yet covered in the Eurocodes. Accordingly, analytical investigations on these new components are required so as to propose, through the present research project, a full analytical method (founded on the component method) able to predict the main joint mechanical properties. In order to validate the proposed analytical models, the behaviour of these new components has been “exposed” during the tests. Table 4.13 summarises the obtained information regarding the new components/concepts. From these experimental results, the analytical models for the new components have been validated. Details about these models can be found in Deliverable D6 [68] of the present project.

Table 4.13 – Obtained information regarding new components

Joint type	Component/concept to be studied	Available information	Tests of reference
B-EP-H joints	Rigidity of the column flanges with lateral plate	yes	A1, A2, A3, A4, B1, B2, B3, B4
	Resistance of the column flanges with lateral plate	No	-
	Compression zone and lever arm	yes	A2, B1
	Behaviour and failure mode of the hammer heads	yes	A2, B1
	Behaviour and failure mode of the beam in the hammer head zone	yes	A1
B-EP-U joints	Rigidity and capacity of reverse U channel in bending	yes	C1, C2, E1, E2
B-EPL-RBS joints	Rigidity of the joints under bending	yes	D1, D2, F1, F2

4.3.3 Load introduction tests

4.3.3.1 Pre-test activities

Test set-up: The different testing set-ups for the column stub tests are shown in Figure 4.72. Set-up 1 aims at studying the friction which can be mobilized at the interface between the concrete core and the steel tube. Set-ups 2 and 3 aim at characterising the shear resistance of the bolts when the loads are applied on the concrete core or on the steel tube, respectively, i.e. when there is a gap (equal to the tube thickness) between the applied shear and the bolt support (set-up 2) and the bolts are subjected to shear + bending and when there is no gap and the bolts are subjected to pure shear only (set-up 3).

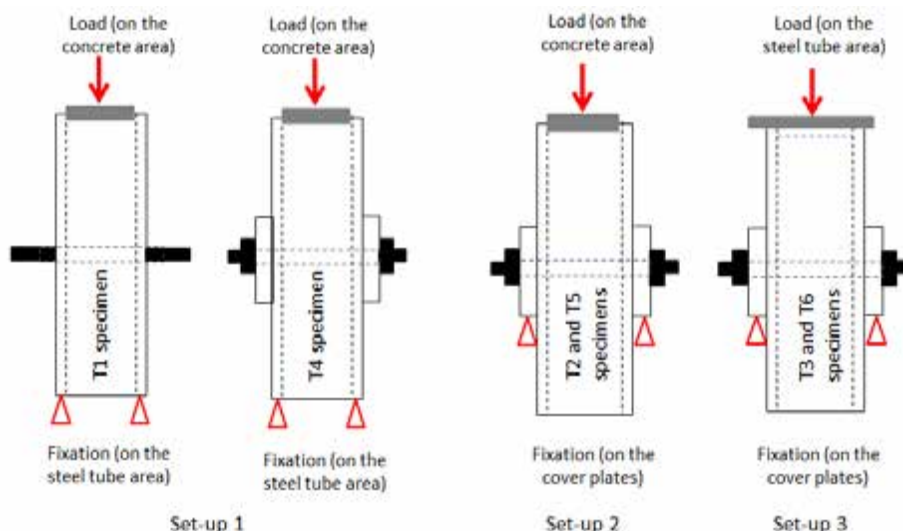


Figure 4.72. Test set-ups for the column stub tests

Material characteristics: the bolts, the steel tube and the concrete were characterized and the results were presented in Table 4.7, Table 4.8 and Table 4.9 (Section 4.3.2.1 – Tests on beam-to-column joints).

Instrumentation: the instrumentations for the specimens are presented in Table 4.14.

Table 4.14 – Instrumentation for the specimens

Quantities to be recorded	Instruments	Referent figures
Tube – bolts slip	D1 and D2	Figure 4.73
Concrete – tube slip	D3 and D4	
Plate – tube slip	D5 and D6	

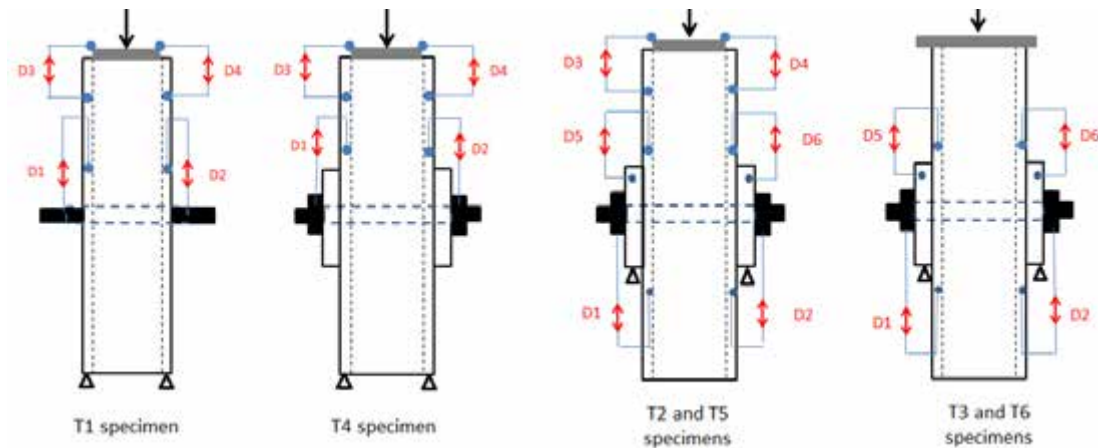


Figure 4.73. Instrumentation for column stubs (T1-T6)

Loading protocol: the quasi-static load procedure is applied for all the tests.

4.3.3.2 Test results and discussions

Table 4.15 summarizes the reached maximal load and the observed failure modes of all the column stub tests. Applied load vs. displacement curves are given in Figure 4.75.

Table 4.15 – Maximal loads and failure modes

Test	Maximal load	Failure modes
T1	1437 (kN)	Significant slip between the concrete and the tube; the bolts are significantly deformed but not failed (Figure 4.74-a)
T2	1218 (kN)	Small slip between the concrete and the tube; the bolt failed in shear; small deformation of the tube in bearing (Figure 4.74-b)
T3	1210 (kN)	small slip between the concrete and the tube; the bolt failed in shear; small deformation of the tube in bearing (Figure 4.74-b)
T4	3516 (kN)	Significant slip between the concrete and the tube; the bolts are considerably deformed but not failed (Figure 4.74-a)
T5	1182 (kN)	Small slip between the concrete and the tube; the bolt failed in shear; small deformation of the tube in bearing (Figure 4.74-b)
T6	1218 (kN)	Small slip between the concrete and the tube; the bolt failed in shear; small deformation of the tube in bearing (Figure 4.74-b)

Note that the failure sections of the bolts are at the interface between the plate and the steel tube, in the unthreaded portion of the shank.

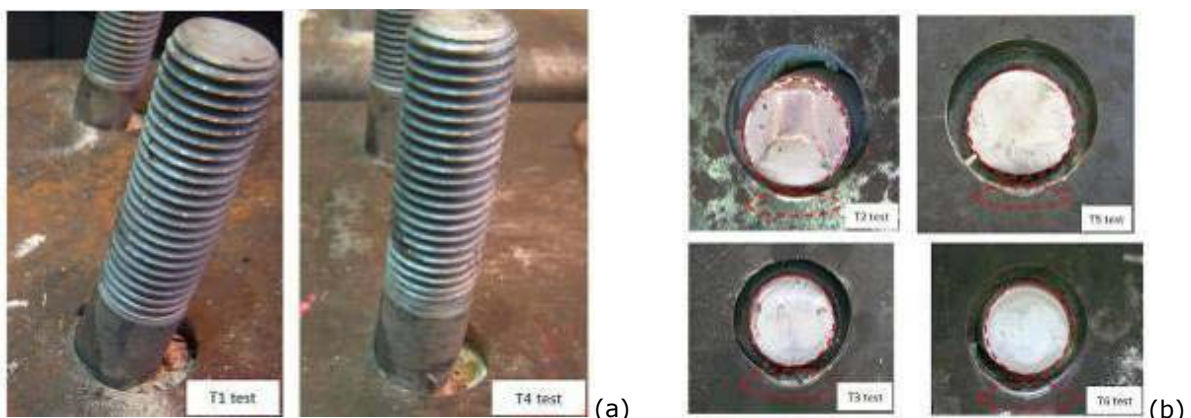


Figure 4.74. Critical zones in: (a) specimens T1 and T4, and (b) specimens T2, T3, T5 and T6

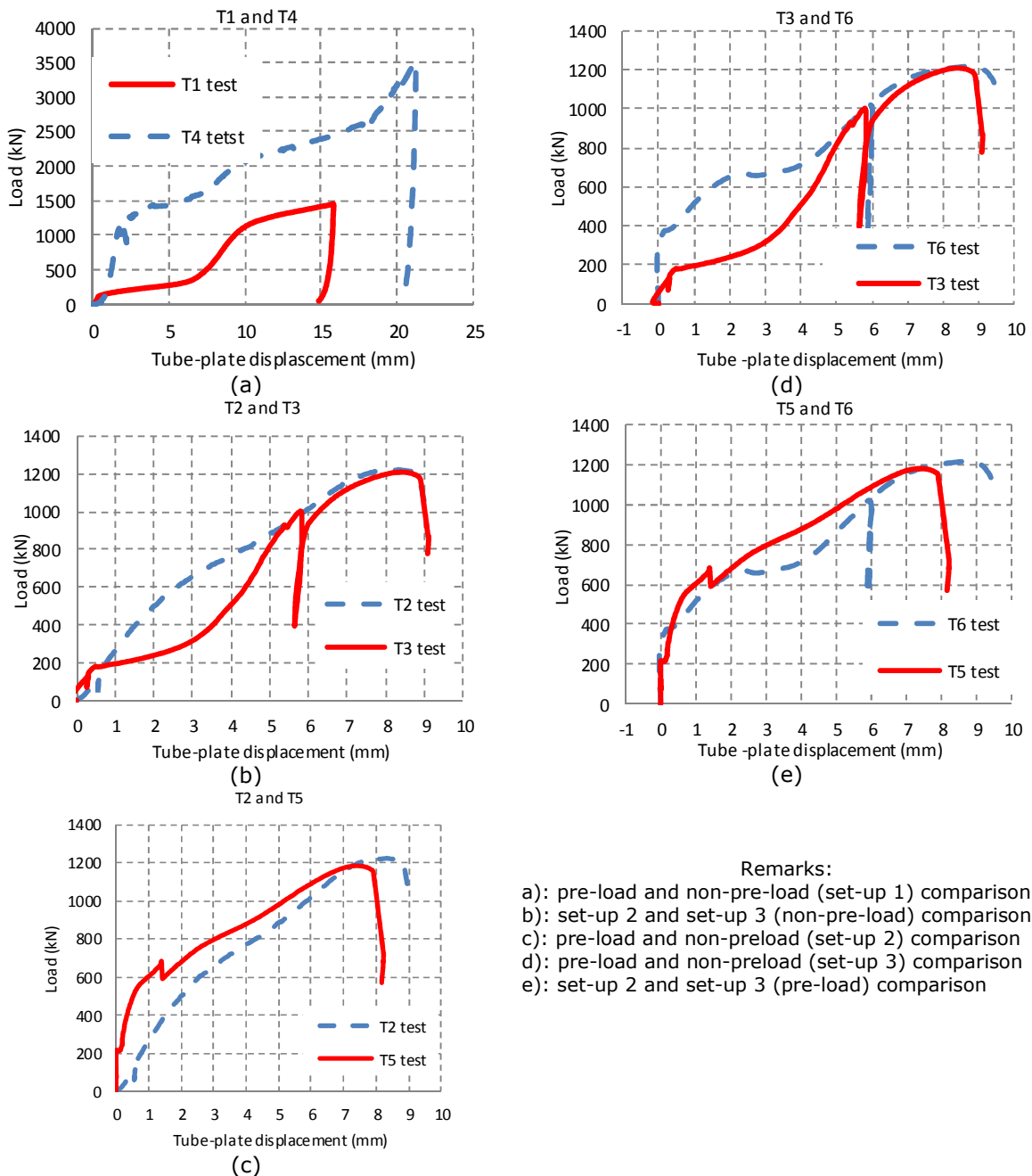


Figure 4.75. Load-displacement curves for the column-stubs tests

- Remarks:
- a): pre-load and non-pre-load (set-up 1) comparison
 - b): set-up 2 and set-up 3 (non-pre-load) comparison
 - c): pre-load and non-preload (set-up 2) comparison
 - d): pre-load and non-preload (set-up 3) comparison
 - e): set-up 2 and set-up 3 (pre-load) comparison

Discussions on the shear resistance of the bolts

The behaviour of the bolts subjected to shear or to shear + bending is studied using the testing set-ups 2 and 3 (see Figure 4.72), i.e. through tests T2, T3, T5 and T6. The maximal loads (about 1200 kN) and the failure modes (bolts in shear) are almost the same for these tests which indicates that:

- There is no effect of the bolt preloading on the bolt shear resistance;
- The bending moment due to the gap (equal to the tube thickness) between the application of the shear through the concrete core and the bolt support (see the testing set-up 2 in Figure 4.72) is not significant and so, does not affect significantly the shear resistance of the bolts.

A quarter of the so-obtained shear resistance (i.e. 300 kN; $\frac{1}{4}$ - because 4 shear plans are present in the tested configuration) can be compared to the shear resistance obtained analytically using the following formula recommended in EN 1993-1-8 (§3.6.1) [3]:

$$F_{shear} = f_{u,bolt} A_{bolt} / \sqrt{3} = 263 \text{ kN} \quad (4.1)$$

where $f_{u,bolt} = 1008 \text{ N/mm}^2$ is the actual ultimate strength of the bolt material and $A_{bolt} = 452 \text{ mm}^2$ the unthreaded bolt shank area.

It can be seen that the analytical formula recommended in EN 1993-1-8 [3] gives a conservative prediction of the shear resistance of the bolts.

Discussions on the bearing resistance of the CFT column

The bearing resistance of the CFT column comes from the contributions of two components: the steel tube wall and the concrete core.

The bearing resistance formula given in EN 1993-1-8 (§3.6.1) [3] can be easily used for the steel tube wall as reported in Table 4.16. However, for the resistance of the concrete core, some assumptions are needed. The concrete within the tube is confined in the latter and its resistant strength needs to be adapted to take this effect into account; this can be done using the recommendations from EN 1994-1-1 (§6.7.4.2(6)) [4] reported in Table 4.16. Also, a length of contact between the bolt shank and the concrete core needs to be considered; it is proposed here to assume a contact length of $2.5 \cdot d$, d being the diameter of the bolt shank in contact with the concrete core, as illustrated in Figure 4.76. The proposed procedure applied to the tested specimen is reported in Table 4.16. In fact, this failure mode, i.e. tube + concrete in bearing, didn't occur during the performed tests. Accordingly, it is impossible to verify the validity of the proposed approach which appears to be anyway reasonable.

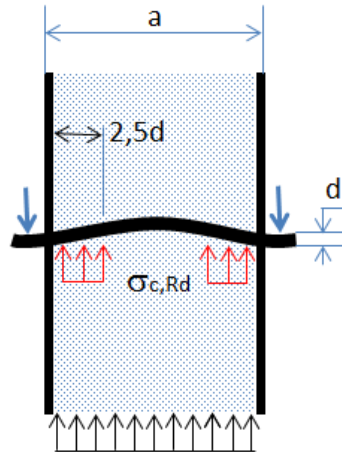


Figure 4.76. Effective length of the bolts for the calculation of the concrete core in bearing

Table 4.16 – Bearing resistance of the tested CFT column

Geometrical and material properties (see the coupon test results)
Bolt ultimate strength $f_{ub}=1008 \text{ N/mm}^2$, steel tube strength $f_u=827 \text{ N/mm}^2$, concrete strength $f_{cm}=45 \text{ N/mm}^2$, nominal diameter of the bolts $d=24 \text{ mm}$, tube width $a=250 \text{ mm}$, tube wall thickness $t=10 \text{ mm}$, cross-section of the concrete $A_c=52900 \text{ mm}^2$, concrete area under the bolt $A_1=24 \cdot 230=5520 \text{ mm}^2$.
Bearing resistance of the tube wall (EN 1993-1-8, §3.6.1, [3])
$F_{b,tube} = 4 \cdot 0,8 \cdot 2,5 f_u d t = 1588 \text{ kN}$ (the factor "4" is linked to the presence of four bearing zones in the tube and the factor "0,8" is used for oversized holes)
Bearing resistance of the concrete
Confined concrete strength (EN 1994-1-1, §6.7.4.2(6), [4]):
$\sigma_{c,Rd} = f_{cd} \left(1 + 3,5 \frac{t}{a} \frac{f_y}{f_{ck}} \right) \sqrt{\frac{A_c}{A_1}} = 45 \left(1 + 3,5 \frac{10}{250} \frac{702}{45} \right) \sqrt{\frac{52900}{2.5520}} = 314 \text{ N/mm}^2$
Bearing resistance (two bolts):
$F_{b,concrete} = 2 \cdot 2 \cdot 2,5 d \cdot d \sigma_{c,Rd} = 1808 \text{ kN}$

Discussions on the steel tube – concrete slip resistance

Tests T1 and T4 were dedicated to the characterisation of the slip resistance between the steel tube and the concrete core. As can be seen in the test results reported in Table 4.15 and Figure 4.75, significant loads were reached during these tests, in particular for Test T4 ($P = 3516 \text{ kN}$).

During Test T4, a slip between the steel tube and the concrete occurred at a load of around 1500 kN . Then, the bolts entered into contact with the steel tubes and shear forces were developing in these bolts; the system was able to sustain an additional load of around 2000 kN . However, as highlighted above, the shear resistance of the bolts has been estimated experimentally as equal to 1200 kN , which means that the bolt in shear was not the only component to support the additional load of 2000 kN .

This "over" resistance has been associated to the development of confinement effects in the concrete core, leading to the high friction between the steel tube and the concrete. A model to

estimate the force in the bolts taking into account the friction has been established. The development of the force in the bolts estimated through the proposed model is given in Figure 4.77; this prediction is in good agreement with the test results. Details on the proposed model can be found in Deliverable D4 [11] of the present project.

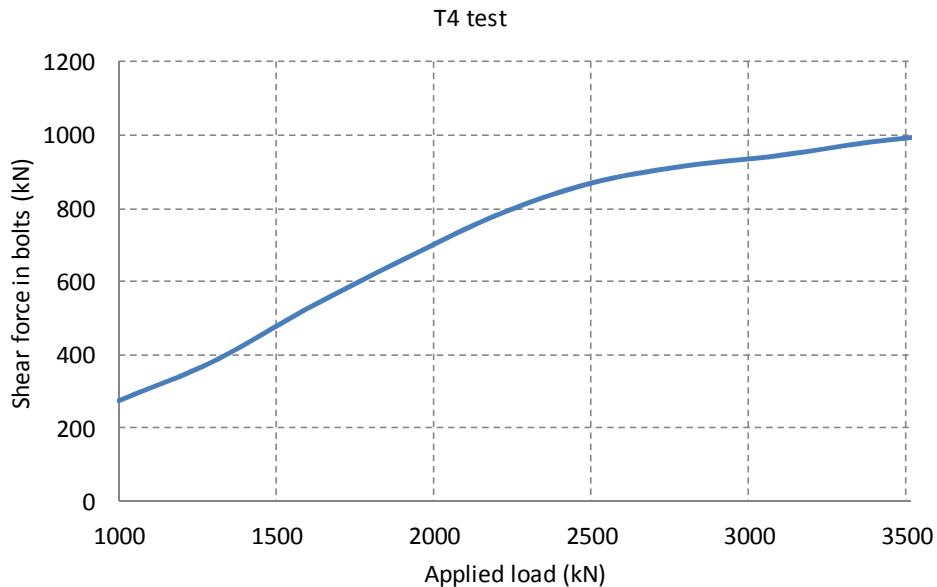


Figure 4.77. Shear force in the bolts during test T4

4.4 Welded beam-to-column joints in moment-resisting dual-steel frames

4.4.1 Experimental program

Experimental tests on large specimens were performed in order to demonstrate that joint detailing and welding technology perform adequately under seismic loading. Four types of joints were investigated:

- Welded stiffened beam-to-column joints with fully-encased wide-flange (FE-WF) columns;
- Welded cover plate beam-to-column joints with fully-encased wide-flange (FE-WF) columns;
- Welded reduced beam section (RBS) beam-to-column joints with concrete filled rectangular hollow section (CF-RHS) columns;
- Welded cover plate (CP) beam-to-column joints with concrete filled rectangular hollow section (CF-RHS) columns.

Table 4.17 summarizes the experimental program performed at University of Ljubljana covering a number of 16 beam-to-column joints with FE-WF columns. In addition, Table 4.18 and Table 4.19 summarise the experimental program performed at Politehnica University of Timisoara covering a number of 16 beam-to-column joints with CF-RHS columns, and 6 column stubs for the load introduction tests.

Table 4.17 – Experimental program on beam-to-column joints with FE-WF columns (UL)

Parameter	Variable	No. of variations	No. of specimens
Joint type	Stiffened and cover-plate	2	16
HSS grade	S460 and S690	2	
Loading procedure	Cyclic: Variable & Constant amplitude	2	
Level of axial force	Low and High	2	

Table 4.18 – Experimental program on beam-to-column joints with CF-RHS columns (UPT)

Parameter	Variable	No. of variations	No. of specimens
Loading	Monotonic & Cyclic	2	16
Joint type	Reduced Beam Section & Cover-Plate	2	
HSS grade	S460 & S690	2	
Failure mode	Weak beam / Weak connection	2	

Table 4.19 – Experimental program on column stubs (UPT)

Parameter	Variable	No. of specimens
Loading	Monotonic & Cyclic	6
Bond	Friction & Friction + Connectors	
HSS grade	S460 & S690	

4.4.2 Tests on welded stiffened and welded cover plate beam-to-column joints with fully-encased wide-flange columns

The current study investigated the concept of stiffened connections, applied to moment resisting frames and dual braced frames. Two different cases of reinforced typology were considered: configuration with a single vertical rib plate, and another one with cover plates attached to the beam flanges. Additionally, a hybrid-steel approach was implemented, where high strength steel (HSS) was used for columns, representing non-dissipative elastic members, and mild carbon steel (MCS) for beams, acting as dissipative members during earthquake. A description of the two joint typologies is made in Section 2.4.2.2, while the design procedure is summarised in Section 5.3.6. To take advantage of the additional fire resistance, structural stiffness and strength, fully encased composite columns were used. Beside two joint types and two different column-beam material combinations, S460/S690 grade steel column and S355 grade steel beam, other parameters of the study were: different cyclic loading histories and the level of axial force in the column, which may be important especially in braced frames. The main parameters of the study are summarized in Table 4.20. Sixteen tests on large scale specimens were performed in order to demonstrate that the joint detailing and the applied welding technology perform adequately under cyclic loading. Description of the test specimens is presented, emphasizing the selection of suitable detailing of both studied beam-to-column joints. Evaluation of experimental results is provided by means of different response parameters in order to compare systematically the behaviour of each connection in terms of strength, stiffness, ductility and energy dissipation capacity. Finally, the experimentally obtained joint deformation capacities were compared to related pre-qualification requirements.

Table 4.20 – Experimental program on beam-to-column joints with FE-WF columns

Parameter	Variable	No. of variations	No. of specimens
Joint type	Stiffened and cover-plate	2	16
HSS grade	S460 and S690	2	
Loading procedure	Cyclic: Variable & Constant amplitude	2	
Level of axial force	Low and High	2	

4.4.2.1 Experimental program and specimen configuration

To investigate and evaluate the seismic performance of hybrid steel building frames made of two different steel grades, taking into account the two selected stiffened joint typologies, four different one sided beam-to-column joint specimens were designed for the tests. Fully encased H-profile steel composite columns were used and the presence of the concrete slab was not considered. Constructional details with member sizes, steel beam-column material combinations as well as composite column cross-section characteristics for all four different specimens are presented in Figure 4.78.

All the joints were designed as full strength connections where plastic hinge is expected to occur in the beam section which is referred to as dissipative region. To address different beam-column MCS-HSS material combinations, each of the two stiffened configuration is represented by two different joints. Specimens RS1 and CP1 comprise beam profile IPE270 in steel grade S355 and steel column profile HEB200 in steel grade S460, hereafter referred to as large column. Specimens RS2 and CP2 are made of beam profile IPE240 in steel grade S355 and steel column profile HEB160 in steel grade S690, hereinafter referred to as small column. Steel profile of the small composite column was welded because hot-rolled profile in steel grade S690 was not available. Reliable inelastic deformation capacity for highly ductile members requires width to thickness ratios of the parts subject to compression be limited to a range that provides cross-section resistance to local buckling well into the inelastic range. Both selected beam cross-sections IPE 240 and IPE 270 meet compactness limit for Class 1 cross-sections in bending according to EN 1993-1-1 [6] and ANSI/AISC 341-10 [7] seismic provisions.

Steel parts of the specimens were fabricated with a standard workmanship quality. Composite column cross-section characteristics were designed in a way that relatively high level of compression axial load-to-design plastic resistance ratio is achieved within available laboratory capabilities. Additional shear studs were applied in the region of both column ends to achieve appropriate load introduction. Longitudinal and transverse reinforcement were defined according to recommendations from EN 1994-1 [4] and EN 1998-1 [1]. Normal strength concrete of grades C25/30 and C30/37 was considered for large and small column, respectively. To facilitate casting, additives were applied to the concrete mixture, which resulted in somewhat greater concrete compressive strengths ranging between 51 and 66 N/mm². Resistance of both composite column cross-sections to combined compression and bending, represented by simplified interaction curve, is shown in Figure 4.79, where interaction curves for the design and the actual material characteristics are plotted. Characteristic and design values of composite column plastic resistances to compression were 8115 and 6710 kN for large column and 7962 and 6829 kN for small column. Taking into account the maximal actuator force of 3000 kN, used to apply the constant column axial force as well as additional axial force in the column because of the transverse force at the tip

of the beam, the ratio axial load/actual composite column plastic resistance ranged between 0.37 and 0.39 in case of the large column and between 0.39 and 0.41 in case of the small column.

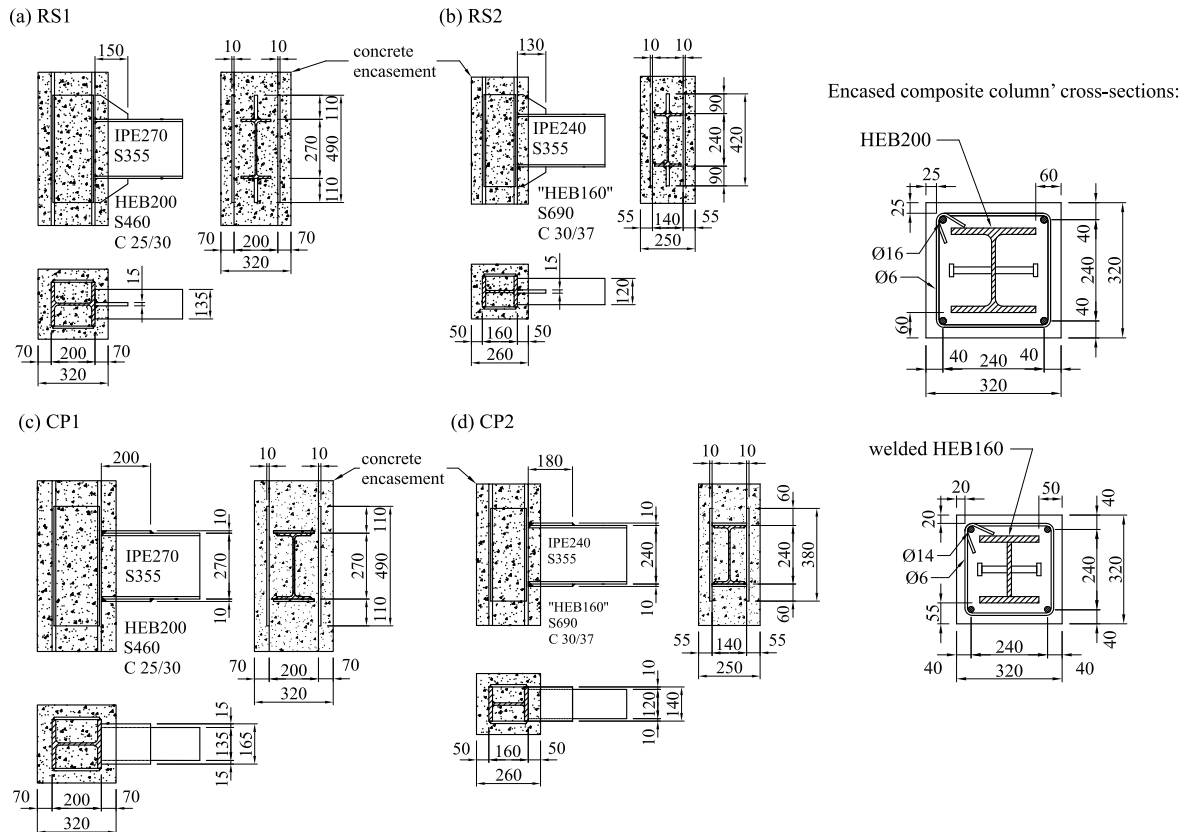


Figure 4.78. Constructional details of four designed stiffened joints

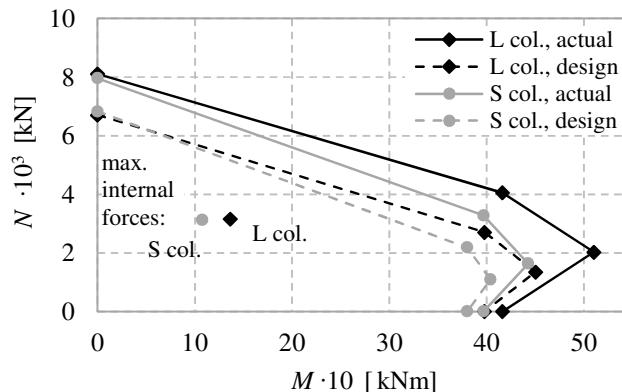


Figure 4.79. N-M interaction curves for large (L) and small (S) composite column cross-section

The same ratio, taking into account the design resistance, ranged between 0.45 and 0.47 and between 0.41 and 0.48 for the large and the small column, respectively. Beside strong column-weak beam requirement fulfilled for all four joint configurations, columns were designed to provide strong column panel zone taking into account additional contribution of concrete in compression and side plates welded to the steel column, see Figure 4.78 and Figure 2.10.

The complete test was designed to simulate the boundary conditions of a beam-to-column exterior connection in a moment-resisting frame or inner connection in a braced frame under typical lateral loading, Figure 4.80. The effect of column axial force may have an influence on connection performance, and its inclusion in the test program was considered as means to obtain more realistic test conditions. The column was assumed to be pin-supported at its both ends. Additional support in loading plane was provided at column mid-height constraining the horizontal displacement at the building's floor level. The column was laterally supported at the bottom, top and mid-height location in order to prevent any horizontal displacements in case of large column axial force. Lateral braces were provided to the beam near the location of plastic hinge and at the free end of the beam, near the application of transverse force, Figure 4.81.

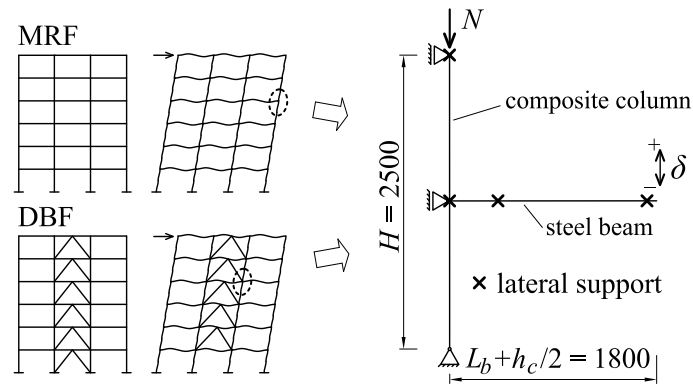


Figure 4.80. Static model of the specimen with boundary conditions and loads applied

Lateral bracing was provided to all ten specimens near the actuator to protect the actuator from damage due to horizontal translation and rotation of the beam following buckling.



Figure 4.81. Experimental test set-up

The average results from the tensile tests on the steel coupons are presented in Table 4.21.

Table 4.21 – Monotonic tensile material properties

Sample type	Steel material	Yield strength, f_y (N/mm ²)	Ultimate tensile strength, f_u (N/mm ²)	f_u/f_y	Elongation at fracture, A (%)
IPE 240, web	S355	435	516	1.19	32
IPE 240, flange	S355	385	486	1.26	31
IPE 270, web	S355	444	514	1.16	33
IPE 270, flange	S355	385	498	1.29	32
"HEB 160" web	S690	808	864	1.07	18
"HEB 160" flange	S690	783	818	1.04	18
HEB 200	S460	468	576	1.23	28
Rib stiffener	S355	450	491	1.09	33
Cover plate	S355	424	501	1.18	34

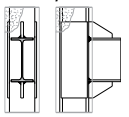
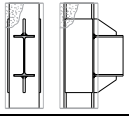
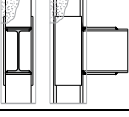
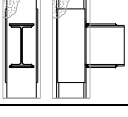
The toughness of all the components was determined by standard Charpy V-notch tests at the temperature of -20 °C, including three specimens for each component. Values of absorbed energy for steel material grade S355 ranged between 108 and 226 J, for grade S460 between 151 and 185 J, and for grade S690 between 91 and 185 J, which is satisfactory.

The instrumentation scheme allowed for the measurement of specimen global and local response quantities, e.g. displacement at the tip of the beam, relative rotation of plastic hinge zone, column rotations, displacement of supports. In addition, uniaxial strain gauges were used to capture strain

response on the beam in and around the yielding zone and at the beam-column interface. Additional strain gauges were placed on the column steel section near beam-to-column connection, Figure 4.92-b.

A quasi-static cyclic loading was used in all the tests. Force controlled loading was used in the elastic range with loading rate 2.5 kN/s, while displacement control loading was used in the plastic range, measured directly in terms of total displacement at the beam tip. Loading rate 1.3 mm/s was used with the maximum measured strain rate of about 0.0009/s. For the first two tests, specimens RS1.1 and RS1.2, Table 4.22, modified protocol from [5] was used according to [69]. The following cyclic sequence was applied: (1) three cycles in elastic range with a semi-amplitude equal to $\frac{1}{4}$, $\frac{1}{2}$, $\frac{3}{4}$, 1 of v_y , where v_y is the yield displacement obtained from preliminary non-linear FEA; (2) three cycles at each amplitude $i \cdot v_y$, with $i = 2, 3, 4, \dots$, up to the complete failure of the specimen. On the basis of the results obtained from the first two tests, displacement increment between the two successive amplitudes was considered to be somewhat too large. Therefore, for the other six specimens tested under cyclic loading with increasing amplitude, Table 4.22, loading procedure according to ANSI/AISC 341-10 [7] was used. Since the study is focused on the determination of beam-to-column joint response under arbitrary loading histories, in addition to variable cyclic loading protocol, two different inelastic constant displacement levels were considered. This allowed damage phenomena due low-cycle fatigue (LCF) to be properly evaluated. From the examination of the local strain response of specimens, previously tested under variable amplitude loading, two constant displacement amplitudes were considered: 35 mm and 60 mm, hereinafter referred to as small and large constant amplitude, respectively. Both constant cyclic amplitudes were applied on each of the four designed joint configurations, see Table 4.22. The values of constant amplitudes were chosen to capture two distinct responses of the beam in plastic hinge region: with and without the presence of local buckling for large and small amplitude, respectively. At the same time the amplitudes had to be different enough in order to produce different fatigue endurance on the same type of specimen. Each test was run until the failure of specimen, characterized by the complete fracture of the beam flange followed by the loss of load resistance.

Table 4.22 – Summary of all 16 test specimens

Specimen	Specimen's column/beam characteristics		Loading protocol	Column axial force
	Steel section	Material combination		
RS1.1		S355/S460	variable	0
RS1.2			variable	3000 kN
RS1.3			constant, small	3000 kN
RS1.4			constant, large	3000 kN
RS2.1		S355/S690	variable	0
RS2.2			variable	3000 kN
RS2.3			constant, small	3000 kN
RS2.4			constant, large	3000 kN
CP1.1		S355/S460	variable	0
CP1.2			variable	3000 kN
CP1.3			constant, small	3000 kN
CP1.4			constant, large	3000 kN
CP2.1		S355/S690	variable	0
CP2.2			variable	3000 kN
CP2.3			constant, small	3000 kN
CP2.4			constant, large	3000 kN

4.4.2.2 Tests results

The presented moment-rotation diagrams comprise the moment determined at the column centreline (M_c) as a function of total joint rotation (θ_T) calculated as the beam tip displacement, divided by the distance between the loading point and the centreline of the column (1800 mm). To be consistent with the loading directions applied in the tests, positive rotation is supposed to be in counter clock direction, Figure 4.81-a. The plastic joint rotation (θ_{pl}), is obtained by subtracting elastic bending and shear deformation of the beam as well as complete contribution from the column: elastic column bending and panel zone deformations. Although the column web panel contribution is generally considered as plastic deformation, it was not included in θ_{pl} . Since all the specimens were designed taking into account the strong column-weak beam concept, and due to additional strength and stiffness resulting from column side plates and concrete encasement, very small elastic deformation of the column panel zone was observed in all the specimens. Hence, θ_{pl} is attributed to the plastic hinge rotation in beam, and is referred to as plastic beam rotation ($\theta_{pl,b}$).

Variable amplitude cyclic tests

The response of specimens RS1.2, RS2.2, CP1.2 and CP2.2 tested under cyclic loading with increasing amplitude in combination with the presence of constant column axial force of 3000 kN is shown in Figure 4.82.

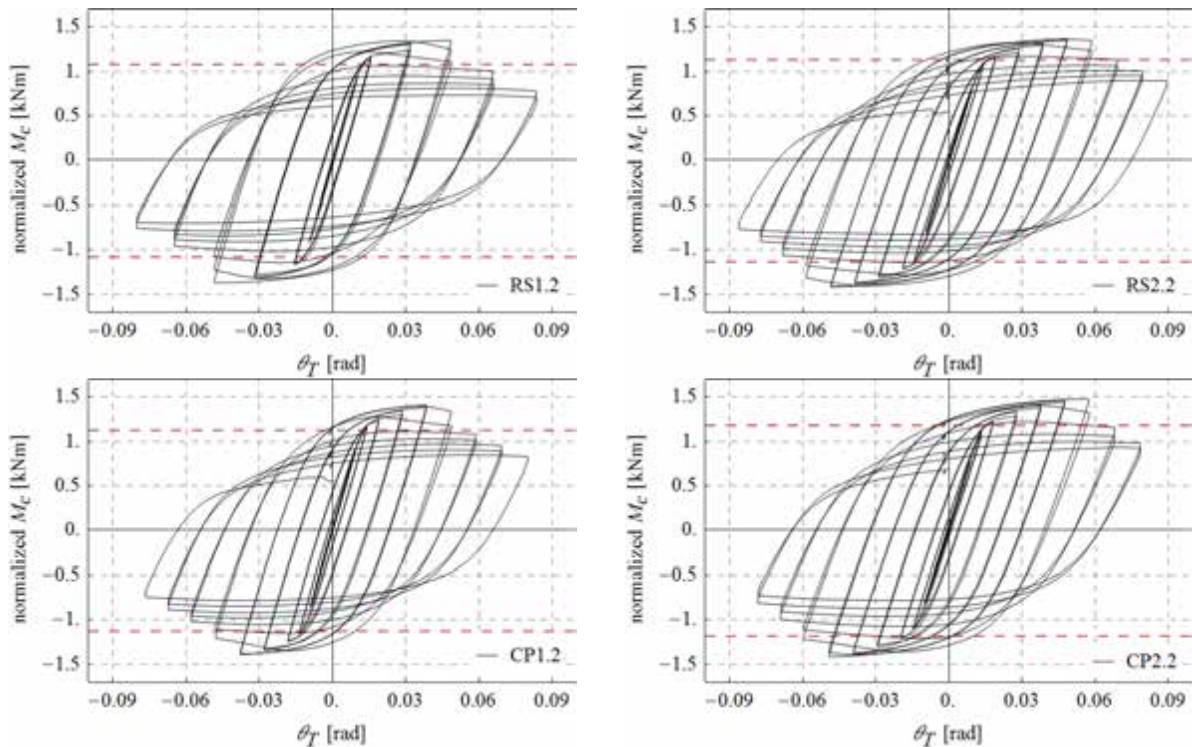


Figure 4.82. Moment vs. total joint rotation relationship for specimens tested under variable cyclic loading with full column axial force

Moment M_c is normalized by the beam plastic moment $M_{pl,b}$, calculated with actual geometric and material characteristics. Dashed lines on each diagram of Figure 4.82 represent the limit associated with 20% drop of maximal strength for positive and negative loading directions, which corresponds to acceptance criterion from EN 1998-1 [1]. The response of the other four specimens, RS1.1, RS2.1 and CP1.1, CP2.1, tested under the same loading protocol, but without column axial force applied during the test, is not presented herein since it is very similar, suggesting that the applied level of the column axial force did not affect the cyclic behaviour of the joints. The comparison of the responses of all eight specimens tested under cyclic loading with increasing amplitude is presented in Figure 4.83. Curves of absolute moment amplitudes as a function of complete joint rotation for the four RS specimens are shown in Figure 4.83-a and for the four CP specimens in Figure 4.83-b. Moment amplitudes corresponding to both loading directions for complete loading history are presented.

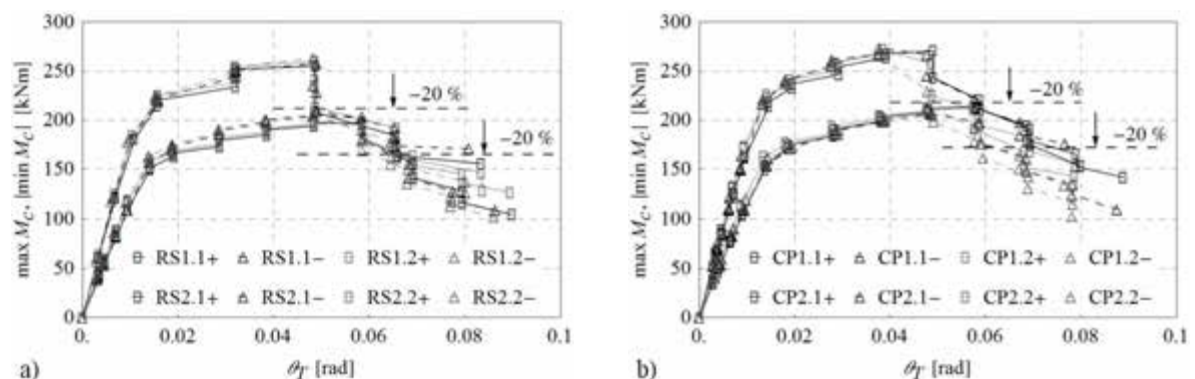


Figure 4.83. Comparison of moment amplitudes vs. total joint rotation for specimens tested under variable amplitude: (a) RS and (b) CP joints

The maximum strengths of two equal specimens RS1.1 - RS1.2 (IPE270 beam), RS2.1 - RS2.2 (IPE240 beam), for RS joint and CP1.1 - CP1.2 (IPE270 beam), CP2.1 - CP2.2 (IPE240 beam) for CP joint are nearly the same because the specimen strengths were controlled by the strength of the beam, being the same for the each of the pairs. Normalized values of maximum moment $M_{c,u}$ are given in Table 4.23 and vary between 1.35 and 1.42 for RS joints and between 1.41 and 1.48 for CP joints. The values belonging to the CP joints are somewhat larger in comparison to those

obtained on the RS joints. The reason for this is inherent in geometric characteristics of both designed joint configurations: the reinforcing cover plates are longer than the ribs, forcing plastic hinge to occur far away from the column face, thus producing shorter distance to the load insertion point. Larger values of $M_{c,u}$ produced by specimens with smaller, more compact beam cross-section IPE240 can also be observed. A very similar response can be noticed between two equal RS and CP joints from Figure 4.83, which shows that the results obtained are repeatable.

Distribution of moment amplitudes over cycles in inelastic range for two representative specimens of RS and CP joint is presented in Figure 4.84-a, and Figure 4.84-b, respectively. For each of two specimens the limit associated with 20% drop of maximal strength is denoted. The label associated with the last cycle without stiffness degradation of more than 20% of its initial value is marked as well.

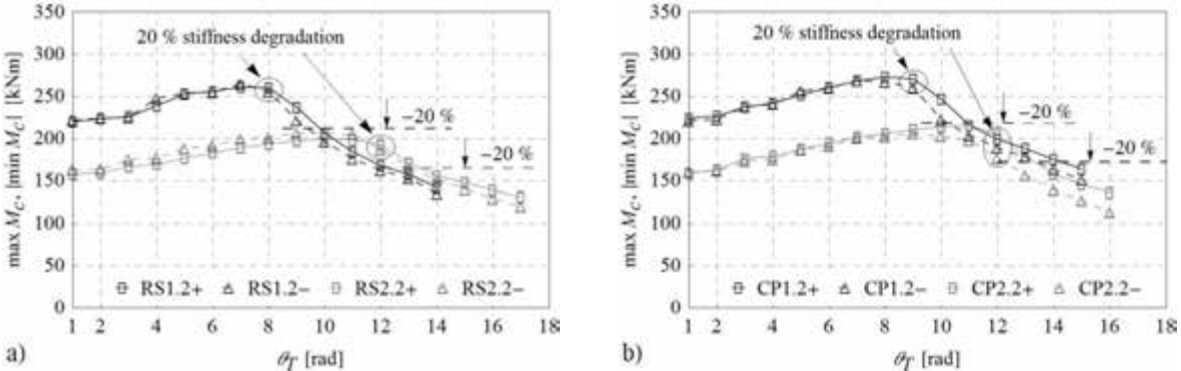


Figure 4.84. Comparison of moment amplitudes vs. number of cycles in inelastic range: (a) specimens RS1.2 and RS2.2, (b) specimens CP1.2 and CP2.2

As can be seen from Figure 4.84, for all four selected specimens 20% fall of initial stiffness occurred prior to the 20% degradation of maximal strength. For the case of all eight specimens tested with variable cyclic loading, the stiffness criterion proved to be equally or even more stringent than strength degradation criterion, see Table 4.25. None of the eight specimens failed prematurely. The degradation of strength and stiffness evident from Figure 4.82 to Figure 4.84 was a consequence of beam local buckling in the plastic hinge zone immediately beyond the end of the strengthened connection. In all eight cases flanges buckled prior to webs. Before the onset of large flange and web local buckling, modest flange buckling occurred, with amplitudes around beam flange thickness. At this state local buckling did not cause strength degradation. In the following cycle buckled flanges in tension were straightened again, which was not the case when large buckling amplitudes had occurred. Finally, failure occurred in the buckled zone of the beam with fracture initiated in the flange as a result of the low-cycle fatigue (see Figure 4.85 & Figure 4.86).

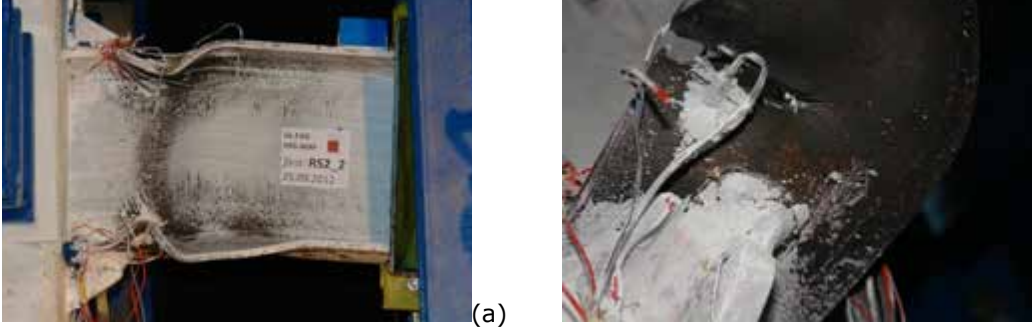


Figure 4.85. Specimen RS2.2 after the failure: a) overall view: beam local buckling with the spread of plastic zone (darker region), b) detail of fracture in the bottom beam flange

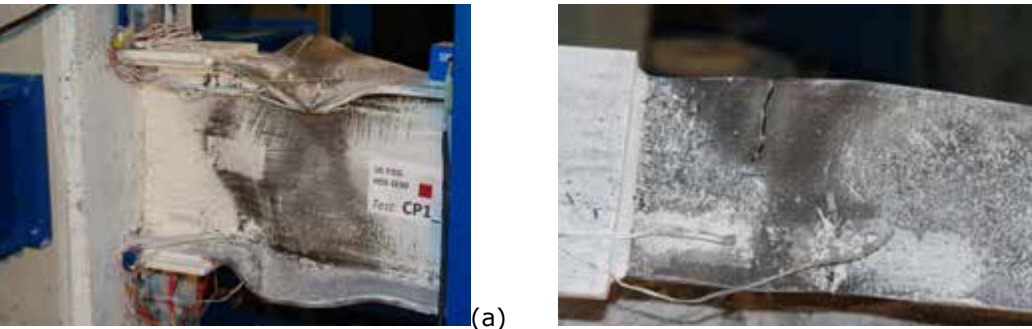


Figure 4.86. Specimen CP1.1 after the failure: a) overall view: beam local buckling with the spread of plastic zone (darker region), b) detail of fracture in the top beam flange

No yielding of reinforcing plates or damage of welds, either in case of RS or in case of CP joints, was observed during the tests. In case of RS joints the first cracks were observed in the heat-affected zone (HAZ) around fillet weld at the end of rib stiffener, Figure 4.84-b, but they did not have any detrimental effect on the response of the specimens, since the final crack always appeared in the largest buckle in the beam flange. Despite distorted and partly fractured beam cross-section due to pronounced local buckling in the dissipative zone, the resistance of all the eight joints just before the failure ranged between 51 and 63% of their maximum strength.

Table 4.23 and Table 4.24 present a summary of experimental response characteristics of test specimens for each of the two joint groups. Beside ultimate moment ($M_{c,u}$) and ultimate moment normalized with actual beam plastic moment ($M_{c,u} / M_{pl,b}$) tables include values of maximum beam plastic rotations (θ_{pl}) and the corresponding cumulative beam plastic rotations ($\Sigma\theta_{pl}$) evaluated for three selected failure criteria. The first criterion represents the state at which fracture occurred, followed by a significant drop of resistance. The second criterion relates to the 20% fall of maximum strength and initial stiffness (values related to the criterion and reported in Table 4.23, Table 4.24 and Table 4.25 correspond to the cycle where first of both falls is detected) and the third one describes the instance with the 20% fall of the actual beam plastic moment $M_{pl,b}$. Corresponding beam plastic rotations and cumulative plastic rotations for the three failure criteria are designated as θ_{pl}^{max} , $\Sigma\theta_{pl}^{max}$, θ_{pl}^{80max} , $\Sigma\theta_{pl}^{80max}$, θ_{pl}^{80b} , $\Sigma\theta_{pl}^{80b}$. Moments and rotations presented in both tables are evaluated with respect to the column centreline.

Table 4.23 – Summary of experimental results for the RS group of specimens

Specimen group:	$M_{c,u}$ (kNm)	$M_{pl,b}$ (kNm)	$M_{c,u}/M_{pl,b}$	θ_{pl}^{max} (rad)	θ_{pl}^{80max} (rad)	θ_{pl}^{80b} (rad)	$\Sigma\theta_{pl}^{max}$ (rad)	$\Sigma\theta_{pl}^{80max}$ (rad)	$\Sigma\theta_{pl}^{80b}$ (rad)
RS1.1	261.3	193.7	1.35	0.071	0.036	0.071	1.505	0.626	1.505
RS1.2	265.1	193.7	1.37	0.074	0.036	0.057	1.832	0.531	1.290
RS1.3	234.1	193.7	1.21	0.006			1.728	1.640	1.670
RS1.4	255.2	193.7	1.32	0.020			2.167	0.930	2.167
RS2.1	209.0	146.0	1.43	0.076	0.041	0.066	2.044	0.852	1.758
RS2.2	206.7	146.0	1.42	0.078	0.044	0.078	2.138	0.921	2.138
RS2.3	175.8	146.0	1.20	0.006			2.305	2.212	2.280
RS2.4	194.3	146.0	1.33	0.017			2.018	1.942	2.018

Table 4.24 – Summary of experimental results for the CP group of specimens

Specimen group:	$M_{c,u}$ (kNm)	$M_{pl,b}$ (kNm)	$M_{c,u}/M_{pl,b}$	θ_{pl}^{max} (rad)	θ_{pl}^{80max} (rad)	θ_{pl}^{80b} (rad)	$\Sigma\theta_{pl}^{max}$ (rad)	$\Sigma\theta_{pl}^{80max}$ (rad)	$\Sigma\theta_{pl}^{80b}$ (rad)
CP1.1	274.9	193.7	1.42	0.062	0.030	0.062	1.547	0.546	1.547
CP1.2	273.1	193.7	1.41	0.069	0.035	0.059	1.658	0.479	1.401
CP1.3	249.0	193.7	1.29	0.005			2.316	2.272	2.316
CP1.4	277.1	193.7	1.43	0.019			2.920	0.881	2.920
CP2.1	216.3	146.0	1.48	0.076	0.039	0.076	1.981	0.815	1.981
CP2.2	215.5	146.0	1.48	0.068	0.042	0.067	1.815	0.893	1.564
CP2.3	180.9	146.0	1.24	0.004			2.302	2.260	2.279
CP2.4	202.9	146.0	1.39	0.017			3.960	2.592	3.960

Values of maximum plastic rotations represent the smaller value of the maximum values for positive and negative loading direction. For all the eight specimens θ_{pl}^{max} ranges between 0.067 and 0.079 rad, without any significant difference between the two stiffened joint types or beam section sizes. Values of θ_{pl}^{80max} vary from 51 to 64% of the corresponding plastic rotation at failure θ_{pl}^{max} , with reduction being more pronounced in case of large beam profile for both stiffened joints. This can be attributed to the smaller beam local buckling effect of the more compact small beam cross-section. For all the specimens the corresponding values of θ_{pl}^{80b} are larger than θ_{pl}^{80max} and range between 77 and 100% of the corresponding plastic rotation at failure θ_{pl}^{max} . Values of cumulative plastic rotation obtained from small beam section are quite larger for both stiffened joints as a result of larger number of cycles to failure that can be seen from Table 4.25. The effect of beam local buckling can be observed also in considerably reduced values of $\Sigma\theta_{pl}^{80max}$ compared to the values $\Sigma\theta_{pl}^{max}$.

Constant Amplitude Cyclic tests

The response of the other eight specimens tested under constant amplitude cyclic loading in combination with constant column axial force of 3000 kN is shown in Figure 4.87 for the small amplitude of 35 mm and in Figure 4.89 for the large amplitude of 60 mm. All the eight specimens tested under constant amplitude cyclic loading revealed good and stable hysteretic response. With systematically chosen test parameters, taking into account two different values of constant amplitude loading (small and large) in combination with two different beam cross-section profiles (IPE240 and IPE270) for each joint type (RS and CP), two distinct types of low-cycle fatigue response, discussed below, were obtained.

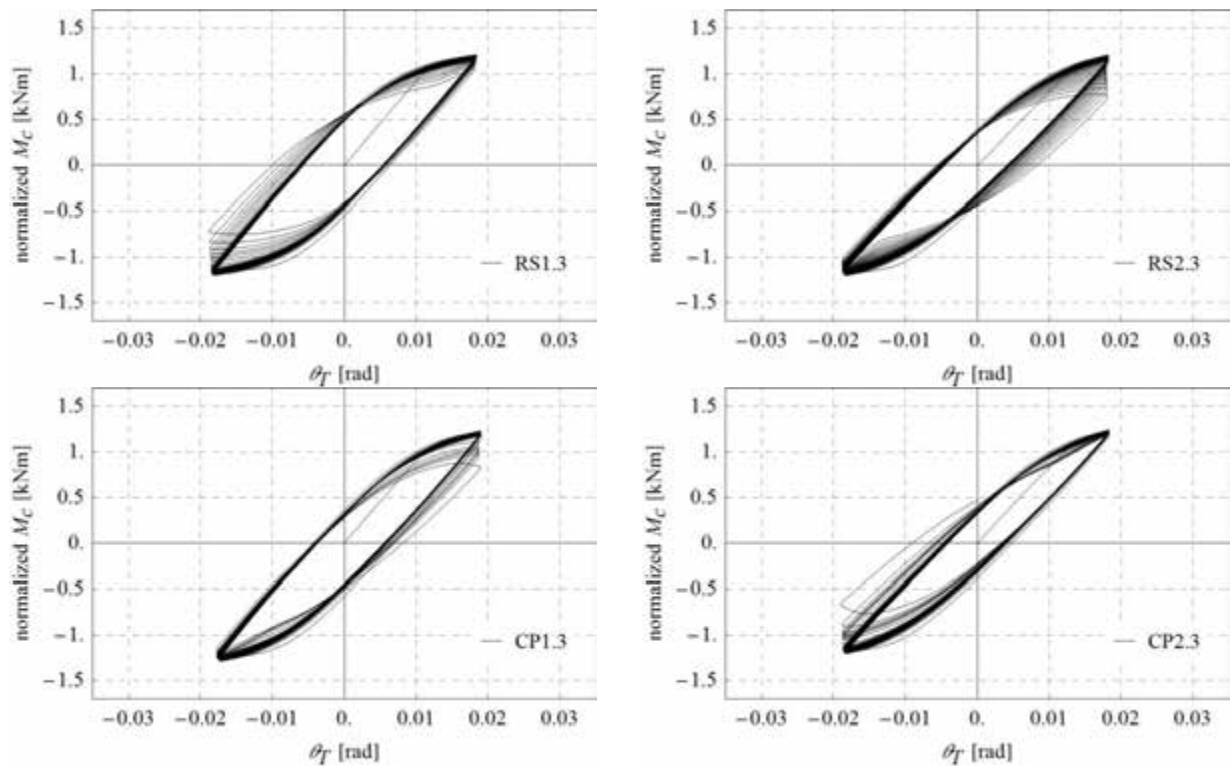


Figure 4.87. Normalized moment versus total joint rotation diagrams for constant amplitude cyclic tests, small amplitude

All four specimens tested with small constant amplitude, RS1.3, RS2.3, CP1.3, CP2.3 did not reveal any beam local buckling prior to LCF fracture. Practically constant value of moment amplitudes throughout the test is characteristic for the above specimens, abruptly reduced only in the last few cycles when fracture of the flanges led to complete joint failure, Figure 4.90-a, Figure 4.90-b for RS2.4 and Figure 4.91-a.

After each test, maximum residual local deformations due to buckling of the beam flanges were measured. In case of specimens CP1.3 and CP2.3 practically no buckling was noticed. Almost the same applies for specimens RS1.3 and RS2.3. Maximum residual amplitude was 1.3 and 0.8 mm for RS1.3 and RS2.3, respectively. In case of RS2.4 maximum residual deformation amplitude on the upper flange was 14.6 mm, whilst the lower flange remained practically straight. In all the five cases no buckling of the beam web was observed. The primary cause of failure in both stiffened joints was fracture as a result of the propagation of ductile cracks initiated at the end of the stiffened region with stable crack propagation until complete fracture of beam flange. In case of the RS joint the first crack initiation was always located in the beam flange at the tip of the rib (fillet weld HAZ), Figure 4.88-a, while in case of the CP joint the first crack was always observed on the beam flange edge in the HAZ of transverse fillet weld, Figure 4.88-b. No yielding or damage of stiffened region of the beam, including welds, was observed.

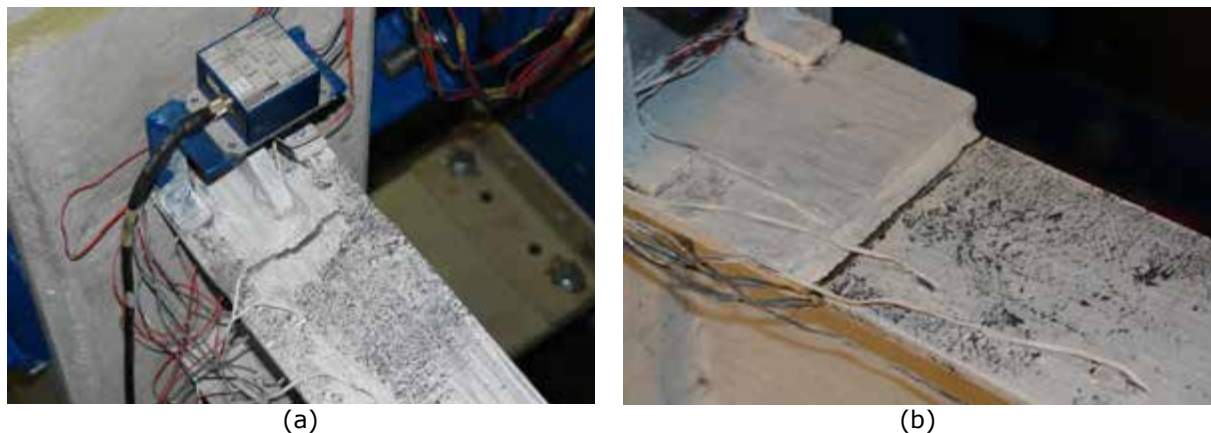


Figure 4.88. Fracture in the upper beam flange: (a) specimen RS1.3, (b) specimen CP2.3

The remaining specimens tested under large constant amplitude, RS1.4, CP1.4 and CP2.4, failed by the progress of the beam local buckling in the plastic hinge zone beyond the end of the strengthened part of the beam.

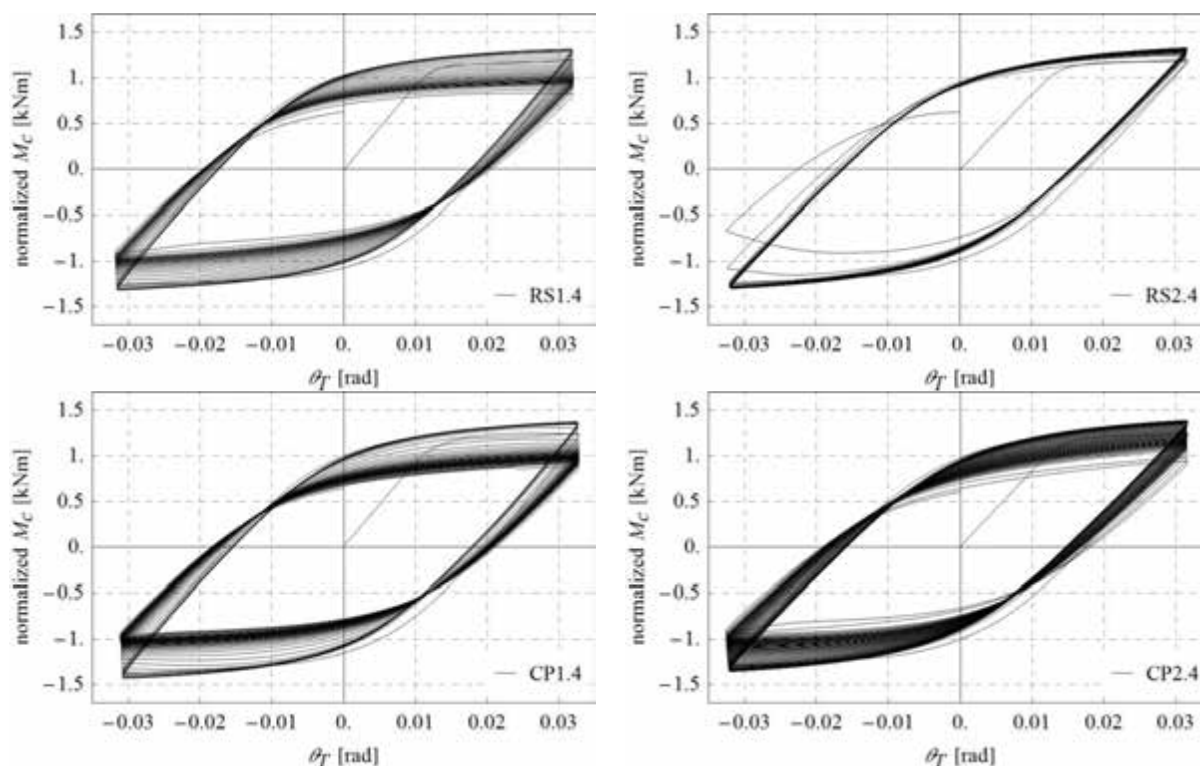


Figure 4.89. Normalized moment versus total joint rotation diagrams for constant amplitude cyclic tests, large amplitude

The buckling took place progressively with the increased number of cycles, leading to the gradual degradation of strength, Figure 4.89, Figure 4.90-b and Figure 4.91-b. Failure of both CP specimens was the same as in case of all eight specimens tested under variable cyclic loading - deterioration of resistance due to the progress of beam flange and web local buckling and cross-section distortion, followed by ductile LCF fracture in the locally most deformed part of the beam flange. However, in case of specimen RS1.4 crack propagation at the end of the rib stiffener in weld HAZ led to complete fracture of the beam flange. No yielding of reinforcing plates or damage of welds in case of both stiffened connections was observed during the tests.

The important difference in the response of specimens tested under small and large constant amplitude is also in the number of cycles to failure, Table 4.25.

Table 4.25 – Total number of complete cycles according to the three failure criteria

Specimen	Load case	N_f	$N_f^{80\max}$	N_f^{80b}	Specimen	N_f	$N_f^{80\max}$	N_f^{80b}
RS1.1	variable	13 ^{LB}	9 ^{†‡}	13	CP1.1	15 ^{LB}	10 [†] , 11 [†]	15
RS1.2	variable	14 ^{LB}	8 [†] , 9 [†]	12	CP1.2	15 ^{LB}	9 [†] , 10 [†]	14
RS1.3	const.	76 ^{FR}	73 [†] , 76 [†]	75	CP1.3	126 ^{FR}	124 [†] , 125 [†]	126
RS1.4	const.	29 ^{FR}	13 [†] , 23 [†]	29	CP1.4	40 ^{LB}	13 [†] , 38 [†]	40
RS2.1	variable	17 ^{LB}	12 [†] , 13 [†]	16	CP2.1	17 ^{LB}	12 [†] , 13 [†]	17
RS2.2	variable	17 ^{LB}	12 [†] , 13 [†]	17	CP2.2	16 ^{LB}	12 ^{†‡}	15
RS2.3	const.	138 ^{FR}	134 [†] , 138 [†]	137	CP2.3	155 ^{FR}	153 [†] , 154 [†]	154
RS2.4	const.	32 ^{FR}	31 ^{†‡}	32	CP2.4	62 ^{LB}	42 [†] , 61 [†]	62

Failure mode: LB - beam local buckling, FR - beam flange fracture.
Failure criterion: † strength, ‡ stiffness.

All four specimens tested under small constant amplitude needed larger number of cycles to complete failure (N_f) than those tested under large constant amplitude. In case of small constant amplitude, the number of cycles to failure varies between 76 and 155, while for large amplitude it is between 29 and 62. In the latter case the increase of local plastic deformation in the plastic hinge zone due to the flange local buckling caused more pronounced LCF effect, which clearly resulted in substantial reduction of fatigue resistance.

In all four tests with small amplitude, RS1.3, RS2.3, CP1.3, CP2.3, and in case of one test with large amplitude, RS2.4, where the beam local buckling did not affect the response of the specimens, the total number of cycles according to the second failure criteria, accounting for 20 % fall of maximal strength and initial stiffness, $N_f^{80\max}$, is very close to the number of cycles to complete failure, N_f^{\max} , Figure 4.90 and Figure 4.91-a. However, in case of the other three specimens tested with large amplitude, RS1.4, CP1.4 and CP2.4, the beam local buckling caused significant reduction of $N_f^{80\max}$, with the values of $N_f^{80\max}/N_f^{\max}$ ratio being 0.57, 0.34 and 0.69 for the three specimens, respectively, Table 4.25.

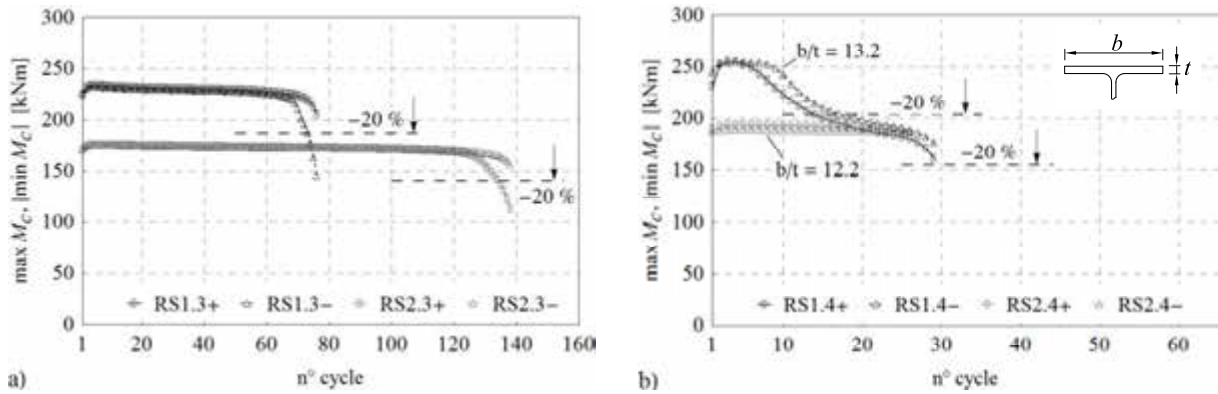


Figure 4.90. Moment amplitudes vs. number of cycles: (a) specimens RS13 and RS23, (b) specimens RS14 and RS24

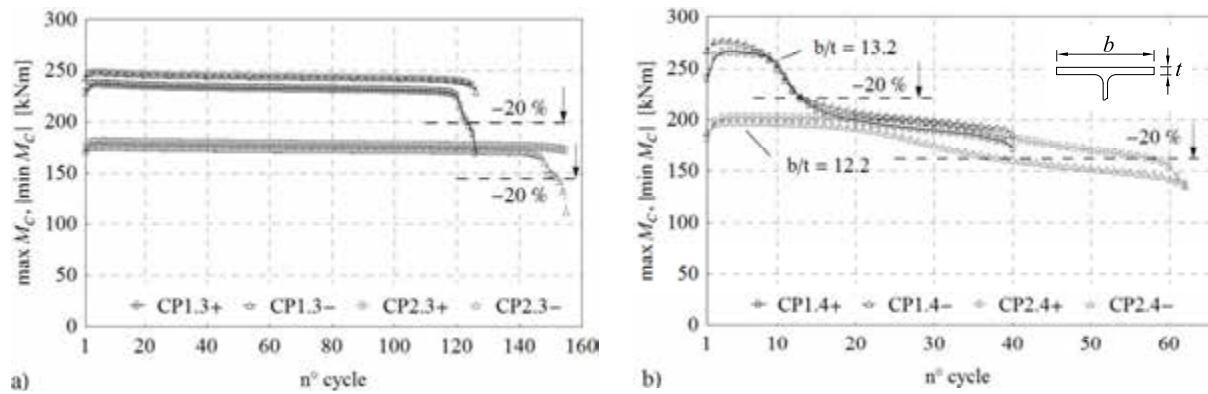


Figure 4.91. Moment amplitudes vs. number of cycles: (a) specimens CP13 and CP23, (b) specimens CP14 and CP24

The effect of beam local buckling on the strength and stiffness degradation was more pronounced in joints with the large beam cross-section IPE270, because they were more prone to local buckling, due to larger flange width-to-thickness ratio, Figure 4.90-b and Figure 4.91-b. Contrary to all eight specimens tested with variable cyclic loading, in case of all specimens tested with constant amplitude loading, the strength criterion proved to be equally or even more stringent than the stiffness degradation criterion, Table 4.25.

4.4.2.3 Interpretation and evaluation of results

Composite column behaviour

The whole inelastic action in all 16 beam-to-column joints was forced into the beam beyond the stiffened connection. Measured rotation contributions from column and beam, outside the plastic hinge region, are shown in Figure 4.92-a.

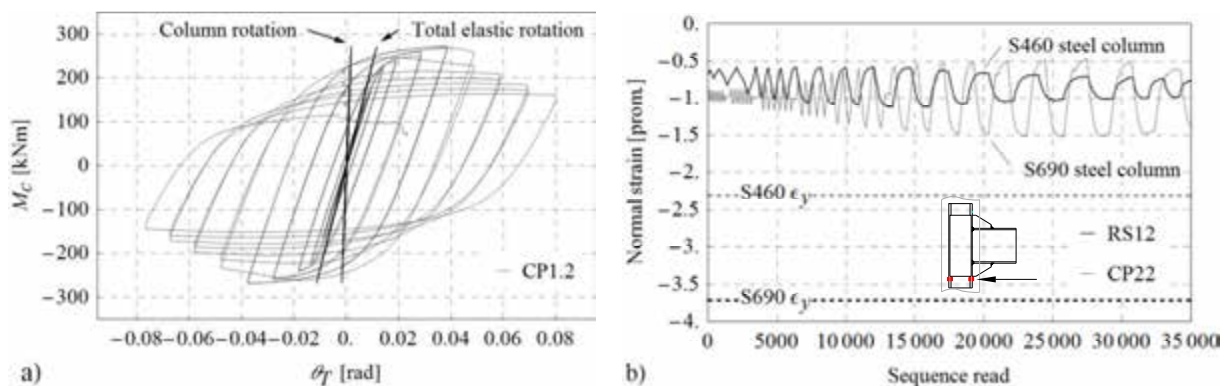


Figure 4.92. Response of composite column: a) elastic column and elastic beam contribution to the total joint rotation for specimen CP1.2, b) recorded normal strains in encased steel sections

Contribution of the column to the total joint rotation: For the group of specimens tested under cyclic loading with increasing amplitude, complete column contribution to the total joint rotation, when maximum strength was reached, ranged between 5.8 and 9.3% in case of large column and between 5.4 and 8.1% in case of small column. Encased steel section remained in elastic state in

all tests. Except for minor cracks around the connection, see Figure 4.93, which have no detrimental effect on joint behaviour, concrete encasement remained undamaged in all the tests.

Influence of the axial force level in the column: No difference was observed in the failure mode for specimens with and without column axial force. Figure 4.92-b shows the level of normal strains measured on flanges of encased steel profile. In spite of considerably strained steel column flange during the test, no damage of welds from column-beam flange interface was observed from metallographic investigation performed after the tests.

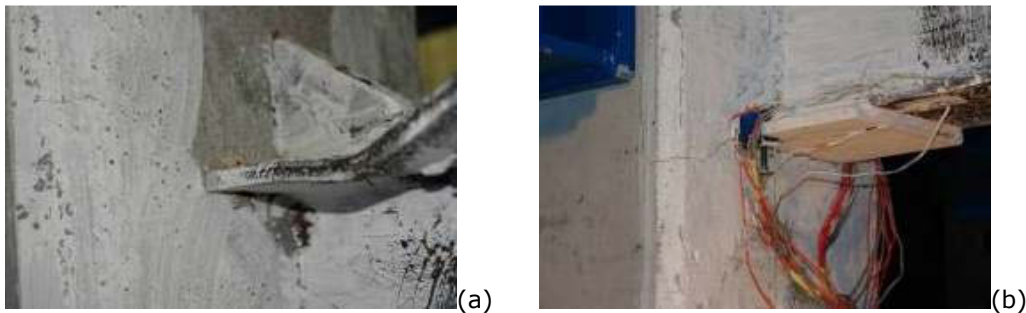


Figure 4.93. Composite column after the test: a) specimens RS14, b) specimens CP11

Energy dissipation capacity

Cumulative plastic rotation $\Sigma\theta_{pl}$, presented in Table 4.23 and Table 4.24, is considered as the primary indicator to evaluate the energy dissipation capacity of the specimens and was computed as in [70], Figure 4.94-a. Comparison of cumulative plastic rotations $\Sigma\theta_{pl}^{80max}$ and $\Sigma\theta_{pl}^{max}$ for all the specimens is presented in Figure 4.94-b.

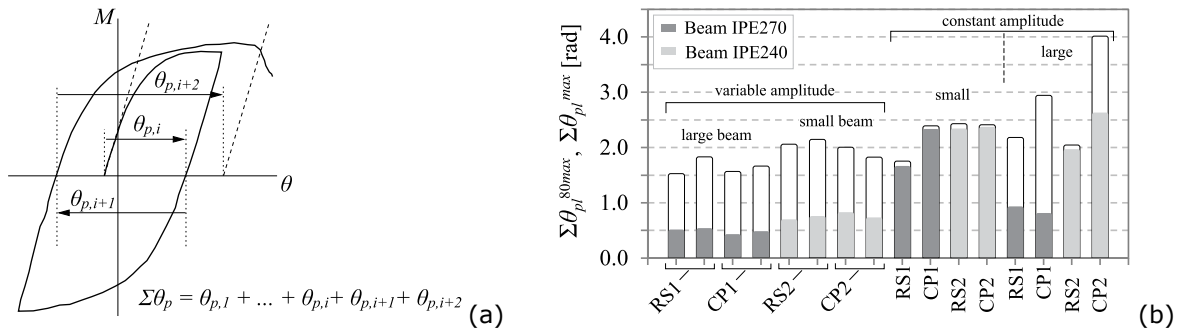


Figure 4.94. (a) Definition of plastic rotation and cumulative plastic rotation, (b) comparison of cumulative plastic rotations for all 16 specimens

In case of all eight specimens tested under variable cyclic loading significant reduction in $\Sigma\theta_{pl}^{80max}$ can be observed, with $\Sigma\theta_{pl}^{80max} / \Sigma\theta_{pl}^{max}$ ratios between 0.28 and 0.41. Larger values of both cumulative plastic rotations can be observed for specimens with small beam section. Cumulative plastic rotations for constant amplitude tests are considerably larger due to increased number of cycles, except for specimens tested with large constant amplitude in combination with large beam section IPE270, where the beam local buckling occurred.

Comparing the response of RS and CP joints, deviation can be observed for RS configuration in terms of lower values of cumulative plastic rotations obtained from constant amplitude tests, Figure 4.94-b and Figure 4.95-a. It seems the reason for this can be attributed to the more pronounced strain concentrations at the end of the rib-stiffener, see Figure 2.10-a. No such obvious differences between the RS and the CP joint in the response of eight specimens tested under variable cyclic loading can be noticed.

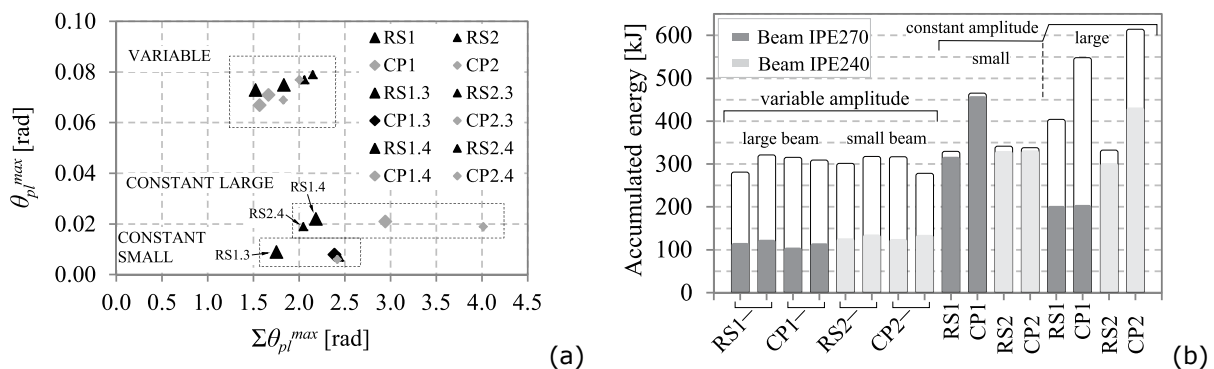


Figure 4.95. a) Maximum rotation vs. cumulative plastic rotation relationship for all 16 specimens, b) Cumulative dissipated energy

The above findings show that: (1) during large amplitude cyclic loading beam local buckling occurred, which led to pronounced LCF failure in buckled zone of the beam irrespective of the joint configuration (applies to variable cyclic loading as well), (2) small amplitude loading resulted in LCF failure of the material without the occurrence of beam local buckling. In the latter case the RS joint configuration proved to be more critical under LCF effects, due to unfavourable higher strain concentrations together with weld residual stress and HAZ at the end of the rib-stiffener.

Comparison of cumulative dissipated energy for all test specimens is presented in Figure 4.95-b. In addition to the total dissipated energy up to the specimen complete failure, the portion of dissipated energy, corresponding to the failure criterion related to 20% fall of maximum strength and initial stiffness, is illustrated. In cases with no buckling the reduction is small, whilst for cases with beam local buckling the reduced portion is not negligible and ranges between 30 and 68%.

Evaluation of results according to the pre-qualification requirements

The response of eight specimens tested under cyclic loading with increasing amplitude was evaluated according to the acceptance criteria of applicable standards currently in use. The required rotation capacity of the plastic hinge region from EN 1998-1 [1] is 0.035 rad for structures of ductility class DCH and 0.025 rad for structures of ductility class DCM. In both cases the rotation capacity should be ensured under cyclic loading without degradation of maximum strength and initial stiffness larger than 20%. For beam-to-column connections used in the seismic force resisting system the ANSI/AISC 341-10 [7] provides the following two requirements: (i) the connection shall be capable of accommodating a total joint rotation of at least 0.04 and 0.02 rad, for special moment frames (SMF) and intermediate moment frames (IMF), respectively; (ii) the measured flexural resistance of the connection, determined at the column face, shall equal at least $0.80 \cdot M_p$ of the connected beam at the aforementioned story drift angles for SMF and IMF, where M_p is nominal plastic beam moment. It should be noted that the AISC acceptance criterion is based on joint rotation, which includes elastic and inelastic rotations from beam and column, while the criterion from Eurocode takes into account total beam rotation and the column web panel shear deformation without the column elastic deformation. In Eurocode it is also not clearly stated whether the rotation limits should account for the rotation capacity of the plastic hinge region or the whole beam. However, also in case when the rotational capacity of the plastic hinge region is used all the eight specimens fulfil the required limit 0.035 rad, see Table 4.23 and Table 4.24.

Values of rotations obtained from all the eight specimens to be compared with required limits from both recommendations are gathered in Table 4.26. Minimal rotations from both loading directions are collected. For all eight joints the value of total beam rotation θ_b , without degradation of maximal strength and initial stiffness greater than 20%, is larger than the more stringent limit value of 0.035 rad from Eurocode standard. Similarly, the value of total joint rotation θ_T is larger than the limit value of 0.04 rad for structures classified as SMF for all tested joints. The later requirement is obviously less stringent and large reserve can be noticed for all the specimens, although complete joint rotation in Table 4.26 presents minimal joint rotation at 20% fall of the actual beam plastic moment $M_{pl,b}$, and not the nominal one as stated in the AISC seismic provisions.

Table 4.26 – Complete beam and complete joint rotations for RS and CP joints

Specimen	θ_b (rad)	θ_T (rad)	Specimen	θ_b (rad)	θ_T (rad)
RS1.1	0.049	0.081	CP1.1	0.048	0.077
RS1.2	0.048	0.065	CP1.2	0.048	0.067
RS2.1	0.059	0.077	CP2.1	0.058	0.088
RS2.2	0.059	0.086	CP2.2	0.058	0.078
Rotation limit	> 0.035*	> 0.04 [†]		> 0.035*	> 0.04 [†]
Pre-qualification requirement according to: * EN 1998-1 [1], [†] ANSI/AISC 341-10 [7]					

It is to be mentioned that the experimental investigation program carried out for the welded beam-to-column joints with FE-WF columns, is presented in detail within Deliverable D5 [13].

4.4.3 Load introduction tests on steel-concrete connection through the use of shot fired nails

The aim of the tests performed on steel-concrete connection was to evaluate the load introduction within composite columns realized as concrete filled tubes of high strength steel (see Figure 4.96). For this purpose load introduction tests were considered on a number of 6 specimens with the objective to assess the efficiency of the shot fired nails in providing the shear connection between the steel tube and the concrete core under monotonic and cyclic loading.



Figure 4.96. Specimen configuration for the load introduction tests

4.4.3.1 Experimental program and specimen configuration

The experimental program on column stubs is summarized in Table 4.27. Consequently, a number of 6 tests on column stubs were considered varying parameters such as: steel tube, steel-concrete connection, and loading procedure. As connectors, a number of 24 Hilti X-DSH32 P10 shot fired nails were considered per column stub. Monotonic and cyclic tests were performed for the three following cases:

- S700-F-M / S700-F-C – connection characterized only by adhesion (chemical bond & friction);
- S700-F-H-M / S700-F-H-C – connection characterized by adhesion combined with connectors;
- S460-F-H-M / S460-F-H-C – connection characterized by adhesion combined with connectors;

Table 4.27 – Experimental program and specimen configuration

Nr.	Specimen	Tube	Bond	Load
1	S700-F-M	RHS 250x10 S700	Friction	Monotonic
2	S700-F-C	RHS 250x10 S700	Friction	Cyclic
3	S700-F-H-M	RHS 250x10 S700	Friction & Nails*	Monotonic
4	S700-F-H-C	RHS 250x10 S700	Friction & Nails*	Cyclic
5	S460-F-H-M	RHS 300x12.5 S460	Friction & Nails*	Monotonic
6	S460-F-H-C	RHS 300x12.5 S460	Friction & Nails*	Cyclic

* 24 Hilti X-DSH32 P10 shot fired nails

4.4.3.2 Experimental test set-up, instrumentation and loading protocol

The experimental test set-up is illustrated in Figure 4.97-a-b. The instrumentation of the specimens (see Figure 4.97-c-d) consisted in the measurement of the force applied by the testing machine and the relative displacement between steel tube and concrete core – for which a number of 4 displacement transducers were used. The parameters used to control of the load introduction tests were the relative displacement “d” measured between steel tube and concrete core, and the force “F”. Monotonic loading was applied by progressively increasing the relative displacement and the ECCS [5] procedure was considered for the cyclic loading.

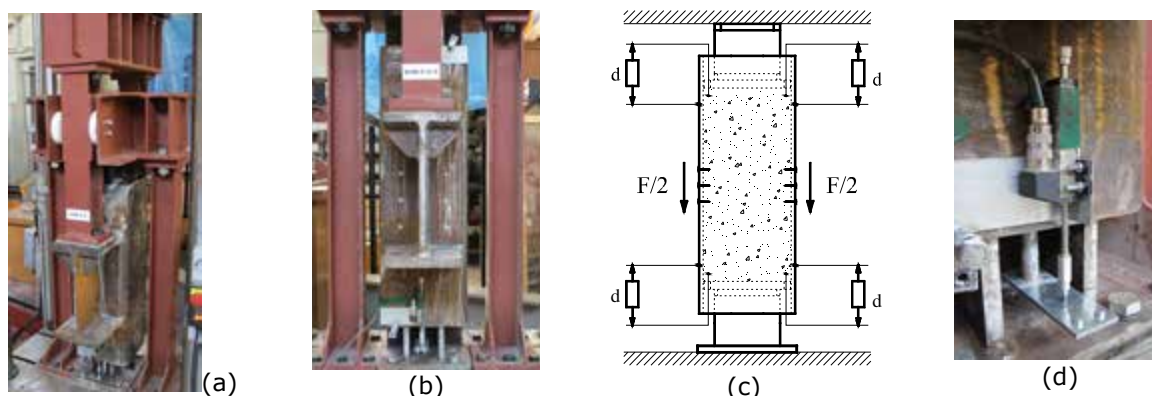


Figure 4.97. Experimental test set-up (a) & (b), instrumentation arrangement (c) & (d)

4.4.3.3 Material properties

The material characteristics of concrete and RHS tubes are identical with those from the beam-to-column joint assemblies (see Section 4.4.4.2 – material properties). In addition, the X-DSH32 P10 nails of 4.5 mm diameter were tested to shear by Hilti AG [71] obtaining an average shear force in amount of 21.85 kN (at 25° C). Consequently, the corresponding shear stress was in amount of 1374 N/mm² and the ultimate strength was computed in amount of 2380 N/mm².

4.4.3.4 Test results

The monotonic tests were performed in the first stage. The obtained force vs. relative displacement curves allowed assessing the yield displacements “ d_y ”, necessary for the ECCS [5] cyclic loading procedure. The yield displacements were computed in amount of: 0.75 mm for the column stub with friction bond only, and 1 mm for the two column stubs with friction and connectors. The results of the experimental investigations are further presented in terms of force vs. relative displacement computed as the average between the measurements of the four displacement transducers. It is to be mentioned that the measurements at the top and bottom side were very close.

The monotonic and cyclic response of the friction, developed between the steel tube and the concrete core, is shown in Figure 4.98-a-b. It can be observed that above a relative displacement of 2 mm the monotonic force transmitted through friction was measured in amount of 200 kN. Under cyclic loading, the force developed through friction was lower (approximately 160 kN corresponding to the maximum amplitude of a cycle, and 20 kN corresponding to the initial position, i.e. 0 mm relative displacement).

The monotonic and cyclic response of the friction combined with the 24 shot fired nails is shown in Figure 4.98-c-d for the column stub with S700 steel tube and respectively in Figure 4.98-e-f for the column stub with S460 steel tube. It can be observed that the shear capacity heavily increased. Under monotonic loading, the transferred forces were approximately 1100 kN corresponding to a relative displacement of 5 mm. Apparently, the capacity limit of the testing device was lower (1100 kN) than the specified 1200 kN, and therefore under monotonic loading, the ultimate capacity of the connectors was not determined. Under cyclic loading the maximum forces were slightly lower. In addition, the force-displacement curve decreased significantly corresponding to relative displacements of 5 mm.

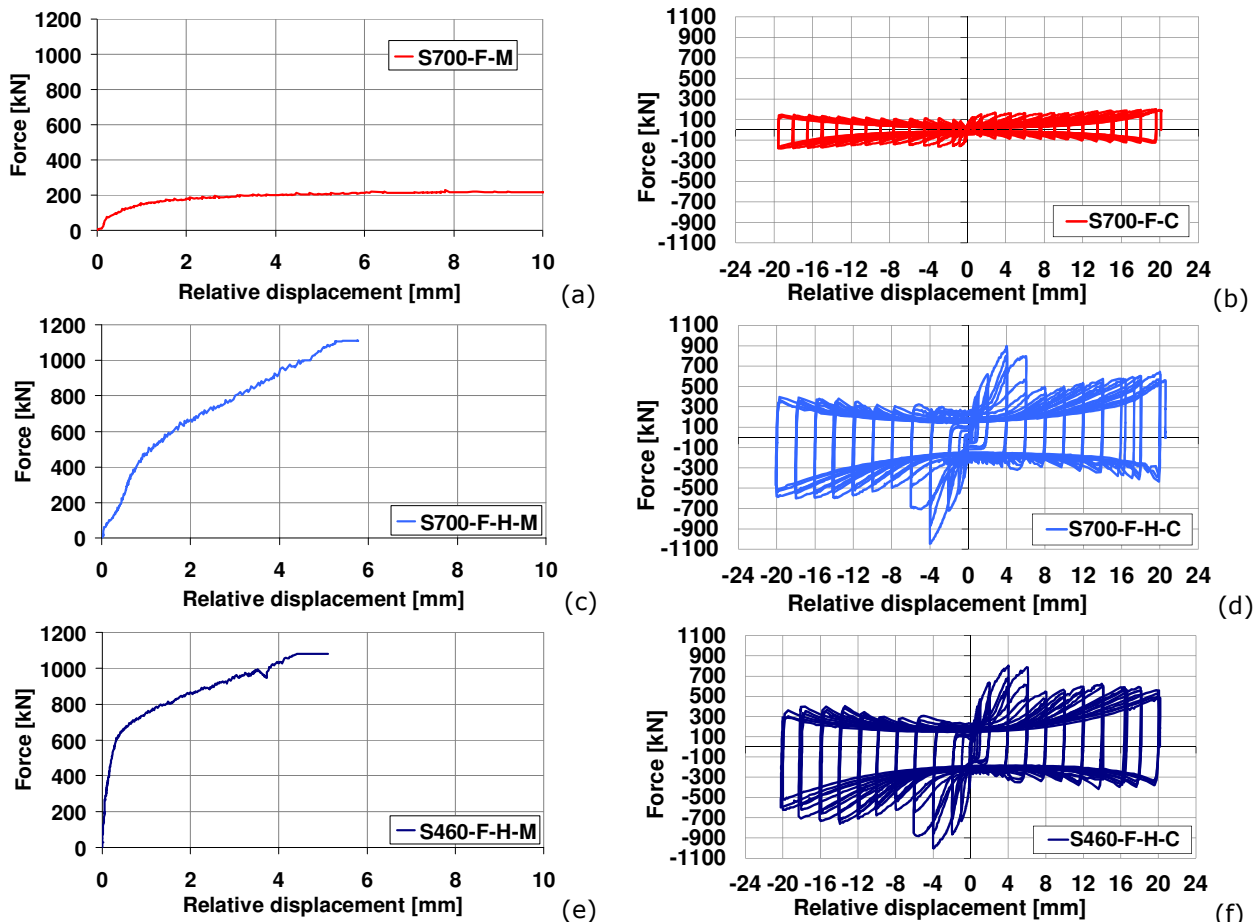


Figure 4.98. Monotonic and cyclic response of friction connection (a) & (b), and friction combined with connectors S700-F-H - (c) & (d), and respectively S460-F-H - (e) & (f)

4.4.3.5 Interpretation of results

A graphical comparison in terms of monotonic response corresponding to the column stubs without nails (S700-F) and with nails (S700-F-H) can be seen in Figure 4.99-a. The response under cyclic loading of the column stubs without and with connectors can be seen in Figure 4.99-c. Consequently, the connectors show a significant contribution under both monotonic and cyclic loading conditions.

A detail of concrete and connector subjected to monotonic loading is shown in Figure 4.99-b. It can be observed that the concrete was crushed in a small amount at the contact with the shot fired nails which were bent. In addition, a detail of concrete and connector after cyclic loading is shown in Figure 4.99-d. It can be observed that under alternating cycles the connectors were broken at the interface between steel tube and concrete core.

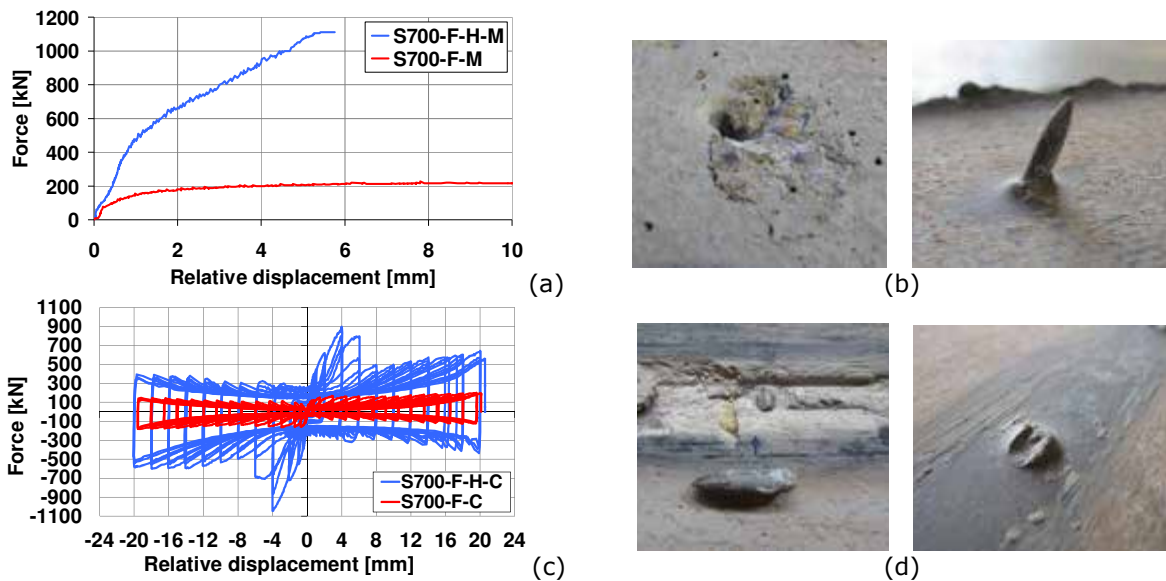


Figure 4.99. Contribution of the connectors under: (a) monotonic loading, and (b) cyclic loading; corresponding failure mode (c) & (d)

The experimental investigation program carried out for the steel-concrete connection is presented more detailed in Deliverable D5 [13]. The conclusions from the investigation can be summarised as follows:

- The shear strength that developed through friction was obtained in amount of 0.4 N/mm^2 , which is equal to the value recommended by EN 1994-1 [4] for rectangular hollow sections.
- It was observed that the connectors can take the major shear contribution to the load transfer from steel tube to the concrete core, in both monotonic and cyclic loading. From the cyclic loading the capacity of the connectors slightly decreased compared to the monotonic loading.
- As previously confirmed by Beck [76], the X-DSH 32 P10 shot fired nails proved a significant contribution to the steel-concrete connection considering the monotonic loading. In addition, the current study proved a significant contribution of the connectors also for the case of cyclic loading conditions and for the use of high strength steel rectangular hollow sections (S460 and S700).

4.4.4 Tests on welded reduced beam section and welded cover plate beam-to-column joints with concrete filled rectangular hollow section (CF-RHS) columns

4.4.4.1 Experimental program and specimen configuration

The experimental program on beam-to-column joints with CF-RHS columns is summarized in Table 4.28. The variations in the configuration of the joints are given by two joint typologies (reduced beam section – RBS, and cover-plate – CP), two steel grades for the rectangular hollow section tubes (S460 and S700) and two intended failure modes (beam and connection zone). In addition two loading conditions were considered for each beam-to-column joint configuration, i.e. monotonic and cyclic loading procedure.

Table 4.28 – Experimental program on welded beam-to-column joints with CF-RHS columns

Parameter	Variable	No. of variations	No. of specimens
Loading	Monotonic & Cyclic	2	16
Joint type	Reduced Beam Section & Cover-Plate	2	
HSS grade	S460 & S690	2	
Failure mode	Weak beam / Weak connection	2	

Considering the two joint typologies (RBS and CP – see Figure 4.100-a-b) and two steel grades for the tubes (S460 and S700), a number of four beam-to-column joint configurations were designed (see Figure 4.100-c). In addition, tests were considered on the corresponding joints for which the beam was strengthened (Figure 4.100-d). Table 4.29 describes for each of the 16 beam-to-column joints, the labelling, column and beam properties, joint typology, loading procedure and intended failure mode.

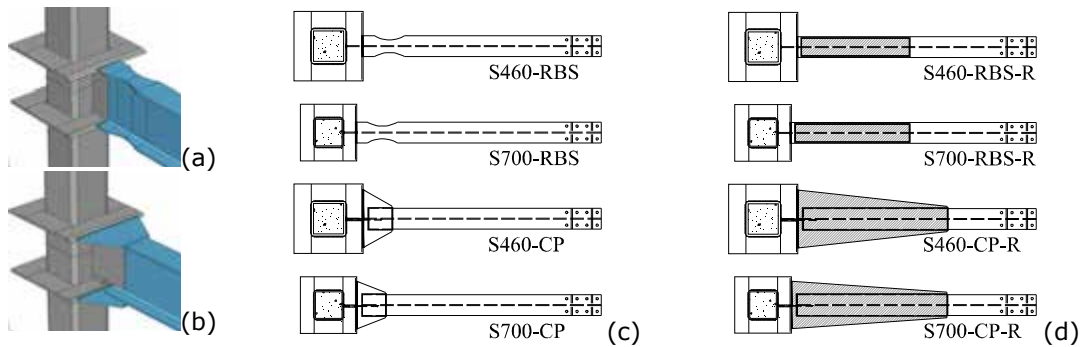


Figure 4.100. Welded external diaphragm beam-to-column joints with reduced beam section (a), cover plates (b), designed joint specimens (c), and corresponding joint specimens with reinforced beam (d)

Table 4.29 – Beam-to-column joint configurations

Nr.	Specimen name	Column	Beam	Joint type	Loading	Intended failure mode
1	S460-RBS-M	RHS 300x12.5 S460	IPE400 S355	RBS	Monotonic	Beam
2	S460-RBS-C				Cyclic	
3	S700-RBS-M	RHS 250x10 S700	IPE400 S355	RBS	Monotonic	Beam
4	S700-RBS-C				Cyclic	
5	S460-CP-M	RHS 300x12.5 S460	IPE400 S355	CP	Monotonic	Beam
6	S460-CP-C				Cyclic	
7	S700-CP-M	RHS 250x10 S700	IPE400 S355	CP	Monotonic	Beam
8	S700-CP-C				Cyclic	
9	S460-RBS-R-M	RHS 300x12.5 S460	IPE400 S355	RBS	Monotonic	Connection
10	S460-RBS-R-C				Cyclic	
11	S700-RBS-R-M	RHS 250x10 S700	IPE400 S355	RBS	Monotonic	Connection
12	S700-RBS-R-C				Cyclic	
13	S460-CP-R-M	RHS 300x12.5 S460	IPE400 S355	CP	Monotonic	Connection
14	S460-CP-R-C				Cyclic	
15	S700-CP-R-M	RHS 250x10 S700	IPE400 S355	CP	Monotonic	Connection
16	S700-CP-R-C				Cyclic	

The intended plastic mechanism corresponding to the four designed beam-to-column joints (see Figure 4.100-c) is related to the formation of the plastic hinge in the beam and an elastic response of the connection and joint components. In contrast, for the beam-to-column joints with strengthened beam (see Figure 4.100-d) the intended failure mode is related to the connection and joint components.

4.4.4.2 Experimental test set-up, instrumentation and loading procedure

Test set-up: The conceptual scheme and an illustration of the experimental test set-up are shown in Figure 4.101. A hydraulic actuator connected at the tip of the beam served as loading device. The column was supported at both ends considering pinned connections. Horizontal and vertical displacements were blocked by the right support, and only the vertical displacements were restrained by the left support. In addition, a lateral support system was used to block the out of plane deformations of the beam.

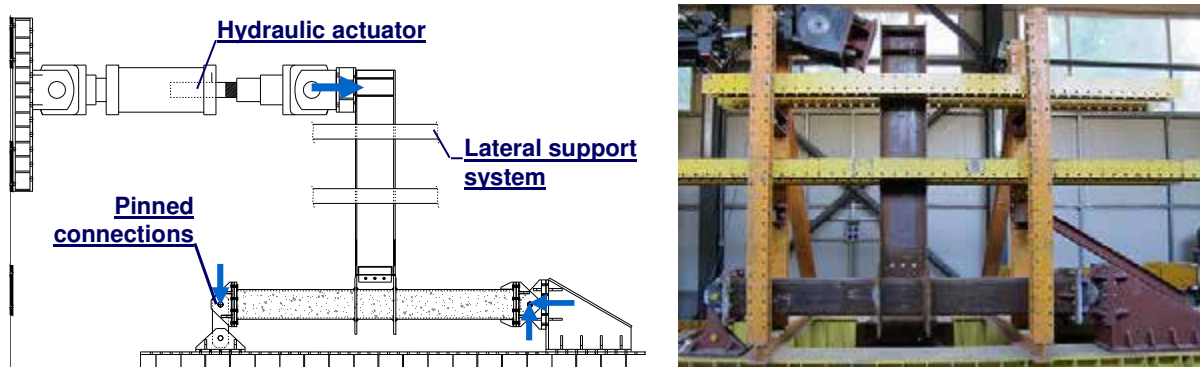


Figure 4.101. Conceptual scheme and illustration of the test assembly

Instrumentation: Both local and global instrumentation were considered. Local instrumentation was aimed to measure the deformations within the dissipative zone, connection zone and column web panel (see Figure 4.102-a). In order to identify the yielding sequence, the joint was prepared by

whitewashing. From the global instrumentation, information was obtained related to the force in the actuator, displacement at the tip of the beam, as well as horizontal and vertical displacement at supports (see Figure 4.102-b).

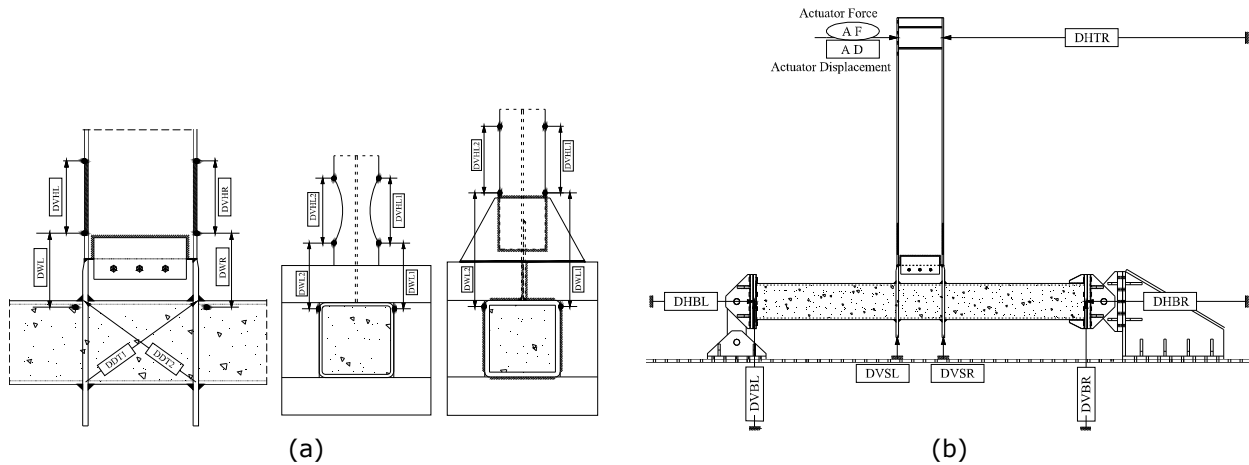


Figure 4.102. Local joint instrumentation (a) and global instrumentation (b)

Loading: The parameters used to control the tests were the inter-storey drift " θ " and bending moment " M ", both computed at column centreline. Monotonic loading was applied by progressively increasing the displacement at the tip of the beam. One unloading-reloading phase was used for a better estimation of the initial stiffness, and the ANSI/AISC 341-10 [7] loading protocol was used for cyclic loading.

Material properties: Experimental tests were performed on material samples with the aim to assess the characteristics of all parts of the joint assemblies. Compression tests on concrete cube samples were performed at 28 days from concrete casting, obtaining an average strength in amount of 35.88 N/mm². In addition, tensile and Charpy V-notch impact tests were performed on steel samples prepared from additional material. Consequently, for each component of the joint assemblies (i.e. beam, cover plates, external diaphragms, RHS tubes, stiffeners, etc.), a number of three samples were prepared and tested. The results are summarized in Table 4.30. From tensile tests, the average values are shown regarding the yield strength (R_{eH}), ultimate strength (R_m), elongation at fracture (A) and elongation at maximum force (A_g). The results from the Charpy V-notch tests are shown in terms of absorbed energy. The results obtained on steel samples allowed assessing the properties of all joint parts and confirmed that the steel grades were in accordance with the code requirements.

Table 4.30 – Tensile and Charpy V-notch test results for steel samples

Steel component / grade			Tensile tests				Charpy V-notch tests		
			R_{eH}	R_m	A	A_g	T	KV _{min}	KV
			N/mm ²	N/mm ²	%	%	°C	J	J
1	IPE 400 flange	S355 JR	393.9	491.9	30.9	16.3	20	27	57.6
2	IPE 400 web *	S355 JR	439.5	507.5	29.1	15.8	20	27	99.6
3	Cover plates	S355 J0	432.7	489.1	30.8	16.2	0	27	266.6
4	Splice plate	S355 J2	415.3	503.0	26.9	15.2	-20	27	221.3
5	RHS 300x12.5	S460 M	497.7	554.1	22.4	7.7	-20	40	247.3
6	RHS 250x10 *	S700 QL	725.4	830.	11.8	-	-20	40	102.3
7	External diaphragm	S460 NL	463.4	618.9	24.2	13.6	-30	40	58.6
8	External diaphragm	S690 QL	725.8	807.1	16.3	5.5	-20	40	233.3
9	Vertical stiffener	S460 NL	495.1	622.4	25.9	13.6	-30	40	152.3
10	Vertical stiffener *	S690 QL	806.9	854.7	14.2	5.7	-20	40	150.6

4.4.4.3 Test results

An illustration of the connection zone prior to the testing is shown in Figure 4.103 for each of the eight beam-to-column joint configurations. Further, the results are shown in terms of moment-rotation curve (computed at column centreline), and illustration of the failure mode. It is to be mentioned that the first testing sequence was represented by the monotonic testing of the eight beam-to-column joint configurations. The second testing sequence was represented by the cyclic testing of the eight similar beam-to-column joint configurations.

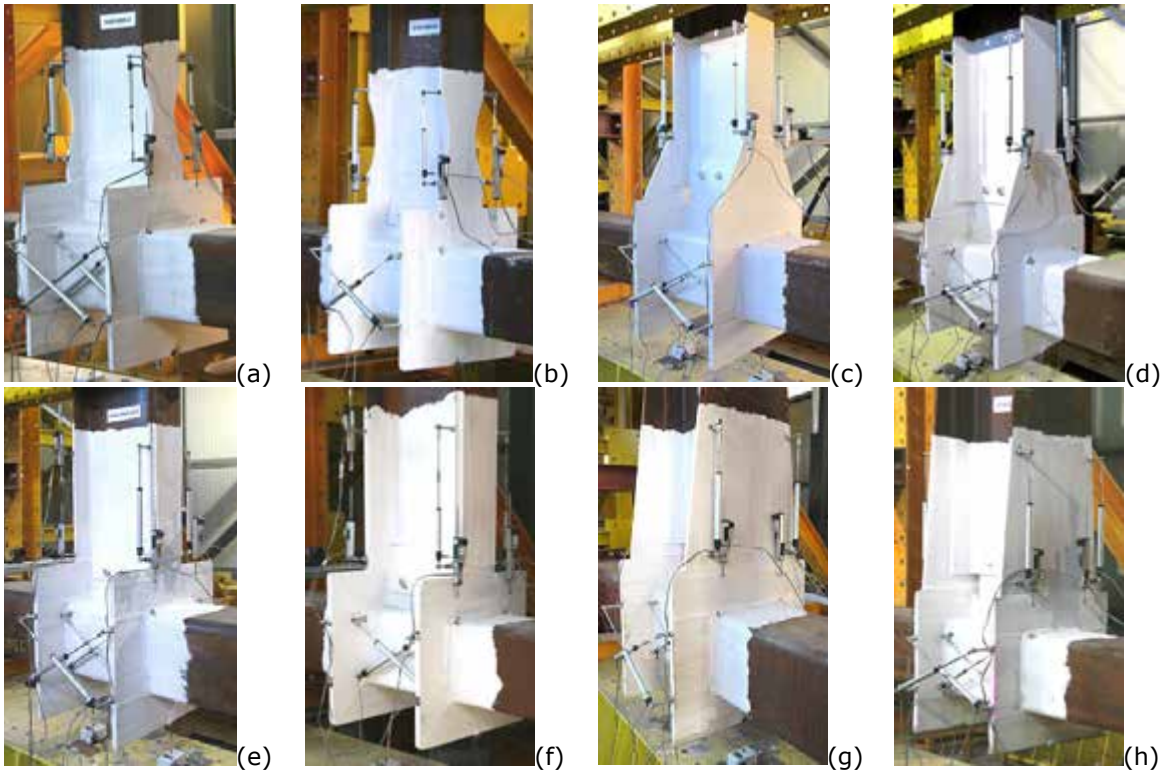


Figure 4.103. State of the joint configurations before testing: (a) S460-RBS, (b) S700-RBS, (c) S460-CP, (d) S700-CP – designed joints; (e) S460-RBS-R, (f) S700-RBS-R, (g) S460-CP-R, (h) S700-CP-R – corresponding joints with reinforced beam

Figure 4.104, Figure 4.105, Figure 4.106 and Figure 4.107 show the response and failure mechanism of RBS joints subjected to monotonic and cyclic loading. The yielding was initiated in the beam flanges within the RBS zone and was followed by large plastic deformations – local buckling of flanges and web under compression. No damage was observed in the external diaphragm and column web panel.

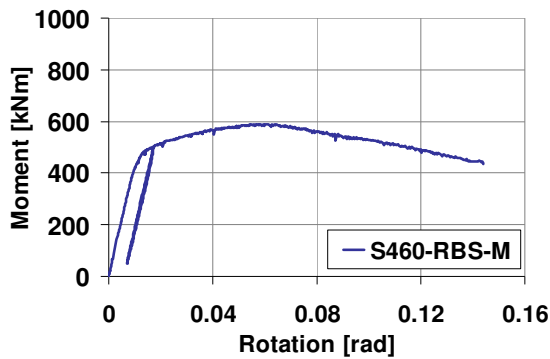


Figure 4.104. S460-RBS-M joint: monotonic response & illustration of failure mode

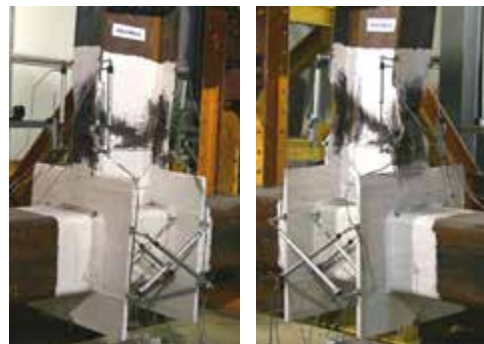
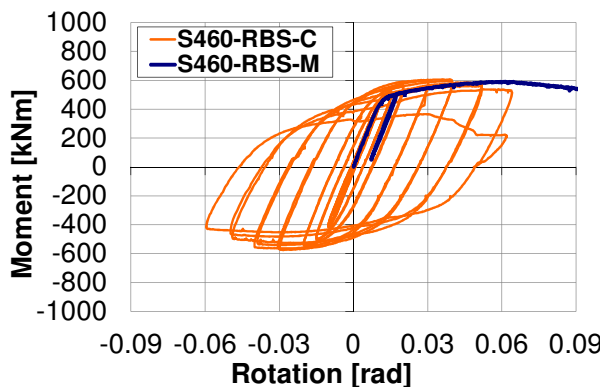


Figure 4.105. S460-RBS-C joint: cyclic response & illustration of failure mode

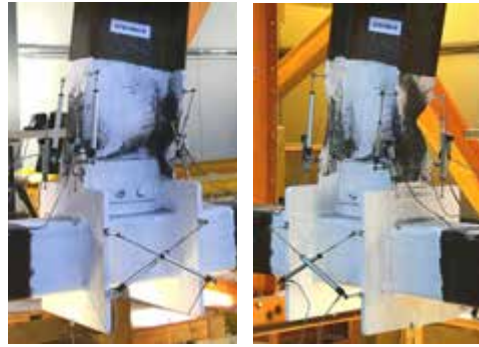
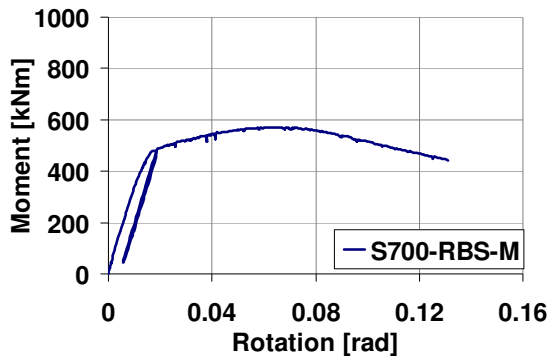


Figure 4.106. S700-RBS-M joint: monotonic response & illustration of failure mode

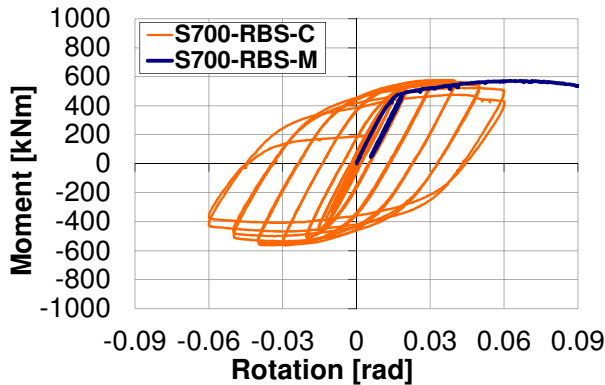


Figure 4.107. S700-RBS-C joint: cyclic response & illustration of failure mode

Figure 4.108, Figure 4.109, Figure 4.110 and Figure 4.111 show the response and failure mechanism of CP joints subjected to monotonic and cyclic loading. The yielding was initiated in the beam flanges near the cover plates and was followed by large plastic deformations – local buckling of flange and web under compression. No damage was observed in cover plates, external diaphragm and column web panel.

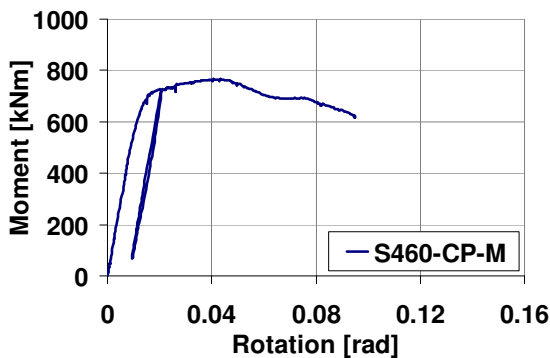


Figure 4.108. S460-CP-M joint: monotonic response & illustration of failure mode

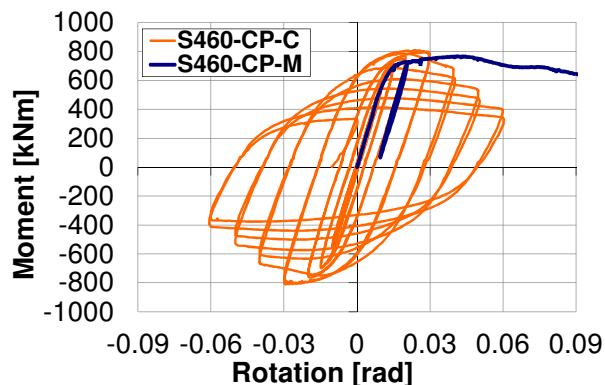


Figure 4.109. S460-CP-C joint: cyclic response & illustration of failure mode

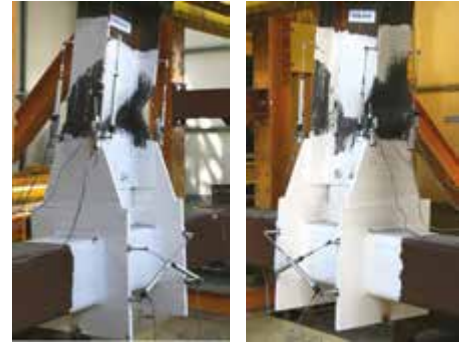
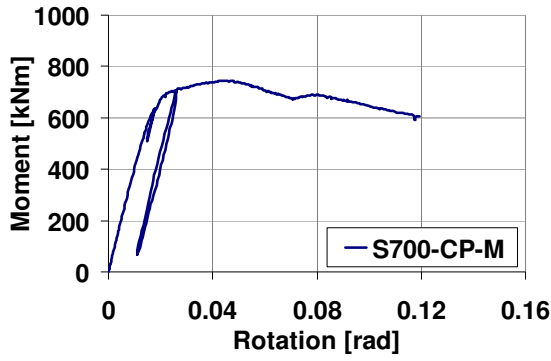


Figure 4.110. S700-CP-M joint: monotonic response & illustration of failure mode

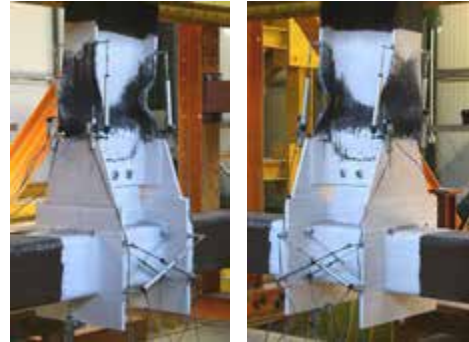
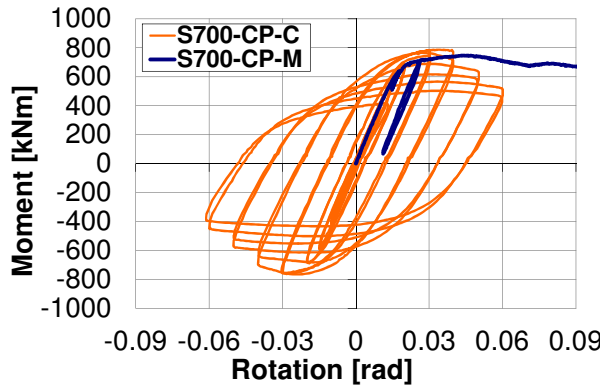


Figure 4.111. S700-CP-C joint: cyclic response & illustration of failure mode

Figure 4.112, Figure 4.113, Figure 4.114 and Figure 4.115 show the response and failure mechanism of the joints with strengthened beam flanges (RBS-R), subjected to monotonic and cyclic loading. The yielding was initiated in beam flanges (between the reinforcing plate and external diaphragm) under compression/tension and was followed by yielding of web and external diaphragm. Finally, the beam flanges fractured in the heat affected zone (HAZ) due to tension forces.

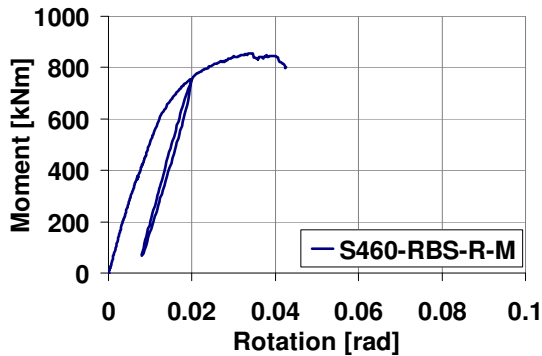


Figure 4.112. S460-RBS-R-M joint: monotonic response & illustration of failure mode

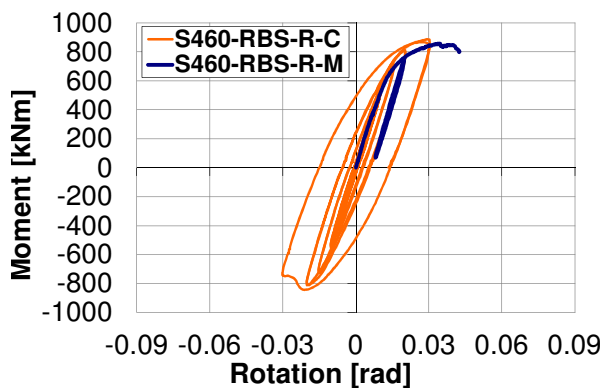


Figure 4.113. S460-RBS-R-C joint: cyclic response & illustration of failure mode

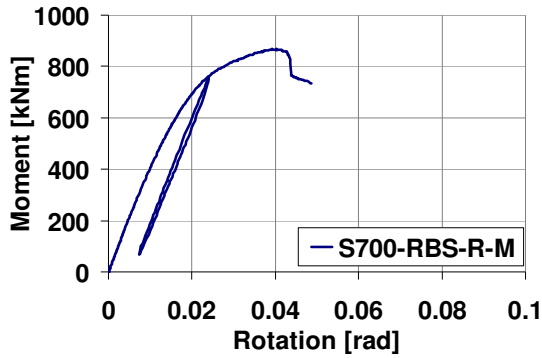


Figure 4.114. S700-RBS-R-M joint: monotonic response & illustration of failure mode

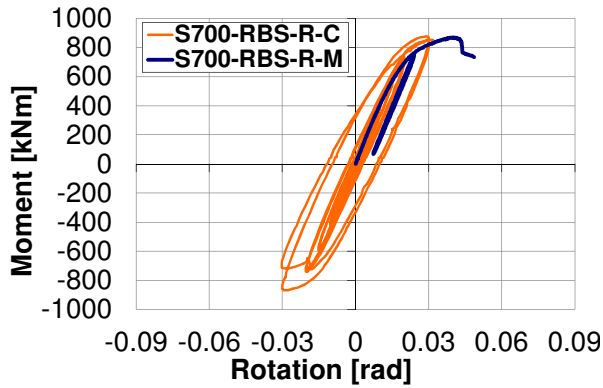


Figure 4.115. S700-RBS-R-C joint: cyclic response & illustration of failure mode

Figure 4.116, Figure 4.117, Figure 4.118 and Figure 4.119 show the response and failure mechanism of joints with extended cover plate (CP-R) subjected to monotonic and cyclic loading. For the S460-CP-R joints, the yielding was initiated in the external diaphragm and was followed by local deformations of cover plates under compression/tension and yielding of the column web panel. For the S700-CP-R joints, the yielding was initiated in the compressed cover plate and was followed by failure of the weld between plates of the external diaphragm, however at forces higher than the design capacity.

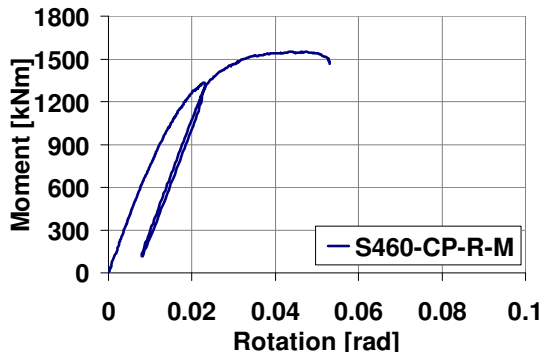


Figure 4.116. S460-CP-R-M joint: monotonic response & illustration of failure mode

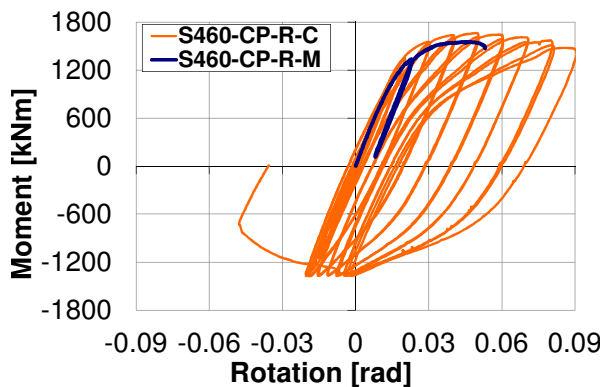


Figure 4.117. S460-CP-R-C joint: cyclic response & illustration of failure mode

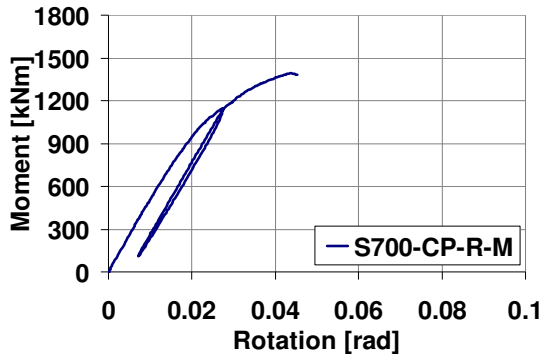


Figure 4.118. S700-CP-R-M joint: monotonic response & illustration of failure mode

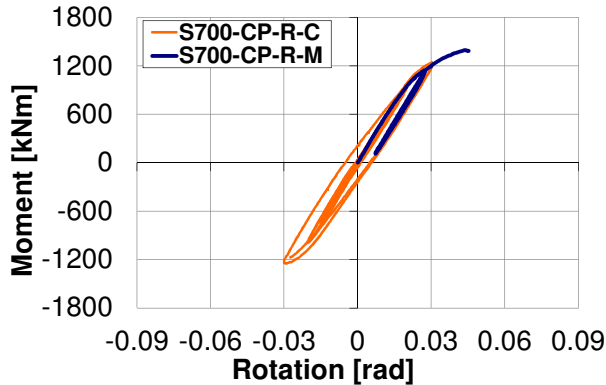


Figure 4.119. S700-CP-R-C joint: cyclic response & illustration of failure mode

4.4.4.4 Interpretation of results

The interpretation of results was made in relation to the following aspects:

- Overstrength of connection zone;
- Contribution of components to the joint rotation;
- Evaluation of the rotation capacity;

With the aim to assess the overstrength of the joint and connection zone, a comparison was made between the four designed joints and the corresponding joints with reinforced beam. Figure 4.120 illustrates the overstrength of the RBS joints and Figure 4.121 illustrates the overstrength of CP joints. The moment-rotation curves were computed at the connection to the external diaphragm, and the overstrength was evaluated corresponding to the yield point and to the maximum capacity. Consequently, the overstrength of the connection zone for the RBS joints (S460 & S700) was evaluated in the amount of 34% & 35% at yield, and respectively 53% & 60% at maximum capacity (see Figure 4.120). The overstrength of the connection zone for the CP joints (S460 & S700) was computed in amount of 55% & 43% at yield, and respectively 101% & 86% at maximum capacity (Figure 4.121).

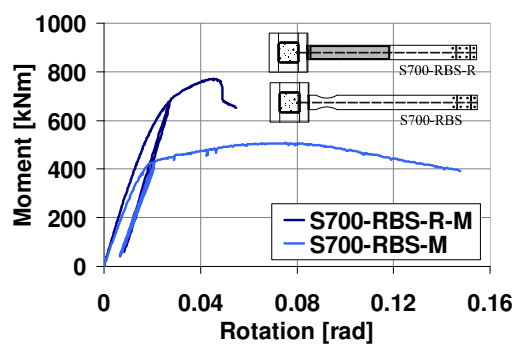
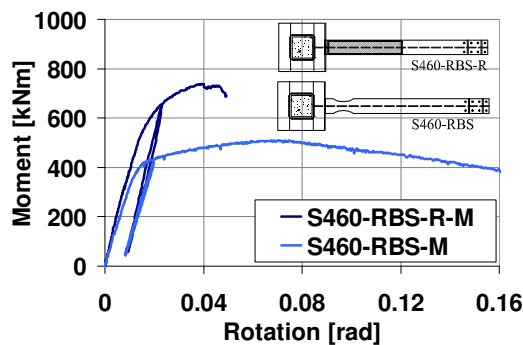


Figure 4.120. Overstrength of connection zone for RBS joints

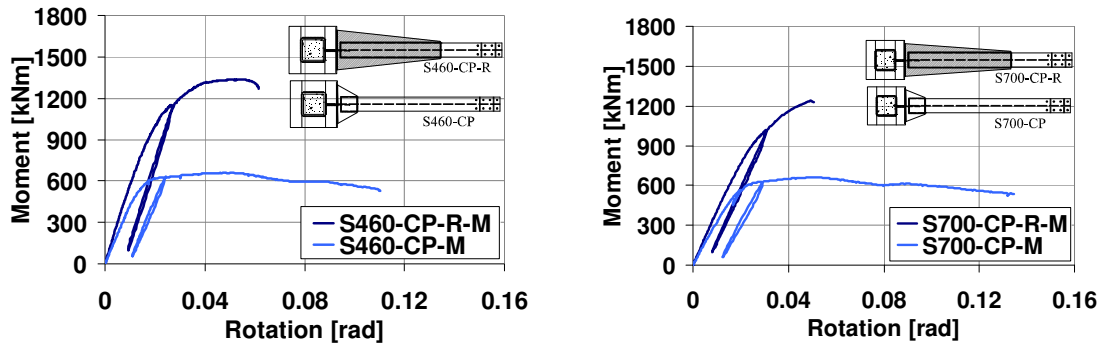


Figure 4.121. Overstrength of connection zone for CP joints

The contribution of components to the joint rotation is further shown for each joint configuration subjected to monotonic loading. The local instrumentation allowed assessing the contribution of the following regions: plastic hinge (dissipative zone), connection (welded connection + external diaphragm), and column web panel. It can be observed in Figure 4.122 for the joints with reduced beam section, and in Figure 4.123 for the joints with cover plates that the main plastic deformations occurred in the dissipative zone of the beam (plastic hinge).

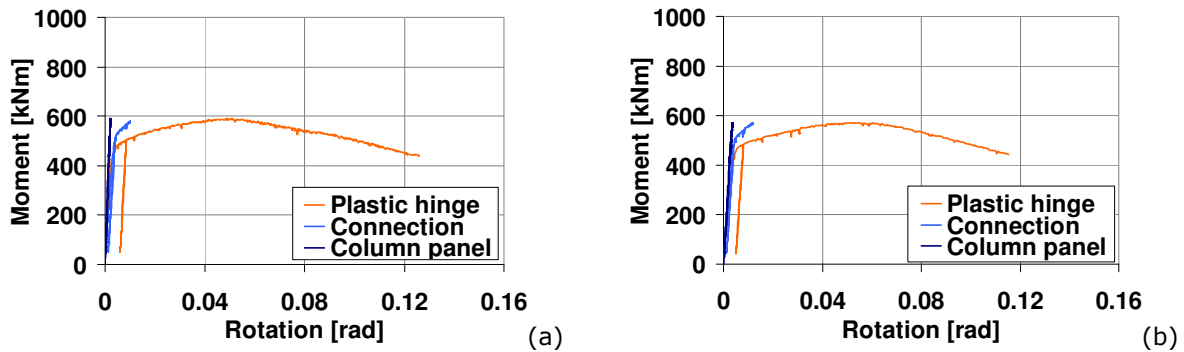


Figure 4.122. Contribution of components joint rotation: (a) S460-RBS-M, (b) S700-RBS-M

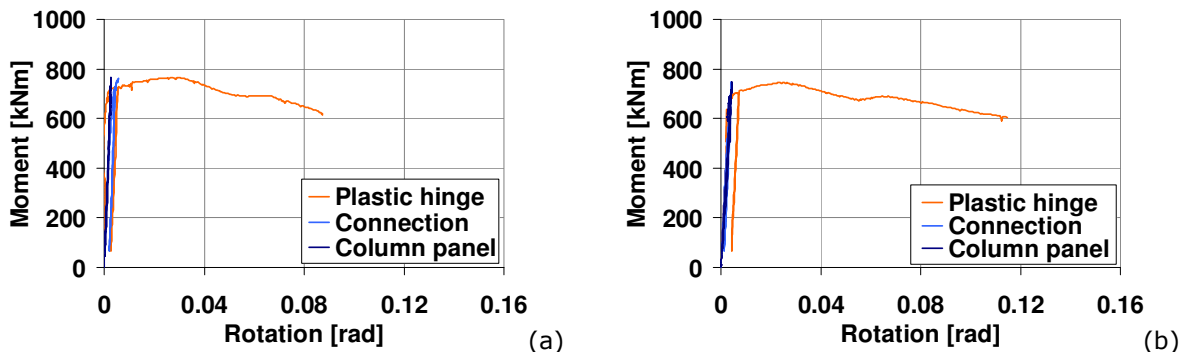


Figure 4.123. Contribution of components to joint rotation: (a) S460-CP-M, (b) S700-CP-M

The contribution of components to overall rotation in case of joints with strengthened beam is shown in Figure 4.124 for reinforced RBS joints and in Figure 4.125 for the reinforced CP joints. The deformations within the reinforced beam zone were proved to be low. The main contribution to the overall joint rotation was given by the connection zone (for reinforced RBS joints), and respectively connection and column web panel (for reinforced CP joint). It is to be noted that the measurements from the connection zone included also the deformations of the external diaphragm.

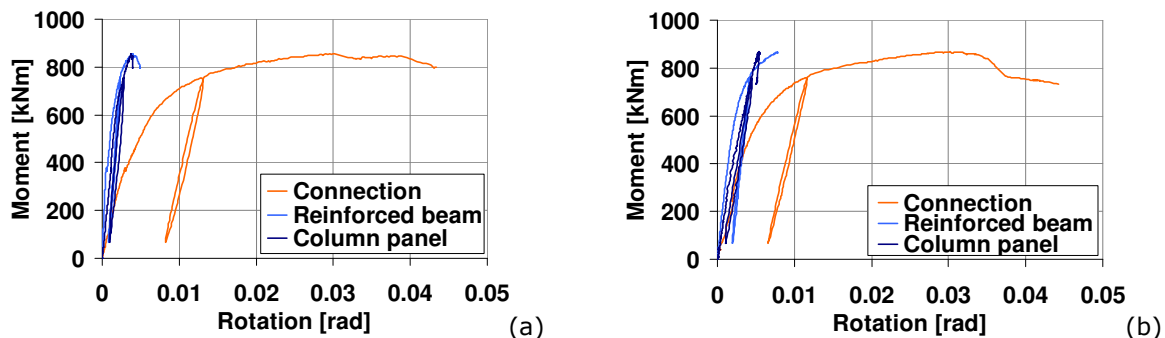


Figure 4.124. Contribution of components to joint rotation: (a) S460-RBS-R-M, (b) S700-RBS-R-M

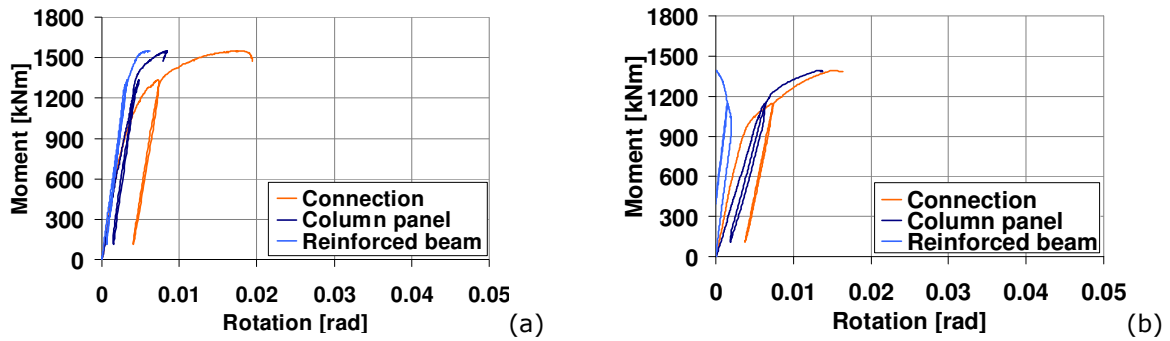


Figure 4.125. Contribution of components to joint rotation: (a) S460-CP-R-M, (b) S700-CP-R-M

Figure 4.126 and Figure 4.127 show the contribution of components to the joint rotation in case of RBS and CP joint assemblies subjected to the cyclic loading. As can be observed the main deformations developed in the plastic hinge.

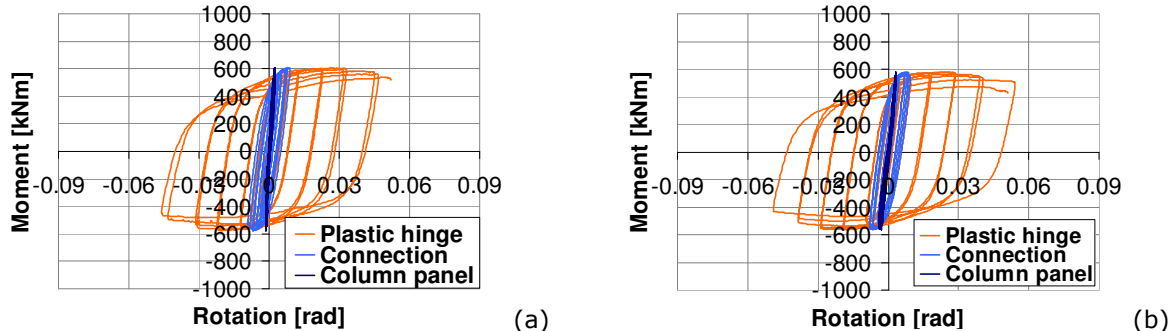


Figure 4.126. Contribution of components to joint rotation: (a) S460-RBS-C, (b) S700-RBS-C

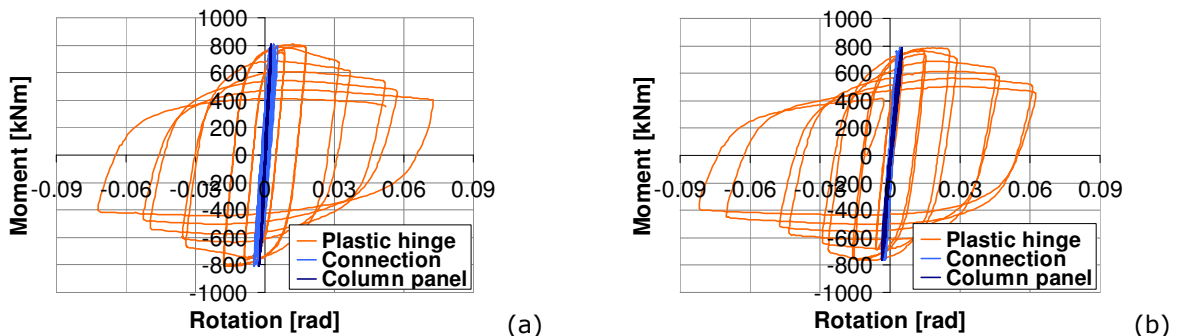


Figure 4.127. Contribution of components to joint rotation: (a) S460-CP-C, (b) S700-CP-C

The rotation capacity of the RBS and CP designed joints was evaluated considering the EN 1998-1 [1] criterion for which the reduction of stiffness and capacity is not greater than 20%. Consequently, the total assembly rotation was corresponding to 50 mrad in case of RBS joints, and 40 mrad in case of CP joints.

4.4.4.5 Numerical investigation of beam-to-CF-RHS column joints

In addition to the experimental tests, extensive numerical simulations have been performed with the finite element modelling software Abaqus [72]. In a first step the material model was calibrated based on results from compression tests on concrete samples and tensile tests on steel samples. The calibrated material model was further used within the numerical models of the beam-to-column joints. Further, based on the calibrated FE models of the joint configurations, the experimental program was extended with the aim to assess the influence of additional parameters on the joint behaviour.

Calibration of the material model

The stress-strain relationship used for concrete (see Figure 4.128), was computed using the results from the compression tests, and an analytical stress-strain model reported in literature [73]. The concrete damaged plasticity model was used, considering as input the stress-strain relationship shown in Figure 4.128, and the plasticity parameters, compression damage and tensile behaviour from Korotkov et al. [74]. The calibration of the material model for the steel grades was performed as well. The input for the plastic behaviour of the steel parts contained by the each beam-to-column joint assembly, are presented in Deliverable D5 [13]. The material models were calibrated

based on results from tensile test. Figure 4.129 illustrates for the IPE400 beam flange, the comparison between test and simulation, in terms of force-displacement curve, for which a good correlation can be observed. The young modulus was considered equal to $E=210000 \text{ N/mm}^2$, and the Poisson ratio was considered equal to $\nu=0.3$.

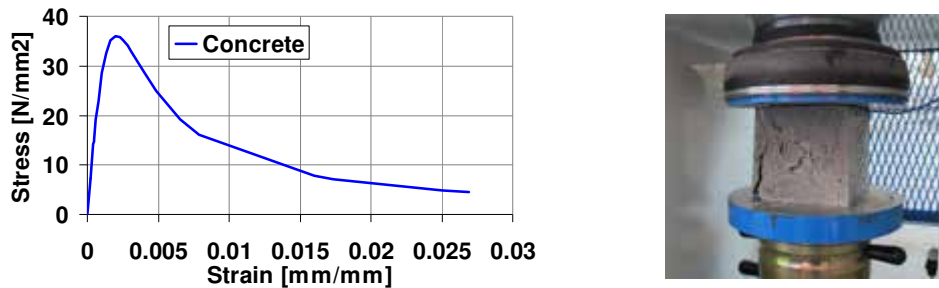


Figure 4.128. Stress-strain relationship for concrete

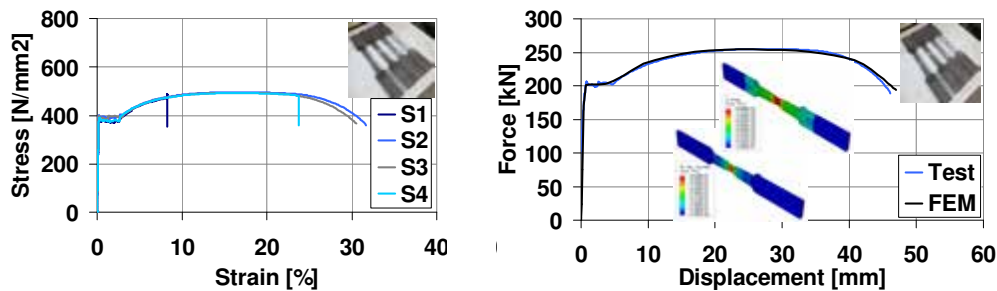


Figure 4.129. Calibration of the material model for steel (IPE400 beam flange)

Calibration of the joint models

Due to the innovative joint configurations, it was needed to have an accurate prediction for the behaviour of the joints in order to avoid unacceptable failure during the experimental tests. Therefore, pre-test numerical simulations have been performed considering the calibrated material model. Consequently, the behaviour of each joint configuration was obtained. It was observed that the results from the pre-test FE simulations were relative close to the test results. The calibration and refinement of the FE joint models was performed using the measured geometry and accounting for the contact tolerances between the out of plane lateral system and beam. The lateral contact was defined considering a small gap between beam flanges and the contact elements (see Figure 4.130).

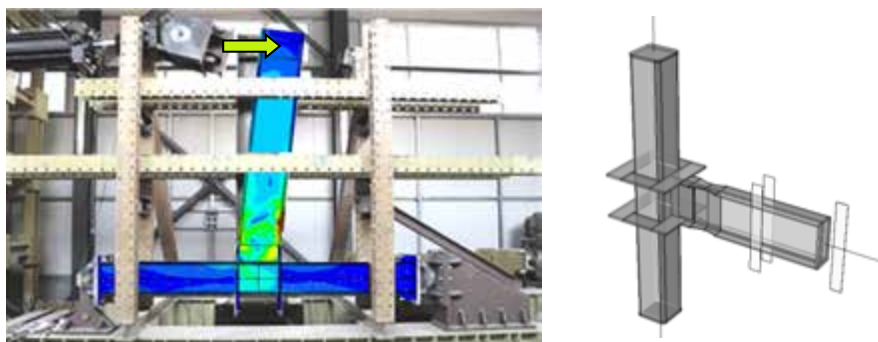


Figure 4.130. Pre-test numerical simulation of the joint behaviour and illustration of the joint model accounting for the out of plane lateral system

From the calibration, a set of numerical models were obtained which were capable to reproduce with a good accuracy the response of the joints in both moment-rotation curve and failure mechanism, i.e. formation of the plastic hinge in the beam (RBS and CP designed joints) and yielding of components (joints with strengthened beam). Consequently, for each joint configuration, a comparison is shown between test and simulation in terms of moment-rotation curve computed at column centreline. The plastic strain is shown in comparison to the failure mode observed during the test. The results from the calibration of the monotonic tests on beam-to-column joints are shown in Figure 4.131 for the joints with reduced beam section, in Figure 4.132 for the joints with cover plates, in Figure 4.133 for the reinforced RBS joints, and finally in Figure 4.134 corresponding to the reinforced CP joints. Within the FE simulations it was not accounted for material fracture, which was observed at some of the joint specimens. Therefore, the capacity did not suffer as in the tests.

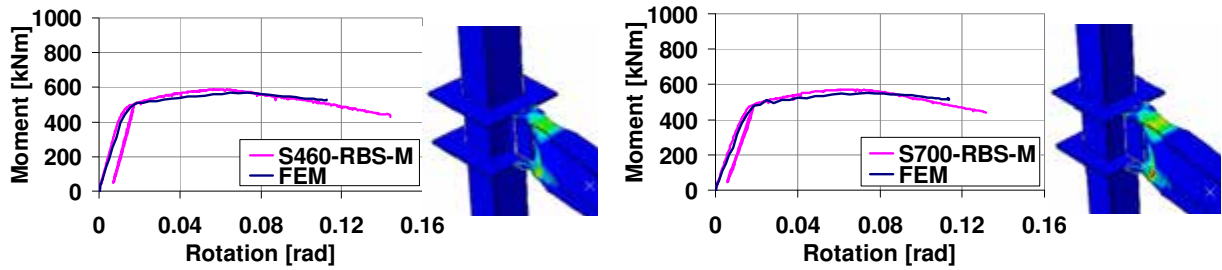


Figure 4.131. Comparison between test and simulation for RBS joints

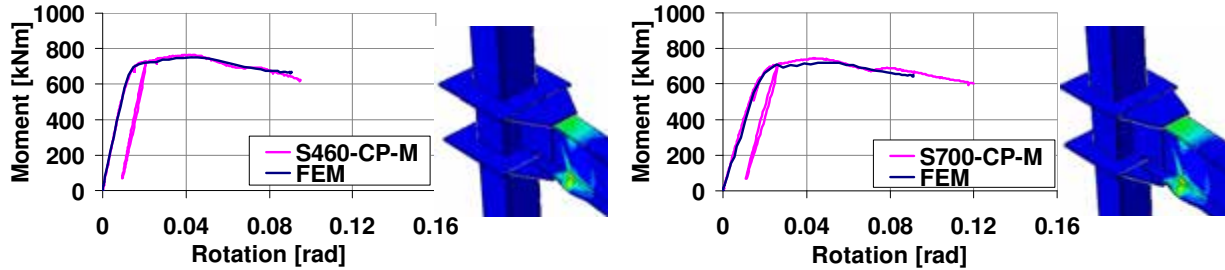


Figure 4.132. Comparison between test and simulation for CP joints

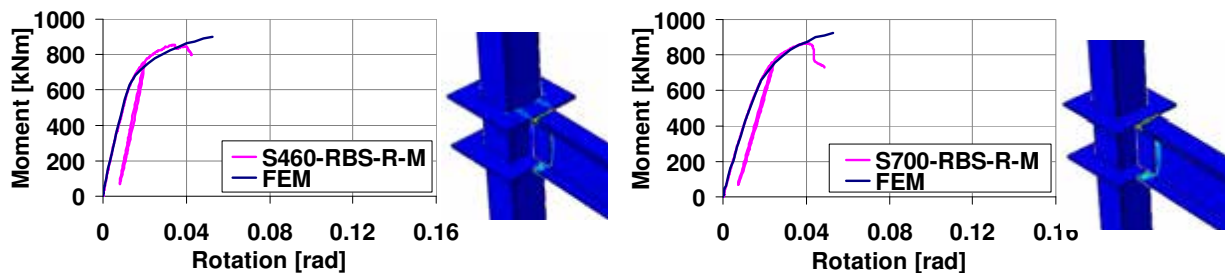


Figure 4.133. Comparison between test and simulation for reinforced RBS-R joints

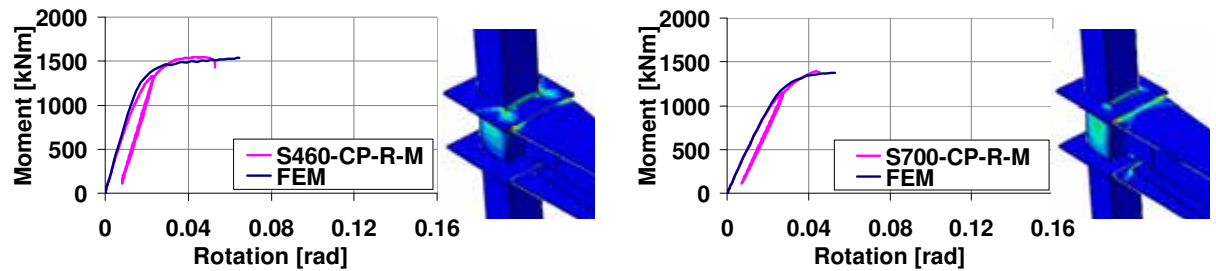


Figure 4.134. Comparison between test and simulation for reinforced CP-R joints

The numerical models calibrated based on the joints subjected to monotonic loading were further used for the calibration based on the cyclic test results. One of the differences was related to the loading procedure. Consequently, a smooth cyclic loading pattern was used, which was characterized by one cycle for each of the following amplitudes: 10, 15, 20, 30, 40, 50, and 60 mrad. Another difference between cyclic and monotonic analyses was related to the material model. A combined isotropic/kinematic cyclic hardening model was therefore adopted. The input for the material model was represented by the yield strength of the steel part, and in addition the cyclic hardening parameters as given by Dutta et al. [75], i.e. $C_1=42096$, $\gamma_1=594.45$, $Q_\infty=60$, $b=9.71$.

The results from the cyclic analysis are shown for each beam-to-column joint configuration in terms moment-rotation curve (computed at column centreline), von Mises stress distribution and equivalent plastic strain. An illustration of the failure mode, as obtained from the experimental investigations, is shown as well. The comparison between test and numerical simulation is shown in Figure 4.135-a-b for the RBS joints, in Figure 4.135-c-d for the CP joints, in Figure 4.136-a-b for reinforced RBS joints, and finally in Figure 4.136-c-d for reinforced CP joints. The results from the numerical investigations of the cyclic tests show a good correlation with the experimental results considering the moment-rotation hysteretic loops as well as the failure mechanism (plastic hinge – buckling of flanges and web of beam in the dissipative zone, yielding of components – failure in the heat affected zone of the reinforced RBS joints, plastic deformations in the external diaphragm and column panel zone). In case of S460-CP-R-C joint, the capacity corresponding to the negative amplitudes was obtained higher in the numerical simulations compared to the test where a crack was developed in the cover plate (between external diaphragm and beam flange) and which did not develop in the FE model.

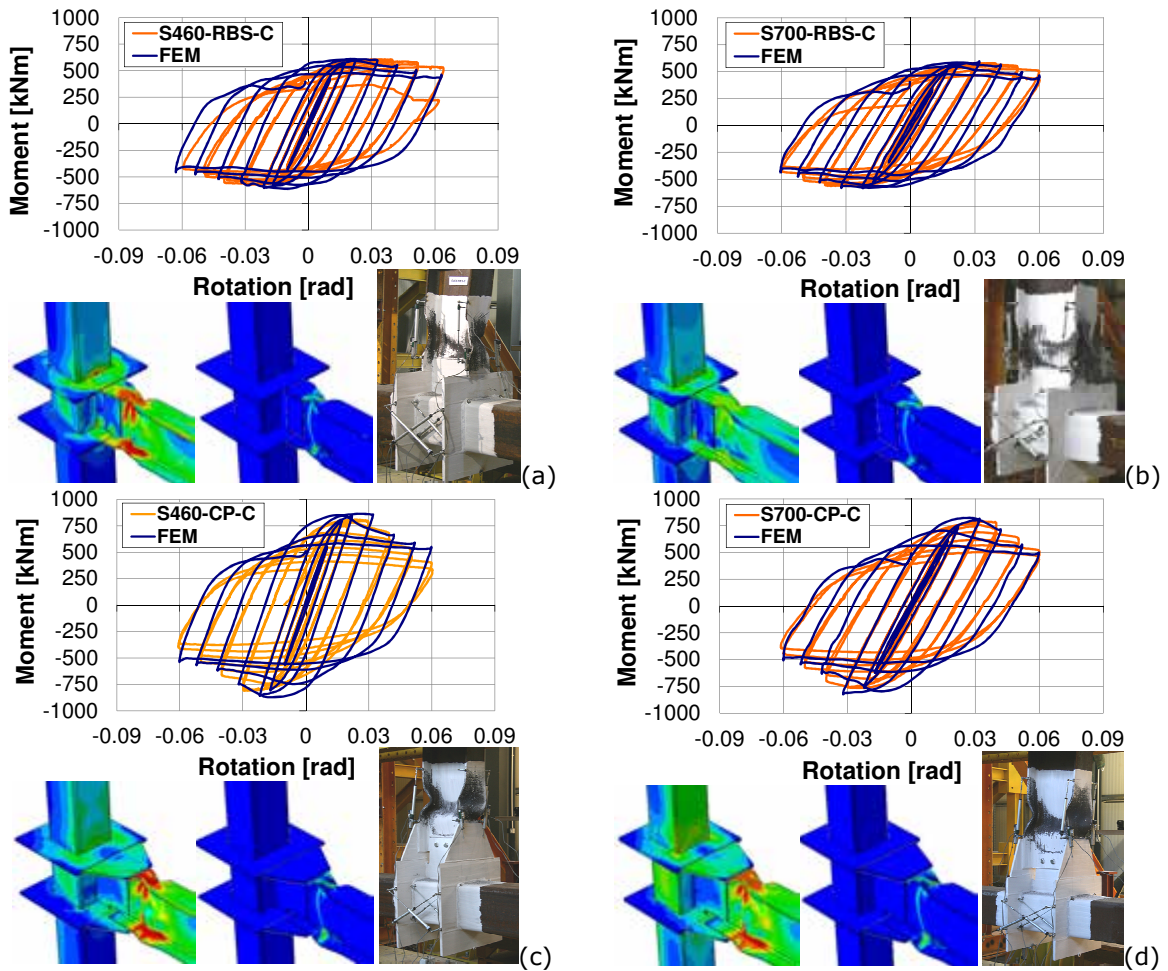


Figure 4.135. Test vs. simulation for RBS and CP designed joints subjected to cyclic loading

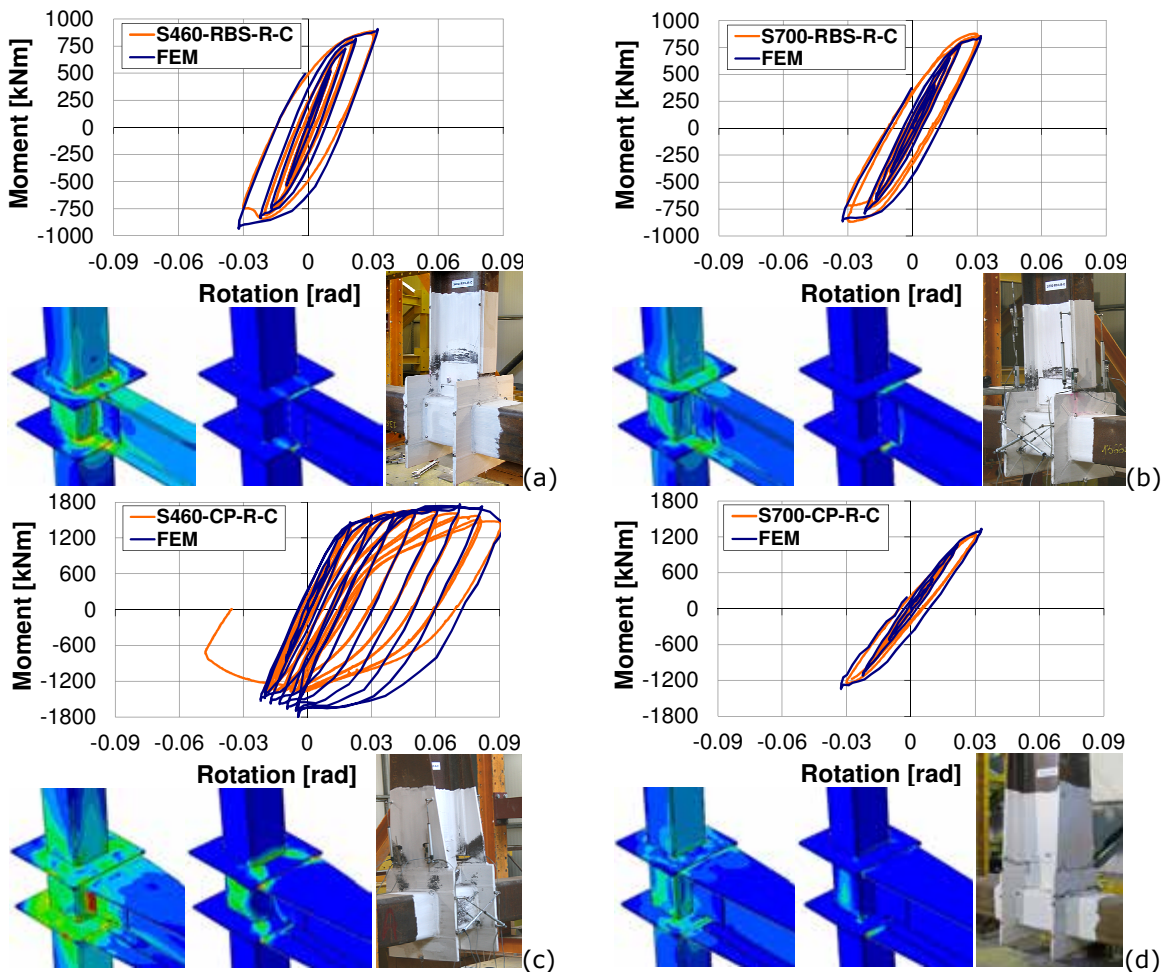


Figure 4.136. Test vs. simulation for reinforced RBS and CP joints subjected to cyclic loading

Extension of experimental program with additional cases

The experimental investigations were conducted on single sided beam-to-column joints. Due to the more complex working conditions of a beam-to-column joint within a 3D building frame, a set of complementary cases were considered for the investigation through FE simulations. The influence of different parameters on the joint behaviour was investigated for the following cases:

- Influence of the concrete core – i.e. the response of the joint without concrete core in comparison to the reference joint with CFT column;
- Influence of the axial force – i.e. the response of the joint with axial force in the column ($N=0.5 \cdot N_{pl}$) in comparison to the reference model;
- Response of the joints with two and respectively four welded beams;

Influence of the concrete core: With the aim to evaluate the influence of the concrete core – i.e. the response of the joint without concrete core in comparison to the reference joints with composite column (CF-RHS) – a set of additional numerical simulations were performed on the calibrated numerical models from which the concrete part was removed (NC – no concrete). The results are shown in terms of moment-rotation curve computed at column centreline. It can be observed in Figure 4.137-a-b for CP joints, that the absence of concrete core did not affect significantly the response (only a minor reduction of the capacity was observed). In contrast, for the reinforced joints (extended cover plate) a significant reduction of capacity can be observed in Figure 4.137-c-d. In these cases, the bending moment and implicitly the shear force in the column web panel were much higher. In other words, the shear force in the column web panel exceeded the capacity of the steel tube in shear, and therefore a higher capacity was corresponding to the joints with concrete core.

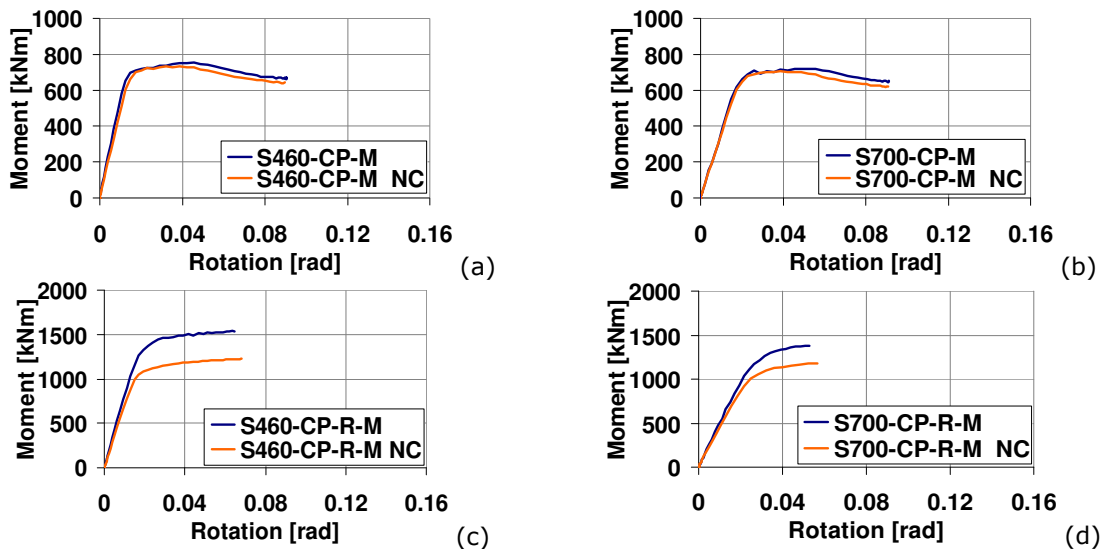


Figure 4.137. Influence of concrete core for: a) & b) CP joints, and c) & d) strengthened CP joints

Influence of axial force in the column: With the aim to assess the influence of the axial force in the column with respect to the behaviour of the beam-to-column joint, FE simulations were performed on one of the joint configurations (i.e. S460-CP) considering an axial force level in the column corresponding to 50% of $N_{pl,Rd,composite}$. In a first step, the column was axially loaded up to the considered level (see Figure 4.138-a), and in a second step the beam was loaded. The stress distribution and implicitly the failure mechanism are shown in Figure 4.138-b. The corresponding moment rotation curve is compared in Figure 4.138-c with the reference model without axial force in the column. It can be observed that the axial force in the column did not affect the response of the joint compared to the reference model, and that the plastic hinge formed in the beam.

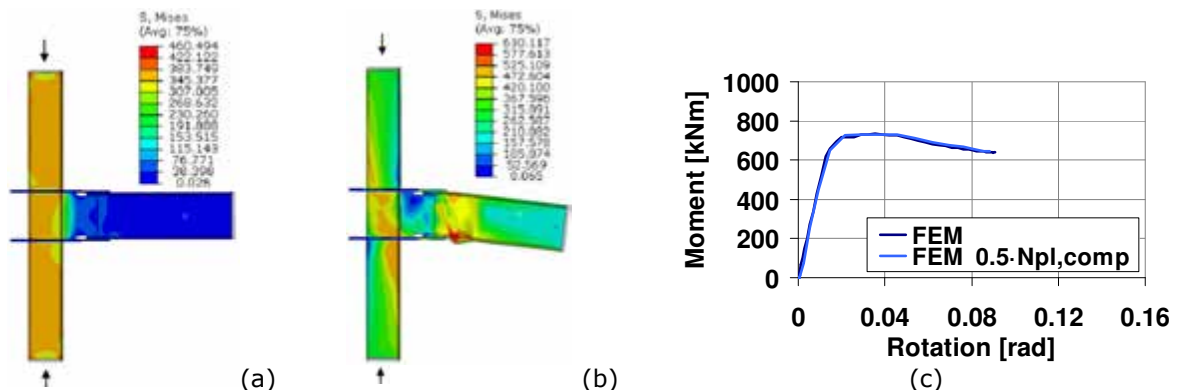


Figure 4.138. Influence of $0.5 \cdot N_{pl,Rd,composite}$ axial force: S460-CP joint

Behaviour of joints with beams welded on two sides: The experimental tests were performed on single sided beam-to-column joints. It was therefore necessary to assess the behaviour of the joints (including column web panel) in the situation of loading from two sides which corresponds to a more demanding scenario. Figure 4.139 shows the stress distribution, plastic strain and moment-rotation curve corresponding to the S700-CP joint. Consequently, a reduction of the stiffness can be observed in a compared to the test curve, but the failure mode was not affected (plastic hinges developed in beams). A similar investigation was performed also for the joint configuration with reduced beam section. Figure 4.140 shows the stress distribution, plastic strain and moment-rotation curve corresponding to the S700-RBS joint. A reduction of the stiffness can be observed also in this case, but the failure mode was not affected (plastic hinges developed in beams). The weak-beam/strong-column concept was therefore confirmed for the CP and RBS joints, considering the case with beams welded on two sides.

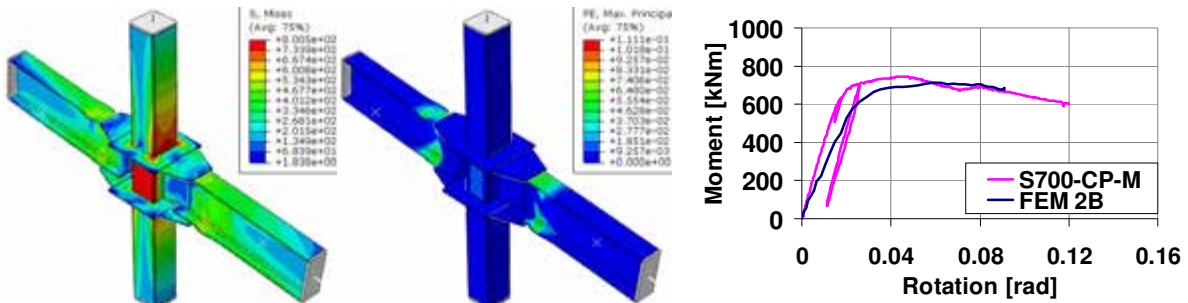


Figure 4.139. Behaviour of S700-CP joint with beams welded on two sides (CFT)

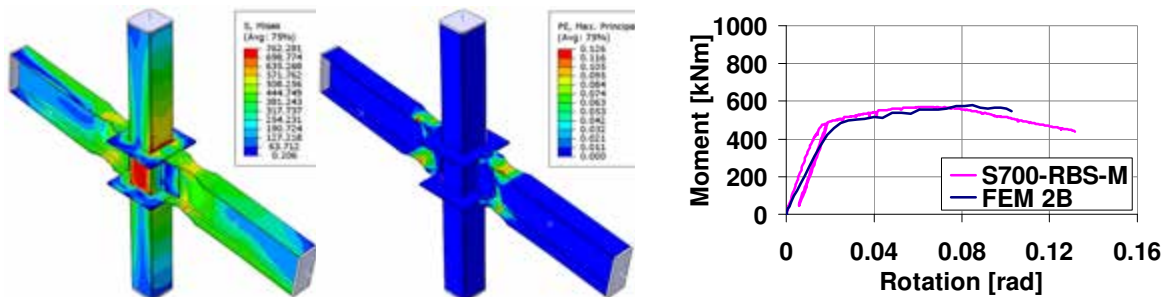


Figure 4.140. Behaviour of S700-RBS joint with beams welded on two sides (CFT)

Behaviour of joints with beams welded on four sides: The response of the joints was also investigated considering the case with four beams welded around the concrete filled tube. As reference, the S700-RBS and S700-CP joint models were used. The loading was applied in displacement control at the tip of the beams, considering a load ratio in amount of 100% on one direction and respectively 50% on the other direction. As a result, the moment rotation curves are shown in Figure 4.141 compared to test data.

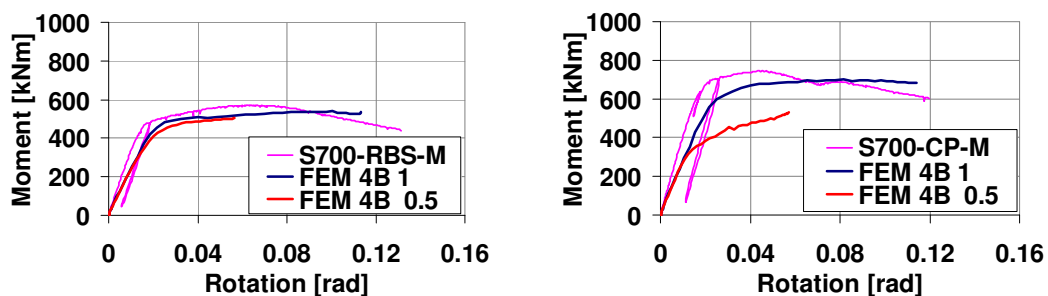


Figure 4.141. Joints with four beams – Moment-rotation curves

Figure 4.142 shows the von Misses stress distribution and the plastic strain in the two joint configurations. As it can be observed, on the main loading direction the moment-rotation curve suffered a small reduction of the stiffness but the capacity or the failure mode was not affected. For the secondary loading direction, the moment rotation curve exhibited the small stiffness reduction and a reduction of the capacity for the S700-CP joint, for which the plastic hinges did not develop in beams as can be observed for the S700-RBS joint. For both joint assemblies, small plastic deformations were observed in the column above the external diaphragm. It is to be mentioned that the members for the joint specimens were chosen from a 2D frame configuration, while the design of a 3D frame would lead to slightly larger column cross sections. However, considering the loading of the joints from two directions it can be observed that the external diaphragm did not suffer plastic deformations.

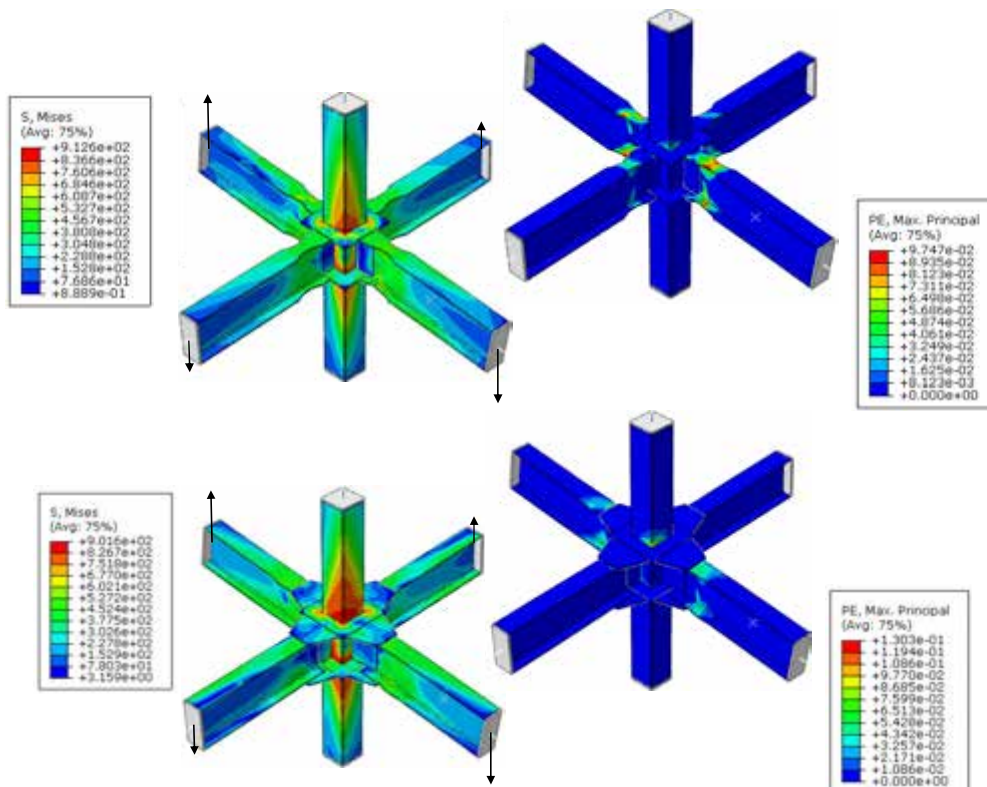


Figure 4.142. Joints with four beams – von Mises stress distribution and plastic strain

It is to be mentioned that the experimental investigation program as well as the numerical investigation program carried out for the welded beam-to-column joints with CF-RHS columns, is presented in detail within Deliverable D5 [13].

4.5 Concluding remarks

Chapter 4 presented the outcomes of the experimental program carried out on joint assemblies and components, and which was focused on the following topics:

- Investigation of weld details and T-stubs;
- Investigation of bolted beam-to-column joints in moment-resisting dual-steel frames;
- Investigation of welded beam-to-column joints in moment-resisting dual-steel frames;
- Investigation of steel-concrete connection (load introduction tests) in case of concrete filled tubes, considering the use of long bolts and respectively shot fired nails.

In the following part a brief presentation is made with regard to the conclusions from the investigation of the above summarised topics.

Investigation of weld details (cruciform joints) and T-stubs

Weld details (cruciform joints):

- For welds designed as full-strength, the loading type did not affect the failure of the connection, i.e. the cyclic quasi-static as well as cyclic dynamic loading had no influence on the behaviour of the weld itself. Only one failure type was observed: the failure occurred for all types of loading conditions in the cross plate (base metal) and no rupture in the weld occurred.
- The most important consequences on the cyclic behaviour of the Cruciform Joints were the reduced ductility and the increased strength for the dynamic loading protocol. Indeed, for cyclic quasi-static loadings more stable hysteretic loops could be observed compared to cyclic dynamic loading.
- The conditions with a strain rate in the range of $0.06 \div 0.12 \text{ s}^{-1}$ (typical for steel members yielding under seismic action) showed an increase in the ultimate strength of welded connections. Additionally, a reduction of ductility was present in the case of high strain rates for monotonic and cyclic loading.
- As the design philosophy of a “full-strength” weld was successful and only failure of the base metal occurred, the influence of the steel grade of the longitudinal plate (S460 / S690) related to the ultimate strength, the type of welding (fillet weld or full penetration weld) and the type of filler metal on the overall strength and ductility of the Cruciform Joint was negligible.

T-stubs:

- The investigation of bolted T-stubs under monotonic quasi-static and cyclic quasi-static loading conditions (86 experimental tests) allowed the evaluation of the strength and ductility.
- The observed failure modes involved combined bending and tension bolt fracture for specimens behaving ductile and nearly pure tension bolt fracture for specimens behaving brittle. Stripping of the nut threads was not observed at all. In one specimen (T-stub series 400) complete cracking of the endplate material in the HAZ occurred.
- The experimental results demonstrate that the end-plate can be deliberately designed, taken into account the thickness and the steel grade, in order to achieve sufficient ductility as requested by code provisions.
- The degree in which cyclic loading affected the ductility of T-stubs is much dependent on the failure mode. Specimens failing by mode 2-3 (brittle) were characterized by an important decrease of ductility coupled with a significant load carrying capacity. On the other hand, ductility of specimens failing in mode 2-1 (ductile) was much more pronounced achieving however a smaller load carrying capacity.
- It can be summarised that the choice of thickness of the end-plate associated with steel grade is important in the conception of a proper connection, in order to obtain a good balance between stiffness, strength and ductility of components.
- As a key outcome it can be concluded in case of bolted T-stub connections and respectively bolted beam-to-column joints, the major contributions of the overall T-stub strength and deformation are the end-plate deformation capacity and the strength of the bolts, as far as its plastic failure mechanism was governed by mode 2.
- The comparison between the experimental results and the corresponding analytical predictions of plastic resistance derived from EN 1993-1-8 [46], taken into account the nominal values for the steel grades, showed remarkable reserves which however might lead to an underestimation of the T-stub components if combined with other components in a joint. The results led to the assumption that the choice of steel grade for the end-plate material does not significantly influence the load carrying capacity. On the contrary the geometry (bolt distance, end-plate thickness, etc.) and the stiffener have a more remarkable influence on the load carrying capacity. For stiffened situations, see e.g. series 200, a uniform load introduction of the bolt and therefore almost a pure tensile stress situation of the bolt provides a nearly independent high load carrying capacity without losing much ductility.

Investigation of bolted beam-to-column joints with PE-WF and CF-RHS columns

- End-plate connections between steel beams with hammer heads and partially-encased composite wide flange column (B-EP-H) joint: this joint solution has a very high resistance and stiffness, as the main sources of the deformation are strengthened. Indeed, the extended part of the end-plate is reinforced by the hammer-head while the column flanges in bending and the column web panel in shear are reinforced by the lateral plates welded on the column flanges. Due to the hammer-head shape, stress concentrations at the beam level can be avoided. It has been demonstrated through these tests that a redistribution of loads between different compression zones, i.e. the hammer-head flange in compression and the beam flange in compression, occurs and should be taken into account in the estimation of the joint resistance. On the economic aspect, using the hammer-heads allows reducing the used material when the overstrength factor conception is applied in the design of joints subjected to seismic actions according to EN 1998-1 [1]. Because the hammer heads and the beams are made from the same material, meaning that it not necessary to apply the overstrength factor for hammer heads components. Moreover, the fabrication of the hammer heads is quite simple as they are extracted from the beam profiles.
- Reverse U channel connections between hammer head beams and composite rectangular hollow section column (B-EP-U) joint: this joint type uses also the hammer-head beams so the advantages given by the hammer-head solution is similar to the B-EP-H joint. However, the U reverse channel is the main source of the joint deformation and is generally the critical component mainly affecting the joint behaviour. The full strength and rigid requirements for B-EP-U joints are more difficult to be met in comparison to the B-EP-H joints.
- Extended end-plate connections between beams with dog-bone and rectangular hollow section composite columns joint using long bolts (B-EPL-RBS) joint: the behaviour of the joints was not totally exposed during the tests, in particular in terms of resistance as the plastic hinges occurred at the dog-bone section of the beams. However, the test results show that the rigidity of the joints is quite high even the use of long bolts. Moreover, the effective load transfer from the beams to the RHS composite columns is also demonstrated by the load introduction tests. It can say that using the long bolts is an efficient solution to connect the I-shaped beam to RHS column, avoiding the intermediate elements (e.g. reverse U channel in B-EP-U joints). In the cases where the resistances of the panel in shear or of the column in transversal compression components are not sufficient, the reinforcement of the lateral column walls by the plates may be considered.

- All joint configurations can be designed to be the full-strength and rigid/or semi-rigid solutions and can be used in moment-resisting dual-steel frames. Moreover, the cyclic tests show that the ductility requirement by EN 1998-1 [1] is satisfied.
- The proposed joint configurations include some new components that are not yet covered in the Eurocodes and the literature. Therefore, the analytical developments on these new components have been performed, and the proposed joints can be now characterized on both resistance and stiffness aspects by using the component method. With a large variation of failure modes, the test results allow validating the analytical developments. The detail on the design guidelines can be found in Deliverable D6 [68].

Investigation of welded beam-to-column joints with FE-WF columns

- Experimental tests performed on the beam-to-column joints proved that the design and geometrical concept along with the welding details applied represent a good solution under variable and constant cyclic loading conditions.
- The design objective for the welded RS and CP connections, based on the capacity design concept, to relocate inelastic action away from the face of the beam-to-column connection, was fulfilled. In both cases connection zone and the column itself remained in elastic state.
- Both designed full strength connections proved to behave well under cyclic tests performed according to the ANSI/AISC 341-10 [7] loading protocol, with plastic rotation capacities greater than 0.044 and 0.051 rad, for bigger and smaller beam cross-sections, respectively, without degradation of strength and stiffness for more than 20% according to EN 1998-1 [1] criterion.
- In case of constant cyclic loading, the CP joint displayed better fatigue performance, attributed to the increased level of unfavourable strain concentrations, larger weld residual stress and HAZ at the end of the rib-stiffener in the RS joint.
- Both designed strengthened connections meet qualification-type requirements according to EN 1998-1 [1] and ANSI/AISC 341-10 [7].
- Both column-beam steel material combinations evidenced good performance. No damage or cracks were observed in the welded region at the column face after the tests.
- Constant axial force applied in the column did not have any noticeable effect on response of the specimens.

Investigation of welded beam-to-column joints with CF-RHS columns

Welded joints with CF-RHS columns have been investigated within the framework of the WP5. Consequently, Tasks 5.3 and 5.4 covered experimental investigations on 8 beam-to-column joint configurations which were subjected to monotonic and cyclic loading. The parameters investigated within the joint tests consisted of loading procedure (monotonic, cyclic), joint type (RBS, CP), steel grade for column (S460, S700), and intended failure mode (beam, connection). The experimental program covered a number of 16 beam-to-column joint specimens. For each case a description was made in relation to the test assembly, observations from test, and the response of the joints subjected to the monotonic and cyclic loading. Interpretation and comparison of results was performed with the aim to assess the participation of components to the joint rotation and the overstrength of the connection zone with respect to the dissipative zone.

The experimental investigations performed on beam-to-column joints under both monotonic and cyclic loading evidenced a good conception and design of the joints (RBS and CP). This observation was justified by the elastic response of the connection zone, formation of the plastic hinge in the beam, and a good response of joint detailing and welded connections. In addition, corresponding to cyclic tests performed according to the ANSI/AISC 341 [7] loading protocol, the RBS and CP designed joints evidenced rotation capacities of 50 mrad (RBS joints) and respectively 40 mrad (CP joints) for which the degradation of strength and stiffness were not greater than the 20% limit defined in EN 1998-1 [1]. From the interpretation and evaluation of results several observations were made, and which are summarized as follows:

- In relation to the contribution of components to joint rotation - for the joints with reduced beam section and with cover plates, the main plastic deformations occurred in the beam (plastic hinge), while the contribution of the external diaphragm and column web panel was low. For the joints with reinforced beam, yielding was initiated in the joint components, i.e. adjacent area of the welded connection and external diaphragm (strengthened RBS joints), and external diaphragm and column web panel (strengthened CP joints).
- In relation to the overstrength of the joints – from the comparison between the four designed joints and the corresponding joints with reinforced beam, the overstrength computed at both yield and at maximum capacity, was observed to satisfy the overstrength requirements, from EN 1998-1 (2004).

Numerical investigations were performed for the welded beam-to-column joints with CF-RHS columns. The aim was to have a better understanding of the joint behaviour and to extend the experimental program with additional cases. The first phase consisted in the calibration of the

numerical models of the joint configurations based on the monotonic and cyclic test results. From the calibration, a set of numerical models were obtained which were capable to reproduce with a good accuracy the response of the joints in both moment-rotation curve and failure mechanism, i.e. formation of the plastic hinge in the beam (designed joints) and yielding of components (joints with strengthened beam). The second phase consisted in the extension of the experimental program with the aim to assess the influence of different parameters on the joint behaviour, i.e.:

- Influence of the concrete core;
- Response of joints with beams welded on two sides (cruciform joints);
- Influence of the axial force;

The outcomes of the parametric study can be summarised as follows:

- The influence of concrete core was proved to be low for the single sided RBS/CP joints (i.e. reduced load level), but significant corresponding to joints with strengthened beam, respectively to joints with multiple beams (i.e. higher load level);
- The axial force in the column did not affect the response of the joint;
- For the joints with beams welded on two sides, a reduction of the stiffness was observed, but the capacity was not affected, nor the failure mode;
- For the joints with beams welded on four sides, a reduction of the stiffness was observed for both loading directions; corresponding to the main loading direction, the capacity was not affected, nor the failure mode (formation of plastic hinges in beams); corresponding to the secondary loading direction, the capacity decreased in case of S700-CP joint and plastic hinges did not develop in beams;
- The joining solution with external diaphragms exhibited a good response for the case of joints with multiple beams, i.e. the response of the external diaphragm was not affected;

From the numerical investigations, particularly based on the calibrated numerical models of the joint configurations, the validation of the analytical model (i.e. the design relations of the components) was performed. Consequently, a comparison between experimental test, numerical simulation and analytical model was made in concerning the dissipative zone, the external diaphragm and the column web panel. The following observations were made:

- The formation of the plastic hinge in the beam was confirmed by the experimental and numerical investigations, and the design capacity of the plastic bending moment was in good agreement with test results and FEM;
- The design capacity of the external diaphragm was confirmed, and the yield lines observed from experimental tests and numerical simulations confirmed the failure mode considered in the analytical model for both RBS and CP joints (development of yield lines);
- The column web panel was activated only for joints with reinforced beam (strong beam – weak column case); the design capacity of the column web panel in shear (steel + concrete) was in very good agreement with the experimental results and FEM simulations; the provisions from EN 1994-1-1 [4] for the column web panel in case of partially encased wide flange (PE-WF) sections in shear were confirmed also for the case of concrete filled rectangular hollow sections (CF-RHS).

Investigation of steel-concrete connection through the use of long bolts

- In case of joints with end-plate connection, long bolts and concrete filled tube columns, the long bolts have a double role, i.e. to assure the connection between beam and column, and respectively to assure the connection between the steel tube and the concrete core. For the study of the latter phenomenon, a set of load introduction tests were performed at the University of Liege.
- Tests with and without bolt preloading have been performed to identify the effect of this preloading on the behaviour of the tested specimen. Also, different testing set-ups have been used in order to be able to characterise the slip resistance between the concrete and the tube, the resistance of the bolts subjected to pure shear and the resistance of the bolts subjected to combined bending and shear.
- The test results proved the effectiveness of the load transfer from the beams to the RHS composite columns through the use of long bolts.

Investigation of steel-concrete connection through the use of shot fired nails

- In case of joints with welded connection and concrete filled tube columns, the load introduction can be provided by shot-fired nails fixed from the exterior of the cross-section. In order to check the effectiveness of the shear connection between steel and concrete, a series of load introduction tests were performed on column stubs at the Politehnica University of Timisoara.
- The investigated parameters consisted of: loading procedure (monotonic, cyclic), connection (friction, friction+connectors) and steel grade (S460, S700). The aim was to assess the efficiency of shot fired nails in providing the connection between steel tube and concrete core.

- The shear strength that developed through friction (between steel tube and concrete core) was obtained in amount of 0.4 N/mm^2 , which is equal to the value recommended by EN 1994-1 [4] for rectangular hollow sections.
- In relation to the specific loading (push-out tests), it was observed that the connectors can take the major shear contribution to the load transfer from steel tube to the concrete core, in both monotonic and cyclic loading. From the investigation of the behaviour and failure mode, it was observed that under monotonic loading the concrete was crushed in a small amount at the contact with the nails which bent. Under alternating cycles the nails eventually fractured at the interface between concrete and steel tube. In addition it was observed that from the cyclic loading the capacity of the connectors slightly decreased compared to the monotonic loading.
- As previously confirmed by Beck [76], the X-DSH 32 P10 shot fired nails proved a significant contribution to the steel-concrete connection considering the monotonic loading. In addition, the current study proved a significant contribution of the connectors also for the case of cyclic loading conditions and for the use of high strength steel rectangular hollow sections (S460 and S700).
- Finite element (FE) simulations (see Deliverable D5 [13]) evidenced a load transfer mechanism based on direct pressure between steel tube / nail / concrete, combined with tension forces within the nail which increased the capacity over the pure shear capacity in amount of 21.85 kN [71].

5 Recommendations for seismic design and performance based evaluation of dual-steel structures

5.1 Introduction

The current chapter is related to the guidance for the structural earthquake design, in the context of the Eurocodes, of medium or high-ductility class (EN1998-1 [1], Table 6.1) dual-steel frames (DSF) utilizing high strength steel members. For the purpose of the guide the term DSF is used with two distinct meanings:

- Frames with dual lateral-load resisting structural system. I.e. frames with moment resisting bays and braced bays;
- Frames with elements fabricated using two grades of steel. I.e. lower/usual grade steel for certain elements and higher grade steel (high strength steel) for other elements.

Design and detailing rules for the DSF typologies are presented in light of the available guidance in EN 1998-1 [1] and supplementary sources. Aspects of joint detailing, with special focus on the behaviours of connections using dissimilar steel grades is discussed. Novel joint typologies are proposed for applications in dual frames, and design methodologies are presented for these joint typologies. The ductility of joints is evaluated respecting the design and detailing rules of this document.

The last part is dedicated to recommendations for performance based design (PBD). While PBD is not the preferred design methodology in everyday practice, this section is intended as an introduction.

Five different dual-steel frame (DSF) typologies are considered in this guide:

- MRF's or moment resisting frames;
- CBF's or concentrically braced frames;
- D-CBF's or dual concentrically braced frames;
- EBF's or eccentrically braced frames;
- D-EBF's of dual eccentrically braced frames.

The MRF's are dual only in the sense of utilizing two types of steel, higher grade for the columns and lower grade for the beams. The columns may or may not utilize concrete composite action, usually tubular steel section with concrete infill, or steel profiles encased in concrete. The beams may or may not rely on composite action with concrete. MRF's are intended by this guide for up to 8 storey heights.

CBF's and EBF's have at least one bay concentrically or eccentrically braced, and a number of un-braced bays with pin-ended floor beams. CBF's and EBF's may be dual in the sense of dual use of steel grades. Columns can use higher grade steel, while pinned beams may use high or low grade steel depending on economic considerations. Link-beams in the braced bays are made of low grade steel in both CBF's and EBF's, and braces are made of low grade steel. The configurations are intended for buildings up to 16 storeys.

D-CBF's and D-EBF's have at least one bay concentrically or eccentrically braced and a number of un-braced bays where the floor beams are rigidly connected to the columns. Hence these configurations are dual structures, since the lateral loads are resisted by two mechanisms: (1) the brace sub-system, and (2) the moment resisting frame sub-system. D-CBF's and D-EBF's may also be dual in the sense of dual use of steel grades. Columns can be of high grade steel. Floor beams and link-beams are of lower grade steel, together with braces. Floor beams may or may not use the composite action, and columns may be of bare steel or composite steel concrete. In this guide, these configurations are intended for buildings up to 16 storeys.

Normal grades or mild carbon steels (MCS) are with yield strength up to $f_y=355$ N/mm², from Table 3.1, EN 1993-1-1 [6]. These grades include:

- S235, S275, S355 in all thickness ranges;
- S275 N/NL, S355 N/NL, S275 M/ML and S355 M/ML in all thickness ranges;
- S275 W, S355 W in all thickness ranges;
- S235 H, S275 H, S355 H, S275 NH/NLH and S355 NH/NLH for tubular sections;

High strength steels (HSS) are steels with yield strength above $f_y=355$ N/mm², from Table 3.1 of EN 1993-1-1 [6], and the higher grades with the upper limit of $f_y = 700$ N/mm².

For the welds of DSF, the filler metal are welding consumables with yield strength above $f_y=460$ N/mm², from Table 1A, EN ISO 2560 [77], and the higher grades with yield strength above $f_y=550$ N/mm², from Table 1A, EN ISO 18276 [78].

Bolts, nuts and washers used in dual steel frames must conform to EN 1993-1-8 [1], Section 3.1. Concrete strength classes C20 to C45 ($f_{ck}=20$ to 45 N/mm², Table 3.1 in EN 1992-1-1 [34]) are

recommended for floors and foundations of DSF's; the use of lightweight aggregate concrete is not covered by this guide. Concrete materials should conform to EN 1992-1-1 [34], Section 3.1 and reinforcing steel to EN 1992-1-1 [34], Section 3.2.

5.2 Design methodology and criteria for dual-steel structures

The traditional design concept for structures resisting earthquake demands meeting two requirements (EN 1998-1 [1], Section 2.1):

- The no-collapse requirement. The design seismic action, an event with 10% probability of exceedance in 50 years (TNCR = 475 years), may cause extensive damage to structural components, but should not cause local or global collapse. This represents an ultimate limit state (ULS) requirement.
- The damage limitation requirement. An event with larger probability of occurrence, e.g. 10% probability of exceedance in 10 years (TNCR = 95 years), should be resisted without damage or limitation of use of the building. This represents a serviceability limit state (SLS) requirement.

Only one elastic calculation needs to be carried out for the structure, greatly simplifying the modelling task of the designer. For DSF's the use of modal response spectrum analysis is recommended (Section 4.3.3.3, EN 1998-1 [1]). The elastic modelling of the structure is carried out for the loads and load combinations for ULS (Eq. 6.10 and Eq. 6.12b from EN 1990 [79]).

The design of earthquake resistant frames depend on: (1) the ability to deform plastically (ductility) of the dissipative elements, and (2) the ability of the non-dissipative elements to direct plastic deformations to the dissipative elements. Hence, the use of different steel grades in the structure offers itself naturally, to:

- Use ductile steel of usually lower grades in the dissipative elements, and
- Use higher steels grades or high-strength steel (HSS) in the non-dissipative elements, where plastic deformation is not supposed to be present and ductility is not demanded of the member.

The above targets can be transformed in actual measures in case of frames, where the anticipated distribution of dissipative elements is known. Some configurations for possible use of mild carbon steel (MCS) and high-strength steel (HSS) are presented in Figure 5.1. It should be noted that, besides the technical considerations, the use of HSS is also a question of cost, and HSS member from Figure 5.1 may be replaced with ordinary grade steel if the change is economically justified.

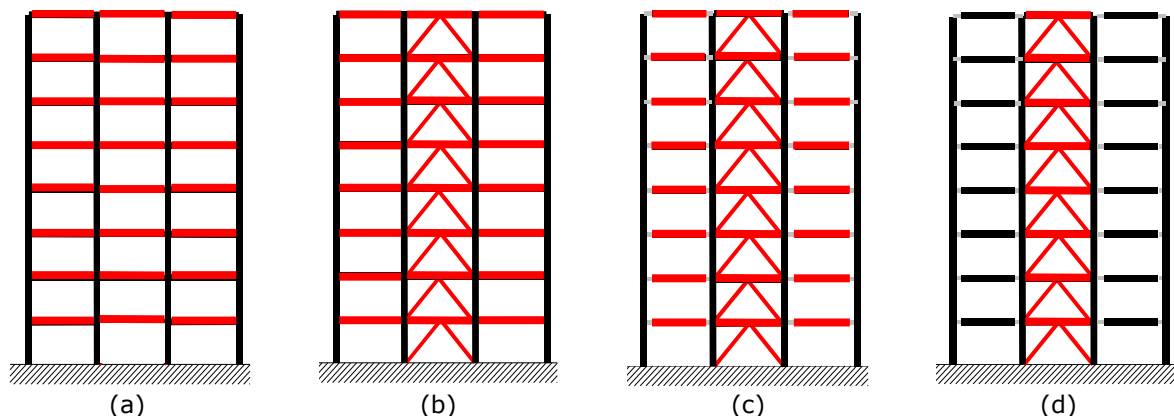


Figure 5.1. Possible use of HSS (black) and mild carbon steel (red) in MRF (a), D-CBF or D-EBF (b), and CBF (c) & (d). Grey are pinned ends of the floor beams

Global analysis of dual-steel frames may be carried out according to procedures used for traditional steel frames: (1) the lateral force method (EN 1998-1 [1], Clause 4.3.3.2) are respected; (2) modal response spectrum analysis (EN 1998-1 [1], Clause 4.3.3.3) or (3) on-linear static pushover analysis, and non-linear time-history analysis Clause 4.3.3.4.2 and 4.3.3.4.3 of EN 1998-1 [1].

According to EN 1998-1 [1], during severe earthquakes it is expected to form an overall ductile mechanism, with uniform formation of plastic zones along the building height.

The final plastic mechanism differs with the structural type. For MRF's it is expected that plastic hinges occur in beams. To achieve this outcome, design codes impose the weak beam/strong column design concept (EN 1998-1 [1], Clause 4.4.2.3(4)). This type of global mechanism for MRF's provide high ductility thanks to distributing plasticity in flexural plastic hinges, as reflected by the high behaviour factor "q" assigned by the codes (EN 1998-1 [1], Section 6.3.2, $q = a_u/a_1 \times q_0$, with $q_0=5$ and a_u/a_1 assumed equal to 1.3).

The designed seismic response of CBF's is different from that of MRF's. The nonlinear behaviour is primarily dependant on the buckling of bracing members and their connections which undergo plastic deformations. Owing to the limited dissipative capacity of bracings and the difficulty to achieve uniform plastic distribution along the building height, the behaviour factors indicated by EN 1998-1 [1] are smaller compared to those used for MRF's. E.g. for CBF's designed according to DCH concept q is equal to 4, for CBF's using cross-braces and 2.5 for CBF's with V braces (EN 1998-1 [1], Table 6.2).

The seismic response of EBF's is influenced by the mechanical behaviour of the link, which is portion of the beam bounded by eccentricity of the bracings. The link is the dissipative element which can yield in shear or in bending. EBF's designed according to the DCH concept are characterized by a q_0 equal to that used for MRF's, $q_0=5$. However, the maximum value of the ratio a_u/a_1 is 1.2.

Dual configurations are characterized by the presence of a braced system (CBF or EBF), acting together with a MRF part. Two different behaviours can be targeted by adopting different design strategies. The dissipative behaviour of dual configurations can be viewed as:

- A primary stiff braced frame with a secondary moment frame with the role to provide plastic distribution along the building height, thus avoiding formation of weak storey mechanism, or
- A primary ductile MRF stiffened by a secondary/sacrificial braced frame, designed to resist wind loads and to provide lateral stiffness to satisfy service-level drift control.

The only type considered in EN 1998-1 [1] is "moment resisting frame combined with concentric bracing" (EN 1998-1 [1] Table 6.2). The behaviour factor recommended for DCH concept is slightly larger than that used for X-CBF's, thanks to the presence of MRF. The q_0 is equal to 4 as that used for CBF's, while the ratio a_u/a_1 is 1.2.

In buildings designed to resist earthquakes it is essential to have some control of the overstrength of the different components, where overstrength means unintended supplementary strength arising from the presence of stronger material in components compared to the strength presumed in the design. Control of the overstrength is essential in order to ensure the formation of dissipative zones in the intended locations (EN 1998-1 [1], Clause 6.2(2)), hence creating the hierarchy of dissipative and non-dissipative elements in the structures. According to EN 1998-1 [1], the following condition needs to be satisfied by the actual maximum yield strength ($f_{y,max}$) of the dissipative zones:

$$f_{y,max} \leq 1.1 \times \gamma_{ov} \times f_y \quad (5.1)$$

where f_y is the nominal yield strength of the steel grade used in the dissipative zone, and γ_{ov} is the overstrength factor used in the design;

According to EN 1998-1 [1] Clause 6.2(3) the adequate value for γ_{ov} is 1.25. Further details on the overstrength factor are available from the technical literature e.g. [35].

5.2.1 Moment-resisting frames (MRF's)

Nonlinear dynamic analyses showed that the MRF's have seismic demands (transient and residual drift ratios, beam ductility) below the proposed limit for limited damage (DL), severe damage (SD) and near collapse (NC) states [9]. At the SD limit state the most of frames had an elastic response. This result is mainly due to design oversizing, but it is consistent with the literature. The use of HSS emphasizes the problems related to excessive frame deformability, suggesting that dual-steel solution for MRF's may lead to inefficient and uneconomical structures.

The design rules for dual-steel MRF's are those given by EN 1998-1 [1]. Owing to the need to satisfy the stiffness requirements (SLS), it is suggested to design MRF's elastically to satisfy the DL/SLS criteria (EN 1998-1 [1], Section 4.4.3), and subsequently to verify the structure against the hierarchy criteria (EN 1998-1 [1], Clause 4.4.2.3(2)). The use of HSS showed to be efficient to guarantee the weak-beam/strong-column behaviour [9].

Pushover analyses showed overall overstrength factors larger than the design behaviour factor ($q=4$). This result is caused by the design procedure, which requires increasing the member size to satisfy the drift limitations. The redistribution factor obtained from pushover curves confirmed the value of 1.3 recommended by EN 1998-1 [1]. The behaviour factors obtained from incremental dynamic analyses (IDA's) for SD limit state have an average of 3.4, and 3.7 for the NC limit state. Both values are smaller than the code value, suggesting the need to calibrate the behaviour factors given by EN 1998-1 [1].

5.2.2 Concentrically braced frames (CBF's)

Nonlinear dynamic analyses showed that CBF's have severe seismic demand in terms of brace ductility for DL, SD and NC states. In particular, at SD limit state most frames exhibited very poor response. This result is mainly due to the small stiffness of the beams in the braced bays.

The design rules for dual-steel CBF's are basically those given by EN 1998-1 [1]. In order to increase the stiffness of the braced beams, it is suggested to design these members in mild carbon steel.

In the most of the cases, pushover analyses showed overall overstrength factors slightly larger than 2. This result is mainly due to the need to fulfil the EN 1998-1 [1] requirements on the brace slenderness. The average redistribution factor obtained from pushover curves is equal to 1.3 for 8-storey and 1.1 for 16 storey frames.

The behaviour factors obtained from incremental dynamic analyses (IDA's) for SD limit state are smaller than the code value with an average value equal to 1.7. The average behaviour factor at NC limit state is equal to 2, still smaller than the code value. These results suggest the need to calibrate the behaviour factors given by EN 1998-1 [1].

5.2.3 Dual concentrically braced frames (D-CBF's)

The nonlinear dynamic analyses showed that the D-CBF's are prone to severe seismic demand in terms of brace ductility for DL, SD and NC states, while small ductility demand is expected for the beams of the MRF parts. In particular, at SD limit state the most of frames exhibit poor response. This result is mainly due to the small stiffness of the beams in the braced bays.

The design rules for dual steel D-CBFs are basically those given by EN 1998-1 [1], namely the requirements for both MRF's and CBF's. However, In order to guarantee that the MRF part has a minimum lateral strength of 25%, the following expression has been taken into account on the basis of the base shear of the structure:

$$V_{Rd,i}^{MRF} \geq 0.25 \times V_{Rd,i}^{DUAL} \rightarrow V_{Rd,i}^{DUAL} = \frac{1}{0.75} \times V_{Rd,i}^{CBF} = \frac{1}{0.75} \times (N_{pl}^+ + 0.3 \times N_{pl}^-)_i \times \cos \alpha_i \quad (5.2)$$

where: $V_{Rd,i}$ the base shear resistance at the i -th storey, N_{pl} is the plastic axial resistance of the brace in tension (+) or in compression (-), and α is the angle that the braces make with the horizontal direction;

As in the case of CBF's, with the aim to increase the stiffness of the braced beams it is suggested to design these members in mild carbon steel.

In most cases, pushover analyses showed overall overstrength factors slightly larger than 2. This result is mainly due to the need to fulfil the EN 1998-1 [1] requirements on the brace slenderness. The average redistribution factor obtained from pushover curves is equal to 1.29.

The behaviour factors obtained from incremental dynamic analyses (IDA's) for SD limit state are smaller than the code value (e.g. $q=4.8$) with an average value equal to 2.3. The average behaviour factor at NC limit state is equal to 2.6, hence still smaller than the code value. These results suggest the need to calibrate the behaviour factors given by EN 1998-1 [1].

5.2.4 Eccentrically braced frames (EBF's)

Nonlinear dynamic analyses showed that the EBF's have a severe seismic demand in terms of link ductility and strength demand for DL, SD and NC states. In particular, at SD limit state most frames exhibit poor response caused by brace buckling. This result is mainly due to the code requirements (EN 1998-1 [1], Section 6.8.3), which are not effective to avoid the brace buckling.

In order to provide a satisfactory response, it is suggested to modify the EN 1998-1 [1] capacity design rules. In particular, it is advisable to apply on the braces the axial forces deriving from the full hardening of the link ($1.5 \cdot V_p$) where they are connected. The remaining rules are those given by EN 1998-1 [1]. Since braces should behave in a stable way (no buckling) and it is important to increase their axial strength, HSS may be used for braces.

In the most cases, pushover analyses showed overall overstrength factors slightly larger than 2. This result is mainly due to the need to fulfil the EN 1998-1 [1] requirements on the storey overstrength variation. The average redistribution factor obtained from pushover curves is 1.3.

The behaviour factors strictly compliant with EN 1998-1 [1], obtained from incremental dynamic analyses (IDA's) for SD limit state, are smaller than the code value with an average value smaller than 4. The EBFs designed with the modified capacity design criteria (namely using $1.5 \cdot V_p$ to calculate the axial force in the bracing) show an excellent performance with average behaviour factors equal to 5.5 and 6 at SD and NC limit states, respectively.

5.2.5 Dual eccentrically braced frames (D-EBF's)

The nonlinear dynamic analyses showed that the D-EBF's have a severe seismic demand in terms of link ductility and strength demand for DL, SD and NC states. In particular, like EBFs, at SD limit state the most of frames exhibit poor response with the most of braces buckled. This result is mainly due to the code requirements, which are not effective to avoid the brace buckling.

In order to provide a satisfactory response, as for the case of EBF's it is suggested to modify the EN 1998-1 [1] capacity design rules. In particular, it is advisable to apply on the braces the axial forces deriving from the full hardening of the link ($1.5 \cdot V_p$) where they are connected. The remaining rules are those given by EN 1998-1 [1]. Since braces should behave in a stable way (no buckling) and it is important to increase their axial strength, HSS may be used for braces.

The design rules for dual steel D-CBFs are basically those given by EN 1998-1 [1], namely the requirements for both MRF's and CBF's. However, In order to guarantee that the MRF part have a minimum lateral strength of 25%, the following expression has been taken into account based on shear base of structure:

$$V_{Rd,i}^{MRF} \geq 0.25 \times V_{Rd,i}^{DUAL} \rightarrow V_{Rd,i}^{DUAL} = \frac{1}{0.75} \times V_{Rd,i}^{EBF} = \frac{1}{0.75} \times V_{p,link,i} \quad (5.3)$$

where: $V_{Rd,i}$ is the base shear resistance at the i -th storey;

In the most cases, pushover analyses showed overall overstrength factors slightly larger than 2. This result is mainly due to the need to fulfil the EN 1998-1 [1] requirements on the storey overstrength variation. The redistribution factor obtained from pushover curves is equal to 1.3.

The behaviour factors, strictly compliant EN 1998-1 [1] obtained from IDA's for the SD limit state, are smaller than the code value with an average value smaller than 4. The EBF's designed with the modified capacity design criteria (namely using $1.5 \cdot V_p$ to calculate the axial force in the bracing) show an excellent performance with average behaviour factors equal to 6 and 7 at SD and NC limit states, respectively.

5.3 Design and detailing rules for connections and joints

5.3.1 Guidelines for welding

Welds are designed as "full-strength" according to the rules for connections in dissipative zones in EN 1993-1-8 [3] and EN 1998-1 [1] with an intended failure in the base metal and not in the weld. For fillet welds the design needs to fulfil the rules of EN 1998-1 [1] clause 6.5.5(3), while full penetration welds are deemed to satisfy the overstrength criterion according to EN 1998-1 [1] Clause 6.5.5(2). The detailed design requirements are presented below. In order to ensure that fillet welds will not behave in a brittle way because of tension, the welds should be designed as "full strength". This means that the rupture strength of full strength welds should be greater than the rupture strength of the adjacent plate. As a consequence in the case of overloading, the plate would fail before the welds.

The "full strength" character of the welds may be achieved by expressing that the design resistance of the weld is higher than or equal to the design resistance of the weakest connected plate. Welds between parts with different material strength grades should be designed using the properties of the material with the lower strength grade. The design resistance of a fillet weld should be determined using either the directional method or the simplified method (EN 1993-1-8 [3], Clause 4.5.3.1). Hereafter the design is made using the directional method (EN 1993-1-8 [3], Clause 4.5.3.2). The minimum weld size to satisfy the full strength requirement and considering the overstrength criteria is therefore expressed as:

$$a \geq \frac{1.1 \cdot \gamma_{ov} \cdot t \cdot f_y \cdot \gamma_{M2} \cdot \beta_w}{\sqrt{2} \cdot \gamma_{M0} \cdot f_u} \quad (5.4)$$

Equation (5.4) indicates that the minimum throat thickness to satisfy the full strength requirement is not related to the length of the weld, but the ratio of f_y/f_u of the weaker part joined. The correlation factor β_w characterises the weld strength in comparison to the base material (recommended values in [68], based on EN 1993-1-8 [3], Table 4.1 and Clause 4.5.3.2).

The design resistance of a full penetration butt weld should be taken equal to the design resistance of the weaker part connected, provided that suitable consumables are used which produce welds having both minimum yield strength and a minimum tensile strength not less than those specified for the parent metal (EN 1993-1-8 [3], Clause 4.7.1(1)). Non-dissipative connections of dissipative members made by means of full penetration butt welds may be assumed to satisfy the overstrength criterion (EN 1998-1 [1] clause 6.5.5(2)), so no specific measures need to be taken to ensure adequate design resistance of full penetration butt welds.

5.3.2 Design of load introduction in composite beam to column joints with concrete-filled tube (CFT) columns

One of the proposed bolted joint configurations is an innovative solution using long bolts passing through a CFT column (joint B-EPL-RBS). The transfer of shear forces within the connection and between the steel tube and the internal concrete core is also a concern. Based on experimental evidences, the analytical design method is proposed to predict the load transfer from the bolt to the steel tube, from the bolt to the concrete core and from the steel tube to the concrete core through the mobilisation of friction effect, taking into account of the confinement of the concrete within the tubular steel column (Table 5.1).

Table 5.1 – Shear load transfer within the B-EPL-RBS joint

Formulas	Notations
<ul style="list-style-type: none"> Load transferred from the bolt to the steel tube: $F_{bolt-tube} = \min \left(nF_s; \frac{A_s E_a}{A_s E_a + A_c E_b} nF_{bolt} \right)$ Load transferred from the bolt to the concrete core (see Table 37): $F_{bolt-concrete} = \min \left(nF_c; \frac{A_c E_b}{A_s E_a + A_c E_b} nF_{bolt} \right)$ Slip resistance between the steel tube and the concrete core: $F_{tube-concrete} = F_{friction} + F_{confi} + F_{bolt}$ 	<p>n: number of bolt used in the considered joint; A_s: the cross-section area of the steel tube; A_c: the cross-section area of the concrete core; E_a: Young modulus of steel tube; E_b: Young modulus of the concrete core; F_{friction}: the friction resistance between the steel tube and the concrete core (EN 1994-1 [4], §6.7.4.2(1) and (2)). F_{confi}: the additional friction due to the confinement of the concrete (EN 1994-1 [4], §6.7.4.2(4)).</p> <ul style="list-style-type: none"> $F_{bolt} = \min(V_{Rd,1}; nF_c; nF_s)$ is the bolt resistance in shear – V_{Rd,1}, F_c and F_s are defined in Table 39 of [68].

In case of joints with welded connection and concrete filled tube columns (when long bolts do not penetrate the concrete core), the load introduction can be provided by shot-fired nails fixed from the exterior of the cross-section. Load introduction tests evidenced significant contribution of the nails to the load transfer from the steel tube to the concrete core [13]. Under monotonic loading conditions, the ultimate capacity of the nails was 37.5 kN, while the pure shear capacity of the nails was significantly lower (21 kN). Under cyclic loading conditions, the ultimate capacity of the connectors decreased in comparison to the monotonic loading conditions. Particularly, considering the two steel tubes (RHS 300x12.5 S460, RHS 250x10 S700) as well as the positive and negative loading, the following ultimate capacity per connector was reported [13]:

- 26.7 kN and respectively 35 kN for the S460-F-H-C column stub specimen;
- 30.6 kN and respectively 36.9 kN for the S700-F-H-C column stub specimen;

For evaluating the ultimate limit states a design resistance of the shot fired nails, the design procedure proposed by Hanswille et al. [80][77] is recommended, corresponding to the pure shear capacity (R_k=21 kN) and affected by a partial safety factor (R_d=R_k/γ_v=21/1.25=16.8 kN). The design procedure is summarised in Table 5.2.

Table 5.2 – Load introduction in CFT columns through shot fired nails

Formulas	Notations
<p>Corresponding to the ultimate limit states, the total number of nails (n) necessary to transfer a part of the design load (F_{Sd}) from the steel tube to the concrete core can be computed with the following relation:</p> $n \geq F_{Sd} \cdot \frac{A_c \cdot f_{cd} + A_s \cdot f_{sd}}{N_{pl,Rd}} \cdot \frac{1}{R_d}$	<p>n: number of shot fired nails; F_{Sd}: design load introduced in the column; A_c·f_{cd}: design plastic resistance to normal forces of the concrete core; A_s·f_{sd}: design plastic resistance to normal forces of the reinforcing bars; N_{pl,Rd}: design plastic resistance to normal forces of the composite section; R_d: design capacity of the connectors;</p> <p>For shot fired nails of type X-DSH32 P10, the pure shear design capacity [80] corresponding to ultimate limit states is:</p> $R_d = \frac{R_k}{\gamma_v} = \frac{21}{1.25} = 16.8kN$

5.3.3 Bolted hammer head end-plate to wide flange column joint

The proposed joint configuration is given in Table 5.3. The stiffened extended end-plate joint, can be used to connect I-shaped beams to partially-encased composite wide flange columns. In the joint, T-shaped hammer heads extracted from the same I-profiles with the beams are utilized, instead of using the traditional haunches. Within the joint zone, the column is strengthened by two lateral plates, reinforcing the column flanges in bending and also the column web in shear. Fillet welds are used to attach the hammer heads, the end-plate to the beam and the lateral plates to the column flanges, while the end-plate are connected to the column flange by four rows of two bolts. This detailing is intended for the rigid and full resistance joint solution for which the plastic hinge is intended to occur at the beam section next to the hammer head ends.

A global design procedure was developed in agreement with the component method as defined in EN 1993-1-8 [3] and EN 1994-1 [4] (Section 8). The design procedure is divided in 6 steps: Step 1: Input data; Step 2: Pre-selection of joint geometrical properties; Step 3: Determination of resistance and stiffness requirements to obtain fully rigid and full strength joints; Step 4: Design of the welds; Step 5: Determination of the joint resistance and stiffness; Step 6: Resistance and stiffness checks. Step 3 and Step 5 are highlighted below. Characterisation of the joint components and identification of the components under bending is presented in Table 5.4. Component assembly for the joint under bending is done in Table 5.5. The full design procedure is given in [68].

Table 5.3 – B-EP-H joint - joint detailing

Elements		Steel materials
1	Double-T steel beam	S355
2a, 2b	Top and bottom hammer-heads	Extracted from the beam profiles
3	Partially-encased wide-flange column	S460 / S700
4	End-plate	S355
5	Bolts	10.9
6	Lateral plates	Same grade with the column profiles

Table 5.4 – B-EP-H joint - component identification

N°	Components	Resistance	γ_{ov}	Stiffness	References
1	Column web and plates in shear	$R_{Rd,1}$	1.0	k_1	Covered in EN1993-1-8 and EN1994-1-1
2	Column web and plates in compression	$F_{Rd,2}$	1.25	k_2	
3	End-plate in bending (row r) (*)	$F_{Rd,3,r}$	1.0	$k_{3,r}$	
4	Bolts in tension	$F_{Rd,4}$	1.25	k_4	
5	Beam web in tension (row r)	$F_{Rd,5,r}$	1.25	$k_{5,r}$	
6	Column web and lateral plates in tension (row r)	$F_{Rd,6,r}$	1.25	$k_{6,r}$	
7	Beam flange and web in compression	$F_{Rd,7}$	1.0	k_7	
8	Column flange in bending (row r)	$F_{Rd,8,r}$	1.25	$k_{8,r}$	[68]
9	Hammer-heads in compression/tension	$F_{Rd,9}$	1.0	k_9	[68]

(*) the calculations for the bolt row 2 (between the two beam flanges) are covered in EN 1993-1-8 [3], while formulas for the bolt row 1 (between the hammer head flange and the beam flange) present a configuration which cannot be directly covered by EN 1993-1-8 [3]. However, recommendations can be found in Jaspert J.P., "Recent advances in the field of steel joints – Column bases and further configurations for beam-to-column joints and beam splices", 1997 (point 3.2.1.3); these recommendations are in full agreement with EN 1993-1-8 [3] design philosophy and are given in [68].

The main challenge of the design is to characterise, from strength and stiffness point of view, the (1) column flange in bending component, (2) the hammer-heads in compression/tension component, and the (3) end-plate in bending component for the bolt row between the hammer head flange and the beam flange. The detailed discussion of the design procedure is presented in the WP6 report of the project [68].

Table 5.5 – B-EP-H joint – component assembly

The joint bending resistance can be estimated using the following procedure:

If $F_{Rd,1} + F_{Rd,2} \leq F_{Rd,4}$ then

$$M_{Rd,j} = F_{Rd,1} \cdot Z_{11} + F_{Rd,2} \cdot Z_{21}$$

If $F_{Rd,1} \leq F_{Rd,4} \leq F_{Rd,1} + F_{Rd,2}$ then

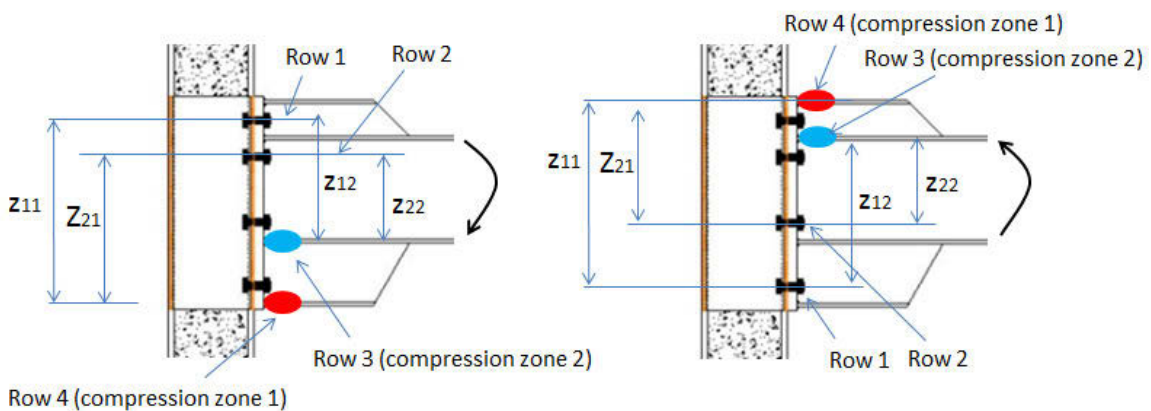
$$M_{Rd,j} = F_{Rd,1} \cdot Z_{11} + \min[F_{Rd,2}; F_{Rd,4} - F_{Rd,1}] \cdot Z_{21} + \min[F_{Rd,2} - \min(F_{Rd,2}; F_{Rd,4} - F_{Rd,1}); F_{Rd,3}] \cdot Z_{22}$$

If $F_{Rd,4} \leq F_{Rd,1}$ then

$$M_{Rd,j} = F_{Rd,4} \cdot Z_{11} + \min[F_{Rd,3}; F_{Rd,1} - F_{Rd,4}] \cdot Z_{12} + \min[F_{Rd,3} - \min(F_{Rd,3}; F_{Rd,1} - F_{Rd,4}); F_{Rd,2}] \cdot Z_{22}$$

In which:

- $F_{Rd,r}$ is the resistance of bolt row r defined as $\min[F_{Rd,k,r}/\gamma_{ov,k}]$ in which
 - $F_{Rd,k,r}$ is the resistance of component k in bolt row r
 - r is the number of the row (see figure here below – only the two most distant bolt rows from the compression zone are considered in the estimation of the bending resistance)
 - k is the number of the considered component (see Table 5.4)
 - $\gamma_{ov,k}$ is the safety coefficient associated to component k (see Table 5.4)
- Z_{ij} are the level arm of row i according to the compression zone j (see figure here below)



Remark: in this procedure, it is assumed that the resistance of bolt row 1 is reached through a ductile failure mode as defined in EN 1993-1-8 [3]; when a brittle mode of failure is identified for bolt row 1, an elastic distribution of the forces between the bolt row 1 and 2 should be assumed as recommended in EN 1993-1-8 [3].

Stiffness: The assembly procedure for “end-plate connections with two or more bolt-rows in tension” as given in EN 1993-1-8 [3] should be applied.

5.3.4 Bolted hammer head end-plate to RHS column joint with U channel

The proposed joint configuration is given in Table 5.6. The reverse channel joint (B-EP-U), is used to connect I-shaped beams to composite rectangular hollow section column. The U reverse channel is used as an intermediate connecting element between the beam and the column to facilitate the bolt assembly. The two lateral faces of the U channel are welded to the lateral faces of the column while the U front face is bolted to the end-plate. The hammer head beams are used as the case of B-EP-H joint (Section 5.3.3). Fillet welds are used to attach the hammer heads, the end-plate to the beam and the U channel to the column faces, while the end-plate are connected to the U channel face by four rows of two bolts.

In comparison with the B-EP-H joint (Section 5.3.3), the deformation of the U channel reduces the rigid and the strength of the present joints. However, the joint may be designed for a rigid and full resistance solution where the plastic hinge is oriented to occur at the beam section next to the hammer head ends.

A global design procedure was developed in agreement with the component method as defined in EN 1993-1-8 [3] and EN 1994-1 [4] (Section 8). The design procedure is divided in 6 steps: Step 1: Input data; Step 2: Pre-selection of joint geometrical properties; Step 3: Determination of resistance and stiffness requirements to obtain fully rigid and full strength joints; Step 4: Design of welds; Step 5: Determination of joint resistance and stiffness; Step 6: Resistance and stiffness checks. Selected steps are highlighted below. Characterisation of the joint components and identification of the components under bending is presented in Table 5.7. Component assembly for the joint under bending is done in Table 5.8. The full design procedure is given in [68].

Table 5.6 – B-EP-U joint – joint detailing

Elements		Steel materials
1	Double-T steel beam	S355
2a, 2b	Top and bottom hammer-heads	Extracted from the beam profile
3	Concrete-filled RHS column	S460 / S700
4	End-plate	S355
5	Bolts	10.9
6a, 6b	Lateral faces & front face of U channel	Same grade with column tube

Table 5.7 – B-EP-U joint - component identification

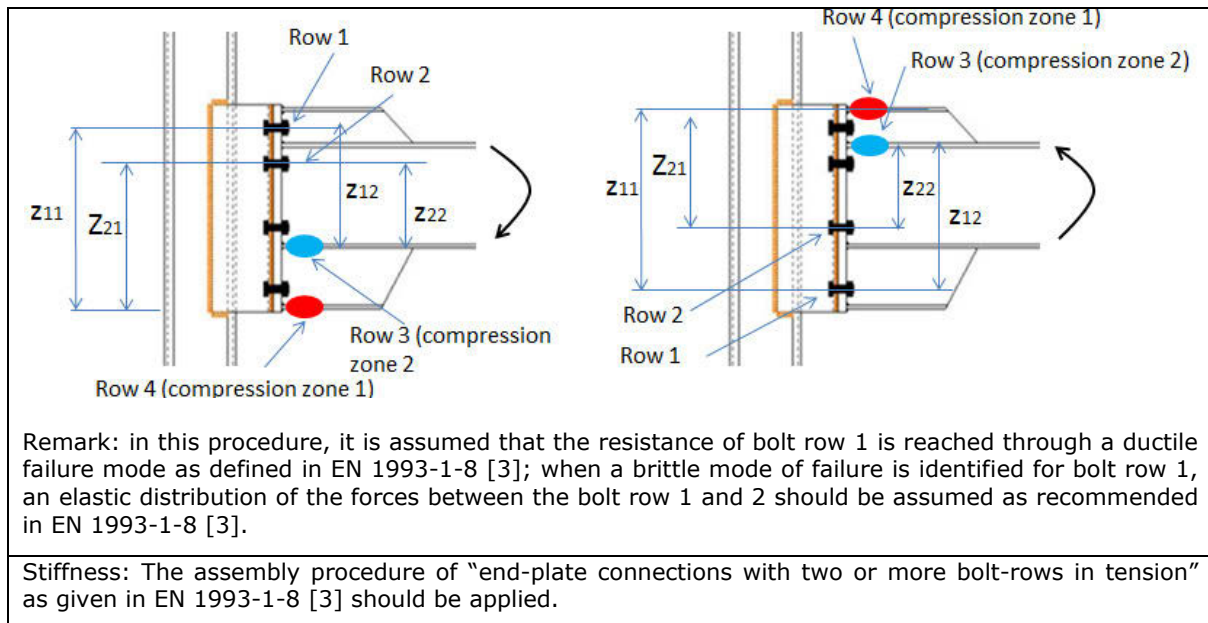
N°	Components	Resistance	γ_{ov}	Stiffness	References
1	Column panel in shear ^(a)	$V_{Rd,p}$	1.0	k_1	EN1993-1-8 and EN1994-1-1
2	Beam web in tension (row r)	$F_{Rd,2,r}$	1.0	$k_{2,r}$	
3	Bolts in tension	$F_{Rd,3}$	1.25	k_3	
4	End plate in bending (row r) ^(b)	$F_{Rd,4,r}$	1.25	$k_{4,r}$	
5	Beam flange and web in compression	$F_{Rd,5}$	1.0	k_5	
6	Reverse U channel in bending	$F_{Rd,6}$	1.25	k_6	[68]
7	Hammer-heads in compression/tension	$F_{Rd,7}$	1.0	k_7	[68]

^(a) the shear area of the two U lateral faces should be included in the shear area of the component.
^(b) the calculations for the bolt row 2 (between the two beam flanges) are covered in EN 1993-1-8 [3], while formulas for the bolt row 1 (between the hammer head flange and the beam flange) present a configuration which cannot be directly covered by EN 1993-1-8 [3]. However, recommendations can be found in Jaspart J.P., "Recent advances in the field of steel joints – Column bases and further configurations for beam-to-column joints and beam splices", 1997 (point 3.2.1.3); these recommendations are in full agreement with EN 1993-1-8 [3] design philosophy and are given in [68].

The main design challenge is the characterization of the (1) reverse U channel component. The detailed discussion of the design procedure is presented in the WP6 report of this project [68].

Table 5.8 – B-EP-U joint - component assembly

<p>The joint bending resistance can be estimated using the following procedure:</p> <p>If $F_{Rd,1} + F_{Rd,2} \leq F_{Rd,4}$ then</p> $M_{Rd,j} = F_{Rd,1} \cdot Z_{11} + F_{Rd,2} \cdot Z_{21}$ <p>If $F_{Rd,1} \leq F_{Rd,4} \leq F_{Rd,1} + F_{Rd,2}$ then</p> $M_{Rd,j} = F_{Rd,1} \cdot Z_{11} + \min[F_{Rd,2}; F_{Rd,4} - F_{Rd,1}] \cdot Z_{21} + \min[F_{Rd,2} - \min(F_{Rd,2}; F_{Rd,4} - F_{Rd,1}); F_{Rd,3}] \cdot Z_{22}$ <p>If $F_{Rd,4} \leq F_{Rd,1}$ then</p> $M_{Rd,j} = F_{Rd,4} \cdot Z_{11} + \min[F_{Rd,3}; F_{Rd,1} - F_{Rd,4}] \cdot Z_{12} + \min[F_{Rd,3} - \min(F_{Rd,3}; F_{Rd,1} - F_{Rd,4}); F_{Rd,2}] \cdot Z_{22}$ <p>In which:</p> <ul style="list-style-type: none"> • $F_{Rd,r}$ is the resistance of bolt row r defined as $\min[F_{Rd,k,r}/\gamma_{ov,k}]$ in which <ul style="list-style-type: none"> ○ $F_{Rd,k,r}$ is the resistance of component k in bolt row r ○ r is the number of the row (see figure here below – only the two most distant bolt rows from the compression zone are considered in the estimation of the bending resistance) ○ k is the number of the considered component (see Table 5.4) ○ $\gamma_{ov,k}$ is the safety coefficient associated to component k (see Table 5.4) • Z_{ij} are the level arm of row i according to the compression zone j (see figure here below)
--



5.3.5 Bolted extended end-plate to RHS column joint with long bolts and reduced beam section

The joint configuration is given in Table 5.9. The unstiffened extended end-plate joint (B-EPL-RBS), is used to connect I-shaped beams to composite rectangular hollow section column. The main idea is the use of the long bolts throughout the column to connect the end-plates, avoiding the intermediate connecting elements (e.g. U reverse channel). As the unstiffened extended end-plate is used, the dog-bone beams are recommended for this joint configuration. Fillet welds are used to attach the end-plate to the beam, while the end-plate is connected to the column by four rows of two bolts. This joint may be considered as rigid and full resistance, and the plastic hinge is located at the dog-bone section of the beam.

Table 5.9 – B-EPL-RBS joint detailing

Elements		Steel materials
1	Double-T steel beam with dog-bone	S355
2	Concrete-filled RHS column	S460 / S700
3	End-plate	The same grade with the beam
4	Repartition plate	The same grade with the beam
5	Long bolts	10.9

A global design procedure was developed in agreement with the component method as defined in EN 1993-1-8 [3] and EN 1994-1 [4] (Section 8). The design procedure is divided in 6 steps: **Step 1**: Input data; **Step 2**: Pre-selection of joint geometrical properties; **Step 3**: Determination of resistance and stiffness requirements to obtain fully rigid and full strength joints; **Step 4**: Design of welds – see Table 5.10; **Step 5**: Determination of the joint resistance and stiffness; **Step 6**: Resistance and stiffness checks. Selected steps are highlighted below. Characterisation of the joint components and identification of the component under bending is done in Table 5.11. Component assembly for B-EPL-RBS joint under bending is shown in Table 5.12. The full design procedure is given in [68].

Table 5.10 – B-EPL-RBS joint - design of welds

Weld (fillet welds)	Throat thickness
Beam flange to end-plate	$a = 0,55t_{fb}$
Beam web to end-plate	$a = 0,55t_{wb}$

Table 5.11 – B-EPL-RBS joint - component identification

Nº	Components	Resistance	γ_{ov}	Stiffness	References
1	Column panel in shear (*)	$V_{Rd,p}$	1,0	k_1	EN 1993-1-8 and EN 1994-1-1
2	Beam web in tension (row r)	$F_{Rd,2,r}$	1,0	$k_{2,r}$	
3	End plate in bending (row r)	$F_{Rd,4,3}$	1,25	$k_{3,r}$	
4	Beam flange and web in compression	$F_{Rd,4}$	1,0	k_4	
5	Column in compression (joint side)	$F_{Rd,5}$	1,25	k_5	
6	Column in compression (opposite side)	$F_{Rd,6}$	1,25	k_6	
7	Bolts in tension	$F_{Rd,7}$	1,25	k_7	

Table 5.12 – B-EPL-RBS joint - component assembly

Resistance:	
$M_{Rd,j} = \sum_{r=1}^2 \min \left(\frac{F_{Rd,k,r}}{1.1 \cdot \gamma_{ov,k}} \right) \cdot z_r$	
with z_r , the distance between bolt row r and the compression centre assumed to be at mid-thickness of the flange; $F_{Rd,k,r}$, the resistance of component k in bolt row r; $\gamma_{ov,k}$, the safety coefficient to be applied to component k.	
Stiffness: The assembly procedure to calculate the stiffness for the “end-plate connections with two or more bolt-rows in tension” as given in EN 1993-1-8 [3] is used for the joint. However, there are two possible assembly procedures for the column (5) and the long bolt (6) components if the preloading of the bolts is taken or not in the process, knowing that the preloading in long bolts significantly increases the global stiffness of the joint.	
Method 1: omission of the bolt preloading	
$k_{5+6} = (1/k_5 + 1/k_6)^{-1}$ for tension zone $k_{5+6} = k_6$ for compression zone	
Method 2: account for the bolt preloading:	
$k_{5+6} = k_5 + k_6$ for both compression and tension The account for the bolt preloading is recommended when failure mode I as defined in EN 1993-1-8 [3] is identified for “end-plate in bending and bolt in tension” component, and $F_b \leq (M_{Ed} / M_{Rd}) F_C / 1,1$, in which F_b is the force in the bolt, F_c is the preloading force and M_{Ed} and M_{Rd} are respectively the design bending loading and the joint bending resistance.	

5.3.6 Welded rib stiffened beam to wide flange column joint, and welded cover plate beam to wide flange column joint

The current section makes a brief description in relation to the design procedure of the following joints:

- Welded rib stiffened beam to wide flange column joint;
- Welded cover plate beam to wide flange column joint;

The welded rib stiffened (RS) joint consists of a hot-rolled I- or H-cross-section beam framing into a fully concrete encased H-cross-section column, see Figure 5.2. The joint represents a stiffened connection solution, in which a single tapered vertical rib plate is welded to both beam flanges. The joint is designed as full strength connection. Thus, plastic hinge is expected to occur in the beam section beyond the end of the reinforcing plates. Complete joint solution takes into account also details regarding fabrication of fully encased composite column with proposed solution for the placement of transverse reinforcement around the beam-to-column connection [68].

The design objective for the RS connection, based on the capacity design concept, is to transfer inelastic action away from the face of the beam-to-column connection, thus reducing the possibility for the appearance of brittle failure conditions. Since full-strength connection with strong column-weak beam concept is applied, plastic hinge is expected to form in the beam section just beyond the end of the reinforcing plates. Plastic hinge in the beam section is the preferred, since flexural yielding of the beam is capable of exhibiting acceptable levels of inelastic behaviour [14], [19]. A

dual-steel approach can be implemented, where HSS is used for the non-dissipative column and MCS for the dissipative beam. Both beam-column MCS/HSS material combinations showed good performance in tests [13], with no damage of welds in the beam-column connection. It is to be mentioned that the solution can be applied also for the case of using MCS for both beams and columns.

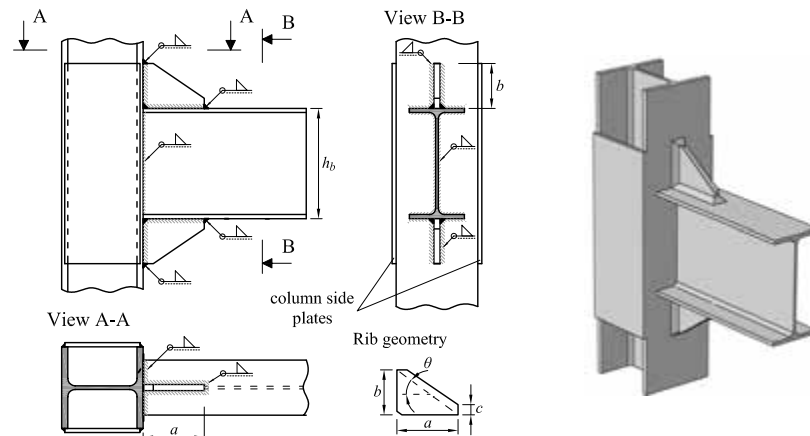


Figure 5.2. Welded RS beam-to-column joint details (concrete column encasement not illustrated)

The welded cover plate (CP) joint consists of a hot-rolled I- or H-cross-section beam framing into a fully concrete encased H-cross-section column, see Figure 5.3. The joint presents stiffened connection solution, in which a flat rectangular cover plate is welded to both beam flanges. The joint is designed as full strength connection. Thus, plastic hinge is expected to occur in the beam section beyond the end of the reinforcing plates. Beam flanges together with the cover plates have to be bevelled prior groove welded to the column flange. Complete joint solution takes into account also details regarding fabrication of fully encased composite column with proposed solution for the placement of transverse reinforcement around the beam-to-column connection [68].

The design objective for the CP connection, based on the capacity design concept, is to transfer inelastic action away from the face of the beam-to-column connection, thus reducing the possibility for the appearance of brittle failure conditions. Since full-strength connection with strong column – weak beam concept is applied, plastic hinge is expected to occur in the beam section just beyond the end of the reinforcing plates. Plastic hinge in the beam section is the preferred site for inelastic action, since flexural yielding of the beam is capable of exhibiting acceptable levels of inelastic behaviour [14], [19]. A dual-steel approach can be implemented, where HSS is used for the non-dissipative column and MCS for the dissipative beam. Both column-beam HSS/MCS material combinations showed good performance in tests [13], with no damage of welds in the beam-column connection. It is to be mentioned that the solution can be applied also for the case of using MCS for both beams and columns.

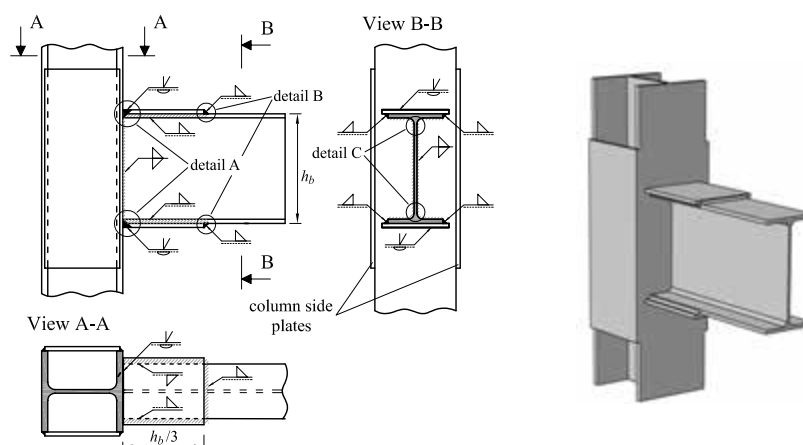


Figure 5.3. Welded CP beam-to-column joint details (concrete column encasement not illustrated)

The design procedure is performed considering the development of the plastic hinge in the beams (see Figure 5.4). Further with the bending moment and shear force from the plastic hinge, the welded connection at column face and the column web panel are designed and/or checked so as to comprise an equal or higher capacity in comparison to the fully yielded and strain hardened plastic hinge. The design procedure for the two welded beam-to-column joints, i.e. rib stiffened (RS) and cover plate (CP) is summarised in Table 5.13. The detailed design procedure is presented within Deliverable D6 [68].

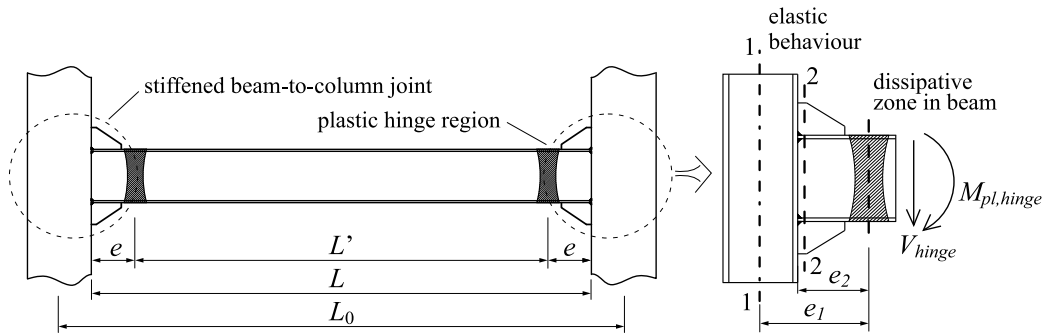


Figure 5.4. Typical beam span with stiffened joint, plastic hinge location and cross-sections used for design check

Table 5.13 – Summary of the design procedure for welded RS and CP joints

RS joint	CP joint
Data: elements & material properties	
For the design of the joints the following considerations are made:	
<ul style="list-style-type: none"> • Beam: wide-flange hot rolled section realised from S355 steel grade; • Column: wide flange section realised from S460 (respectively S690) steel grade and fully encased in concrete; • Rib stiffener and cover plates: realised from plates of S355 steel grade; 	
Selection of component size	
In order to achieve reliable inelastic deformation capacity, the beam should meet the compactness limits for cross-sectional class 1 or at least class 2 according to EN 1993-1-1 [6]. In addition, according to EN 1998-1 [1], Section 6.6, the beam should be verified to have sufficient resistance against lateral and lateral torsional buckling in accordance with EN 1993-1-1 [6], Clause 6.3.5, assuming the formation of plastic hinges at both ends of the beam. In addition, for the choice of the component size it can be considered:	
<ul style="list-style-type: none"> • The following trial values for preliminary rib sizing can be used [12], [19]: rib height $b = \frac{1}{2} \cdot h_b$; rib diagonal angle $\theta = 30^\circ - 40^\circ$; rib length $a = b / \tan(\theta)$, trimmed length $c = 25$ mm and rib thickness $t = 1.35 \cdot t_f$, with t_f being the thickness of the beam flange (for standard European I- and H- beam profiles); 	<ul style="list-style-type: none"> • Trial values for preliminary cover-plate sizing can be used [14], [15], [16]: rectangular plate with a thickness equal to that of the beam flange, $t_{cp} = t_f$, width equal to the beam flange width, increased at least by two times the plate thickness to provide space for longitudinal fillet welds placement, $b_{cp} = b_b + 2 \cdot t_{cp}$ and length $l_{cp} = \frac{3}{4} \cdot h_b$, see Figure 5.3;
Evaluation of plastic hinge location	
<ul style="list-style-type: none"> • Based on the test results, the centreline of a plastic hinge is assumed to be located at a distance of one-quarter of the beam depth from the end of the rib-stiffener, respectively cover plate. 	
Evaluation of efforts in the plastic hinge	
The probable maximum moment ($M_{pl,hinge}$) and shear force (V_{hinge}) in the plastic hinge are determined by considering that a fully yielded and strain hardened plastic hinge develops in the beam.	
$M_{pl,hinge} = \gamma'_{ov} \cdot M_{pl,b}^{nom} = 1.1 \cdot \gamma_{ov} \cdot M_{pl,b}^{nom}$ $V_{hinge} = V_{Ed,G} + \gamma'_{ov} \cdot V_{Ed,M}$	
Based on the test results, and taking into account the probable material overstrength and strain hardening of the steel material in the dissipative zone of the beam, the value of the overstrength factor to be used in the design is recommended in amount of $\gamma'_{ov} = 1.1 \cdot \gamma_{ov} = 1.5$.	
Welded connection at column face	
The design criterion adopted is that the region of the connection at the face of the column should remain nominally elastic under the maximum bending moment and shear force developed by the fully yielded and strain hardened beam.	
The capacity of the welded stiffened connection is computed in terms of bending moment and shear force, and compared with the level of actions. It is assumed that the shear force is carried by the beam web, where the value of shear force is less than half the plastic shear resistance, neglecting its effect on the moment resistance. In addition the following:	

- The size of the ribs is determined taking into account the moment at the face of the column and using the elastic section modulus of the stiffened section for the moment resistance, treating the beam and the reinforcing plates as an integral section;
- The cover plate geometric characteristics b_{cp} and t_{cp} are determined by applying the design criterion that stiffened connection at the column face remains nominally elastic under maximum moment developed by the connected beam. The final length of the cover plate l_{cp} is chosen to permit the placement of sufficiently long longitudinal fillet welds to develop at least the yield strength of the cover plate.

Column web panel

The capacity of the column web panel is checked considering the following aspects:

- The shear resistance check of the column panel is performed according to EN 1998-1 [1], where the design shear force in the web panel due to action effects ($V_{wp,Ed}$) should take into account the plastic resistance of the adjacent dissipative zones in the beams, but without the possible overstrength. Since provisions from EN 1998-1 [1] do not provide additional information on the relation, the shear force in the column panel is determined using the procedure from EN 1993-1-8 [3], Clause 5.3(3), Figure 5.5:

$$V_{pz} = \sum M_b / h_b - V_c,$$

where: $\sum M_b$ is the sum of bending moments in the beam at the column face; h_b is the beam height; V_c is the average shear force in the column;

- In case of a single-sided joint configuration (assumption is true for external joints and approximately true for joints adjacent to concentrically braced bays, $\beta=1.0$), the shear force in the column panel zone $V_{wp,Ed}$ is computed as follows (see Figure 5.4):

$$V_{wp,Ed} = M_{Ed}^{2-2,nom} / h_b - V_c,$$

$$M_{Ed}^{2-2,nom} = M_{pl,hinge}^{nom} + V_{hinge}^{nom} \cdot e_2$$

- Design plastic shear resistance of unstiffened column web panel ($V_{wp,a,Rd}$) is computed according to EN 1993-1-8 [3], Clause 6.2.6.1(2);
- In case of concrete encased steel column web the design shear resistance of the panel, determined in accordance with EN 1993-1-8 [3], may be increased to allow for the encasement (if conditions from EN 1998-1 [1], Clause 7.5.4(7) are satisfied);
- The design shear resistance of concrete encasement to the column web panel ($V_{wp,c,Rd}$) is computed according to EN 1994-1-1 [4], Clause 8.4.4.1. Consequently, the panel zone resistance is defined as the sum of contributions from the concrete and steel shear panel, according to EN 1998-1 [1], Clause 7.5.4(7).
- The contribution of the column side plates throughout the effective width of the column web in case of composite column and transverse web stiffeners or supplementary web plates in case of steel column may also be taken into account, if needed.

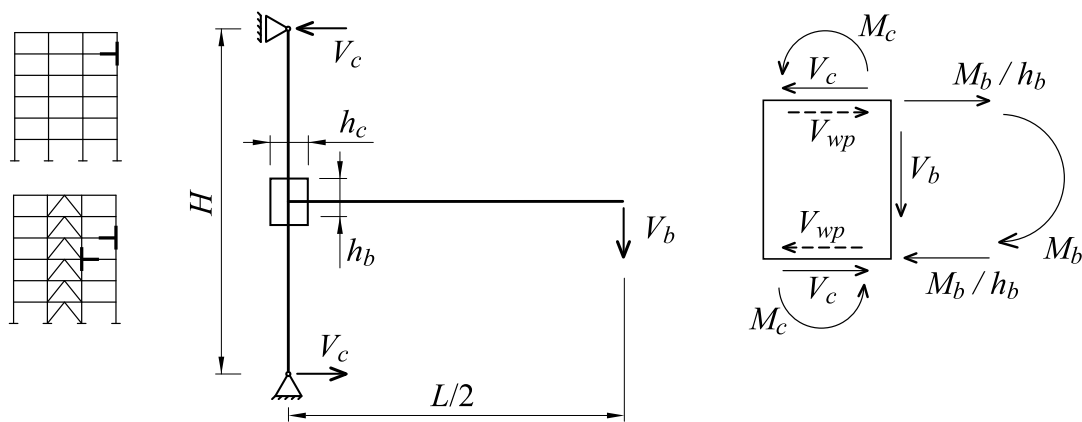


Figure 5.5. Sample frame with single-sided joint configuration, internal forces in panel zone

5.3.7 Welded external diaphragm reduced beam section to RHS column joint, and welded external diaphragm cover plated beam to RHS column joint

The current section makes a brief description in relation to the design procedure of the following joints:

- Welded external diaphragm reduced beam section (RBS) to concrete filled rectangular hollow section (CF-RHS) column joint;
- Welded external diaphragm cover plate (CP) beam to concrete filled rectangular hollow section (CF-RHS) column joint;

The RBS joint (see Figure 5.6-a) connects a wide-flange hot rolled beam with a CFT column using field welding. A reduced beam section is used in order to alleviate stresses in the beam-column connection and control the location of the plastic hinge. An external diaphragm is shop-welded to the column in order to transfer the forces from beam to the side walls of the column. Beam flanges are welded to the external diaphragm using full-penetration butt welds. The preparation details for full penetration welds between external diaphragm and beam flanges are shown in Figure 5.6-b. As can be seen, the thickness of the external diaphragm obtained from design was higher than the flange thickness. Therefore, in order to avoid the concentration of the stresses due to thickness variation, the preparation details shown in Figure 5.6-b were proposed. The solution does not require weld access holes, and the advantage is that no preparations are necessary for beam flanges. A shear tab bolted connection between the beam web and vertical column stiffener was considered for erection only. The final connection of the beam web is realised using full-penetration weld, using the shear tab as backing plate. The design of the reduced beam section was done based on provisions from AISC 358-05 [18]. The design procedure was adapted to the particular joint configuration employing CFT column reinforced with external diaphragm. The RBS joint specimen is shown in Figure 5.6-c.

The CP joint (see Figure 5.7-a) connects a wide-flange hot rolled beam with a CFT column using field welding. An external diaphragm is shop-welded to the column in order to reduce the out-of plane bending of the column walls. Cover plates are used in order to reinforce the beam-column connection, forcing the plastic hinge to form in the beam. The cover plates are welded to the external diaphragm using full-penetration butt welds. The preparation details shown in Figure 5.7-b are based on the weld access-hole details recommended in FEMA-350 [19]. As can be seen, the thickness of the external diaphragm obtained from design was higher compared to the thickness of the cover plates. Therefore, in order to avoid the concentration of the stresses due to thickness variation, the preparation details shown in Figure 5.7-b were proposed. The advantage is that no preparations are necessary for cover plates. A bolted connection between the beam web and vertical column stiffener was considered for erection only. The final connection of the beam web is realized using fillet welds. The CP joint specimen is illustrated in Figure 5.7-c.

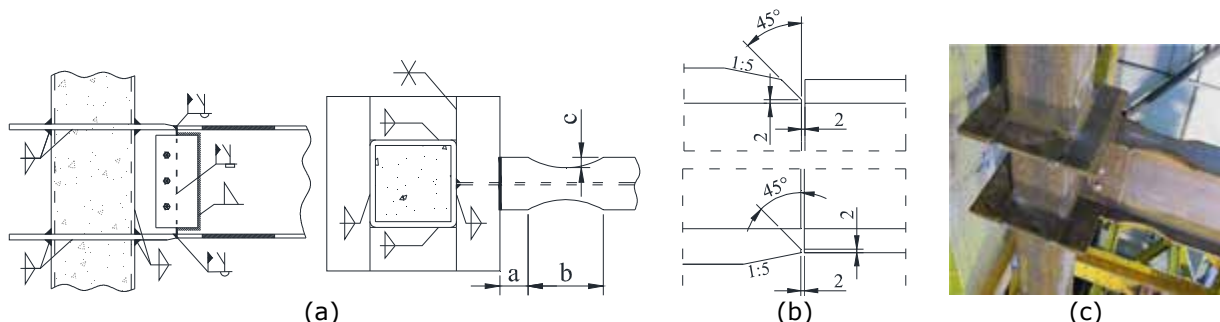


Figure 5.6. RBS joint: a) configuration, b) preparation details, c) specimen illustration

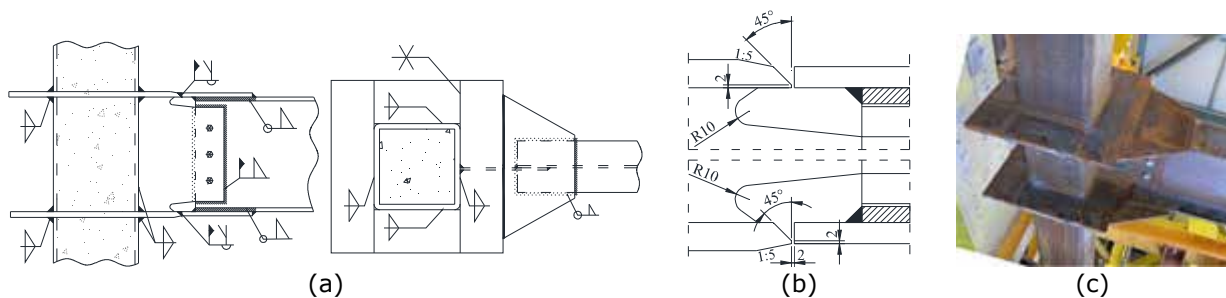


Figure 5.7. CP joint: a) configuration, b) preparation details, c) specimen illustration

The design was performed considering the development of the plastic hinge in the beams (see Figure 5.8-a). Further with the bending moment and shear force from the plastic hinge, the welded connections and the components of the joint, i.e. cover plates, external diaphragm (see Figure 5.8-b) and column web panel (see Figure 5.8-c) were designed and/or checked so as to comprise an equal or higher capacity in comparison to the fully yielded and strain hardened plastic hinge. A

summary of the design procedure for the two welded beam-to-column joints with reduced beam section (RBS), and with cover plates (CP) is summarised in Table 5.14. In addition to the capacity of the joint, the characterisation of the joint stiffness is performed further on.

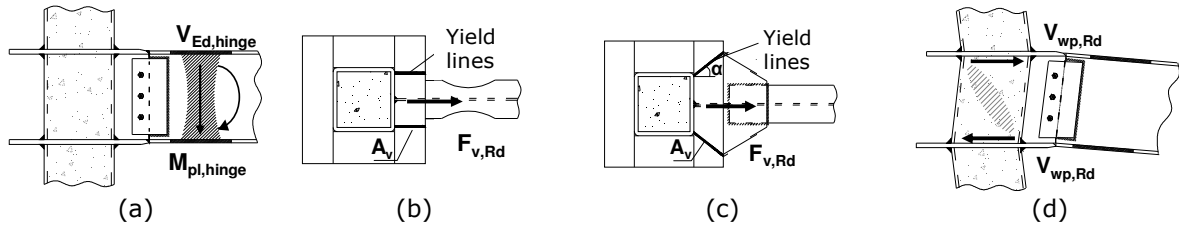


Figure 5.8. Design steps for RBS and CP joints

Table 5.14 – Summary of the design procedure for welded RBS and CP joints

RBS joint	CP joint
<u>Data: elements & material properties</u>	
For the design of the joint the following considerations are made:	
<ul style="list-style-type: none"> • Beam: wide-flange hot rolled section realised from S355 steel grade; • Column: rectangular hollow section (RHS) realised from S460 (respectively S690 / S700) steel grade and filled with concrete; • Cover plates: realised from plates of S355 steel grade; • External diaphragm: shop welded from plates of S460 (respectively S690) steel grade; • Vertical column stiffener: realised from plates of S460 (respectively S690) steel grade; 	
<u>Selection of component size</u>	
For the choice of the component size it can be considered:	
<ul style="list-style-type: none"> • External diaphragm: the thickness should be equal or higher then the thickness of the beam flanges ($t_{ed} \geq t_f$), and the width should satisfy the following relation ($b_{ed} \geq 0.42 \cdot b_c$), where b_c is the width of the column; • Geometry of the reduced beam section: the minimum values for a, b, c dimensions (see AISC 358-05 [18] recommendations) should be considered as starting values; 	<ul style="list-style-type: none"> • External diaphragm: the thickness should be equal or higher then the thickness of the cover plates ($t_{ed} \geq t_{cp}$), and the width should satisfy the following relation ($b_{ed} \geq 0.42 \cdot b_c$), where b_c is the width of the column; • Cover plates: the thickness should be equal or higher then the thickness of the beam flanges ($t_{cp} \geq t_f$), and the width should satisfy the following relations ($b_c + 2 \cdot b_{ed} > b_{cp} > b_c$); • Welded connection (CP to flanges): throat thickness should be equal to $0.7 \cdot t_{min}$, and the length should be equal or higher then the width of the beam flanges, distance between beam end and welded connection (CP to external diaphragm) can be approximated equal to 50 mm;
<u>Evaluation of plastic hinge location</u>	
<ul style="list-style-type: none"> • The position of the plastic hinge is related to the centre of the reduced beam section. 	<ul style="list-style-type: none"> • According to PEER 2000/07 [14], the centre of the plastic hinge is located at a distance equal to $h_{beam}/3$ from the cover plate ending.
<u>Evaluation of efforts in the plastic hinge</u>	
The probable maximum moment ($M_{pl,hinge}$) and shear force ($V_{Ed,hinge}$) in the plastic hinge are determined by considering that a fully yielded and strain hardened plastic hinge develops in the beam.	
$M_{pl,hinge} = \frac{\gamma_{sh} \cdot \gamma_{ov} \cdot W_{pl} \cdot f_y}{\gamma_{M0}} \quad V_{Ed,hinge} = V_{Ed,G} + \frac{2 \cdot M_{pl,hinge}}{L}$	
<u>Welded connection (CP to beam flange)</u>	
The capacity of the welded connection is checked considering:	
-	<ul style="list-style-type: none"> • Actions evaluated at the beam end; • Capacity computed assuming that the flanges carry the moment only, while the web carries the shear force. The strength of the welded connection is determined as the sum of the resistance of the four fillet welds between cover plate and beam flange. $F_{w,Rd} = 2 \cdot (F_{w,Rd,1} + F_{w,Rd,2})$

$F_{w,Rd} = 2 \cdot \left[\left(\frac{a_1 \cdot l_1}{\sqrt{3}} + \frac{a_2 \cdot l_2}{\sqrt{2}} \right) \cdot \frac{f_u}{\beta_w \cdot \gamma_{M2}} \right]$	
Welded on-site connection	
The capacity of the welded on-site connection is checked considering:	
<ul style="list-style-type: none"> • Actions evaluated at the on-site connection; • Capacity computed in terms of bending moment and shear force, based on the gross cross-section of the beam (no weld access holes are considered). 	<ul style="list-style-type: none"> • Actions evaluated at the on-site connection; • Capacity computed assuming that the cover plates carry moment only, while the web carries the shear force.
External diaphragm	
The capacity of the external diaphragm is checked considering:	
<ul style="list-style-type: none"> • Actions evaluated at column face; • Capacity in shear of the external diaphragm computed assuming the formation of yield lines (see Figure 5.8-b) and neglecting the direct connection to the column wall: $F_{v,Rd} = \frac{2 \cdot A_v \cdot f_y}{\sqrt{3} \cdot \gamma_{M0}}$	<ul style="list-style-type: none"> • Actions evaluated at column face; • Capacity in shear of the external diaphragm computed assuming the formation of yield lines (see Figure 5.8-c) and neglecting the direct connection to the column wall: $F_{v,Rd} = \frac{2 \cdot A_v \cdot f_y}{\gamma_{M0} \cdot \sqrt{1 + 2 \cdot \cos^2 \alpha}}$
Column web panel	
The capacity of the column web panel is checked considering:	
<ul style="list-style-type: none"> • Shear force in column web panel is determined using the procedure from EN 1993-1-8 [3] (5.3(3)). In addition, the shear force in the column panel zone corresponds to fully-yielded plastic hinges in the beams framing into the joint. According to EN 1998-1 [1], no over-strength is required ($\gamma_{sh}=1.0$ & $\gamma_{ov}=1.0$). • Capacity computed for both steel tube and concrete core. The shear strength of the steel tube is determined according to EN 1993-1-8 [3], while the shear strength of the concrete core is determined according to EN 1994-1 [4] (8.4.4.1). $V_{wp,s,Rd} = \frac{0,9 \cdot A_v \cdot f_y}{\sqrt{3} \cdot \gamma_{M0}} \quad V_{wp,c,Rd} = 1,0 \cdot v \cdot A_c \cdot f_{cd} \cdot \sin \theta$ <ul style="list-style-type: none"> • The capacity of the composite section (concrete and steel) of the column web panel, according to EN 1998-1 [1], should be taken as 80% of the two sections together. However, considering only the contribution of the steel section might lead to higher shear strength. $V_{wp,Rd} = \max(V_{wp,s,Rd}; 0,8 \cdot (V_{wp,s,Rd} + V_{wp,c,Rd}))$	

According to EN 1993-1-8 [3] (Section 6.3), the rotational stiffness of a joint should be determined from the flexibilities of its basic components, each represented by an elastic stiffness coefficient k_i . According to the code provisions, the stiffness coefficients can be assumed to be equal to infinite for: beam web in tension, beam flange and web in compression, plates in tension or compression. Furthermore, the stiffness coefficient for the external diaphragm in shear can be assumed to be infinite if the design is made considering a full strength external diaphragm, and $b_{ed} \geq 0.42 \cdot b_c$; where b_c is the width of the column and b_{ed} is the width of the external diaphragm. Consequently, the contribution to the joint stiffness is given only by the column web panel in shear (see Equation (5.5)). According to EN 1993-1-8 [3] the stiffness coefficient corresponding to an unstiffened joint is k_1 (see Equation (5.6)). Where the steel column web is encased in concrete, the stiffness of the panel may be increased to allow for the encasement (EN 1994-1-1 [4]); the addition $k_{1,c}$ to the stiffness coefficient k_1 may be determined with Equation (5.7).

$$S_j = \frac{E \cdot z^2}{\mu \cdot \left(\frac{1}{k_1 + k_{1,c}} \right)} \quad (5.5)$$

$$k_1 = \frac{0.38 \cdot A_{vc}}{\beta \cdot z} \quad (5.6)$$

$$k_{1,c} = 0.06 \cdot \frac{E_{cm}}{E_a} \cdot \frac{b_c \cdot h_c}{\beta \cdot z} \quad (5.7)$$

5.3.8 Design and detailing rules for bracing connections

EN 1998-1 [1] does not provide detailed design rules for brace connections. Reference is made to the general design requirements for connections in dissipative zones, according to which two approaches are possible: dissipative and non-dissipative connections.

Generally, non-dissipative connections are preferred. In this case the connection should be designed for the expected strength of braces developed as a result of plastic deformations: yielding in tension and buckling in compression [81], [82], [83]. As a result of brace flexural buckling three plastic hinges form in the brace (one at the middle and two at the ends), unless true pinned connections are adopted, which results in one plastic hinge at the middle of the brace.

According to the principle stated above, in tension, the connection should be designed to resist with sufficient overstrength the tensile strength of the brace. In compression, bending moments will develop as a result of brace inelastic buckling. Consequently, either the connection should be strong enough to allow plastic hinges to form in the brace, or the connection should be detailed in a manner that would allow ductile hinging in the connection itself (see Figure 5.9).

When brace buckling is to be accommodated in the connection, several options are available. One of the most widely used is to provide a linear clearance in the gusset plate with a minimum width of twice the gusset plate thickness (see Figure 5.9-a). This clearance provides for a ductile deformation in the gusset plate, allowing the end of the brace to rotate out of plane almost freely. Very large gusset plate thickness may result in connections designed according to this approach. A more economical design of the connection (smaller gusset plate thickness) can generally be obtained if a recently introduced design approach based on an elliptical hinge is adopted [84] (see Figure 5.9-b). A third option is possible, which allows for in-plane rotations of the brace by adopting a knife plate perpendicular to the gusset plate (see Figure 5.9-c).

Significant inter-storey drifts may occur in eccentrically braced frames after brace buckling/yielding. If the beam to column connection is not designed to accommodate rotations that develop at beam ends, gusset plates are prone to rupture. Two possible solutions that have been validated experimentally are shown in Figure 5.10. The first one accommodates the rotation in the flexible connections between the beam and column [85], and between the gusset plate and the column. The second one uses a rigid moment connection at the beam-column-gusset plate interface [86], accommodating the rotation in a flexible beam connection at some distance away from the gusset plate zone.

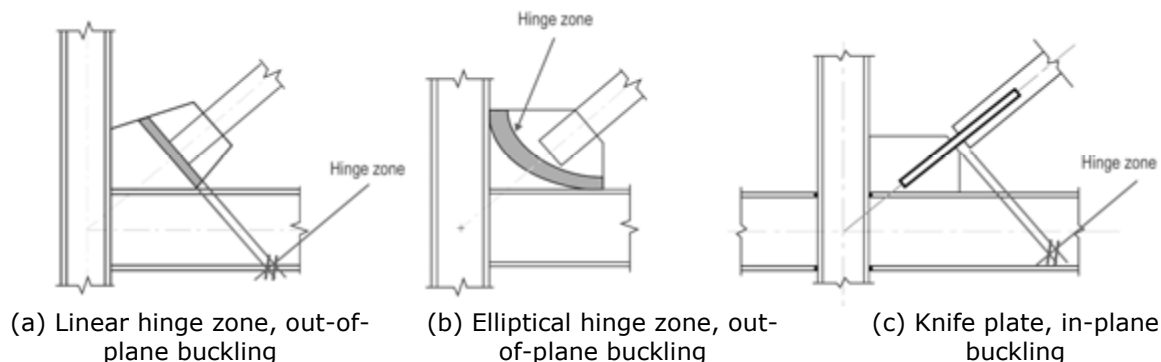


Figure 5.9. Gusset plate connections detailed to accommodate brace buckling by yielding in the connection gusset or knife plate [83]

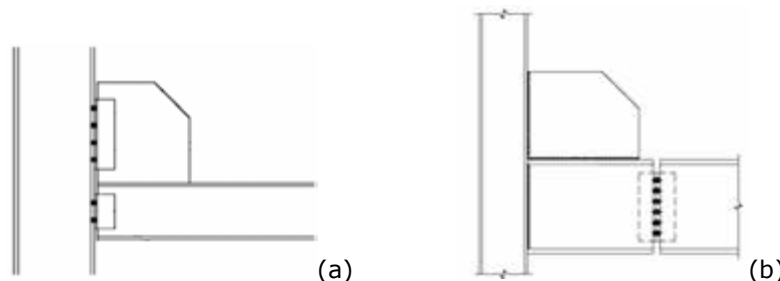


Figure 5.10. Beam-to-column connections that allow rotation: (a) Stoakes & Fahnestock [85], and (b) Thornton & Muir [86]

5.3.9 Design and detailing rules for column bases

Design requirements for column base anchoring are not specified directly in EN 1998-1 [1]. The designer has two possible solutions in overcoming this problem. The first possibility is to assume that column base anchoring should resist the same forces as the foundation it connects to. In this case, design forces are determined according to paragraph 4.4.2.6(4) of EN 1998-1 [1]. The

second option is to treat column base anchoring as any other connection, in which case the paragraph 6.5.5(3) would apply. There is a small difference between the values of forces the two approaches would yield. Thus in the first case, the overstrength factor γ_{Rd} amounts to 1.2, while in the second one the default value of the corresponding overstrength factor is $1.1 \cdot \gamma_{OV} = 1.375$. In either case, requirements for design of column base design in EN 1998-1 [1] effectively ascribe them to non-dissipative components, which should have enough strength to allow development of the plastic mechanism in the structure.

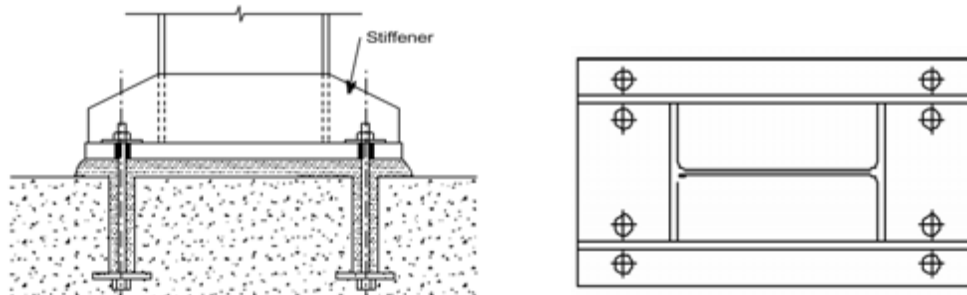


Figure 5.11. Typical column base detail [87]

Figure 5.11 shows a typical column base detail, consisting of a stiffened end-plate fixed using anchor rods to the foundation. Design criteria for base plate connections are available in EN 1993-1-8 [3]. Other column base details may be adopted, including embedding the lower portion of column into a foundation pocket, or the use of baseplates strengthened by additional horizontal steel members [87].

5.4 Recommendation for performance based evaluation

5.4.1 Framework for performance based evaluation

The framework of performance based evaluation can be articulated into the following steps:

- the definition of seismic performance levels;
- the definition of seismic hazard (in accordance to EN 1998-1 [1]);
- the definition of q factor;
- the definition of overall overstrength;
- the definition of failure criteria and relevant acceptance criteria.

According to the seismic performance matrix by SEAC (Vision code 2000) [88], structures designed against earthquakes must fulfil specific requirements for different level of seismic intensity, which correspond to criteria such as stiffness, strength and ductility. Table 5.15 summarizes the performance levels and acceptance criteria for three limit states.

Table 5.15 – Performance levels and acceptance criteria

Limit state	Performance criterion	Acceptance criterion
Serviceability (SLS)	stiffness	Interstorey drift/member buckling
Damageability (DLS)	strength	Interstorey drift/member capacity
Ultimate (ULS)	ductility	Interstorey drift/member residual capacity

Each performance level is referred to a pre-defined level of seismic hazard, represented by magnitudes or accelerations. The ground motion acceleration for the three performance levels (limit states) introduced in Table 5.15 may be determined as a function of the return periods, which are related to probability of exceedence (p) and target design life (T_o) by means of the following Equation:

$$T = -\frac{T_o}{\ln(1-p)} \quad (5.8)$$

For DLS and ULS, respectively, the return periods are univocally accepted to be 475 and 970 years, respectively.

On the other hand, for SLS there are different proposals (ranging from 10 to 75 years) due to the difficulties in choosing a rational criterion for non-damage limit states, which depend on the type of non-structural elements. If the acceleration for DLS A_d is considered as a basic design value for ground motion acceleration, the accelerations for SLS and ULS are determined with Equation (5.9) [1], [89]:

$$\frac{a_{gR}}{a_{gR475}} \cong \left(\frac{T_L}{T_{L475}} \right)^{1/k} \quad (5.9)$$

In particular, since in EN 1998-1 [1] the serviceability analyses were undertaken by multiplying the records by a factor of 0.4 (buildings of class I and II).

The design q factors allow the use of simple elastic models to estimate the non-linear capacity of a structure to resist earthquake. These factors depend on the ability of the structure to dissipate energy through ductile behaviour.

EN 1998-1 [1] states that the behaviour (q) factor can be obtained as the average ratio between the seismic intensity inducing an ultimate limit state (ULS) in the structure taking into account its non-linear behaviour, and the design seismic intensity used with a conventional linear model.

Practically, for a given earthquake the q factor corresponds to the ratio between the seismic intensity A_u (in the sense of the peak value of the acceleration) which causes an ultimate limit state (failure) and the seismic intensity A_y associated to the elastic limit state of the structure. In line with this definition, q can be derived from a series of dynamic inelastic analyses, for which the peak ground acceleration is increased step by step (incremental dynamic analysis or IDA) [90], [91], [92].

According to EN 1998-1 [1] (Clause 4.3.3.4.2.4) the overstrength factor (V_u/V_1) can be determined by pushover analyses. In particular, two lateral load distributions should be used for the pushover load: (i) 1st mode force distribution; (ii) uniform pattern (proportional to masses). The assumed value is the lower for the two lateral load distributions.

The performance demand should be established by means of incremental non-linear dynamic analyses (IDA's). Each IDA should be performed by scaling a set of accelerograms. It is recommended to choose the scaling factors so that: (1) the acceleration for first yielding identified, (2) the demand at serviceability $0.4 \cdot \text{PGA}$ and (3) ultimate $1 \cdot \text{PGA}$ design targets are included. Accelerations should be scaled step by step above $1 \cdot \text{PGA}$ up to levels where damage limitation (DL) and severe damage (SD) limit states are identified.

If the goal is to assess the seismic performance of a generic configuration of steel frames, a set of criteria should be defined on the basis of the following considerations:

- In order to investigate the influence of different geometrical variations, a broad range of designs need to be included in the analyses.
- Several earthquake ground motions need to be used. Three or seven accelerograms are recommended (EN 1998-1 [1], Clause 3.2.3.1.2 & 4.3.3.4.3(3)) for representing each ground motion. If different soil conditions are studied, separate ground motions need to be considered of each soil conditions.
- Individual failure criteria, based on the limiting behaviour of each structural element need to be defined in order to assess behaviour factors.
- In each examined structure collapse is assumed when one of the failure criteria is exceeded. This is a conservative assumption, because local failure will need to occur in more than one area before overall collapse could be experienced.

With the above assumptions, a performance criteria correspond to failure under seismic loading can be associated with:

- buckling, local buckling, fracture and low cycle fatigue;
- the failure of a structural member;
- all phenomena causing deterioration of capacity or out-of service of the structure.

In the proposed method the amplitude corresponding to the acceleration A_u is the minimum value corresponding to all possible theoretical states of collapse:

$$A_u = \min(A_\theta, A_m, A_C, A_R, A_{br}, A_{link}) \quad (5.10)$$

where:

- A_θ is the acceleration corresponding to the maximum permitted inter-story drift (3% for MRF and 2% for brace frames);
- A_C corresponds to the column buckling;
- A_R corresponds to the maximum permitted local rotation (defined according to EN 1998-3 [21]);
- A_{br} corresponds to the maximum permitted brace deformation in tension and compression (defined according to EN 1998-3 [21]);
- A_{link} corresponds to the maximum permitted link rotation (defined according to EN 1998-3 [21]).

5.4.2 Modelling criteria for structural components

The brace hysteretic behaviour is recommended to be simulated by using two non-linear elastic fibre beam-column elements connected together with initial imperfection taking into account for buckling of braces [93]. The advantage of this physical-theory model is less dependence on experimental parameters. The basic input data are only the material properties, the brace geometry and distribution of fibers at the critical sections. The recommended modelling assumptions are:

- Brace member should be subdivided only in two inelastic beam-column elements;
- The initial camber/imperfection given by Dicleli & Calik [43] generally result in good prediction of the buckling;
- At least 200 fibres should be adopted to mesh the cross section for an accurate representation of inelastic strains;
- Distributed plasticity elements with at least 4 integrating section.

The beam hysteretic behaviour is recommended to be simulated using a nonlinear fibre element calibrated on the basis of tests [41]. The modelling assumptions are given in the following:

- Beams should be modelled with an inelastic beam-column element;
- At least 200 fibres should be adopted to mesh the cross section;
- Distributed plasticity elements with more than 5 integration sections have to be used.

Links are modelled by means of an inelastic fibre element and by bi-linear kinematic spring at both ends. The central element has the same length and section properties as the link and simulates the flexural behaviour (the shear stiffness of this element is set to zero). The two end springs are zero-length, they connect the beam segments outside the link to the flexural element of the link and reproduce the shear behaviour of the link. Only relative vertical displacements are permitted between the nodes of the shear element. The stiffness of the translational spring which causes this relative movement is defined to simulate the effect of the shear deformability of half a link. If short links are considered, the ultimate link shear force and bending moment are given by:

$$V_u = 1.5V_p \quad (5.11)$$

$$M_u = 0.5eV_u \quad (5.12)$$

being e the link length;

The post-yielding stiffness of the shear springs is defined as follows:

$$K_v = \frac{0.5V_p}{0.08} \quad (5.13)$$

being 0.08 the maximum plastic rotation in radians;

For frames, it can usually be assumed that columns are fixed at the base and continuous through the height, but concerning beams and braces each typology has its specific characteristic:

- Moment-resisting frame (MRFs) – beam-to-columns joints have been assumed rigid and full strength or pinned; or flexibility and strength characteristics need to be modelled with a dedicated spring element at the ends of the beams;
- Centrally braced frame (CBFs) – non-braced bays of the frame usually have pinned beam ends. The stiffness of brace-end connections play important role on the performance of braces and needs to be modelled, unless pinned connection can be assumed;
- Eccentrically braced frame (EBFs) – Same notes as for CBFs;
- Dual-centrally braced frame (D-CBFs) – non-braces bays may have rigid and full strength beam connections, or flexibility and strength characteristics need to be modelled with a dedicated spring element at the ends of the beams. See CBF frame notes for modelling braces;
- Dual-eccentrically braced frame (D-EBFs) – Same notes as for D-EBFs;

The P-Delta effects of the seismic mass not tributary to the analysed frames need to be considered by employing a leaning column or pendulum system (Figure 5.12), connected to the frames with lateral stiffness.

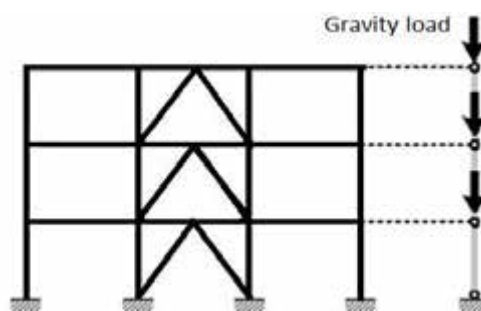


Figure 5.12. Leaning column

In Figure 5.13 the effectiveness of the recommended modelling techniques is exemplified using the cyclic response from experimental testing conducted on one storey-one bay steel concentrically braced frames [42].

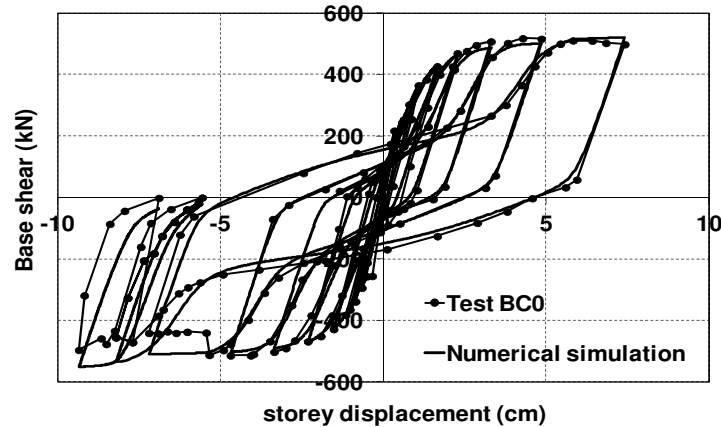


Figure 5.13. 2D Frame numerical vs. experimental response: cyclic condition

5.4.3 Model validation for non-linear dynamic analysis

In order to validate the modelling techniques for dynamic analyses, the inertial properties and viscous damping have been calibrated on the results of shaking table tests carried out by Uang & Bertero [94] on a 3D prototype steel concentrically braced building having six storeys and a square plan, with three frames in both directions and a composite floor system. The structure was subjected to the Miyagi-Ken-Okii 1978, earthquake (N-S component only).

Mass distribution on the frame was respected and viscous damping was modelled as tangent stiffness-proportional Rayleigh damping updated at every load increment. The assumed damping ratios were 2% at both first and second vibration mode. The comparison between the numerical and experimental response curve in terms of roof displacements show acceptable match.

5.4.4 Acceptance criteria for structural components

The recommended acceptance criteria of member deformations, corresponding to the different performance levels are mainly consistent with those given by EN 1998-3 [21]. Since EN 1998-3 [21] does not provide indications for links of EBFs and D-EBFs, the performance limits given by Malley and Popov [95] are recommended. Table 5.16 summaries the acceptance criteria for assessing the seismic performance of dual-steel structures.

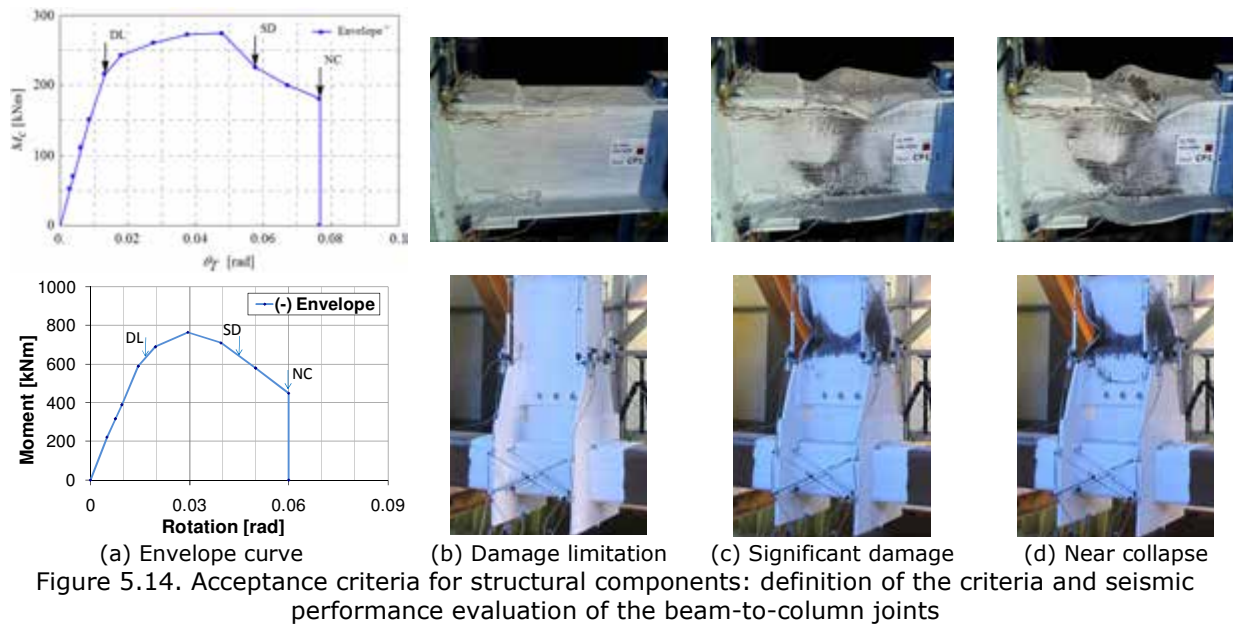
Table 5.16 – Acceptance criteria at each limit state

Limit state	Interstorey drift ratio ^(*)	Bracing in tension ^(**)	Bracing in compression ^(**)	Beam ^(*)	Beam ^(**)	Column/bracing in EBF	Link ^(***)
DL	0.75% (transient)	0.25 Δ_t	0.25 Δ_c	10 θ_y	$\frac{M}{M_y} = 0$	buckling	$\gamma \leq 0.005rad$
SD	0.40% (residual)	7 Δ_t	4 Δ_c	60 θ_y	$\frac{M}{M_y} \leq 1$	buckling	$(\gamma - \gamma_y) \leq 0.08rad$
NC	3.0% (transient)	9 Δ_t	6 Δ_c	80 θ_y	$\frac{M}{M_y} \leq 1$	buckling	$(\gamma - \gamma_y) \leq 0.10rad$

(*) MRF / (**) CBF and D-CBF / (***) EBF and D-EBF

In relation to the acceptance criteria for structural components, a proposal was elaborated within the project by UPT [96], concerning the definition of the acceptance criteria and evaluation of the seismic performance of the beam-to-column joints investigated in WP4 and WP5, and which were designed to develop the plastic hinge in the beam. Consequently, for the seismic performance evaluation, an envelope curve was constructed for each joint configuration. Further, the deformations (rotations) corresponding to the three performance levels (damage limitation – DL, significant damage – SD, near collapse – NC) were identified (see Figure 5.14). It was considered that the yield rotation (θ_y), computed using the ECCS [5] procedure, corresponds to the Damage Limitation performance level. The rotation related to the Significant Damage performance level was considered to correspond to the intersection between the envelope curve and the $0.8 \cdot M_{max}$ strength limit, but not more than 0.75 times the deformation at Near Collapse performance level.

Finally, the rotation associated to Near Collapse, was considered to correspond to the intersection between the envelope curve and the $0.2 \cdot M_{max}$, but not more than the maximum deformation attained during the test.



In relation to the performance of the joints, the following observations were made:

- Corresponding to the Significant Damage performance level, all joint configurations evidenced rotation capacities larger than the 40 mrad, and therefore the seismic performance of the joints was considered acceptable;

The state of the joints corresponding to the three performance levels (see Figure 5.14) was observed to reflect in a realistic manner the definition related to each performance level (see Table 5.17).

Table 5.17 – Performance levels (description & identification criteria)

Performance Level	Description of the performance level	Criteria used for the identification of the performance level
Damage Limitation (DL)	Light damage, with the component retaining the initial strength and stiffness.	Deformation at which permanent, visible damage occurred in the experiments but not greater than 0.67 times the deformation at Significant Damage (SD) performance level.
Significant Damage (SD)	Significant damage, with some margin against total collapse of the component.	Deformation at $0.8 \cdot M_{max}$ strength limit, but not more than 0.75 times the deformation at Near Collapse (NC) performance level.
Near Collapse (NC)	Heavy damage, with low residual strength and stiffness of the component.	Deformation at $0.2 \cdot M_{max}$, but not more than the maximum deformation attained during the test.

Note: the seismic performance of the joints is considered as acceptable if the rotation corresponding to the Significant Damage performance level is larger than 0.04 rad;

5.5 Concluding remarks

The Guidelines developed within WP6 and which were presented in Chapter 5, summarise earthquake design options for frames of the (1) moment resisting (2) concentrically braced and (3) eccentrically braced varieties in pure steel and as with composite columns. Usage of high strength steel (HSS) for the non-dissipative and mild carbon steel (MCS) for the dissipative elements is supported. The configurations of frames where moment resisting bays and braced bays are acting together are also covered.

The guide covers the use of steel grades up to $f_y=700$ N/mm², and concrete classes C20 to C45 ($f_{ck}=20$ to 45 N/mm²).

The design recommendations follow the seismic design principles of EN 1998-1 [1], with the aim of forming a global plastic mechanism at the collapse stage of the frames. The main departure points from the letter of EN 1998-1 [1] are:

- More specific recommendations for the q factors in the dual-steel scenarios;
- More specific welding requirements when the welding of HSS elements are concerned;
- Proposing a set of specific connection typologies, and associated design examples, for the judicious use of HSS and MCS together.

The guide also formulates recommendations on using performance based design for the evaluation of the seismic performance of the frames.

6 Technical and economic efficiency

6.1 Introduction

The investigation of the technical and economical efficiency was performed as part of WP7. The aim was to evaluate the technical and economic benefit of the dual-steel approach involving HSS, i.e. the benefit of dual-steel structures vs. conventional ones. Consequently, the following activities were performed:

- Design of 15 case study frames;
- Design of the beam-to-column joints corresponding to the moment resisting bays of the dual braced frames (D-CBF and D-EBF); several joint typologies were considered:
 - ED-RBS – welded external diaphragm reduced beam section joint with CFT columns;
 - RS – welded rib stiffened joint with FE-WF columns;
 - HH – bolted joint with hammer heads and PE-WF columns;
 - LB-RBS – bolted joint with extended end-plate, reduced beam section and long bolts with CFT columns.
- Evaluation of the technical and economic efficiency of the designed frame configurations and respectively joint typologies.

The design of the frames was performed by GIPAC, while the design of the different joint typologies was performed by the Politehnica University of Timisoara, University of Ljubljana, and University of Liege. Furthermore, the evaluation of the technical and economic efficiency was performed by University of Pisa in collaboration with the steel industry (Stahlbau Pichler SRL).

The economical efficiency was evaluated for the 15 case study frames by taking into account in a simplified manner the beam-to-column joint typology (see Section 6.3.2 and Section 6.3.3). Furthermore, the economic efficiency was evaluated for each of the four connection typologies as well, see Section 6.3.4.2.

The activities conducted within WP7 are linked to the activities conducted within other work packages. Particularly, the design of the case study frames was based on the outcomes of WP1 and WP2. The beam-to-column joint typologies considered for the moment resisting bays of the dual frames (D-CBF & D-EBF), were chosen based on the solutions proposed within WP1, which were further investigated as part of WP4 and WP5, and respectively for which design procedures were developed within WP6.

6.2 Case study reference frames

6.2.1 Design of reference frames

A number of 15 frame configurations (see Figure 6.1) were selected and designed on a more detailed level. The design of the frames was performed by GIPAC, while the design of the different joint typologies was performed by UPT, UL, and ULG. The frames were characterised by stiff soil conditions, eight stories and 7.5 m span. The frames were considered as dual frames (MRF+CBF, and MRF+EBF), and as standard braced frames (CBF, EBF). The parameters from the case study frames are: frame type (D-CBF, CBF, D-EBF, EBF), steel grade for non-dissipative members (S355, S460, S690), and typology of the beam-to-column joints from the moment resisting bays of the dual frames (welded dog-bone, rib stiffened, long bolts, and hammer head joints).

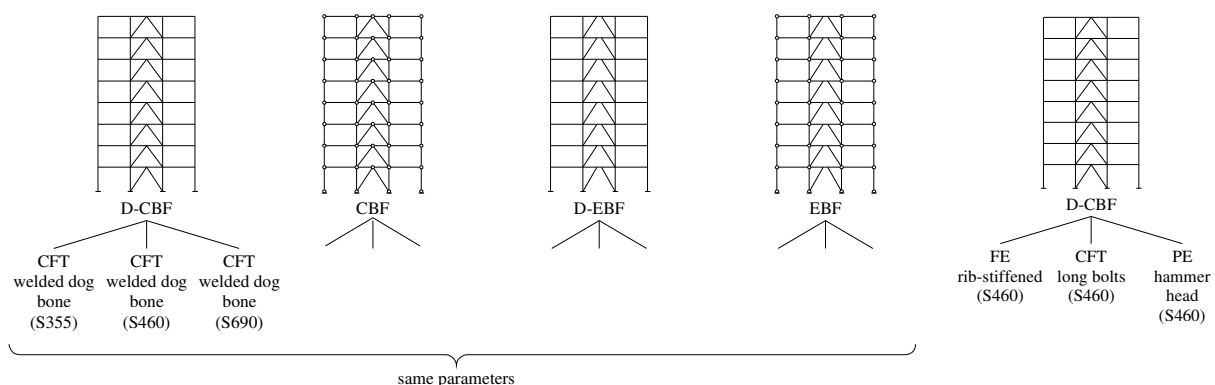


Figure 6.1. Analysis cases for the evaluation of technical and economic efficiency

The description of the 15 case study frames is made in Table 6.1. Consequently, for each configuration, the code system is presented, the label used for a better understanding of the frame parameters, the type of the frame, the type of the column, the steel grade for non-dissipative

members (i.e. columns from 1-4 storeys), and respectively the joint typology (i.e. pinned for the standard braced frames, and full strength for the dual braced frames).

Table 6.1 – Case study frames (code, labelling, frame type, column type, steel grade, joint)

Nr.	Code	Frame label	Frame	Column	Steel gr.	Joint
1	CBF_10213	CBF_CFT_S355	CBF	CFT	S355	°
2	CBF_11213	CBF_CFT_S460	CBF	CFT	S460	°
3	CBF_12213	CBF_CFT_S700	CBF	CFT	S700	°
4	D-CBF_10213	D-CBF_CFT_S355_RBS	D-CBF	CFT	S355	ED-RBS
5	D-CBF_11213	D-CBF_CFT_S460_RBS	D-CBF	CFT	S460	ED-RBS
6	D-CBF_12213	D-CBF_CFT_S700_RBS	D-CBF	CFT	S700	ED-RBS
7	D-CBF_11211	D-CBF_FE_S460_RS	D-CBF	FE	S460	RS
8	D-CBF_11212	D-CBF_PE_S460_HH	D-CBF	PE	S460	HH
9	D-CBF_11213	D-CBF_CFT_S460_LB-RBS	D-CBF	CFT	S460	LB-RBS
10	EBF_10213	EBF_CFT_S355	EBF	CFT	S355	°
11	EBF_11213	EBF_CFT_S460	EBF	CFT	S460	°
12	EBF_12213	EBF_CFT_S700	EBF	CFT	S700	°
13	D-EBF_10213	D-EBF_CFT_S355_RBS	D-EBF	CFT	S355	ED-RBS
14	D-EBF_11213	D-EBF_CFT_S460_RBS	D-EBF	CFT	S460	ED-RBS
15	D-EBF_12213	D-EBF_CFT_S700_RBS	D-EBF	CFT	S700	ED-RBS

Note:
° - pinned connection
ED-RBS - welded external diaphragm reduced beam section joint
RS - welded rib stiffened joint
HH - bolted hammer head joint
LB-RBS - bolted reduced beam section joint with long bolts

A detailed presentation concerning the design of the frames is made by GIPAC within [98] (report on the design of frames in WP7). The results from the design are presented in both, the report [98] and Deliverable D7 [97].

6.2.2 Design of beam-to-column joints

The beam-to-column joint typologies considered for the moment resisting bays of the dual frames (D-CBF & D-EBF), were chosen based on the solutions proposed and investigated within the project. The considered joint typologies and the partner institutions responsible with the design of the joints can be summarized as follows:

- ED-RBS – welded external diaphragm reduced beam section joint with CFT column (see Figure 6.2-a) – Politehnica University of Timisoara;
- RS – welded rib stiffened joint with FE column (see Figure 6.2-b) – University of Ljubljana;
- HH – bolted hammer head joint with PE column (see Figure 6.2-c) – University of Liege;
- LB-RBS – bolted reduced beam section joint with long bolts and CFT column (see Figure 6.2-d) – University of Liege.

In case of the dual frame configurations (D-CBF & D-EBF) listed in Table 6.1, the designed joints corresponding to the moment resisting bays (see Figure 6.2), are presented in Deliverable D7 [97].

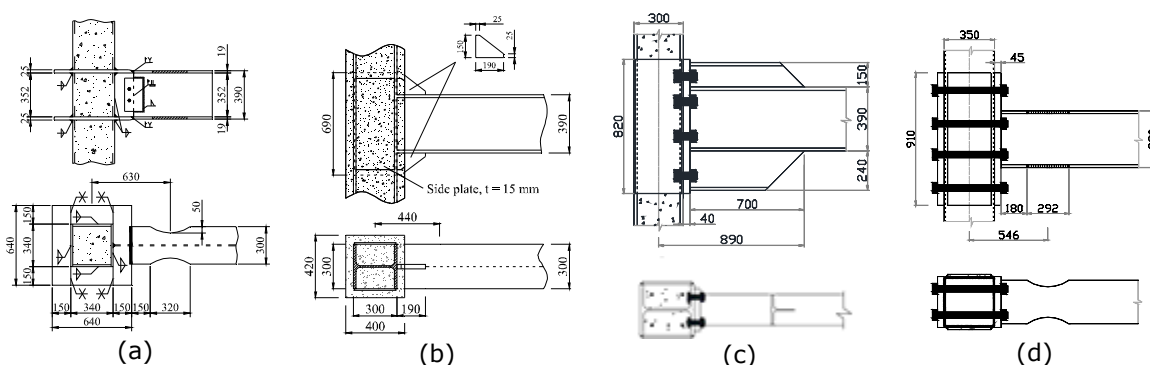


Figure 6.2. Designed beam-to-column joints: (a) ED-RBS – welded external diaphragm reduced beam section joint; (b) RS – welded rib stiffened joint; (c) HH – bolted hammer head joint; (d) LB-RBS – bolted reduced beam section joint with long bolts

6.3 *Evaluation of the technical and economic efficiency*

6.3.1 *Evaluation of frame weight*

In order to evaluate the general price of the pre-defined frames, the weight of the frame has been evaluated by multiplying the length of the steel members by the weight corresponding to 1 m length. In addition, the weight of the concrete from the columns has been considered too. Concrete price has been taken from PREBETON CALCESTRUZZI S.P.A. catalog.

The weight of the connections has been considered and taken as the 20% of the total weight of the steel members. Connection weight has been added, taking as reference the frame made of members with S355 steel grade. The detailed evaluation of the frame weight is presented within Deliverable D7 [97].

6.3.2 *Evaluation of unitary price of frames*

6.3.2.1 *General considerations*

Economic calculations have been realized in order to evaluate the general unitary price (referring to the mass unit) of the previously defined frames. The work has been performed in collaboration with the steel industry STAHLBAU PICHLER SRL (Bolzano, Italy). Stahlbau Pichler has provided information, limitations and overall ideas about technical feasibility and economic convenience on the different typology of frames and connections. In particular:

- Within Section 6.3.2.2, the general price of the frames has been evaluated without taking into account the specific typology of beam-to-column connection;
- After evaluating an overall price of the frames, in Section 6.3.2.3, technical and economic considerations have been supplied in order to analyze the differences between different beam-to-column connections;
- General price based on the concept of precast structures:
 - Beam and column elements pre-realized within the factory, with relative plates and weldings;
 - Dimension of manufacturing that allow an easy transportation;
 - Connection bolts and welding foreseen in the building site with their relative cost.

6.3.2.2 *Average unitary frame price*

The average price of the presented frames can be estimated in amount of 2150 €/t. In order to underline the parameters that influence this amount, a subdivision can be realized as summarised in Table 6.2.

Some items have not been taken into consideration in the definition of the price. In particular:

- Fire resistance – depends on the degree of resistance demanded to the structure;
- Surface treatment – can be estimated in 300 €/t for zinc-coating and in 120 €/t for sandblast and primer treatments.

Table 6.2 – Average unitary frame price

Item	Description	Economic influence
Design	Technical Office; Details "Engineerization"; Calculations; Executive design; Design checks;	16 €/t
Drawing	Static elements approval drawings	60 €/t
Materials	Steel (beams, columns and plates), Concrete	1080 €/t
Production	Pre-manufacturing within the factory	450 €/t
Quality controls	Performed within the factory	54 €/t
Transportation	Supposed a range of transportation of 500 km; Means of transportation;	40 €/t
Installation	Necessary equipment; Laying; Need of high altitude works;	370 €/t
Bolts	Supposed hot zinc-coated	80 €/t
		2150 €/t

6.3.2.3 *Influence of the connection typology*

The evaluation of the beam-to-column connection price for the different typology that have been proposed is characterized by a relative interest. The main reasons are:

- The price of the details has to be related always to the structural completeness;
- What is really important is the price of the frames, designed using different typologies of details;

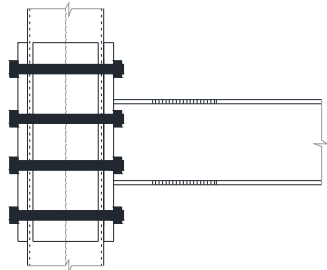
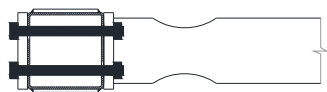
- A detail configuration can be expensive itself, but can be designed in order to determine a decrease of the global weight of the frame. This can consequently reduce the total price of the frame and of the underlying foundations.

Joint with long bolts

This frame solution can be indicatively taken as REFERENCE and related to the frame general price, previously detailed in Section 6.3.2.2, and respectively in Table 6.3.

Long bolts connection, including the necessary plates, represent an important slice of the final price. The installation is complex and slow, with consequences on the item economic influence. Flange connections need expensive and not easy butt welds.

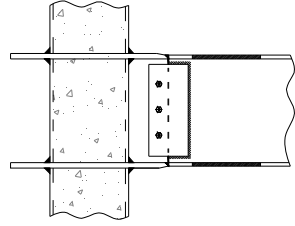
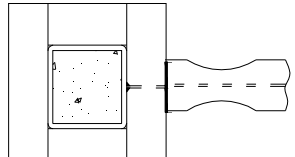
Table 6.3 – Average unitary frame price – Long bolts joint

Item	Description	Economic influence	
Design	Technical Office; Details "Engineerization"; Calculations; Executive design; Design checks;	16 €/t	
Drawing	Static elements approval drawings	60 €/t	
Materials	Steel (beams, columns and plates), Concrete;	1080 €/t	
Production	Pre-manufacturing within the factory	450 €/t	
Quality controls	Performed within the factory;	54 €/t	
Transportation	Supposed a range of transportation of 500 km; Means of transportation;	40 €/t	
Installation	Necessary equipment; Laying; Need of high altitude works;	370 €/t	
Bolts	Supposed hot zinc-coated;	80 €/t	
		2150 €/t	

Joint with external diaphragm and reduced beam section

This is probably the most expensive solution. This is due to the great amount of necessary welds, to the high cost of the composite columns. Furthermore, this connection is characterized by the presence of bolts, which have to be realized in situ, and welds (of the plates between the beams and the column stubs). In Table 6.4, the price of the frame has been evaluated in all its items, and an economic evaluation with the reference frame has been performed.

Table 6.4 – Average unitary frame price – External diaphragm RBS joint

Item	"Reference" frame	Current frame	Differences	
Design	16 €/t	16 €/t		
Drawing	60 €/t	60 €/t		
Materials	1080 €/t	1080 €/t		
Production	450 €/t	500 €/t		
Quality controls	54 €/t	54 €/t		
Transportation	40 €/t	40 €/t		
Installation	370 €/t	570 €/t	(+) 200 €/t Beam / stub plate welds	
Bolts	80 €/t	80 €/t		
	2150 €/t	2350 €/t	(+) 200 €/t	

Joint with rib stiffeners

This solution needs a construction site assembly. The beam-to-column connections overtake the limit size and they are not transportable in one piece. Therefore beams and ribs have to be welded to the columns "in situ".

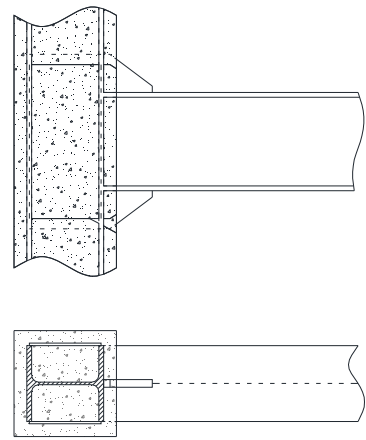
This solution requires a high installation time. This is due to the welds, necessary to connect the beams and the ribs to the column. Furthermore, the composite columns have to be realized in situ. Time is necessary for the realization of the formworks and for the concrete pours.

Despite the fact that the frame realized with rib-stiffened details seems to be characterized by a lower price, and because of the previously defined reasons, Stahlbau Pichler SRL advises against this solution.

In Table 6.5, the price of the frame has been evaluated in all its items, and an economic evaluation with the reference frame has been performed.

Table 6.5 – Average unitary frame price – Rib-stiffened joint

Item	"Reference" frame	Current frame	Differences
Design	16 €/t	16 €/t	
Drawing	60 €/t	60 €/t	
Materials	1080 €/t	1080 €/t	
Production	450 €/t	150 €/t	(-) 300 €/t No need of specific pre-manufacturing
Quality controls	54 €/t	54 €/t	
Transportation	40 €/t	40 €/t	
Instalation	370 €/t	500-550 €/t	(+) 130-180 €/t Welds; Concrete formworks and pours
Bolts	80 €/t	0 €/t	(-) 80 €/t Absence of bolts
	2150 €/t	1900 - 1950 €/t	(-) 200-250 €/t



Joint with hammer heads

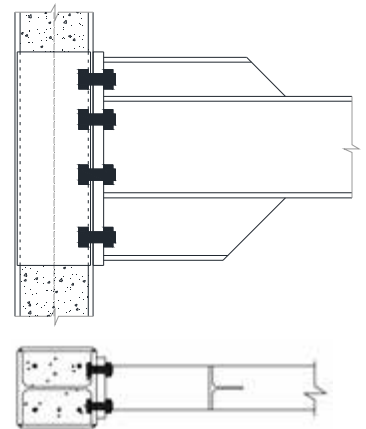
Under the point of view of the unitary price (per mass unit), this joint solution can be considered a good alternative to the reference one. The majority of the production operations can be performed within the factory. Frames can be assembled with their hammer-head and brought on-site already assembled.

This reduces the installation price, but not the installation process. In fact, it necessitate of in-site concrete castings to realize the composite columns. Connections are characterized by the presence of bolts. However, they have ordinary dimension, therefore they don't represent an expensive item in the calculation of unitary price. The connection is completed by the welding of the external plates.

In Table 6.6, the price of the frame has been evaluated in all its items, and an economic evaluation with the reference frame has been performed.

Table 6.6 – Average unitary frame price – Hammer-head joint

Item	"Reference" frame	Current frame	Differences
Design	16 €/t	16 €/t	
Drawing	60 €/t	60 €/t	
Materials	1080 €/t	1080 €/t	
Production	450 €/t	500 €/t	(+) 50 €/t Pre-manufacturing within the factory
Quality controls	54 €/t	54 €/t	
Transportation	40 €/t	40 €/t	
Instalation	370 €/t	270 €/t	(-) 100 €/t (smaller plates, ordinary bolts)
Bolts	80 €/t	40 €/t	(-) 40 €/t Ordinary bolts
	2150 €/t	2060 €/t	(-) 90 €/t



6.3.2.4 Influence of the steel grade

According to the information provided by Stahlbau Pichler SRL the differences in the frames price due to different steel graded (S355, S460 and S690) can be evaluated as shown in Table 6.7. Particular attention has to be focus on the "MINIMUM REQUIRED", i.e. the minimum amount of

high strength steel section (S460 and especially S690 rate) below which the industry refuses to produce. This can be evaluated in around 50 t/profile.

Table 6.7 – Evaluation of the influence of steel grade in unitary frame price

Steel grade	Frame price (average)	Difference	Percentage
S355	2150 €/t	Reference	-
S460	2200 €/t	30 – 70 €/t	3%
S690	2250 €/t	100 – 150 €/t	5%

6.3.3 Frame price

The frame prices has been evaluated by multiplying the weight of steel and concrete by the respective unitary price corresponding to 1 tonne. Steel price refers to the joint typology. For each joint typology, the evaluation of the unitary price was realised in the previous chapter. Concrete price has been taken, from PREBETON CALCESTRUZZI S.P.A. catalog, as 142 €/m³. The price of the connections are grouped in Table 6.8.

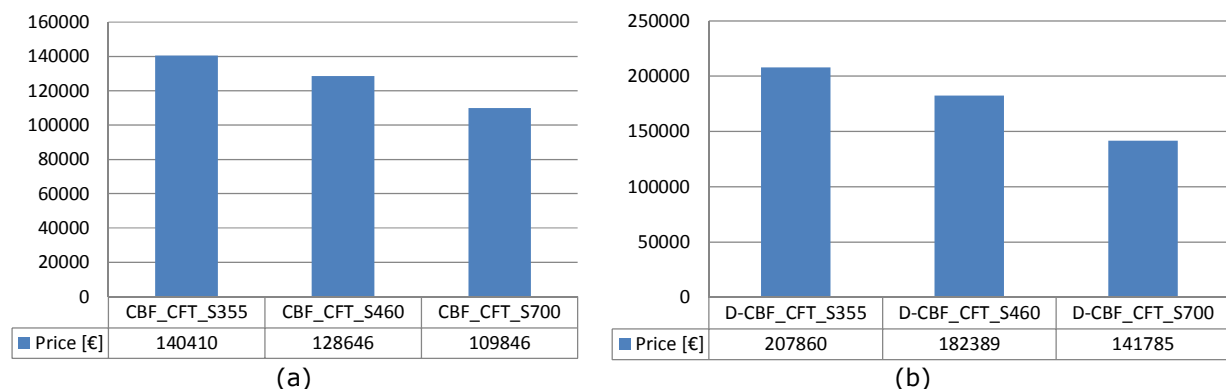
Further with the obtained frame prices a comparison was made for the assessment of the economic benefit of using higher steel grades in non-dissipative members (columns particularly).

Table 6.8 – Frames price resume

Nr.	Frame label	Steel unitary price	Concrete unitary price	Frame price
1	CBF_CFT_S355	2350 €/t	59 €/t	140410 €
2	CBF_CFT_S460	2350 €/t	59 €/t	128646 €
3	CBF_CFT_S700	2350 €/t	59 €/t	109846 €
4	D-CBF_CFT_S355_ED-RBS	2350 €/t	59 €/t	207860 €
5	D-CBF_CFT_S460_ED-RBS	2350 €/t	59 €/t	182389 €
6	D-CBF_CFT_S700_ED-RBS	2350 €/t	59 €/t	141785 €
7	D-CBF_FE_S460_RS	1950 €/t	59 €/t	122507 €
8	D-CBF_PE_S460_HH	2060 €/t	59 €/t	134968 €
9	D-CBF_CFT_S460_LB-RBS	2150 €/t	59 €/t	139456 €
10	EBF_CFT_S355	2350 €/t	59 €/t	97413 €
11	EBF_CFT_S460	2350 €/t	59 €/t	89537 €
12	EBF_CFT_S700	2350 €/t	59 €/t	74261 €
13	D-EBF_CFT_S355_ED-RBS	2350 €/t	59 €/t	122266 €
14	D-EBF_CFT_S460_ED-RBS	2350 €/t	59 €/t	114390 €
15	D-EBF_CFT_S700_ED-RBS	2350 €/t	59 €/t	102603 €

6.3.3.1 Economic benefit of using higher steel grades in non-dissipative members (columns particularly)

Figure 6.3 illustrates the economic benefit of using high strength steel in some of the non-dissipative members in case of CBF's, D-CBF's, EBF's, and D-EBF's. In each case, a comparison was made showing the economic impact of the steel grade (S355, S460, S700) used within the columns. The price of frames are taken according to Table 6.8. As can be observed, the use of higher steel grades (S460, S700) for non-dissipative members (particularly in columns), lead to the reduction of costs in all cases compared to the homogeneous solution (only S355).



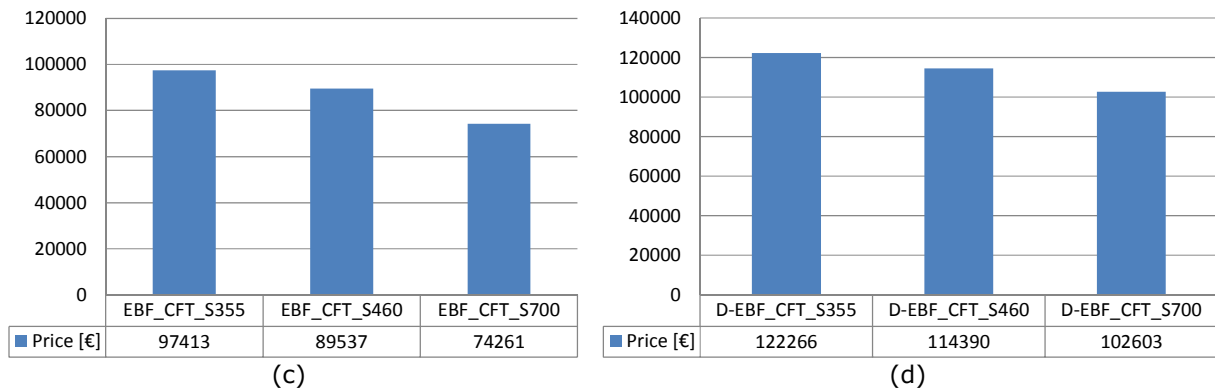


Figure 6.3. Economic benefit of dual-steel frames, i.e. the use of high strength steel in some particular non-dissipative members in case of: (a) CBF's, (b) D-CBF's, (c) EBF's, (d) D-EBF's

6.3.4 Beam-to-column joint price

The costs related to the beam-to-column joints are related to a set of economic indicators as well as to the costs associated with the fabrication of the connection.

6.3.4.1 Economic indicators

The economic indicators affecting the costs of the beam-to-column joints can be summarised as follows:

- Fundamental importance, with important reflection on the final price, is to be conferred to the construction velocity, thus the simplicity to assemble, in situ, the pieces of the frame. Factory operations and controls are to be preferred in order to limit and simplify in situ ones;
- For medium-small steel cross-sections (up to, indicatively IPE500), on equal static performances, IPE profiles cost less than HE ones;
- For medium-high steel cross-sections, on equal static performances, there is an inversion and IPE profiles cost more than HE ones;
- On equal static performances, "open" cross section, even HEM, are to be preferred compared to "closed" ones. The difference can be considered around 20-30% [200-300 €/t], due to the necessary pre-manufacturing operations (e.g. pre-lamination);
- Manufacturing cost decrease, in percentage, with the increase of the weight of the cross sections.

6.3.4.2 Connection price

In relation to the price of the connections, a study has been performed for each beam-to-column joint typology, particularly ED-RBS, RS, HH, and LB-RBS joints designed corresponding to storey 1-4, 5-7 and respectively 8. Within the study it was considered that the costs for the realization of the connection are related to the raw materials (plates, bolts, welding wire) and respectively to the workmanship (direct labor expenses, contributions for direct labor, indirect wages, contributions indirect wages, amortization, and electricity and gas expenses).

Figure 6.4-a and Figure 6.4-b show the costs related to the realization of a connection between a beam and a column corresponding to storeys 1-4 of the D-CBF's and respectively D-EBF's, both realized using S355, S460 and S700 steel grades for columns and plates of the external diaphragm. The costs are represented in relative terms. The costs were evaluated based on raw materials and workmanship.

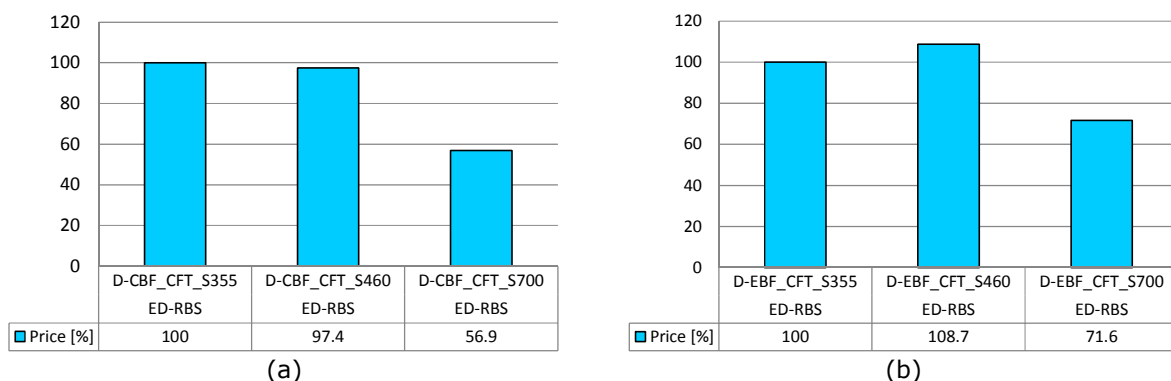


Figure 6.4. Economic impact of the steel grade (S355, S460, S700) for the connection corresponding to the moment resisting bays of (a) D-CBF's, and (b) D-EBF's with CFT columns

As it can be observed, the use of S460 steel grades lead to a small reduction of the costs for the ED-RBS joint designed for the D-CBF, while the costs of the joint designed for the D-EBF were slightly higher. It is to be mentioned that the welding wire was more expensive compared to the joint of S355 steel grade, and the ratio between the increase of costs due to welding wire and the reduction of welding volume was not so significant. In contrast for the joints of S700 steel grade, a significant reduction of costs can be observed. These are related to the reduction of raw materials (plates) and reduction of the welding volume (length of welds and thickness of the welded plates).

Figure 6.5 shows the economic impact of the connection type corresponding to D-CBF's with different column cross sections (CFT, FE, PE). The particular connections are as follows: welded external diaphragm reduced beam section (ED-RBS) connection, welded rib stiffened (RS) connection, bolted hammer head (HH) connection, and bolted reduced beam section connection with extended end-plate and long bolts (LB-RBS). It can be observed that the most economical solutions are represented by the welded rib stiffened connection for FE columns, and bolted hammer head connection for PE columns. However, considering the welded rib stiffened joint, two approaches are available:

- Fabrication of the welded connection (beam-to-column) within the factory, and therefore additional costs would be necessary for a splice connection (site assembly);
- Fabrication of the welded connection (beam-to-column) on site, and therefore additional costs would be necessary due to the difficulty of the welding process, and the quality control.

It is to be mentioned that the costs related to formwork in case of FE and PE columns were not taken into account, and that the CFT columns present the advantage that no formwork is necessary and that the erection time of the structure is faster. In case of joints with long bolts, the higher costs are represented by the price of the long bolts.

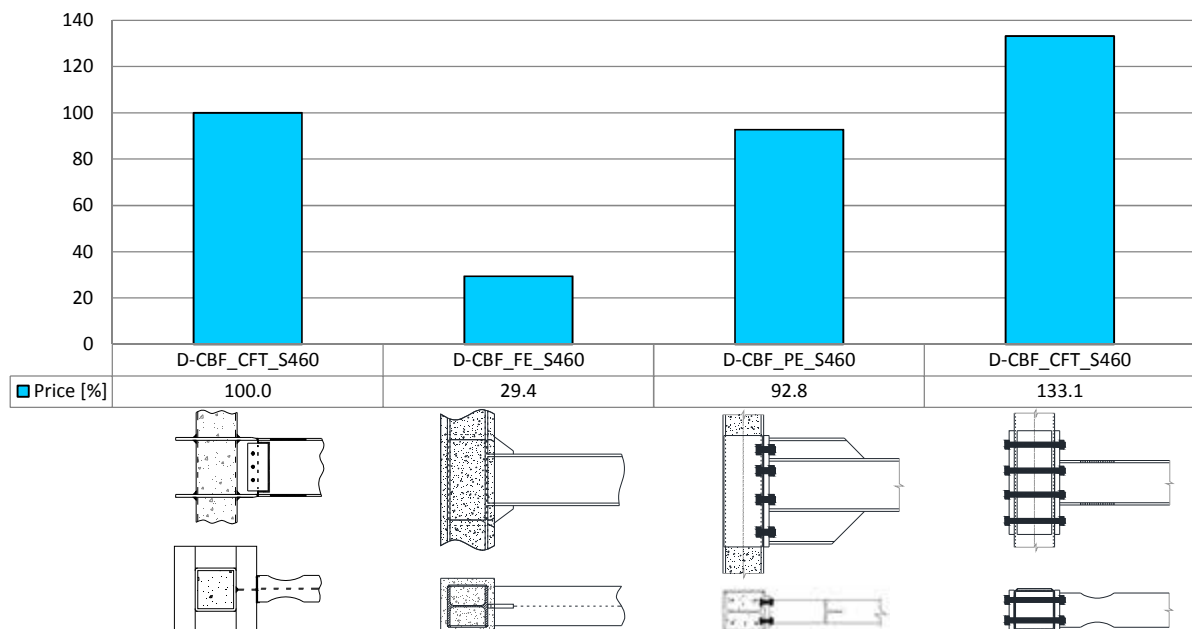


Figure 6.5. Economic impact of connection type corresponding to D-CBF's with different column cross sections (CFT, FE, PE)

6.4 Concluding remarks

Within Chapter 6, the outcomes of the activities performed as part of WP7 were presented. The aim was to evaluate the technical and economic benefit of the dual-steel approach involving HSS, i.e. the benefit of dual-steel structures vs. conventional ones. Consequently, the following activities were performed:

- Design of 15 case study frames;
- Design of the beam-to-column joints corresponding to the moment resisting bays of the dual braced frames (D-CBF and D-EBF); several joint typologies were considered:
 - ED-RBS – welded external diaphragm reduced beam section joint with CFT columns;
 - RS – welded rib stiffened joint with FE-WF columns;
 - HH – bolted joint with hammer heads and PE-WF columns;
 - LB-RBS – bolted joint with extended end-plate, reduced beam section and long bolts with CFT columns.
- Evaluation of the technical and economic efficiency of the designed frame configurations and respectively joint typologies.

The design of the frames was performed by GIPAC, while the design of the different joint typologies was performed by the Politehnica University of Timisoara, University of Ljubljana, and University of Liege. Furthermore, the evaluation of the technical and economic efficiency was performed by University of Pisa in collaboration with the steel industry (Stahlbau Pichler SRL).

The design of the frames in WP7 was performed for the following frame configurations: CBF's, D-CBF's, EBF's, and D-EBF's. It is to be mentioned that based on the outcomes from WP2, it was observed that the use of HSS was not an effective solution for MRF's, as the seismic design procedure was governed by damage limitation. Consequently, MRF's were not considered for the evaluation of the technical and economic efficiency of dual-steel structures. In addition, the study is limited to 8-storey frame configurations.

With the above mentioned considerations, the activities carried out within WP7 were related to the evaluation of the general price of the each frame and the price for each connection typology. The first step has been the calculation of the frame weights. These have been obtained by multiplying the length of the every members by the weight corresponding to 1 m length. Weight of the connections has been taken as the 20% of the total steel weight and added, as well as the weight of the concrete. The general price has been obtained by multiplying the weight of steel and concrete, of each member by the price corresponding to 1 ton.

The general price of the frames has been evaluated without taking into account the specific typology of beam-to-column connection. After evaluating an overall price of the frames, technical and economic considerations have been supplied in order to analyzed the differences between joining solutions.

It appeared quite difficult to realize a detailed economical evaluation of the price of the pre-defined frames and connections. This is due to the fact that many aspects, both technical and related to the on-site application, effect the evaluation. However some interesting conclusion can be drawn:

- The average weight of the 15 presented frames can be estimated in 97 t. In particular it swings between 60 tons of the frame EBF 1.2.2.1.3 to 157 tons of the frame D-CBF 1.0.2.1.3.
- The average price of the presented frames can be estimated in 2150 €/t. It depends for a half to the necessary material, and for the other half to production and realization parameters. The most influence of them are the pre-manufacturing operations to be done within the factory, the installation operations and the presence of bolt equipment.
- According to the information provided by Stahlbau Pichler SRL, the difference in the frame price, due to different steel grade from S355 (taken as reference) seems to be around 3-5%. Particular attention has to be focus on the minimum required, i.e. the minimum amount of high strength steel section (S460 and especially S690 rate) below which the industry refuses to produce. This can be evaluated in around 50 t/profile.

From the point of view of the economical indicators, the most important is to confer primary importance to the construction velocity, thus the simplicity to assemble, in situ, the pieces of the frame. Furthermore it has to be taken into account that for medium-small steel cross-sections (up to, indicatively, IPE500), on equal static performances, IPE profiles cost less than HE ones. For medium-high steel cross-sections, instead, there is the inversion of the tendency. Last consideration is that manufacturing cost decrease, in percentage, with the increase of the weight of the cross sections.

As a general conclusion, based on the computed price of the frames, and the price associated with the fabrication of the connections, it was observed that that the use of higher steel grades in non-dissipative members and connections, represented an effective solution from the technical and economical point of view, which lead to the reduction of the costs. These were related to the reduction of the steel consumption within members and connections, as well as the reduction of the welding volume.

7 Conclusions

In recent years, significant developments in steel processing allowed obtaining high strength steels (HSS). Nowadays, in Japan and USA, HSS's are widely used for bridge and building construction. On the contrary, in the European context, there are still a limited number of applications on buildings, and especially in seismic regions, although some examples exist for the use of HSS in bridge structures. The use of high strength steel within seismic resistant structures could be done considering two approaches: (i) dual-steel structures in which mild carbon steel (MCS) is used for dissipative members and HSS is used in non-dissipative members; (ii) structures realised of HSS, i.e. S460 which is characterised by a certain amount of ductility and therefore could be used in structures of medium ductility class (DCM). With these considerations, the aim of "HSS-SERF" project was to investigate and evaluate the seismic performance of dual-steel building frames, realised from two different steel grades: mild carbon steel and high strength steel. In addition, the main objectives can be summarized as follows:

- To find reliable structural typologies (e.g. moment-resisting frames, concentrically braced frames, eccentrically braced frames) and connection detailing for dual-steel building frames, and to validate them by tests and advanced numerical simulations;
- To develop design criteria and performance based design methodology for dual-steel structures using HSS;
- To recommend relevant design parameters (i.e. behaviour factor q , over-strength factor Ω) to be implemented in further versions of the seismic design code (EN 1998-1 [1]) in order to apply capacity design approach for dual-steel framing typologies;
- To evaluate technical and economic benefit of dual-steel approach involving HSS;

The research activities of the project were divided into several working packages. Consequently, the main research activities can be summarised as follows:

- Design and evaluation of the seismic performance of dual-steel multi-storey frames;
- Investigation of weld details and T-stubs (correlated to welded and bolted joint assemblies);
- Investigation of bolted beam-to-column joints with columns realized as partially encased wide flange sections (PE-WF), and respectively concrete filled tubes (CFT);
- Investigation of welded beam-to-column joints with columns realized as fully encased wide flange section (FE-WF), and respectively concrete filled tubes (CFT);
- Investigation of the load introduction for CFT columns through the use of long bolts, and respectively shot fired nails;
- Elaboration of guidelines for conceptual design and performance based design (PBD) of dual-steel building frames under seismic actions;
- Evaluation of technical and economic efficiency of dual-steel structures;

The main results and conclusions from the research activities of "HSS-SERF" project, are presented in the following part.

A number of 18 dual-steel frame configurations were designed within WP1, according to the current code provisions, and following the initial plan. The design of the frames allowed the identification of realistic member sizes for both mild carbon steel beams and high strength steel composite columns. Several practical solutions for bolted and welded beam-to-column joints were identified and designed. These are: bolted joints with hammer-heads, joints with long bolts for concrete filled tubes, welded joints with fully encased wide-flange columns and rib or cover plate stiffened beam, as well as welded joints with concrete filled tube and reduced beam section and cover plate stiffened beam. In addition, new T-stub configurations whose design is not covered by Eurocode rules, were identified and considered further in the experimental program. As a result, the studies performed in the first stage of the project contributed to the detailing of the experimental program and to its adjustment according to the requirements of the connection typologies resulted from the design of the considered structural typologies.

In WP2, a comprehensive parametric study was defined by selecting and designing a set of 120 frames representative for the design practice, extending the initial set of frames to include standard concentrically and eccentrically braced frames, two additional height ranges, two span ranges, and two different types of seismic action (corresponding to stiff and soft soil). An extensive numerical program was carried out for the seismic performance evaluation of the 120 frame configurations, which lead to the following observations:

- The use of HSS was proven to be an efficient solution especially in columns for CBF's (simple & dual), and in both columns and braces for EBF's (simple & dual); in contrast, the use of HSS was not an effective solution for MRF's, the seismic design procedure being governed by damage limitation;

- MRF's evidenced an adequate seismic performance with low ductility demands, and the exhibited overstrength was larger than the behaviour factor used in design;
- CBF's & D-CBF's: the dual-system structures presented higher over-strength and behaviour factors compared to the simple solutions; however, in all cases the behaviour factors were smaller compared to the values from EN 1998-1 [1], mainly due to the large brace ductility demand in compression; in addition, the frames with flexible beams in the braced bays showed the poorest performance – hence, the use of HSS for beams of braced bays is not advisable. Although, EN 1998-1 [1] makes no difference between the soil condition regarding to overstrength and behaviour factors, the frames designed on soft soil presented smaller overstrength and behaviour factors;
- EBF's & D-EBF's: the static and dynamic analyses showed that the performance of the structures designed according to EN 1998-1 [1] are affected by the brace buckling; consequently, the behaviour factors were significantly lower compared to the values recommended by EN 1998-1 [1]; the same set of structures designed with modified capacity design criterion showed an effective performance avoiding the brace buckling, thus experiencing behaviour factors consistent to the codified values;
- For MRF's, EBF's and D-EBF's, the total behaviour factors (q_t) obtained from incremental dynamic analyses, corresponding to SD limit state, are larger than the codified ones. However, in case of the analysed CBF and D-CBF structures, smaller behaviour factors were obtained from IDA in comparison with the considered values from the initial design. These results suggest that care should be taken for design of CBF's and D-CBF's.

It is to be highlighted that the activities of WP2 were correlated with the activities of WP1, in which several of the examined frame configurations have been designed, activities of WP6, where guidelines for conceptual design and performance based design of dual-steel building frames have been developed, and respectively activities of WP7, in which a number of 15 case study frames were selected and designed on a more detailed level for the evaluation of technical and economic efficiency. Furthermore, the frames designed in WP1, from which cross-section of members were selected for beam-to-column joint assemblies (see WP4 & WP5), were validated within WP2.

In WP3, extensive experimental investigations were carried out on weld details, bolted T-stubs, and material samples. It is to be highlighted that the activities conducted in WP3 were linked to the activities conducted in other work packages. Particularly, the form, geometry and configuration of specimens were planned in cooperation with WP4 for the bolted connections and WP5 for the welded connections. Indeed, the experimental investigation program on T-stubs has been adapted to the needs of WP4. The design of bolted beam-to-column joints with concrete filled rectangular hollow section (CF-RHS) columns, and partially encased wide flange (PE-WF) columns revealed very specific details which imposed specific T-stub configurations, different from the standard and well-established ones that were initially assumed in WP3. Consequently, in addition to the originally proposed T-stub configurations (unstiffened and stiffened), two new and more complex types of T-stubs ("Box Section" T-stub & Unstiffened T-stub with long bolts) were included in the testing program. These new and more complicated types of T-stubs needed additional efforts for instrumentation and test set-up. In order to cover the statistical effect originally planned by the multiple repetitions of the same types of specimens, numerical and analytical calculations were performed. Furthermore, the combination of HSS and MCS requires practical experiences in welding technology. Therefore welding procedures for the dual-steel cases (HSS and MCS) have been fixed in collaboration with the Italian Institute of Welding. Additionally, based on the outcomes of WP3, a set of guidelines for welding of dissimilar steel grades were developed within WP6.

The experimental investigations on weld details were aimed at studying the influence of: steel grade (S460, S690), filler metal (G46, G69), type of weld (fillet weld, full penetration weld), loading procedure (monotonic, cyclic), and loading rate (0.00025 s^{-1} , 0.06 s^{-1} , 0.12 s^{-1}). Consequently, the following observations can be drawn:

- For welds designed as full-strength, the loading type did not affect the failure of the connection, which occurred for all types of loading conditions in the base metal.
- As the design philosophy of a "full-strength" weld was successful, and only failure of the base metal occurred, the influence of the steel grade of the longitudinal plate (S460 / S690), the type of welding (fillet weld or full penetration weld) and the type of filler metal on the overall strength and ductility of the Cruciform Joint was negligible.

The experimental investigations on T-stubs were aimed at studying the components which are of relevance in bolted beam-to-column joints where mild carbon steel beams are connected to high strength steel columns. Several T-stub configurations were considered, particularly: un-stiffened T-stub with normal bolts, stiffened T-stub, "box-section" T-stub, and un-stiffened T-stub with long bolts. The outcomes of the investigation can be summarised as follows:

- The observed failure modes of bolted T-stubs involved combined bending and tension bolt fracture for specimens behaving ductile and nearly pure tension bolt fracture for specimens

behaving brittle. Stripping of the nut threads was not observed at all. In one specimen (Series 400) complete cracking of the end-plate material in the HAZ occurred.

- The choice of thickness for the end-plate associated with steel grade is important in the conception of a proper connection, in order to obtain a good balance between stiffness, strength and ductility of components.
- The major contributions to the overall T-stub strength and deformation were the end-plate deformation capacity and the strength of the bolts, as far as its plastic failure mechanism was governed by mode 2.
- The choice of steel grade for the end-plate material does not significantly influence the load carrying capacity. In contrast, the geometry (bolt distance, end-plate thickness, etc.) and the stiffener have a more remarkable influence on the load carrying capacity. For stiffened situations (Series 200), a uniform load introduction of the bolt and therefore almost a pure tensile stress situation of the bolt provides a nearly independent high load carrying capacity without losing much ductility.

In WP4, a number of 16 bolted beam-to-column joint assemblies and 6 column stub specimens were investigated. Three types of bolted beam-to-column joints were developed: (a) partially encased wide flange column with reinforced end-plate connection; (b) concrete filled tube column with reinforced end-plate connection; (c) concrete filled tube column with end-plate connection and long bolts. It is to be highlighted that the activities performed within WP4, were linked to the activities conducted within other work packages. Particularly, the design of the tested specimens was realised in WP1, the T-stubs extracted from the bolted joint configurations were investigated within WP3, the experimental results from WP4 have been used to validate the design guidelines of the joints within WP6, and the proposed joints were also used to evaluate the technical and economic efficiency of dual-steel structures in WP7. The test campaign within WP4 aimed to characterize the behaviour of these new bolted beam-to-column joints, and to investigate the influence of the following parameters: steel grade for the columns (S460, S700), loading procedure (monotonic, cyclic), failure mode (beam, connection zone). From the study, the following observations can be drawn:

- The experimental investigations evidenced a stable hysteretic behaviour of the joints for which the plastic deformations developed in the dissipative zone of the beam.
- The test campaign allowed demonstrating the ability of the proposed bolted joint configurations to exhibit a full strength and fully rigid character.
- The analytical provisions of EN 1993-1-8 have been extended in order to be able to characterise the proposed joint configurations. The analytical models developed for the innovative joint components have been validated against the experimental results.
- All joint configurations can be designed as full-strength and rigid/or semi-rigid solutions and can be used in moment-resisting dual-steel frames. Moreover, the cyclic tests show that the ductility requirement by EN 1998-1 is satisfied.
- In case of joints with end-plate connection, long bolts and concrete filled tube columns, the long bolts have a double role, i.e. to assure the connection between beam and column, and respectively to assure the connection between the steel tube and the concrete core. For the study of the latter phenomenon, a set of load introduction tests were performed, which evidenced the effectiveness of the load transfer from the beams to the RHS composite columns through the use of long bolts.

In WP5, experimental investigations were conducted on welded beam-to-column joint assemblies, particularly joints with fully encased wide flange (FE-WF) columns and welded connections (rib stiffened and cover plate), and respectively joints with concrete filled rectangular hollow section (CF-RHS) columns and welded connections (reduced beam section and cover plate). The activities conducted within WP5 were linked to the activities conducted within other work packages. Particularly, the design of the tested specimens was realised in WP1, the welding procedures for the dual-steel cases (HSS and MCS) have been established within WP3, the experimental results from WP5 have been used to validate the design guidelines of the joints developed in WP6, and the proposed joints were also used to evaluate the technical and economic efficiency of dual-steel structures in WP7.

In case of joints with fully encased wide flange columns, experimental investigations were performed on a number of 16 beam-to-column joints with the aim to assess the influence of the following parameters: joint type (rib stiffened RS, cover plate CP), steel grade for the column (S460 & S690), loading procedure (cyclic with variable amplitude & cyclic with constant amplitude), axial force level in the column. From the study, the following observations can be drawn:

- The proposed joints proved that the design and geometrical concept along with the considered weld details represent a good solution under variable and constant cyclic loading conditions.
- The design objective for the welded RS and CP connections, based on the capacity design concept, to relocate inelastic action away from the face of the beam-to-column connection, was fulfilled. In both cases connection zone and the column itself remained in elastic state.

- Both designed full strength connections proved to behave well under cyclic tests performed according to the ANSI/AISC 341-10 [7] loading protocol, with plastic rotation capacities greater than 0.044 and 0.051 rad, for bigger and smaller beam cross-sections, respectively, without degradation of strength and stiffness for more than 20% according to EN 1998-1 [1] criterion.
- In case of constant cyclic loading, the CP joint displayed better fatigue performance, attributed to the increased level of unfavourable strain concentrations, larger weld residual stress and HAZ at the end of the rib-stiffener in the RS joint.
- Constant axial force applied in the column did not have any noticeable effect on response of the specimens.

In case of joints with concrete filled tubes, experimental investigations were performed on a number of 16 beam-to-column joint assemblies with the aim to assess the influence of the following parameters: loading procedure (monotonic, cyclic), joint type (reduced beam section RBS, cover plate CP), steel grade for the column (S460, S700), and failure mode (beam, connection zone). Furthermore, a series of load introduction tests were performed on column stubs with the aim to assess the efficiency of the shot fired nails in providing the connection between steel tube and concrete core. The investigated parameters were: loading procedure (monotonic, cyclic), type of connection between steel tube and concrete core (friction only, friction combined with connectors), steel grade (S460, S700). From the study, the following observations can be drawn:

- The monotonic and cyclic tests on beam-to-column joints evidenced a good conception and design of the joints (RBS and CP). This observation was justified by the elastic response of the connection zone, formation of the plastic hinge in the beam, and a good response of joint detailing and welded connections.
- Corresponding to cyclic tests performed according to the ANSI/AISC 341-10 [7] loading protocol, the designed joints evidenced rotation capacities of 50 mrad (RBS joints) and respectively 40 mrad (CP joints) for which the degradation of strength and stiffness were not greater than the 20% limit defined in EN 1998-1 [1].
- From the load introduction tests on column stubs – the shear strength that developed through friction (between steel tube and concrete core) was obtained in amount of 0.4 N/mm², which is equal to the value recommended by EN 1994-1 [4] for rectangular hollow sections. In relation to the specific loading (push-out tests), it was observed that the connectors can take the major shear contribution to the load transfer from steel tube to the concrete core, in both monotonic and cyclic loading.

In addition to the experimental program, extensive numerical investigations were carried out for the beam-to-column joints. The numerical simulation program helped gaining better understanding of the joint behaviour, and allowed the development and validation of simple design procedures for the studied joint configurations, and respectively the extension of the experimental program with the aim to assess the influence of different parameters on the joint behaviour.

In WP6, based on the outcomes of WP1, WP2, WP3, WP4 and WP5, guidelines were developed for the conceptual design and performance based design of dual-steel building frames under seismic actions. Particularly, based on WP1 and WP2, guidelines for conceptual design and performance based design of dual-steel building frames were developed. Additionally, based on the outcomes of WP3, a set of guidelines for welding of dissimilar steel grades were developed. The experimental and numerical investigations carried out within WP4 and WP5 on bolted and welded beam-to-column joints, were used to validate the design guidelines of the joints within WP6. As a result, the main outline of the guidelines was related to the design and detailing rules for connections and joints, and design methodology and criteria for MRF's, CBF's and EBF's. Furthermore, several worked examples have been prepared covering all beam-to-column joint typologies investigated within the project.

In WP7, the evaluation of technical and economic efficiency of dual-steel structures vs. conventional ones was performed. For this purpose, a number of 15 frame configurations were selected and designed on a more detailed level. The following frame typologies were considered: CBF's, D-CBF's, EBF's, and D-EBF's. It is to be highlighted that the activities performed within WP7 were linked to the activities of WP1, WP2, WP4 and WP5. Particularly, based on the outcomes of WP2, it was observed that the use of HSS was not an effective solution for MRF's, as the seismic design procedure was governed by damage limitation. Consequently, MRF's were not considered for the evaluation of the technical and economic efficiency of dual-steel structures, and in addition, the study was limited to 8-storey frames. In addition, several beam-to-column joint typologies (designed in WP1 and investigated within WP4 and WP5), were considered as part of the case study frames within WP7. The economical efficiency was evaluated for the 15 case study frames by taking into account also the type of the beam-to-column joints (in a simplified manner). Furthermore, the economic efficiency was evaluated for different connection typologies as well. As a general conclusion, based on the computed price of the frames, and the price associated with the fabrication of the connections, it was observed that that the use of higher steel grades in non-

dissipative members and connections, represented an effective solution from the technical and economical point of view. The reduction of costs corresponding to the use of higher steel grades, was related to the reduction of the steel consumption within members and connections, as well as the reduction of the welding volume.

In the light of the accomplished research activities and the corresponding results, the main contributions of the project can be summarised as follows:

- The investigated frame typologies based on the dual-steel approach with composite columns, are solutions with a high innovative character in the European context; the dual-steel structures are not yet covered by the current code provisions (EN 1998-1 [1], EN 1993-1-8 [3], EN 1994-1 [4]); these configurations are to be taken into account within the further versions of the relevant Eurocodes;
- Principles and design recommendations for dual-steel frames (guidelines);
- Characterisation in terms of global ductility and over-strength demands of dual-steel frames realised in simple and dual configuration;
- Proposal of a series of innovative beam-to-column joint typologies with composite steel-concrete columns (i.e. PE, FE and CFT) for which the structural performance was confirmed by experimental and numerical investigations;
- Recommendations for weld details and appropriate component method design approaches.

At last, it is to be mentioned that a particular application of the dual-steel concept was implemented within the research project "DUAREM" – Full-scale experimental validation of dual eccentrically braced frame with removable links. The project involved a full scale pseudo-dynamic test of a dual structure (Eccentrically Braced Frame with removable links combined with Moment Resisting Frames) realized using the dual-steel concept (Mild Carbon Steel in dissipative members and High Strength Steel in non-dissipative members). The full-scale pseudo-dynamic tests was carried out at the ELSA facility of the Joint Research Centre in Ispira, Italy, and enabled a realistic evaluation and validation of the structural concept and dual-steel solutions developed within "HSS-SERF" Project.

List of figures

Figure I. General flow chart of research.....	7
Figure II. Design of dual-steel multi-storey frames (MRF, D-EBF, D-CBF), choice of members (beams, columns) and design of beam-to-column joint specimens.....	9
Figure III. Bolted beam-to-column joint configurations	9
Figure IV. Welded beam-to-column joint configurations	9
Figure V. Analysis cases for the seismic performance evaluation	10
Figure VI. Welded details and T-stub typologies (Univ. of Stuttgart)	11
Figure VII. Experimental investigation of bolted beam-to-column joints (Univ. of Liege)	12
Figure VIII. Experimental investigation of welded beam-to-column joints (Univ. of Ljubljana).....	13
Figure IX. Experimental investigation of welded beam-to-column joints (Univ. of Timisoara)	13
Figure X. Load introduction tests: steel-concrete connection through long bolts (Univ. of Liege)	14
Figure XI. Load introduction tests: steel-concrete connection with shot fired nails (Univ. of Timisoara)	14
Figure XII. Advanced numerical investigations of beam-to-column joint assemblies subjected to monotonic and cyclic loading conditions (calibration of numerical models)	14
Figure XIII. Analysis cases for the evaluation of technical and economic efficiency	15
Figure XIV. Designed beam-to-column joints for the moment resisting bays: (a) ED-RBS – welded external diaphragm reduced beam section joint; (b) RS – welded rib stiffened joint; (c) HH – bolted hammer head joint; (d) LB-RBS – bolted reduced beam section joint with long bolts	16
Figure XV. Full-scale experimental validation of dual eccentrically braced frame with removable links ...	16
Figure 1.1. General flow chart of research	20
Figure 2.1. Structural configurations	23
Figure 2.2. Types of composite columns: (a) FE-WF, (b) PE-WF, (c) CFT	24
Figure 2.3. Types of soil conditions	25
Figure 2.4. Definition of parametric study	25
Figure 2.5. Design of dual-steel multi-storey frames (MRF, D-EBF, D-CBF), choice of members (beams, columns) and design of beam-to-column joint specimens.....	28
Figure 2.6. Bolted beam-to-column joint configurations (Univ. of Liege)	28
Figure 2.7. Welded beam-to-column joint configurations: (a) rib stiffener and (b) cover plate joints with FE-WF columns, (c) reduced beam section and (d) cover plate joints with CF-RHS columns	28
Figure 2.8. Bolted beam-to-column joints: (a) "joint configuration 1", (b) "joint configuration 2", (c) "joint configuration 3".....	30
Figure 2.9. Rib- and cover plate- stiffened connection configurations studied	31
Figure 2.10. Welded RS and CP beam-to-column joint details (concrete encasement is not illustrated) .	31
Figure 2.11. Welded RBS joint: configuration & preparation details for full penetration welds	32
Figure 2.12. Welded beam-to-column joint with cover plates: joint configuration and preparation details for full penetration welds between external diaphragm and cover plates (top & bottom) .	32
Figure 3.1. Investigated frame typologies	34
Figure 3.2. PSA spectra of the scaled records	36
Figure 3.3. PSA spectra of the scaled records fulfilling EN 1998-1 [1] criteria, so that $PSA_{average} > 0.9 \cdot PSA_{target}$. (average & average $\pm 1\sigma$ are represented)	37
Figure 3.4. Earthquake records adopted in the analysis for stiff soil	38
Figure 3.5. Earthquake records adopted in the analysis for soft soil	39
Figure 3.6. Comparison between numerical and experimental curves: (a) cyclic tests on beams by D'Aniello et al. [41]; (b) cyclic tests on single storey MRF by Wakawayashi et al. [42]....	42
Figure 3.7. Brace model vs. experimental response: (a) axial behaviour, (b) out-of-plane behaviour	42
Figure 3.8. Link model vs. experimental response (W10x33 by Okazaki & Engelhardt [45]).....	43
Figure 3.9. Ductility demand ratios	43
Figure 3.10. Overstrength demand ratios	44

Figure 3.11. Brace ductility demand for the three limit states	45
Figure 3.12. Rotation demand in beams of MRF spans: (a) 8-storeys, (b) 16-storeys	45
Figure 3.13. Brace ductility demand for the three limit states	46
Figure 3.14. Link ductility demand for the three limit states	47
Figure 3.15. Link overstrength vs. link demand: (a) 8-storeys, (b) 16-storeys	48
Figure 3.16. Rotation demand in beams of MRF spans: (a) 8-storeys, (b) 16-storeys	48
Figure 3.17. Link ductility demand for the three limit states	49
Figure 3.18. Link overstrength vs. link demand	49
Figure 3.19. Interstorey drift demand for the three limit states: (a) 4 & 8 storey frames corresponding to stiff soil, (b) 4 & 8 storey frames corresponding to soft soil	50
Figure 3.20. Interstorey drift demand for the three limit states	52
Figure 3.21. Interstorey drift demand for the three limit states	53
Figure 3.22. Interstorey drift demand for the three limit states	55
Figure 3.23. Interstorey drift demand for the three limit states	56
Figure 4.1. Experimental programme on bolts	60
Figure 4.2. Results from tensile tests on bolts: (a) pure material, (b) thread insert & set of bolt	61
Figure 4.3. Stress-strain curve for tensile tests on steel grade S355	61
Figure 4.4. Yield strength and ultimate strength for steel grade S355	61
Figure 4.5. Tensile tests on steel grade S460	62
Figure 4.6. Yield strength and ultimate strength for steel grade S460	62
Figure 4.7. Tensile tests on steel grade S690	62
Figure 4.8. Yield strength and ultimate strength for steel grade S690	62
Figure 4.9. Modulus of elasticity	62
Figure 4.10. Elongation after fracture (A) [%]	62
Figure 4.11. Stress-strain curves of filler metal G46	63
Figure 4.12. Stress-strain curves of filler metal G69	63
Figure 4.13. Testing scheme - indenter lines	63
Figure 4.14. Close up (indenter lines)	63
Figure 4.15. Comparison of hardness of filler metal G46 and different base metal (S460 / S690)	64
Figure 4.16. Comparison of hardness of filler metal G69 and different base metal (S460 / S690)	64
Figure 4.17. Close up CJ-501-FW-G46-S460	64
Figure 4.18. Close up CJ-502-FPW-G46-S460	64
Figure 4.19. Fabrication for Cruciform Joint specimens	65
Figure 4.20. Modified loading protocol	66
Figure 4.21. Final instrumentation for Cruciform Joint specimens - Displacement Transducers	66
Figure 4.22. Test results for Cruciform Joints under monotonic quasi-static loading	67
Figure 4.23. Comparison F_{max} for mq-s / md_0.06 / md_0.12	67
Figure 4.24. 504-9_ mq-s_#1	68
Figure 4.25. 504-16_ cd_0.06_#1	68
Figure 4.26. 504-18_ cd_0.12_#1	68
Figure 4.27. Comparison F_{max} for cq-s / cd_0.06 / cd_0.12	68
Figure 4.28. Comparison of mq-s & cq-s	68
Figure 4.29. Comparison of md_0.06 & cd_0.06	68
Figure 4.30. Comparison D_{max} for mq-s / md_0.06 / md_0.12	69
Figure 4.31. Comparison D_{max} for cq-s / cd_0.06 / cd_0.12	69
Figure 4.32. Plastic strains in the weld	69
Figure 4.33. Plastic strains of specimens with (a) fillet welds, and (b) full penetration welds	69
Figure 4.34. Plastic strains at longitudinal plate	70
Figure 4.35. Extraction from joint configuration – T-stub specimens (visualisation)	71
Figure 4.36. Differentiation of T-stub failure modes	71
Figure 4.37. Modified loading protocol with X=6	72
Figure 4.38. Modified loading protocol with X=9	72
Figure 4.39. T-stub instrumentation (e.g. series 100)	73

Figure 4.40. Load carrying capacity for T-stub (a) series 100, and (b) series 200	74
Figure 4.41. FE-results e.g. T-stub series 100 (a) end-plate S460, and (b) end-plate S690	74
Figure 4.42. FE-results (a) development of prying forces, and (b) bolt failure.....	74
Figure 4.43. (a) F-D-curve: Unstiffened T-stub (series 100); (b) & (c) Immediately before failure.....	75
Figure 4.44. (a) F-D-curve: Unstiffened T-stub (series 200); (b) & (c) Immediately before failure.....	75
Figure 4.45. F-D-curve: T-stub series 300	75
Figure 4.46. Load carrying capacity: T-stub series 300	75
Figure 4.47. F-D-curve: T-stub series 400	76
Figure 4.48. Load carrying capacity: T-stub series 400	76
Figure 4.49. Punching failure	76
Figure 4.50. F-D-curve TST-301-3_cq-s	76
Figure 4.51. Failure mode TST-401-4_cq-s	77
Figure 4.52. Cyclic F-D-curve TST-401-4_cq-s.....	77
Figure 4.53. Experimental vs. analytical: (a) series 100; (b) series 200	77
Figure 4.54. Experimental vs. analytical: a) series 300; b) series 400	78
Figure 4.55. B-EP-H joint configuration	79
Figure 4.56. B-EP-U joint configuration	79
Figure 4.57. B-EPL-RBS joint configuration	79
Figure 4.58. End-plate details	80
Figure 4.59. Reverse U channel details.....	80
Figure 4.60. Dog-bone detail (D and F specimens).....	80
Figure 4.61. Different reinforcements of the beams.....	81
Figure 4.62. Description of column stub specimens	81
Figure 4.63. Test set-up for the beam-to-column joints	83
Figure 4.64. Instrumentation for A1, A2, B1 and B2 specimens (detail for C, D, E, F specimens can be found in Deliverable D4 [11] of the present project).....	84
Figure 4.65. Plastic-hinge failure mode.....	85
Figure 4.66. B-EP-H joint – failure in the connection (4 bolts in the tension zone failed and the hammer head in compression yielded).....	85
Figure 4.67. Failure mode of the B-EP-U joints (reverse U channels yielded)	85
Figure 4.68. Load – point load displacement curves for B-EP-H joint	86
Figure 4.69. Load – point load displacement curves for B-EP-U joints.....	86
Figure 4.70. Load – point load displacement curves for B-EPL-RBS joints	87
Figure 4.71. k_b factor for the joint types.....	87
Figure 4.72. Test set-ups for the column stub tests.....	88
Figure 4.73. Instrumentation for column stubs (T1-T6).....	89
Figure 4.74. Critical zones in: (a) specimens T1 and T4, and (b) specimens T2, T3, T5 and T6	89
Figure 4.75. Load-displacement curves for the column-stubs tests	90
Figure 4.76. Effective length of the bolts for the calculation of the concrete core in bearing.....	91
Figure 4.77. Shear force in the bolts during test T4	92
Figure 4.78. Constructional details of four designed stiffened joints	94
Figure 4.79. N-M interaction curves for large (L) and small (S) composite column cross-section	94
Figure 4.80. Static model of the specimen with boundary conditions and loads applied	95
Figure 4.81. Experimental test set-up	95
Figure 4.82. Moment vs. total joint rotation relationship for specimens tested under variable cyclic loading with full column axial force	97
Figure 4.83. Comparison of moment amplitudes vs. total joint rotation for specimens tested under variable amplitude: (a) RS and (b) CP joints	97
Figure 4.84. Comparison of moment amplitudes vs. number of cycles in inelastic range: (a) specimens RS1.2 and RS2.2, (b) specimens CP1.2 and CP2.2	98
Figure 4.85. Specimen RS2.2 after the failure: a) overall view: beam local buckling with the spread of plastic zone (darker region), b) detail of fracture in the bottom beam flange.....	98
Figure 4.86. Specimen CP1.1 after the failure: (a) overall view: beam local buckling with the spread of plastic zone (darker region), (b) detail of fracture in the top beam flange.....	98

Figure 4.87. Normalized moment versus total joint rotation diagrams for constant amplitude cyclic tests, small amplitude	100
Figure 4.88. Fracture in the upper beam flange: (a) specimen RS1.3, (b) specimen CP2.3	100
Figure 4.89. Normalized moment versus total joint rotation diagrams for constant amplitude cyclic tests, large amplitude	101
Figure 4.90. Moment amplitudes vs. number of cycles: (a) specimens RS13 and RS23, (b) specimens RS14 and RS24	102
Figure 4.91. Moment amplitudes vs. number of cycles: (a) specimens CP13 and CP23, (b) specimens CP14 and CP24.....	102
Figure 4.92. Response of composite column: a) elastic column and elastic beam contribution to the total joint rotation for specimen CP1.2, b) recorded normal strains in encased steel sections	102
Figure 4.93. Composite column after the test: a) specimens RS14, b) specimens CP11	103
Figure 4.94. (a) Definition of plastic rotation and cumulative plastic rotation, (b) comparison of cumulative plastic rotations for all 16 specimens	103
Figure 4.95. a) Maximum rotation vs. cumulative plastic rotation relationship for all 16 specimens, b) Cumulative dissipated energy	103
Figure 4.96. Specimen configuration for the load introduction tests	105
Figure 4.97. Experimental test set-up (a) & (b), instrumentation arrangement (c) & (d).....	105
Figure 4.98. Monotonic and cyclic response of friction connection (a) & (b), and friction combined with connectors S700-F-H - (c) & (d), and respectively S460-F-H - (e) & (f).....	106
Figure 4.99. Contribution of the connectors under: (a) monotonic loading, and (b) cyclic loading; corresponding failure mode (c) & (d)	107
Figure 4.100. Welded external diaphragm beam-to-column joints with reduced beam section (a), cover plates (b), designed joint specimens (c), and corresponding joint specimens with reinforced beam (d)	108
Figure 4.101. Conceptual scheme and illustration of the test assembly.....	108
Figure 4.102. Local joint instrumentation (a) and global instrumentation (b).....	109
Figure 4.103. State of the joint configurations before testing: (a) S460-RBS, (b) S700-RBS, (c) S460-CP, (d) S700-CP – designed joints; (e) S460-RBS-R, (f) S700-RBS-R, (g) S460-CP-R, (h) S700-CP-R – corresponding joints with reinforced beam	110
Figure 4.104. S460-RBS-M joint: monotonic response & illustration of failure mode	110
Figure 4.105. S460-RBS-C joint: cyclic response & illustration of failure mode	110
Figure 4.106. S700-RBS-M joint: monotonic response & illustration of failure mode	111
Figure 4.107. S700-RBS-C joint: cyclic response & illustration of failure mode	111
Figure 4.108. S460-CP-M joint: monotonic response & illustration of failure mode	111
Figure 4.109. S460-CP-C joint: cyclic response & illustration of failure mode	111
Figure 4.110. S700-CP-M joint: monotonic response & illustration of failure mode	112
Figure 4.111. S700-CP-C joint: cyclic response & illustration of failure mode	112
Figure 4.112. S460-RBS-R-M joint: monotonic response & illustration of failure mode	112
Figure 4.113. S460-RBS-R-C joint: cyclic response & illustration of failure mode	112
Figure 4.114. S700-RBS-R-M joint: monotonic response & illustration of failure mode.....	113
Figure 4.115. S700-RBS-R-C joint: cyclic response & illustration of failure mode	113
Figure 4.116. S460-CP-R-M joint: monotonic response & illustration of failure mode	113
Figure 4.117. S460-CP-R-C joint: cyclic response & illustration of failure mode	113
Figure 4.118. S700-CP-R-M joint: monotonic response & illustration of failure mode	114
Figure 4.119. S700-CP-R-C joint: cyclic response & illustration of failure mode	114
Figure 4.120. Overstrength of connection zone for RBS joints.....	114
Figure 4.121. Overstrength of connection zone for CP joints.....	115
Figure 4.122. Contribution of components joint rotation: (a) S460-RBS-M, (b) S700-RBS-M	115
Figure 4.123. Contribution of components to joint rotation: (a) S460-CP-M, (b) S700-CP-M.....	115
Figure 4.124. Contribution of components to joint rotation: (a) S460-RBS-R-M, (b) S700-RBS-R-M ...	115
Figure 4.125. Contribution of components to joint rotation: (a) S460-CP-R-M, (b) S700-CP-R-M.....	116
Figure 4.126. Contribution of components to joint rotation: (a) S460-RBS-C, (b) S700-RBS-C	116
Figure 4.127. Contribution of components to joint rotation: (a) S460-CP-C, (b) S700-CP-C.....	116
Figure 4.128. Stress-strain relationship for concrete.....	117
Figure 4.129. Calibration of the material model for steel (IPE400 beam flange).....	117

Figure 4.130. Pre-test numerical simulation of the joint behaviour and illustration of the joint model accounting for the out of plane lateral system	117
Figure 4.131. Comparison between test and simulation for RBS joints.....	118
Figure 4.132. Comparison between test and simulation for CP joints.....	118
Figure 4.133. Comparison between test and simulation for reinforced RBS-R joints.....	118
Figure 4.134. Comparison between test and simulation for reinforced CP-R joints.....	118
Figure 4.135. Test vs. simulation for RBS and CP designed joints subjected to cyclic loading	119
Figure 4.136. Test vs. simulation for reinforced RBS and CP joints subjected to cyclic loading	119
Figure 4.137. Influence of concrete core for: a) & b) CP joints, and c) & d) strengthened CP joints	120
Figure 4.138. Influence of $0.5 \cdot N_{pl,Rd,composite}$ axial force: S460-CP joint	120
Figure 4.139. Behaviour of S700-CP joint with beams welded on two sides (CFT)	121
Figure 4.140. Behaviour of S700-RBS joint with beams welded on two sides (CFT)	121
Figure 4.141. Joints with four beams – Moment-rotation curves.....	121
Figure 4.142. Joints with four beams – von Misses stress distribution and plastic strain	122
Figure 5.1. Possible use of HSS (black) and mild carbon steel (red) in MRF (a), D-CBF or D-EBF (b), and CBF (c) & (d). Grey are pinned ends of the floor beams	128
Figure 5.2. Welded RS beam-to-column joint details (concrete column encasement not illustrated)	138
Figure 5.3. Welded CP beam-to-column joint details (concrete column encasement not illustrated)	138
Figure 5.4. Typical beam span with stiffened joint, plastic hinge location and cross-sections used for design check	139
Figure 5.5. Sample frame with single-sided joint configuration, internal forces in panel zone.....	140
Figure 5.6. RBS joint: a) configuration, b) preparation details, c) specimen illustration.....	141
Figure 5.7. CP joint: a) configuration, b) preparation details, c) specimen illustration.....	141
Figure 5.8. Design steps for RBS and CP joints	142
Figure 5.9. Gusset plate connections detailed to accommodate brace buckling by yielding in the connection gusset or knife plate [83]	144
Figure 5.10. Beam-to-column connections that allow rotation: (a) Stoakes & Fahnestock [85], and (b) Thornton & Muir [86].....	144
Figure 5.11. Typical column base detail [87]	145
Figure 5.12. Leaning column.....	147
Figure 5.13. 2D Frame numerical vs. experimental response: cyclic condition	148
Figure 5.14. Acceptance criteria for structural components: definition of the criteria and seismic performance evaluation of the beam-to-column joints	149
Figure 6.1. Analysis cases for the evaluation of technical and economic efficiency.....	151
Figure 6.2. Designed beam-to-column joints: (a) ED-RBS – welded external diaphragm reduced beam section joint; (b) RS – welded rib stiffened joint; (c) HH – bolted hammer head joint; (d) LB-RBS – bolted reduced beam section joint with long bolts	152
Figure 6.3. Economic benefit of dual-steel frames, i.e. the use of high strength steel in some particular non-dissipative members in case of: (a) CBF's, (b) D-CBF's, (c) EBF's, (d) D-EBF's.....	157
Figure 6.4. Economic impact of the steel grade (S355, S460, S700) for the connection corresponding to the moment resisting bays of (a) D-CBF's, and (b) D-EBF's with CFT columns.....	157
Figure 6.5. Economic impact of connection type corresponding to D-CBF's with different column cross sections (CFT, FE, PE).....	158

List of tables

Table I – Working packages: WP leaders and partners involved in specific tasks.....	8
Table II – Frame configurations for preliminary design in WP1	8
Table 2.1 – Frame configurations for preliminary design in WP1	28
Table 2.2 – Cross-section of members for “joint configuration 1”.....	29
Table 2.3 – Cross-section of members for “joint configuration 2”.....	29
Table 2.4 – Cross-section of members for “joint configuration 3”.....	30
Table 2.5 – Cross-section of members for welded joints with FE-WF columns.....	30
Table 2.6 – Cross-section of members for welded joints with CFT columns.....	31
Table 3.1 – Parameter variations.....	34
Table 3.2 – 8-storey frames: aspect ratios.....	34
Table 3.3 – Performance levels vs. seismic intensity levels.....	35
Table 3.4 – Basic data of the earthquakes behind the selected records.....	35
Table 3.5 – Period ranges for fitting the records	36
Table 3.6 – Scale factor based on equality of areas under spectra, corrected to fulfil the EN 1998-1 [1] requirement ($PSA_{average} > 0.9 \cdot PSA_{target}$).....	37
Table 3.7 – Acceptance criteria at each limit state.....	41
Table 3.8 – Overstrength factors for MRF’s	51
Table 3.9 – Behaviour factors for MRF’s.....	51
Table 3.10 – Overstrength factors for CBF’s	52
Table 3.11 – Behaviour factors for CBF’s	53
Table 3.12 – Overstrength factors for D-CBF’s.....	54
Table 3.13 – Behaviour factors for D-CBF’s	54
Table 3.14 – Overstrength factors for EBF’s	55
Table 3.15 – Behaviour factors for EBF’s.....	56
Table 3.16 – Overstrength factors for D-EBF’s.....	57
Table 3.17 – Behaviour factors for D-EBF’s	57
Table 4.1 – Extract from tensile tests on bolts shown in Figure 4.2.....	61
Table 4.2 – Cruciform Joint variations	65
Table 4.3 – Experimental programme on T-stubs.....	72
Table 4.4 – Test program on the beam-to-column joints	80
Table 4.5 – Test program on the column stubs ^(a)	81
Table 4.6 – Results of the tightening tests on bolts	82
Table 4.7 – Results of the tensile tests on bolts	82
Table 4.8 – Coupon tests on plates, profiles and hollow sections	82
Table 4.9 – Compression tests on concrete cubes	83
Table 4.10 – Instrumentation for the beam-to-column specimens	83
Table 4.11 – Summary of the test results on the beam-to-column joints	84
Table 4.12 – Summary of joint characterization from the test results.....	87
Table 4.13 – Obtained information regarding new components	88
Table 4.14 – Instrumentation for the specimens.....	89
Table 4.15 – Maximal loads and failure modes.....	89
Table 4.16 – Bearing resistance of the tested CFT column.....	91
Table 4.17 – Experimental program on beam-to-column joints with FE-WF columns (UL).....	92
Table 4.18 – Experimental program on beam-to-column joints with CF-RHS columns (UPT)	92
Table 4.19 – Experimental program on column stubs (UPT).....	92
Table 4.20 – Experimental program on beam-to-column joints with FE-WF columns.....	93
Table 4.21 – Monotonic tensile material properties.....	95
Table 4.22 – Summary of all 16 test specimens.....	96

Table 4.23 – Summary of experimental results for the RS group of specimens	99
Table 4.24 – Summary of experimental results for the CP group of specimens	99
Table 4.25 – Total number of complete cycles according to the three failure criteria.....	101
Table 4.26 – Complete beam and complete joint rotations for RS and CP joints.....	104
Table 4.27 – Experimental program and specimen configuration	105
Table 4.28 – Experimental program on welded beam-to-column joints with CF-RHS columns	107
Table 4.29 – Beam-to-column joint configurations	108
Table 4.30 – Tensile and Charpy V-notch test results for steel samples	109
Table 5.1 – Shear load transfer within the B-EPL-RBS joint	132
Table 5.2 – Load introduction in CFT columns through shot fired nails.....	132
Table 5.3 – B-EP-H joint - joint detailing.....	133
Table 5.4 – B-EP-H joint - component identification.....	133
Table 5.5 – B-EP-H joint – component assembly.....	134
Table 5.6 – B-EP-U joint – joint detailing	135
Table 5.7 – B-EP-U joint - component identification.....	135
Table 5.8 – B-EP-U joint - component assembly	135
Table 5.9 – B-EPL-RBS joint detailing.....	136
Table 5.10 – B-EPL-RBS joint - design of welds	136
Table 5.11 – B-EPL-RBS joint - component identification.....	137
Table 5.12 – B-EPL-RBS joint - component assembly.....	137
Table 5.13 – Summary of the design procedure for welded RS and CP joints.....	139
Table 5.14 – Summary of the design procedure for welded RBS and CP joints.....	142
Table 5.15 – Performance levels and acceptance criteria.....	145
Table 5.16 – Acceptance criteria at each limit state.....	148
Table 5.17 – Performance levels (description & identification criteria)	149
Table 6.1 – Case study frames (code, labelling, frame type, column type, steel grade, joint).....	152
Table 6.2 – Average unitary frame price	153
Table 6.3 – Average unitary frame price – Long bolts joint	154
Table 6.4 – Average unitary frame price – External diaphragm RBS joint.....	154
Table 6.5 – Average unitary frame price – Rib-stiffened joint.....	155
Table 6.6 – Average unitary frame price – Hammer-head joint	155
Table 6.7 – Evaluation of the influence of steel grade in unitary frame price	156
Table 6.8 – Frames price resume.....	156

List of acronyms and abbreviations

HSS-SERF – High Strength Steel in Seismic Resistant Building Frames

UPT - Universitatea "Politehnica" din Timisoara

RIVA - Riva Acciaio S.p.A

VTT - Valtion teknillinen tutkimuskeskus

ULG - University of Liege

UL – University of Ljubljana

USTUTT - Universität Stuttgart

UNINA - University of Naples "Federico II"

GIPAC - Gabinete de Informática e Projecto Assistido por Computador Lda.

RUUKKI - Ruukki Construction Oy

B-EPL-RBS – bolted extended end plate to RHS column joint with long bolts and reduced beam section

B-EP-H – bolted hammer head end plate joint

B-EP-U – bolted hammer head end plate to RHS column joint with U channel

CBF – Concentrically Braced Frames

CFT – Concrete Filled Tube

CP – Cover Plate

D-CBF – Dual Centrally Braced Frames

DCH – ductility class high (a design concept of EN1998-1)

D-EBF – Dual Eccentrically Braced Frames

DL – damage limitation (limit state in a performance based setting)

DLS – damageability limit state

DSF – dual-steel frame

EBF – Eccentrically Braced Frames

FEM – Finite Element Method

FE-WF – Fully Encased Wide Flange

FPW – Full Penetration Welds

FW – Fillet Welds

HSS – High Strength Steel

IDA – incremental dynamic analysis

MCS – Mild Carbon Steel

MRF – Moment Resisting Frames

NAD – national application document

NC – near collapse (limit state in a performance based setting)

PBD – performance based design

PE – Partially Encased

PE-WF – Partially Encased Wide Flange

RBS – Reduced Beam Section

RHS – Rectangular Hollow Section

RS – rib stiffened

SD – severe damage (limit state in a performance based setting)

SLS – serviceability limit state

ULS – ultimate limit state

W-RS – welded rib stiffened beam to wide flange column joint

W-ED-RBS – welded external diaphragm reduced beam section to RHS column joint

List of references

- [1] EN 1998-1 / CEN. Eurocode 8: Design of structures for earthquake resistance - Part 1: General rules, seismic actions and rules for buildings, EN 1998-1, European Committee for Standardisation, Brussels; 2005.
- [2] Seismostruct (2010), Version 5.0.5, Seismosoft – Earthquake Engineering Software Solution, Pavia, Italy.
- [3] EN 1993-1-8, (2005), Eurocode 3: Design of steel structures - Part 1-8: Design of joints, CEN, European Committee for Standardization.
- [4] EN 1994-1-1, (2004), Eurocode 4: Design of composite steel and concrete structures - Part 1-1: General rules and rules for buildings, EN 1994-1-1. Brussels, European Committee for Standardisation; 2004.
- [5] ECCS 1986. Recommended testing procedures for accessing the behaviour of structural elements under cyclic loads, ECCS No.45, European Convention for Structural Steelwork, Technical Committee 1 - Structural Safety and Loadings, Technical Working Group 1.3 - Seismic Design; 1986.
- [6] EN 1993-1-1 / CEN. Eurocode 3: Design of steel structures - Part 1-1: General rules and rules for buildings, EN 1993-1-1. Brussels, European Committee for Standardisation; 2005.
- [7] ANSI/AISC 341-10 / AISC. Seismic provisions for structural steel buildings, ANSI/AISC 341-10. Chicago, Illinois, American Institute of Steel Construction; 2010.
- [8] Autodesk Robot Structural Analysis Professional 2010.
- [9] Landolfo R., D’Aniello M., La Manna Ambrosino G., Portioli F., Tenchini A., Rebelo C., Da Silva L. S., Serra M., Ludovic Fulop., Deliverable D2 - Report on seismic performance of dual-steel structures and evaluation of q-factors associated with different performance levels. (document id: hss-d-0002-wp2-unina-v3).
- [10] Silva L.S., Rebelo C., Serra M., Tenchini A., Deliverable D1 – Design specifications and drawings of joint specimens (document id: hss-d-0001-wp1-gipac-v1).
- [11] Jaspart J.-P., Hoang L., Demonceau J.-F., Tremeeea A., Braconi A., Kuhlmann U., Kleiner A., Kesti J., Deliverable D4 – Prequalification criteria for bolted beam-to-column joints in dual-steel frames (document id: hss-d-0004-wp4-ulg-v1)
- [12] Lee CH., Seismic design of rib-reinforced steel moment connections based on equivalent strut model. Journal of Structural Engineering-Asce 2002; 128(9): 1121-1129.
- [13] Beg D., Cermelj B., Rejec K., Lopatic J., Dubina D., Vulcu C., Stratan A., Ciutina A., Tremeeea A., Braconi A., Kuhlmann U., Kleiner A., Kesti J., Deliverable D5 - Prequalification criteria for welded beam-to-column joints in dual-steel frames (document id: hss-d-0005-wp5-ul-v1).
- [14] Kim T., Whittaker A.S., Gilani A.S.J, Bertero V., Takhirov S.M., Cover-plate and flange-plate reinforced steel moment-resisting connections. Report to sponsor SAC Joint Venture, Pacific Earthquake Engineering Research Center (PEER), College of Engineering, University of California, Berkeley; 2000.
- [15] Kim T, et al. Cover-plate and flange-plate steel moment-resisting connections. Journal of Structural Engineering-Asce 2002; 128(4): 474-482.
- [16] Kim T, et al. Experimental evaluation of plate-reinforced steel moment-resisting connections. Journal of Structural Engineering-Asce 2002; 128(4): 483-491.
- [17] Engelhardt MD and Sabol TA. Reinforcing of steel moment connections with cover plates: benefits and limitations. Engineering Structures 1998; 20(4-6): 510-520.
- [18] ANSI/AISC 358-05 (2005), "Prequalified Connections for Special and Intermediate Steel Moment Frames for Seismic Applications", American Institute of Steel Construction.
- [19] FEMA 350. SAC. Recommended seismic design criteria for new steel moment-frame buildings. Prepared by the SAC Joint Venture for the Federal Emergency Management

- Agency, Sacramento, California; 2000.
- [20] Owens G.W., Knowles P.R., Dowling P.J., Steel Designer Manual. Steel Construction Institute, Blackwell science Ltd, 2000.
- [21] EN 1998-3: Eurocode 8: Design of structures for earthquake resistance – Part 3: Assessment and retrofitting of buildings, CEN, 2005.
- [22] Kesti J., Rodriguez A., Pastor N., Arnedo A., Casafont M., Bretones M.A., Hakola I., Arola J., Fülöp L.A., and Sivill A., Seismic design of light gauge steel framed buildings, Luxembourg: European Commission - Directorate General for Research, 2007.
- [23] Balling R., Balling L., and Richards P., "Design of Buckling-Restrained Braced Frames Using Nonlinear Time History Analysis and Optimization," Journal of Structural Engineering, vol. 135, May. 2009, pp. 461 - 468.
- [24] Elghazouli A.Y., Assessment of capacity design approaches for steel framed structures. Journal of Steel Structures 2005;5(5):465-75
- [25] Mazzolani F.M., Piluso V., ECCS Manual on Design of Steel Structures in Seismic Zones. Technical Committee 13 - Seismic Design, N° 76/1994. ECCS – European Convention for Constructional Steelwork; 1994.
- [26] Elnashai A.S., Broderick B.M., (1996). Seismic response of composite frames II. Calculation of behaviour factors. Eng Struct 1996;18(9): 707-723
- [27] Malley J., Popov E., Design considerations for shear links in eccentrically braced frames, UCB/EERC-83/24.
- [28] Spacone E., Ciampi V., Filippou FC., Mixed formulation of nonlinear beam finite element. Comput Struct 1996;58(I): 71-83.
- [29] Calabrese A., Almeida J.P., Pinho R., Numerical issues in distributed inelasticity modelling of RC frame elements for seismic analysis. J. Earthq. Eng 2010; 14(1): 38-68.
- [30] Martinez-Rueda J.E., Elnashai A.S., Confined concrete model under cyclic load. Mater Struct 1997;30: 139-147.
- [31] Mander J.B., Priestley M.J.N., Park R. Theoretical stress-strain model for confined concrete. J Struct Eng 1988;8(114): 1804-1826.
- [32] Susantha K.A.S., Ge H., Usami T., Uniaxial stress-strain relationship of concrete confined by various shaped steel tubes. Eng Struct 2001;23(10): 1331-1347.
- [33] Menegotto M., Pinto P.E., Method of analysis for cyclically loaded R.C. plane frames including changes in geometry and non-elastic behaviour of elements under combined normal force and bending. In: Symposium on the Resistance and Ultimate Deformability of Structures Acted on by Well Defined Repeated Loads; 1973.
- [34] EN 1992-1-1, Eurocode 2: Design of concrete structures - Part 1-1: General rules and rules for buildings. CEN; 2004.
- [35] Braconi A., Finetto M., Degee H., Hausoul N., Hoffmeister B., Gündel M., Karmanos S. A., Pappa P., Varelis G., Rinaldi V., Obiala R., Hjaij M., Somja H., Badalassi M., Caprili S., Salvatore W., (2013), Optimising the seismic performance of steel and steel-concrete structures by standardising material quality control (OPUS), RFSR-CT-2007-00039, Final Report, ISBN 978-92-79-29037-4.
- [36] Abramowitz M., Stegun I.A., Handbook of Mathematical Functions, National Bureau of Standards, Applied Math. Series; 1964.
- [37] Szabó B.A., Babuška I., Finite Element Analysis, John Wiley & Sons; 1991.
- [38] Correia A.A., Virtuoso F.B.E., Nonlinear analysis of space frames. In: Proceedings of the Third European Conference on Computational Mechanics: Solids, Structures and Coupled Problems in Engineering, (Mota Soares et al. Eds.); 2006.
- [39] Priestley M.J.N., Grant D.N., Viscous damping in seismic design and analysis. J Earthq Eng 2005; 9(1): 229-255.
- [40] D’Aniello M, La Manna Ambrosino G, Portioli F, Landolfo R. Modelling aspects of the seismic response of steel concentric braced frames. Steel and Composite Structures 2013;15(5): 539-566.

- [41] D'Aniello M, Landolfo R, Piluso V, Rizzano G. Ultimate Behaviour of Steel Beams under Non-Uniform Bending. *J Construct Steel Res* 2012;78: 144–158.
- [42] Wakawayashi M, Matsui C, Minami K, Mitani I. Inelastic Behaviour of Full Scale Steel Frames, Kyoto University Research Information Repository, Disaster Prevention Research Institute annuals; 1970.
- [43] Diceli, M. and Calik, E. (2008). Physical Theory Hysteretic Model for Steel Braces *J. Struct. Eng.*, 134(7), 1215–1228.
- [44] Black, R. G., Wenger, W. A. B., Popov, E. P., (1980), Inelastic buckling of steel struts under cyclic load reversals, Rep. No. UCB/EERC-80/40, Berkeley, Calif.
- [45] Okazaki T., Engelhardt M. D. (2007). Cyclic loading behavior of EBF links constructed of ASTM A992 steel. *Journal of constructional Steel Research*, 63, 751-765.
- [46] EN 1993-1-8: 2010-12 - Eurocode 3: Design of steel structures - Part 1-8: Design of joints.
- [47] Kuhlmann U., Kleiner A., Beg D., Blaž Č., Jaspart J.-P., Demonceau J.-F., Hoang L., Tremea A., Kesti J., Deliverable D3 - Report on performance of welded details and T-stubs, and recommendations of welding procedures to be used in dual-steel structures for welded connections between HSS and MCS. (document id: hss-d-0003-wp3-ustutt-v1)
- [48] EN ISO 6892-1:2009-12 - Metallic materials - Tensile testing -Part 1: Method of test at room temperature.
- [49] EN ISO 5817:2006-10 - Welding - Fusion-welded joints in steel, nickel, titanium and their alloys (beam welding excluded) - Quality levels for imperfections.
- [50] EN ISO 9015-1:2011-05 - Destructive tests on welds in metallic materials - Hardness testing - Part 1: Hardness test on arc welded joints.
- [51] EN 14399-4:2005-06 - High-strength structural bolting assemblies for preloading - Part 4: System HV- Hexagon bolt and nut assemblies.
- [52] EN 14399-6:2005-06 - High-strength structural bolting assemblies for preloading - Part 6: Plain chamfered washers.
- [53] EN 10025-2:2005-04 - Hot rolled products of structural steels – Part 2: Technical delivery conditions for non-alloy structural steels.
- [54] EN 10025-6:2009-08 - Hot rolled products of structural steels – Part 6: Technical delivery conditions for flat products of high yield strength structural steels in the quenched and tempered condition.
- [55] EN ISO 15614-1:2012-06 - Specification and qualification of welding procedures for metallic materials - Welding procedure test - Part 1: Arc and gas welding of steels and arc welding of nickel and nickel alloys.
- [56] EN 1998-1:2004-12 - Eurocode 8: Design of structures for earthquake resistance - Part 1: General rules, seismic actions and rules for buildings.
- [57] EN 1011-1:2002-09 - Welding - Recommendations for welding of metallic materials - Part 1: General guidance for arc welding.
- [58] EN 1090-2:2008-12 - Execution of steel structures and aluminium structures - Part 2: Technical requirements for steel structures.
- [59] Schlecker M., Investigations on load carrying capacity on Cruciform Joints made of mild carbon steel and high strength steel under monotonic as well as cyclic loading conditions, Universität Stuttgart, Institut für Konstruktion und Entwurf, Diploma Thesis, Nr. 2013-13X (in German).
- [60] Dubina D., Stratan A., Behaviour of welded connections of moment resisting frames beam-to-column joints; *Engineering Structures* 24 (2002) p. 1431–1440.
- [61] Schwab C., Numerical investigations on load carrying capacity on Cruciform Joints made of mild carbon steel and high strength steel under monotonic quasi-static loading conditions, Universität Stuttgart, Institut für Konstruktion und Entwurf, Diploma Thesis, Nr. 2013-42X (in German).
- [62] ANSYS, INC: ANSYS Release V14.0 User`s Manual, Canonsburg, USA.
- [63] Ling Y., Uniaxial True Stress-Strain after Necking, *AMP Journal of Technology* Vol. 5, 1996.

- [64] Bridgman P. W., *Studies in Large Plastic Flow and Fracture*, New York, 1952.
- [65] Piluso V., Rizzano, G.: Experimental analysis and modelling of bolted T-stubs under cyclic loads, *Journal of Constructional Steel Research* 64 (2008) p. 655–669.
- [66] CIDECT Report: 5BP-4/05, Development of full consistent design approach for bolted and welded joints in building frames and trusses between steel members made of hollow and/or open sections – Application of the component method, Volume 1 - Practical guidelines, Jaspart J.P., Pietrapertosa C., Weynand K., Busse E., Klinkhammer R., November 2005.
- [67] Kittel M., Investigations on load carrying and deformation capacity under monotonic and cyclic quasi-static loading conditions, Universität Stuttgart, Institut für Konstruktion und Entwurf, Diploma Thesis, Nr. 2014-4X (in German).
- [68] Fülöp L.A., Vulcu C., Stratan A., Dubina D., D’Aniello M., Landolfo R., Cermelj B., Beg D., Comelieu L., Demonceau J.F., Hoang L., Kleiner A., Kuhlmann U., Deliverable D6 – Report on conceptual design and performance based design of dual-steel building frames under seismic actions.
- [69] Calado L, Influence of column size, in Moment resistant connections of steel frames in seismic areas, *Design and reliability*, F.M. Mazzolani, Editor E & FN Spon, London; 2000, p. 267-290.
- [70] Nakashima M, et al. Tests on welded beam-to-column subassemblies. I: Global behaviour. *Journal of structural engineering* 1998; 124(11): 1236-1244.
- [71] Hilti AG, Prüfbericht nr. 172268, Prüfobjekt: Hilti Nägel X-DSH 32 P10 Special, Auftragsnummer 555236, 25-27.05.1998.
- [72] Abaqus (2007) Analysis User’s Manual I-V. Version 6.7. ABAQUS, Inc., Dassault Systèmes.
- [73] Ali A.M., Farid B.J., and Al-Janabi A.I.M., “Stress-strain relationship for concrete in compression made of local materials”, *JAU: Eng. Sci.*, Vol. 2, pp 183-194, 1990.
- [74] Korotkov V., Poprygin D., Ilin K., Ryzhov S., “Determination of dynamic reaction in concrete floors of civil structures of nuclear power plant in accidental drops of heavy objects”, *ABAQUS Users’ Conference*, Boston 25-27 May, 2004, pp. 399-408.
- [75] Dutta A., Dhar S., Acharyya S.K., “Material characterization of SS 316 in low-cycle fatigue loading”, *Journal of Materials Science*, Vol. 45, Issue 7, pp. 1782-1789, 2010.
- [76] Beck H., “Nailed shear connection in composite tube columns”, *Second European Conference on Steel Structures*, Prague, 26-29 May 1999, pp. 565–568.
- [77] EN ISO 2560 Welding consumables – Covered electrodes for manual metal arc welding of non-alloy and fine grain steels – Classification (2009)
- [78] EN ISO 18276 Welding consumables – Tubular cored electrodes for gas-shielded and non-gas-shielded metal arc welding of high strength steels – Classification (2005)
- [79] EN 1990, Eurocode 0: Basis of structural design. Brussels, European Committee for Standardisation; 2002.
- [80] Hanswille G., Beck H., Neubauer T., “Design concept of nailed shear connections in composite tube columns”, *Proceedings of the International Symposium on Connections between Steel and Concrete*, RILEM Publications SARL, Print-ISBN: 2-912143-25-X, e-ISBN: 2351580346, Stuttgart, Germany, September 10-12, pp. 1056-1065, 2001.
- [81] Astaneh-Asl, A. (1998), *Seismic Behavior and Design of Gusset Plates for Braced Frames*, Steel Tips, Structural Steel Education Council, Moraga, CA.
- [82] Thornton, W.A. (2001). *Seismic design of connections in concentrically braced frames*, Cives Engineering Corporation, Roswell, Georgia, USA.
- [83] Sabelli, R., Roeder, C.W., and Hajjar, J. (2013). *Seismic Design of Steel Special Concentrically Braced Frame Systems: a Guide for Practicing Engineers* NEHRP Seismic Design Technical Brief No. 8, produced by the NEHRP Consultants Joint Venture, for the National Institute of Standards and Technology, Gaithersburg, MD, NIST GCR 13-917-24.
- [84] Roeder, C.W., Lumpkin, E.J., and Lehman, D.E. (2011). *Balanced design procedure for special concentrically braced frame connections*, Elsevier, *Journal of Constructional Steel Research*, Vol. 67 No. 11, pp. 1760-72.

- [85] Stoakes, C. D. and Fahnestock, L.A. (2010), Flexural Behavior of Concentrically-Braced Frame Beam-Column Connections, Proceedings, 2010 Structures Congress, ASCE, Orlando, FL.
- [86] Thornton, W.A. and Muir, L.S. (2008), Vertical Bracing Connections in the Seismic Regime, Proceedings of the Sixth International Workshop on Connections in Steel Structures, AISC, Chicago, IL.
- [87] ECCS (1999). Column bases in steel building frames.
- [88] SEAOC, Vision 2000 - A Framework for Performance Based Earthquake Engineering, Vol.1 1995
- [89] Gioncu V, Mazzolani F. (2002), Ductility of Seismic-Resistant Steel Structures, Taylor & Francis, ISBN0419225501
- [90] Ballio G., ECCS approach for the design of steel structures against earthquakes, In:Symposium on steel in buildings. IABSE-AIPC-IVBH report, V.48. 1985. p. 373-80
- [91] Mazzolani F.M., Piluso V., Theory and design of seismic resistant steel frames. London: Spon; 1996
- [92] Sanchez-Ricart & Plumier A., Parametric study of ductile moment-resisting steel frames: A first step towards Eurocode 8 calibration, 2008
- [93] Ikeda K., Mahin S.A. (1986), Cyclic Response of Steel Braces, Journal of Structural Engineering-ASCE 1986; 112(2): 342-361.
- [94] Uang A., Bertero V., Earthquake simulation tests and associated studies of a 0.3-scale model of a six-storey concentrically braced steel structures. Report N. UCB/EERC-86/10 in University of California, Berkely, 1986
- [95] Malley J., Popov E., Design Considerations for shear links in eccentrically braced frames, UCB/EERC-83/24
- [96] Stratan A., Dubina D., Vulcu C., Proposal for the seismic performance evaluation of the beam-to-column joints investigated within HSS-SERF project. (document id: hss-tn-0040-wp6-upt-v1)
- [97] Caprili S., Ferrini M., Salvatore W., Tremea A., Deliverable D7 - Evaluation of technical and economic efficiency of dual-steel structures vs. conventional ones. (document id: hss-d-0007-wp7-riva-v1)
- [98] Tenchini A., Moura, A., Rebelo C. Da Silva L.S., - GIPAC - "Seismic design of braced frames accounting for connection behaviour", (document id: hss-r-0001-wp7-gipac-v4))

HOW TO OBTAIN EU PUBLICATIONS

Free publications:

- one copy:
via EU Bookshop (<http://bookshop.europa.eu>);
- more than one copy or posters/maps:
from the European Union's representations (http://ec.europa.eu/represent_en.htm);
from the delegations in non-EU countries (http://eeas.europa.eu/delegations/index_en.htm);
by contacting the Europe Direct service (http://europa.eu/eurodirect/index_en.htm) or
calling 00 800 6 7 8 9 10 11 (freephone number from anywhere in the EU) (*).

(*) The information given is free, as are most calls (though some operators, phone boxes or hotels may charge you).

Priced publications:

- via EU Bookshop (<http://bookshop.europa.eu>).

Priced subscriptions:

- via one of the sales agents of the Publications Office of the European Union
(http://publications.europa.eu/others/agents/index_en.htm).

The aim of “HSS-SERF” project was to investigate and evaluate the seismic performance of dual-steel building frames, realized from two different steel grades: Mild Carbon Steel and High Strength Steel.

A comprehensive set of dual-steel frames (moment resisting, concentrically and eccentrically braced) were designed, which allowed the identification of realistic member sizes for both mild carbon steel and high strength steel components. Several practical solutions for bolted and welded beam-to-column joints were identified and designed. Further, an extensive numerical program was carried out for the seismic performance evaluation of frames. The ductility and over-strength demands, and q-factors associated with different performance levels were evaluated. Furthermore, experimental and numerical investigations were carried out on joint assemblies and components. Guidelines were elaborated for the conceptual design and performance based design of dual-steel frames under seismic actions, and the technical and economic efficiency of dual-steel structures vs. conventional ones were finally evaluated.

The main outcomes of the project consist in: (i) development and characterisation in terms of global ductility and over-strength demands of dual-steel frames with composite columns (innovative solutions in European context); (ii) development of design recommendations; (iii) proposal of innovative solutions for beam-to-column joints with composite columns; (iv) recommendation for weld details and appropriate component method design approaches; (v) evaluation of technical and economic efficiency of the dual-steel approach.

Studies and reports

